A novel scaffold for cell-based lung tissue engineering

Ana Yuliyanova Kyoseva

PhD

March 2022

Keele University

Abstract

Chronic obstructive pulmonary disease (COPD) is the fourth leading cause of death worldwide and numbers are rising. Tissue engineering approaches have the potential to improve lung function and treat diseases such as COPD. Our aim is to investigate a highly porous and elastic gelatine scaffold, Surgispon®, for potential uses in cell-based lung tissue engineering by generating an alveolar-like structure. Surgispon scaffolds were crosslinked for stability, and their pore size, pore connectivity, and cytotoxicity were investigated. Human lung epithelial (A549) and fibroblast (35FLH) cell lines and primary porcine lung cells were cultured on Surgispon scaffolds, both separately and in co-cultures. Surgispon was used to create an air-liquid interface (ALI) to differentiate primary lung cells, and migration studies were performed in combination with decellularised lung tissue. Uncrosslinked Surgispon dissolved rapidly in solution, crosslinking promoted stability beyond 60 days in cell culture conditions. Pore size and interconnectivity were determined via imaging and µCT analysis, establishing similarity to alveolar diameter. Surgispon scaffolds supported cell attachment and growth, with no requirement for chemical coating. Primary lung epithelial cells differentiated into ciliated cells and self-organised into bronchospheres/organoids when cultured on Surgispon with an ALI. Cell migration occurred both from scaffold to tissue and vice versa, demonstrating the potential use of Surgispon scaffolds in clinical COPD research. In summary, Surgispon® scaffolds are an effective alveolar mimic due to being suitable for 3D cell culture, differentiation, and featuring interconnective pores of a size approximate to alveolar diameter. These features promote the prospect of Surgispon scaffolds as a potential scaffold and/or cell delivery system for use in lung tissue engineering and to help combat respiratory disease.

Table of Contents

List of abbreviations

µCT	Micro Computed Tomography
35FLH	Immortalised Adult Lung Fibroblasts
A549	Lung Epithelial Cell Line
ALI	Air-Liquid Interface
AT1	Pneumocyte Alveolar Type 1
AT2	Pneumocyte Alveolar Type 2
BAL	Bronchoalveolar Lavage
BSA	Bovine Serum Albumin
CaMg	Calcium Magnesium Salt
COL	Collagen Type I
COL+FIB	Collagen Type I And Fibronectin
COPD	Chronic Obstructive Pulmonary Disease
CTGF	Connective Tissue Growth Factor
D-35FLH	Deactivated Immortalised Adult Lung Fibroblasts
DAPI	4’,6-Diamidino-2-Phenylindole
DC	Dendritic Cell
DMEM	Dulbecco's Modified Eagle Medium
DMSO	Dimethyl Sulfoxide
DNase	Deoxyribonuclease
D-PLF	Deactivated Primary Porcine Lung Fibroblasts
dsDNA	Double Stranded DNA
EBV	Endobronchial Valve
ECM	Extracellular Matrix
EDTA	Ethylene Diamine Tetra-Acetic Acid
EGF	Epidermal Growth Factor
ELVR	Endoscopic Lung Volume Reduction
EPCs	Endothelial Progenitor Cells
EthD-1	Ethidium Homodimer-1
FBS	Foetal Bovine Serum
FDA	The Food And Drug Administration
FGF	Fibroblast Growth Factor
FIB	Fibronectin
GTA	Glutaraldehyde
HGF	Human Hepatocyte Growth Factor
IFN	Interferons
Ig E	Immunoglobulin E
IL	Interleukin
IL-10	Interleukin-10
IMS	Industrial Methylated Spirit
iPSCs	Induced Pluripotent Stem Cells

ITS	Insulin, Transferrin, Selenium
LABAs	Long-Acting B-Adrenergic Agonists
LCL	Liquid Crosslinked
L-Glu	L-Glutamine
LTOT	Long Term Oxygen Therapy
LVRS	Lung Volume Reduction Surgery
MSCs	Mesenchymal Stem Cells
MTT	3-(4,5-Dimethylthiazol-2-Yl)-2,5-Diphenyltetrazolium Bromide
NEAA	Non-Essential Amino Acids
NHS	National Health Service
PBS	Phosphate-Buffered Saline
PCL	Poly-Ɛ-Caprolactone
PLEC	Primary Porcine Lung Epithelial Cells
PLF	Primary Porcine Lung Fibroblasts
PSA	Penicillin/Streptomycin/Amphotericin B
RBC	Red Blood Cell
RI	ROCK Inhibitor
ROCK	Rho-Associated Protein Kinase
SABAs	Short-Acting B-Adrenergic Agonists
scRNA-seq	Small Conditional RNA Sequencing
SDC	Sodium Deoxycholate
ssDNA	Single Stranded DNA
TCP	Tissue Culture Plastic
TGF-B	Tissue Growth Factor-B
Th2	T-Helper Type 2
UK	United Kingdom
USA	United States Of America
VCL	Vapour Crosslinked

List of figures

List of tables

Schematics

Acknowledgements

I would like to thank my supervisors, Prof. Dr. Nicholas Forsyth for being there when most needed, his knowledge, support and guidance; Prof. Ying Yang for all the support, knowledge and home-like warmth she provided, along with gifted postdoctoral researcher Dr. Tina Dale and both supervisors' group members.

I am also deeply grateful to Keele University, ACORN funding, North Staffordshire Medical Institute, The Royal Society, Tongji University and EPSRC for Centre of Doctoral Training (CDT) in Regenerative Medicine, for allowing me to complete my laboratory research and travel to numerous conferences.

Many thanks go to my friends and colleagues at Guy Hilton Research Centre, Keele University, past and present, for being there at all times and creating a friendly atmosphere which made it a great place to come to work every day. Special thanks go to The Core group for allowing me being in their circle, to BiyololoMuh group, and to my high school friends who are virtually with me all the time.

Finally, I cannot thank my family enough; my wonderful husband Dr. Matt Köse-Dunn and our cat Luna. I could not have completed this work without his support, knowledge, love and spell checks.

Disclaimer

I declare that this is an original work and all sources of information are fully acknowledged and cited.

Chapter 1

Introduction

1.0 Introduction

The respiratory system is one of the most important functional systems in any mammal, used for gas exchange and to provide oxygen to the whole body. Anatomically, this system comprises of the upper and lower respiratory tract; where the upper includes the nasal cavity, pharynx and larynx, while the lower includes the trachea, bronchi and lungs (**Fig 1.1**).

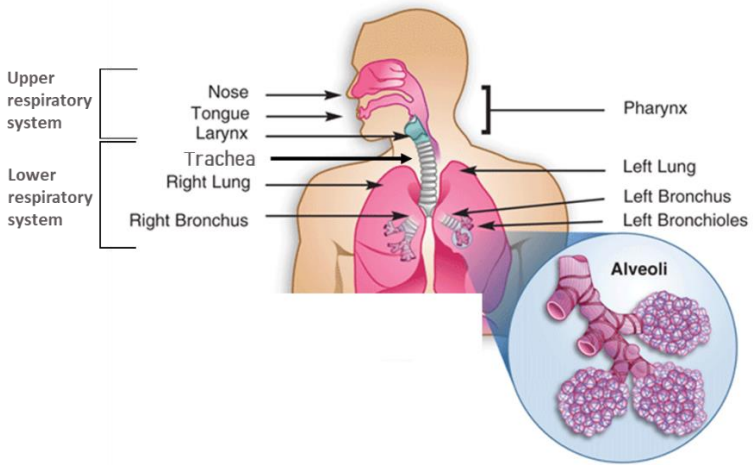

Figure 1.1: Upper and lower respiratory system. Respiratory system consists of two parts: upper and lower respiratory tracts. Upper respiratory tract includes the nose and nasal passages, the pharynx, tongue and the portion of the larynx. The lower respiratory tract includes the portion of the larynx trachea, both lungs bronchi and bronchioles.

The respiratory system starts with the nose, the nasal cavity is a large space in the nose and consists of two (right and left) parts (Harkema et al., 2016). Airflow starts from nose/mouth and carries to pharynx (throat), which is part of both respiratory and digestive systems as it carries both air and food. The bottom of the pharynx ends with the epiglottis; a small tissue that covers the trachea, protects it and allows air to reach the lungs. The larynx (commonly known as the voice box) is the last organ in the upper respiratory system, it is located in the

top part of the trachea, it helps breathing and protects the trachea against food aspiration (Herbert et al., 2018).

This project is concerned with the lower respiratory system, most notably the lungs, which are the primary respiratory organ of the human body. They receive deoxygenated blood from the heart and supply oxygenated blood to the body. The lungs are part of the lower respiratory system that begins with the trachea and leads to main bronchus, which then branches out into sequentially smaller airway structures. The main bronchus further branches into the lobar bronchus, segmental bronchus, subsegmental bronchus, conducting bronchiole, terminal bronchiole, respiratory bronchiole, alveolar duct, alveolar sac and alveolus ("Bronchial Anatomy: Overview, Gross Anatomy, Microscopic Anatomy," n.d.). The lung is not a static tissue, and has colour changes linked to age. In adults the lungs are mostly dark grey and patchily mottled (Lowery et al., 2013)..

Lung tissue can be affected by a number of diseases including cancer, pneumonia, asthma, and chronic obstructive pulmonary disease (COPD). Respiratory diseases in the UK represent an enormous financial burden, estimated to cost the UK £11.1 billion annually, a huge burden on the National Health Service (NHS), and being responsible for the loss of many lives. In the UK around 12 million people are affected by respiratory disease, of which 8 million are asthma, 1.2 million are COPD, and over 150,000 are interstitial lung diseases (such as pulmonary fibrosis). The UK has the fourth highest lung disease mortality rate in Europe, and there has been no marked improvement in the past 10 years(Burki, 2017).

Organ transplantation is still the main treatment for end stage respiratory disease patients. This option is, however, limited by the shortage of organ donors. While advances in surgical

technique have improved early survival, the long term median survival time after transplantation is only 6.5 years (Chambers et al., 2018).

Lungs are capable of regenerating and repairing themselves at the microscopic and cellular levels. Unfortunately, at the macroscopic level damage by degeneration, infection or surgically resected lung tissue cannot repair itself *in vivo*. Lung tissue engineering approaches can investigate whether lung tissue can be generated *in vitro* (Kotton and Morrisey, 2014). With lung tissue engineering it might be possible to grow lung cells, tissues or organs in *in vitro* conditions and then replace the damaged lung tissue, allowing the body to repair itself or to replace the damaged lung entirely (Rosenberg et al., 2017).

1.1 Lung Structure and Anatomy

In the human body the two lungs are located behind the rib cage, near the backbone on either side of heart, and are surrounded by the pleural membrane (Hsia et al., 2016). The pleural membrane consists of two layers of serous membrane which cover and protect each lung. The outer layer (parietal pleura) attaches the lungs to the wall of the thoracic cavity and the inner layer (visceral pleura) covers the lungs, with the thin space between the two pleural layers known as the pleural cavity and normally contains a small amount of pleural fluid (Charalampidis et al., 2015), as seen in **Figure 1.2**.

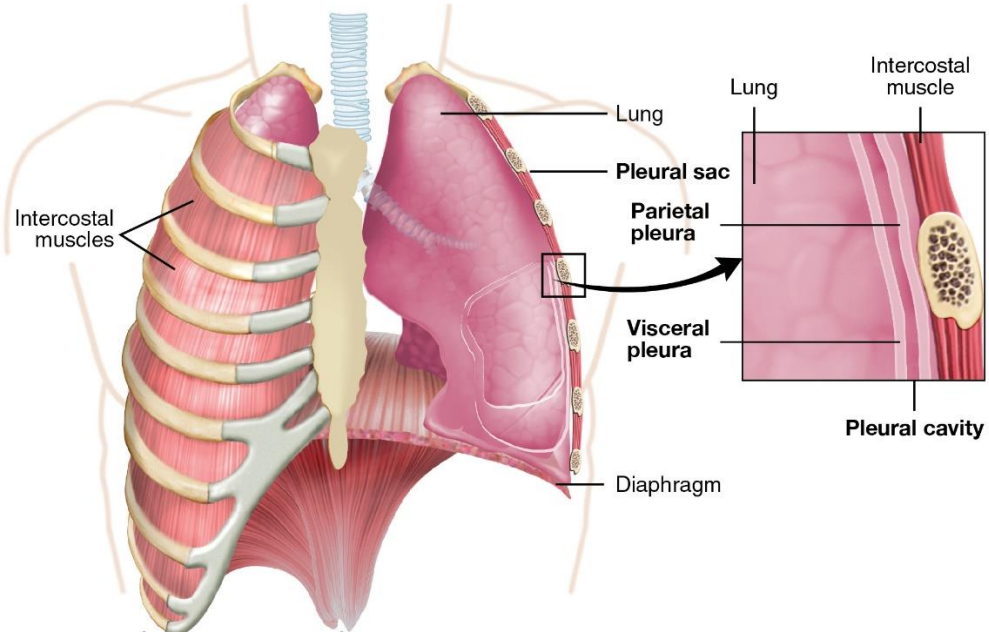

Figure 1.2: The lung and surrounding pleura. The lungs are shown under the ribcage and surrounded by the pleural sac. This sac consists of two layers of serous membrane: the outer parietal pleura and the inner visceral pleura, with the pleural cavity in-between. The diaphragm is also shown beneath the lungs (Image from Wikimedia Commons with Creative Commons Licence).

The muscles of respiration and the diaphragm act together to increase the intrathoracic volume, creating a negative pressure within the pleural space which surrounds the lung and causes expansion of the lung. The resultant reduction in intra-alveolar pressure prompts the conduction of air through the upper respiratory tract into the trachea and airways and then into the alveoli, where gaseous exchange occurs (Charalampidis et al., 2015). The process of breathing exposes the lung to noxious agents, including gases, dust particles, bacteria and viruses. The mucous barrier, mucociliary escalator (Bustamante-Marin and Ostrowski, 2017), branching pattern of the airways and the cough reflex (Dicpinigaitis, 2017) are all anatomical defences against these insults.

The respiratory system can be divided into a conducting zone and a respiratory zone (**Fig.1.3**). The conducting zone provides a route for incoming and outgoing air and consists of the trachea and bronchial tree. The trachea is formed by 16 to 20 stacked, C-shaped pieces of hyaline cartilage that are connected by dense connective tissue. The fibroelastic membrane allows the trachea to stretch and expand slightly during inhalation and exhalation, whereas the rings of cartilage provide structural support and prevent the trachea from collapsing. In addition, the trachealis muscle can be contracted to force air through the trachea during exhalation. The trachea branches into the right and left primary bronchi. The primary bronchi enter the lungs at the hilum. The hilum is a concave region where blood vessels, lymphatic vessels and nerves also enter the lungs. The bronchi continue to branch into the bronchial tree (respiratory tree). The bronchial tree is the collective term used for these multiple branched bronchi (Bizzintino *et al*., 2011).

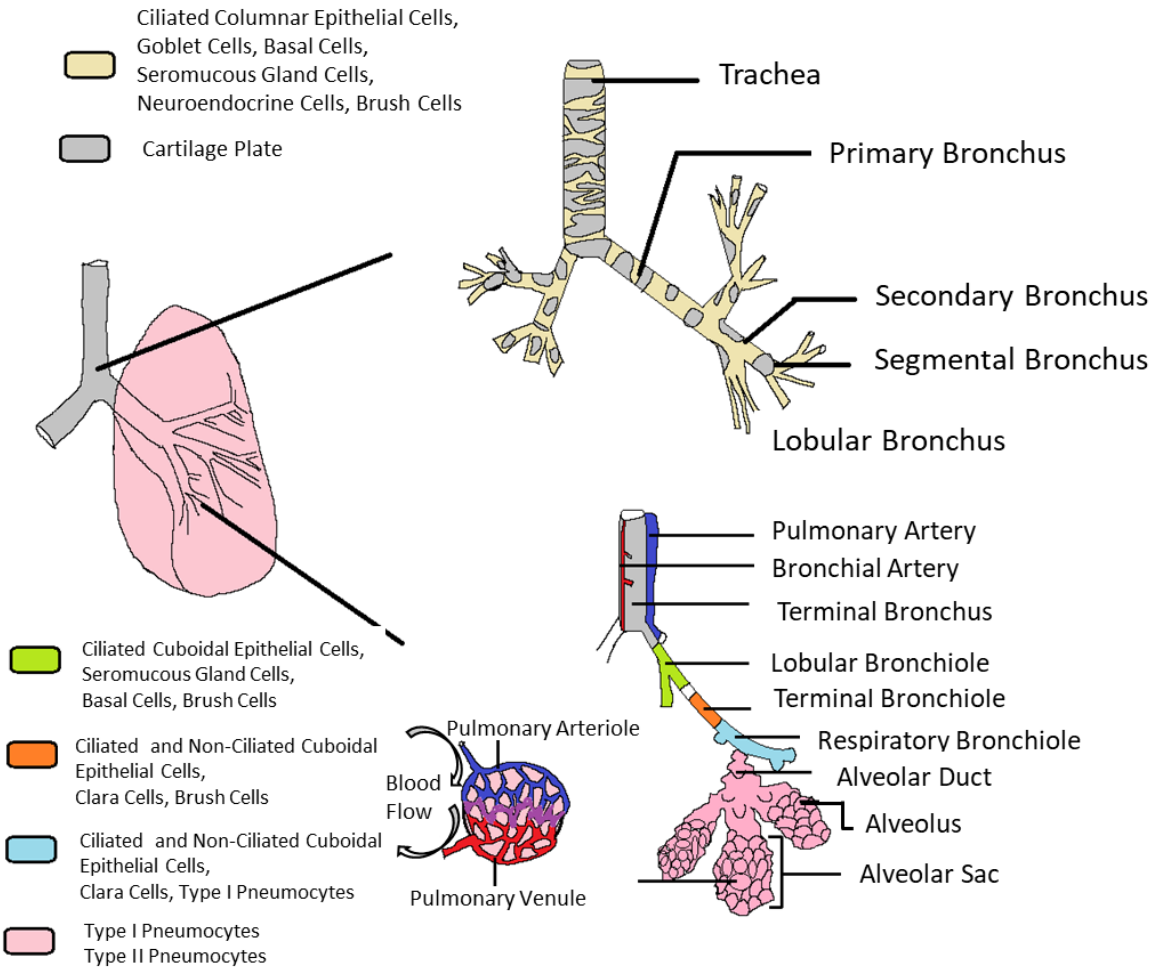

Figure 1.3: A diagram showing the lower respiratory system. The diagram features a lung (on the left) with two magnified inserts, the top insert showing the conducting zone and the lower insert showing the respiratory zone. The left hand lower insert shows deoxygenated (blue, pulmonary arteriole) and oxygenated (red, pulmonary venule) blood supply to a magnified single alveolus. The distribution of different cells is indicated by colour, with legends on the left.

The respiratory zone begins where the terminal bronchioles join a respiratory bronchiole (the smallest type of bronchiole), this zone includes structures that are directly involved in gas exchange. The terminal bronchioles are divided into respiratory bronchioles and these respiratory bronchioles subdivide into 2-11 alveolar ducts (atria). The area around each of the alveolar ducts contains numerous alveoli and alveolar sacs. An alveolus (singular, plural is alveoli) is a sphere lined with epithelium and supported by a thin elastic membrane. 90% of

the alveolar surface is covered by type I pneumocytes, these specialized epithelial cells are responsible for gas exchange. Type II pneumocytes are also present, and secrete a mixture of lipoproteins called surfactant. This fluid coats the inside of the respiratory membrane to reduce surface tension and help diffusion of the gas. Therefore, surfactant helps prevent the alveoli from collapsing or sticking shut as air moves (Rizzo, 2015).

1.1.1 Microstructure of Lung

Lungs have a complex microstructure with airways and alveolar sacs to make gas exchange possible (Hsia et al., 2016). Starting from the trachea, there are mucosa and submucosa layers (Brand-Saberi and Schäfer, 2014). The mucosa layer has a high number of mucus-secreting goblet cells and ciliated pseudostratified columnar epithelium on the basement membrane with a thin lamina propria. These contribute to the mucociliary elevator and keep foreign bodies out of the lungs. In thinner bronchi, there are less goblet cells and the epithelium become mainly ciliated with cuboidal cells.

1.1.2 Alveolar Microstructure

Alveoli are made up of numerous different cell types such as epithelial cells, fibroblasts, macrophages, vascular cells and fibroblastic mesenchymal cells (**Fig 1.4**), as well as complex microstructural niches, all highly designed in order to best allow for gas exchange.

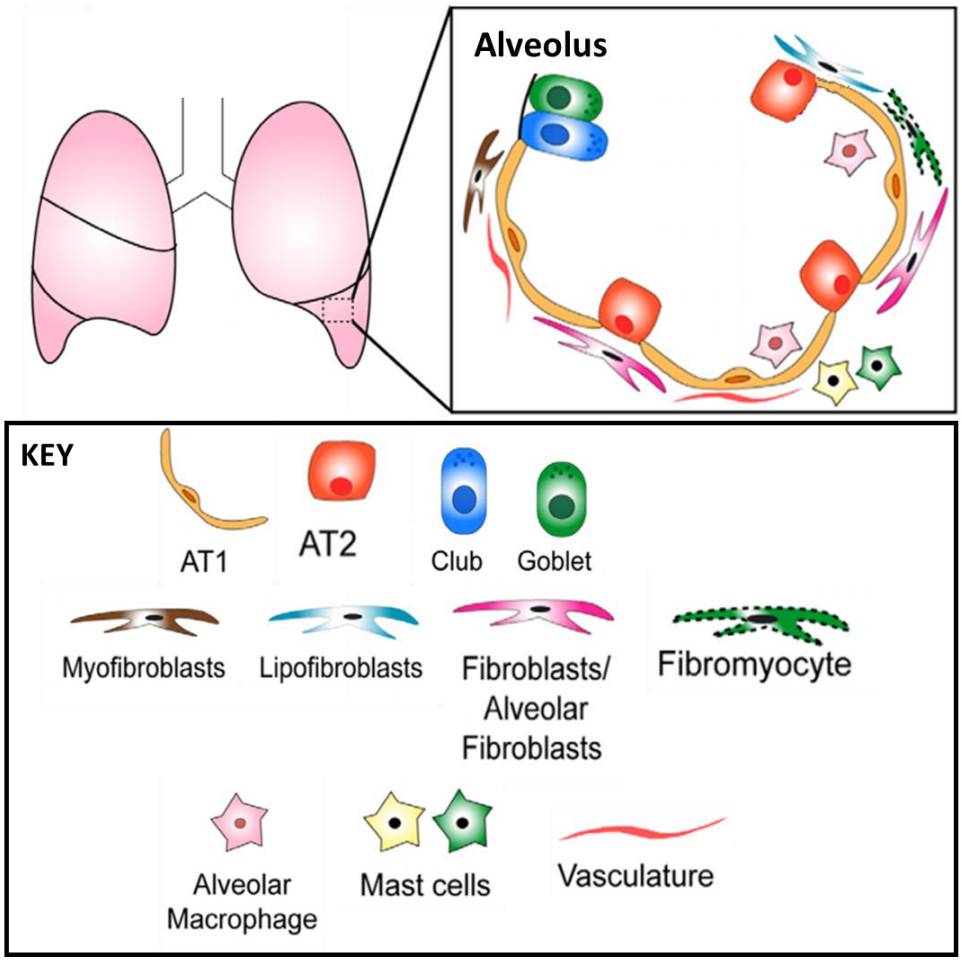

Figure 1.4: The cellular structure of an alveolus. There are two main types of epithelial cells in alveoli: the gas exchanging AT1 (pneumocyte alveolar type 1) and surfactant producing AT2 (pneumocyte alveolar type 2). There are alveolar macrophages in the alveolar space and two populations of mast cells. Fibroblast heterogeneity also exists in alveoli as mesenchymal cells: lipofibroblasts, myofibroblasts, fibromyocytes, and alveolar fibroblasts. (Adapted from Evans et al., 2020).

1.1.2.1 Epithelial cells

Alveoli are mainly made up of two types of epithelial cells: pneumocytes type I and type II, also known as alveolar type I (AT1) and alveolar type II (AT2) cells. (Evans and Lee, 2020). AT1s are thin flat cells that cover ~95% of the alveolar surface area, allowing for optimal gas exchange. There are nearly twice as many AT2s as AT1s, but AT2s only cover ~5% of the alveolar surface area due to their cuboidal morphology (Chen and Liu, 2020). Both AT1 and 2

cells are derived from multipotent alveolar progenitor cells during lung development (Barkauskas et al., 2017; Zacharias et al., 2018).

AT2 cells have a number of important characteristics: AT2s can differentiate into AT1s, secrete surfactant proteins, transport sodium ions and alveolar fluid, and play an important role in the lung immune response (Lee et al., 2018).

AT2 cells have been shown to exist in the lung as a heterogeneous population, with specific subgroups of AT2 acting as adult tissue stem cells, having a role in repair and regeneration (Zacharias et al., 2018). Under normal physiological conditions, only ∼1% of AT2 cells displayed this progenitor function, producing both AT1 cells through differentiation and AT2 cells through self-renewal (Chen and Liu, 2020; Desai et al., 2014). However, when under pathological conditions or after lung injury, AT2 cells can be recruited and enter the progenitor state depending on the type and extent of the injury. In one study, injury induced by *P. aeruginosa* resulted in 30-70% of AT2 cells expressing stem cell antigen 1 markers in repair phase (Liu et al., 2015). This shows that AT2 cells in the lung are a dynamic and responsive cell population with an important role in repair.

Another vital role of AT2 cells is the synthesis, storage and secretion of the various components of pulmonary surfactant. Surfactant is composed of about 90% lipid (mainly phospholipids) and 10% proteins, most significantly the surfactant proteins (SP) A, B, C and D. Most surfactant components are assembled and stored within AT2 organelles known as lamellar bodies (Knudsen and Ochs, 2018a). Surfactant is recycled by AT2 cells or degraded by alveolar macrophages, but can also move into the upper airways and mucociliary escalator, facilitating lower airway clearance (Watson et al., 2019).

Surfactant is vital for the mechanical stability of the alveoli, allowing for expansion and contraction of alveoli without collapse, as alveoli have a tendency to collapse due to their spherical shape, small size and the contribution of water vapor to surface tension. Surfactant helps to lower surface tension thus preventing collapse (Nkadi et al., 2010).

As well as having a role in mechanical stability, surfactant has further roles in the immune response, specifically SPA and SPD. These two surfactant proteins are hydrophilic calcium-dependent lectins, also termed collectins. SPA and SPD bind to and aggregate pathogens (bacteria, fungi, viruses) and other small foreign substances such as pollen and nanoparticles, having both a bactericidal role (Watson et al., 2019) and recruiting alveolar macrophages to enhance pathogen uptake (Carreto-Binaghi et al., 2016). SPA and SPD also bind to and promote the clearance of apoptotic cells, as well as having immunomodulatory effects on dendritic cells and T cells (Watson et al., 2019).

Alongside the production of surfactant proteins, AT2 cells have further roles in innate local immunity. The lungs are constantly assaulted by inhaled particulates, toxins and microorganisms, despite this the lung doesn't typically exhibit chronic inflammation. This is due to innate immunity provided by AT2 cells (and potentially AT1 cells). AT2 cells secrete a wide variety of anti-inflammatory and antimicrobial substances other than SPA and SPD, including lysozymes, beta defensins, cathelicidin, lipocalin 2, antioxidants such as glutathione, and components of the complement system (Mason, 2006; Nkadi et al., 2009; Qian et al., 2013; Stegemann-Koniszewski et al., 2016). This variety of antimicrobial substances in the alveolar fluid allows the lung to deal with inhaled substances throughout normal function.

Upon infection, AT2 cells markedly enhance the lung defences and increase production and secretion of protective substances. Additional substances are also produced, including

chemokines and cytokines (such as interleukin (IL) β, Ilα, IL-6, and tumour necrosis factor (TNF)). Thanks to expression of toll-like receptors (TLRs), AT2 cells can recognise Gram-positive/negative bacteria as well as some viruses, with secretion changing to adapt to the infection (viral infections also involve secretion of IL-8 and some type I interferons). This indicates that AT2 cells have a role in adaptive immunity and may even stimulate the adaptive immune response (Mason, 2006; Nkadi et al., 2009; Qian et al., 2013; Stegemann-Koniszewski et al., 2016).

Due to the clear importance of AT2 cells in the alveolar microenvironment, they are an important cell type for study. However, there remain inabilities to culture and maintain primary AT2 cells in a well differentiated state, and cell lines (such as A549 lung epithelial cells) fail to reproduce all of the morphological, functional, molecular and genetic markers of AT2 cells (Beers and Moodley, 2017). A potential avenue for AT2 cell study is stem cell biology and reprogrammed progenitors.

Research has shown that AT2 cells can behave like stem cells in either 2D cultures of human AT2s cells or 3D lung organoid culture, and these cells can self-renew and differentiate into AT1 cells (Barkauskas et al., 2017; Fuchs et al., 2003). In addition, AT2 cells have an improved proliferation and re-differentiation capacity to AT1 cells when cultured in cell-derived organoid cultures (Zacharias et al., 2018).

1.1.2.2 Fibroblasts

There are a diverse range of fibroblast phenotypes in the alveoli, including alveolar fibroblasts, lipofibroblasts, and myofibroblasts, with the lung displaying regional heterogeneity (Evans and Lee, 2020; Kotaru et al., 2006). Lipofibroblasts are lipid-enriched interstitial fibroblasts with an important role in lung development, homeostasis and repair

(Rehan and Torday, 2014). Myofibroblasts are not typically present in adult lung tissue, but instead arise during injury repair processes through expression of smooth muscle actin in typical fibroblasts resulting in specialisation (Phan, 2012). The remainder are alveolar fibroblasts (Evans and Lee, 2020; C. Wang et al., 2018).

Fibroblasts in the alveoli have several important roles: producing and regulating lung extracellular matrix (ECM) components, serving as effector cells during injury repair, and regulating interstitial fluid volume/pressure. Typically, lung fibroblasts reside within the ECM in the interstitial space until they are required for wound repair or there are changes in ECM quality (White, 2015).

Fibroblasts and myofibroblasts are the main producers of ECM components (Bonnans et al., 2014), with the ECM being is a dynamic and complex structure composed of fibrous proteins, glycoproteins and proteoglycans that makes up the noncellular parts of tissues in the body. In the lung the ECM is found in two main areas, the basement membranes (thin layers of ECM under epithelial and endothelial cell layers, surrounding muscle, fat and nerves) and the interstitial spaces (meshwork that connects structural cell types within tissues, maintaining 3D structure, where the majority of fibroblasts reside and produce additional ECM) (White, 2015).

Interstitial ECM of the alveoli is composed of type I and III collagen and elastin, along with glycosaminoglycans, fibronectin, and proteoglycans, formed into a relaxed meshwork to allow for expansion and contraction (Burgstaller et al., 2017). As well as collagen I and III, lung ECM also contains types IV and V, with the former being a key component of the basement membrane. Elastin is responsible for the elastic recoil in lung tissue and the ability to respire, and is highly flexible and resilient to allow for ventilation throughout life. Proteoglycans are

scattered throughout the ECM, can store water and biochemical factors, and assist with cellular movement. Fibronectin is essential for cell adhesion to the ECM, affecting cell morphology, motility, and differentiation, while also having a role in ECM remodelling. These components of the ECM are vital for continued respiration, with loss or damage to any component potentially leading to lung dysfunction (Balestrini and Niklason, 2015).

An important characteristic of the ECM is the stiffness, as there is constant stress and strain in the alveoli due to expansion and contraction during the respiratory cycle. The composition and biomechanical properties of lung ECM can affect its stiffness and consequently the stiffness of the lung and the ability to respire. Throughout the lung, ECM has different stiffness depending on the local microenvironment, with alveolar wall ECM differing in stiffness to airway wall and airway epithelium ECM. (White, 2015). ECM stiffness can change due to aging and disease, with ECM stiffness being increased with fibrotic disorders (Liu et al., 2010) and decreased with conditions such as emphysema (Parameswaran et al., 2011). A stiffer ECM promotes profibrotic behaviour in fibroblasts, including myofibroblast differentiation and additional ECM production, due to the way that fibroblasts prefer to adhere and proliferate on stiffer ECM surfaces (White, 2015).

Due to the importance of ECM for lung structure and function, it has been the subject of study across numerous organs. However, every organ has a unique ECM containing hundreds of proteins and other components (known as the matrisome), with identification and study of ECM components often presenting a challenge due to the need to remove all cellular and nuclear material from a tissue sample in order to isolate the ECM remainder. These decellularization techniques can affect the ECM, resulting in samples being damaged and changes in matrix stiffness, so choice of technique is important (Melo et al., 2014).

1.1.2.3 Macrophages

Macrophages are one of the most abundant immune cell types present in the lung under normal conditions, ready to act to defend the lungs from toxins, particulates and microorganisms inhaled from the outside world. At least two macrophage populations exist in the lung, namely alveolar macrophages (AMs) and interstitial macrophages (IMs), each with their own distinct locations, properties, functions, and integrin expression patterns (CD11c expression is high and CD11b expression is low in AMs, vice versa in IMs) (Byrne et al., 2015; Hussell and Bell, 2014; Schyns et al., 2018).

AMs are located in the airway lumen and on the epithelial surface of the alveoli, making up 90-95% of the cellular content in the alveoli under normal conditions (Morales-Nebreda et al., 2015). They have a role in host defence and are generally suppressive, acting against pathogens, removing apoptotic cells, and remove waste material from the epithelium such as inhaled particles small enough to reach the alveoli (Allard et al., 2018). This is done via high phagocytic ability, as well as secretion of antimicrobials, nitrous oxide, TNF-α and interferon (Byrne et al., 2015). Maintenance of lung microstructure is vital with even minor structural or functional changes serving as indicators for lung disease (Guilliams et al., 2013). IMs are located in the lung parenchyma and have a more regulatory function, maintaining lung homeostatic, preventing immune-mediated allergic airway inflammation, (Schyns et al., 2018) releasing specific cytokines associated with the adaptive immune response, such as interleukin-10 (Byrne et al., 2015)

Macrophage phenotypes are highly diverse, forming a continuum of activation states depending on the microenvironment and infection status. Whether AMs display certain phenotypes depends on the tissue environment, but generally alveolar macrophages can be

a challenge to characterise as the exist in a complex and unique environment (Hussell and Bell, 2014). AMs are generally anti-inflammatory through phagocytosis of apoptotic cells, but can also produce inflammatory cytokines in response to danger. In addition, some AMs are derived from circulating monocytes recruited from bone marrow, and some AMs are resident in the alveolus. Overall, a number of mechanisms surrounding AMs require further study, but they remain a vital part of the alveoli microstructure (Allard et al., 2018).

1.1.2.4 Mast cells

Mast cells are multifunctional immune cells found across many different tissues but are highly concentrated in the airways as these are exposed to foreign substances and toxins from the outside world (Erjefält, 2014). Mast cells can both excite and inhibit inflammatory responses (Metz et al., 2007) and have an important role in the immunopathology of a number of respiratory diseases, including COPD (Ballarin et al., 2012).

Mast cells can also be involved in allergy, where surface IgE cross-linking leads to degranulation, release of histamine/other mediators, and an acute allergic response, such as airway closing. This is then followed by production of prostaglandins and release of cytokines, resulting in chronic inflammation and the late phase reaction (Erjefält, 2014). In addition, mast cells also detect infection and have a role in defence, again important for COPD where respiratory infections are a major cause of exacerbation (Sethi, 2010).

Mast cells exist as a number of subtypes, classically connective (MCTC) and mucosal (MCT) mast cells. However, there are further subpopulations in different tissues, including alveoli. Alveolar MCT and MCTCs differ from other lung mast cells populations (including bronchi and small airways) in expression of mast cell related molecules, potentially to prevent anaphylactic degranulation (Andersson et al., 2009). Mast cells have a key role in asthma

through expression of the high-affinity IgE receptor FceRI, however, alveolar mast cells are characterized by low FceRI expression (Andersson et al., 2011).

1.1.2.5 Club cells

Club cells are cubical cells that do not have cilia and do not secrete mucus, also known as bronchiolar cells. These cells mainly secrete uteroglobin/blastokinin and a number of substances that provide protection for surfactant and small airways, serve as progenitor cells for both themselves and ciliated cells, and can protect the airways from harmful/toxic compounds inhaled into the lungs (Rokicki et al., 2016).

1.1.2.7 Goblet cells

The main function of goblet cells is the production and secretion of mucus, which serves as a barrier to prevent water loss and to remove inhaled foreign substances from the lung. The major components of mucus are mucin glycoproteins, of which over 20 types exist (Ma et al., 2018). Changes in the number of goblet cells are typically a feature of lung disease, with an increased number of goblet cells found in COPD (Kim et al., 2015) and asthma, and a decreased number in cystic fibrosis (Ma et al., 2018)

1.1.2.8 Pores of Kohn

Interalveolar pores, termed pores of Kohn, are small channels between alveoli lined by epithelium (typically AT2 cells), which cross interalveolar septa to link adjacent alveolar airspaces, as seen in **Fig. 1.5**. Humans have up to seven pores per alveolus, ranging in size from 2-13 μm. There are several theorised roles for the pores of Kohn, such as collateral ventilation. The interalveolar pores of Kohn (**Fig.1.5A**), along with bronchoalveolar Lambert's channels (**Fig.1.5B**) and interbronchiolar Martin's channels (**Fig.1.5C**), all serve as collateral ventilation pathways that can bypass standard ventilation (Terry and Traystman, 2016).

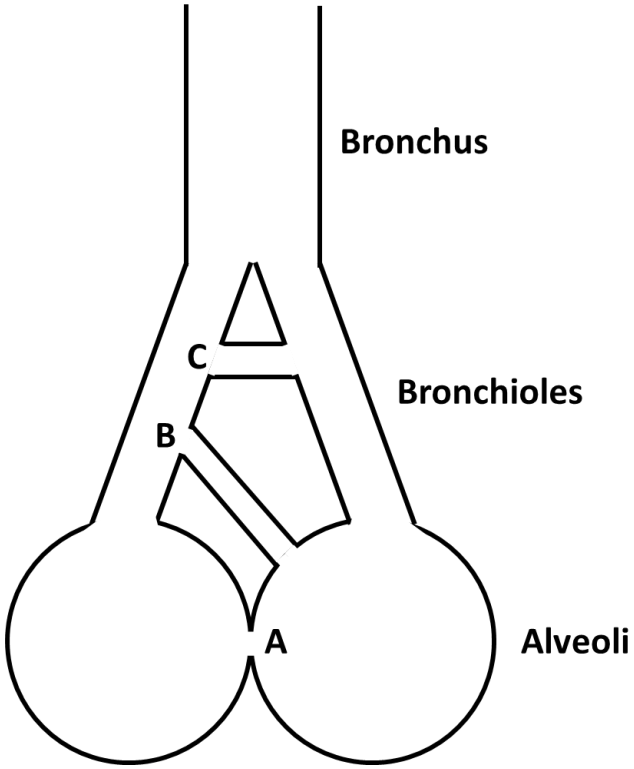

Figure 1.5: Collateral ventilation pathways of the bronchioles and alveoli. A) interalveolar pores of Kohn (3-13 µm diameter), B) bronchoalveolar Lambert's channels (120 µm diameter), C) interbronchiolar Martin's channels (30 µm diameter). Adapted from (Terry and Traystman, 2016).

Pores of Kohn develop at around 4 years of age, and collateral ventilation in general may increase with age due to potential enlargement of the various collateral channels. This collateral ventilation is also affected by diseases such as COPD and asthma, as well as the composition of inhaled gases (Terry and Traystman, 2016).

Other potential roles for the pores of Kohn are: sustaining the flow of air in the event of blockage of one of the alveolar ducts; provide routes of migration for alveolar macrophages or other cells, acting as surfactant-filled reservoir connections between alveoli, and are likely the structures that erode during the early stages of emphysema (Oldham and Moss, 2019).

1.2 Lung Diseases

Lung disease refers to disorders that affect the lungs and lead to respiratory distress. Breathing problems caused by lung disease may prevent the body from getting enough oxygen. Asthma, chronic obstructive pulmonary disease (COPD), lung cancer, lower respiratory tract infections, pulmonary fibrosis, and infections such as tuberculosis (TB), influenza, and pneumonia are all examples of lung diseases (Robinson, 2016).

Lung diseases are some of the most common medical conditions in the world, with more than 1 billion people worldwide suffering from acute or chronic respiratory conditions (European Respiratory Society, 2017). These lung diseases represent an immense worldwide health burden, with an estimated 334 million cases of asthma (Global Asthma Report 2014), and 200 million cases of COPD (65 million of moderate to severe) (Burney et al., 2015). In terms of mortality, lung diseases make up five of the 30 most common causes of death: COPD is third, lower respiratory tract infection fourth, lung cancers sixth, TB twelfth, and asthma twenty-eighth (GDB Mortality Collaborators, 2016).

The United Kingdom is an outlier in terms of lung disease, with higher mortality and morbidity than other western countries, potentially due to smoking, pollution, or delivery of healthcare (Salciccioli et al., 2018). The most common lung diseases in the UK are asthma and COPD, with the latter affecting 4.5% of all people aged over 40 and being the fifth most common cause of death (nearly 30,000 deaths every year) (NICE Guidelines: COPD 2018). Due to their common prevalence in the population and/or impact on the NHS, lung cancer, asthma and COPD are discussed in more detail.

1.2.1 Lung cancer

Lung cancer is a disease in which abnormal (malignant) lung cells multiply and grow uncontrollably. These cancerous cells can invade nearby tissues and potentially spread to other parts of the body (metastasize). The two major kinds of lung cancer are named for the way the cells look under a microscope (Herbst et al., 2008). These are small-cell lung cancer and non-small lung cancer (**Fig 1.6**), with small-cell lung cancer tending to behave more aggressively. Non-small cell lung cancer describes several types of lung cancers that act in a similar way and generally spread more slowly (benign) than small cell lung cancer, this category includes adenocarcinomas, squamous cell carcinomas and large-cell carcinomas.

Another distinction to be made with lung cancers is describing where the cancer originated: when cancer starts in the lungs and is unrelated to previous cancers (and the tumour contains lung cancer cells), it is known as primary lung cancer. If the cancer has spread to the lung from another part of the body, and the tumour contains cancer cells from that area, it is known as secondary lung cancer.

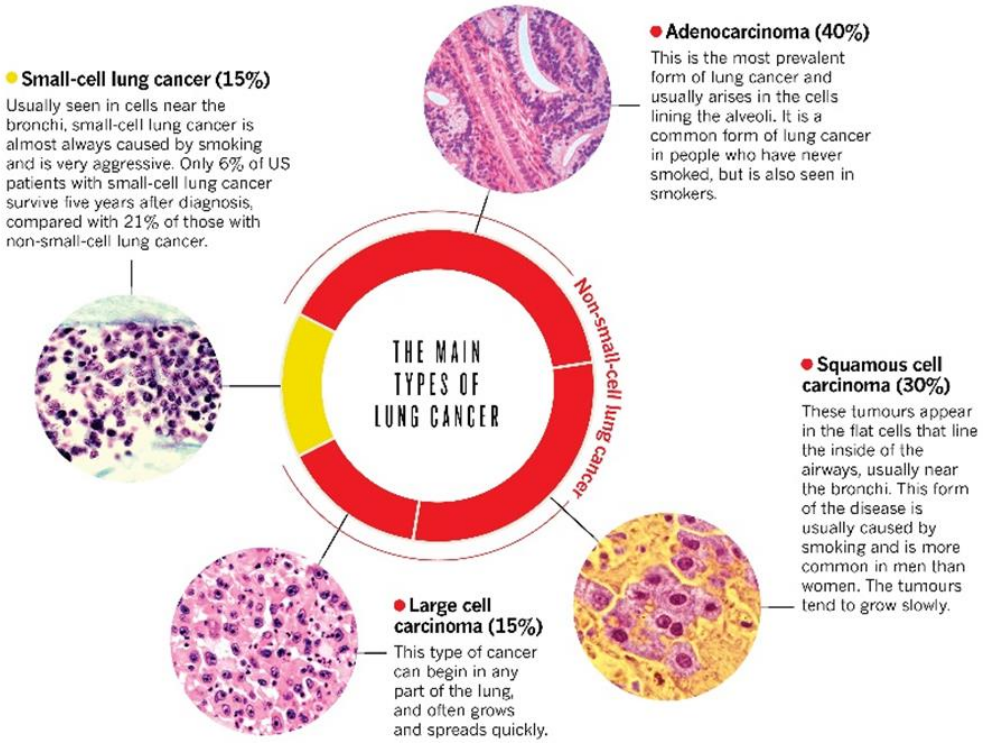

Figure 1.6: Difference between lung cancer types. Non-small cell lung cancer can be large carcinoma, squamous cell carcinoma, or adenocarcinoma. Most common non-small cell lung cancer type is adenocarcinoma (%40). Small cell lung cancer is the 15% of the all lung cancers.

Treatments depend on the type of lung cancer, where the cancer is and if it has spread to other parts of the body, age of the patient, and overall health (Hirsch et al., 2017). Surgery is the standard approach to remove the lung tissue that has the cancerous tumour. Frequently this can require removal of a large proportion of a lung including complete removal. Where cancer spread has yet to occur, surgical removal can be sufficient to cure the patient. Alternative approaches include radiation therapy where high-energy X-rays are focused onto the tumour. The energy from the x-rays can be enough to induce cancer cell death helping relieve pain and improving overall quality of life. Chemotherapy utilises medicinal approaches to kill cancer cells where delivery can be either intravenous or orally (von Dincklage *et al.*, 2013).

1.2.2 Asthma

Asthma is characterised by chronic inflammation of the airways, with a history of respiratory symptoms that vary in intensity over time: cough, tightness in chest, wheezing, and shortness of breath. Asthma is a heterogenous condition, including allergic, non-allergic and late-onset phenotypes (Global Initiative for Asthma 2020; Rehman et al., 2018, Martinez 2007).

Asthma is caused by a combination of complex genetic and environmental factors that is not fully understood. Environmental risk factors for asthma include: tobacco (including second hand smoke), pollution (particulates, nitrogen dioxide), obesity, occupation, microbes and stress (Toskala and Kennedy, 2015). Banning smoking in public areas was linked with a reduction in the rate of respiratory diseases and asthma symptoms in Scotland (Mackay et al., 2010).

Genetically, over 600 candidate genes have been identified, with genome-wide association studies (GWASs) used to further explore the genome. More recently, epigenetic studies have also been performed, but overall direct causative mechanisms of asthma remain mostly unknown (Toskala and Kennedy, 2015).

Asthma is part of the atopic triad along with eczema and allergies, with some patients progressing through life from eczema to asthma to allergic rhinitis. These conditions are closely related, with up to 80% of children with eczema also having asthma or allergies to pollen, mould, certain foods or dust mite proteins (Belgrave et al., 2015). Allergic reactions to these allergens can trigger asthma, other triggers including viral infection, air pollution, exercise, and physical/emotional stress (Rehman et al., 2018). In asthma the walls of the bronchial tubes become inflamed and hypersensitive. During the asthmatic reaction the airways constrict, limiting the flow of air into and out of the lungs and creating difficulties in

breathing, resulting in the asthma symptoms of wheezing, coughing, and tightness of the chest. These symptoms are generally reversible with treatment but some patients show poor reversibility and these make the definition of asthma incomplete (Patel and Teach, 2019).

The inflammation in the lower airway in asthma is type 2 (chronic) inflammation, named for the type 2 T helper (Th2) lymphocyte (Lambrecht and Hammad, 2013). Asthma exacerbations have an early phase and a late phase, with the former initiated by IgE antibodies that respond to environmental triggers. The IgE then binds to mast cells and basophils, with the mast cells degranulating and releasing cytokines, histamine, prostaglandins and leukotrienes, which lead to smooth muscle contraction, excess mucus production (due to goblet cell metaplasia), and airway tightening. In addition, Th2 cells release interleukins (IL) 4, 5 and 13, which sustains inflammation, activates eosinophils and is attributed to remodelling and fibrosis (Sinyor and Concepcion Perez, 2020).

The late phase involves infiltration of eosinophils, basophils, neutrophils, macrophages and helper/memory T-cells into the airway, simulated by the chemoattractants from mast cells. These newcomers result in bronchoconstriction and further inflammation. Eosinophils in particular have a significant role, causing airway epithelial cell damage/death, dysfunction of airway cholinergic nerve receptors, airway hyperresponsiveness, mucus hypersecretion and airway remodelling through fibrosis and collagen deposition (Possa et al., 2013). While active, eosinophils release leukotrienes (similarly to mast cells), which acts as a potent bronchoconstrictor and causes more eosinophils to migrate to the airways (Possa et al., 2013)

Sustained epithelial injury in asthma can lead to airway remodelling (**Fig.1.7**), where epithelial cells transition to mesenchymal cells, resulting in an increase in smooth muscle content in the airway. Eosinophils also have a role, by interacting with mast cells and causing release of TGF-

B and cytokines. These remodelling mechanisms may worsen inflammation and aggravate asthma over time (Holgate, 2013).

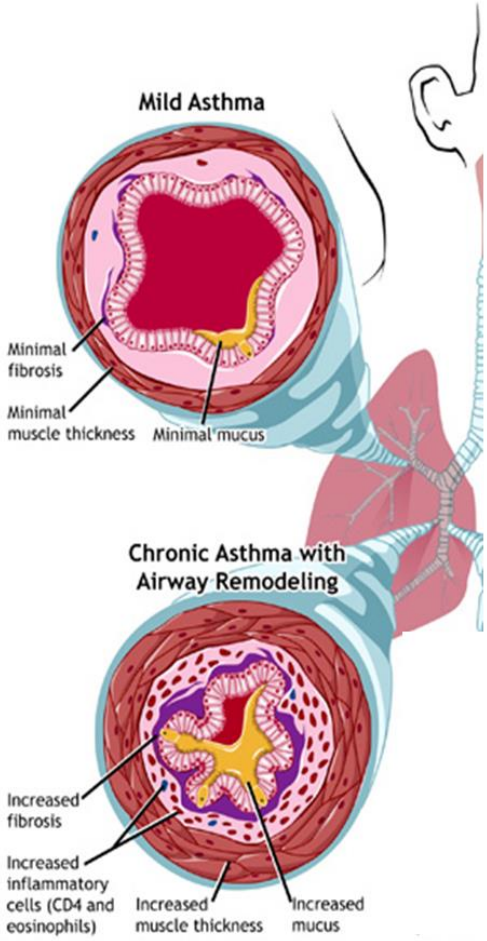

Figure 1.7: A schematic of asthma. Mild asthma causes a minimal level of fibrosis, muscle thickening and mucus build up in the airways. Chronic asthma causes increased levels of fibrosis, muscle thickening and mucus build up, as well as increased inflammatory cells (CD4 and eosinophils). Image adapted from NIH NIAID 'Asthma: Mild and Chronic.

1.3 Chronic obstructive pulmonary disease (COPD)

Respiratory diseases are a global critical health issue and the third leading cause of death in the UK and the United States of America (USA) (Gotts and Matthay, 2013). As of 2012, COPD

was the fourth-ranked cause of death worldwide, affecting female and male patients equally (Lozano et al., 2012).

The global initiative for COPD (GOLD) has defined COPD as “a common preventable and treatable disease characterised by persistent and progressive airflow limitation, associated with an enhanced chronic inflammatory response in the airways and lung to toxins or gases. Exacerbations and comorbities contribute to overall severity in individual patients.” (GOLD 2020).

COPD comprises numerous disease processes, including: airway thickening/narrowing that obstructs expiratory outflow; chronic mucus hypersecretion leading to chronic cough, excess phlegm production and chronic bronchitis; and emphysema, where distal airspaces are abnormally dilated and there is destruction of alveolar walls. (Forey et al., 2011) Chronic bronchitis and emphysema often occur together, and COPD presents a number of different clinical phenotypes, with differences in age of onset and frequency of exacerbations (**Fig 1.8**). (Central, 2012; Qureshi et al., 2014).

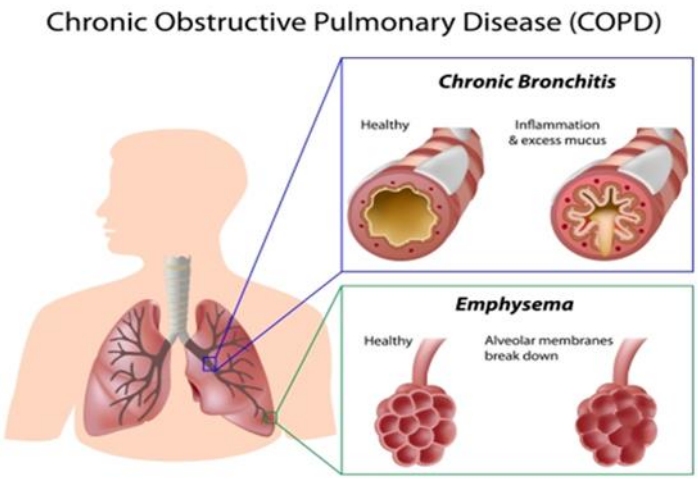

Figure 1.8: COPD: chronic bronchitis and emphysema. The difference between healthy and unhealthy tissue can be seen in the image., with chronic bronchitis presenting thickened inflamed airways, while emphysema presents destruction of alveolar airway membranes (Image from Alila Medical Media).

1.3.1 Risk factors for COPD: Environmental

Tobacco smoking is the main environmental risk factor for COPD, as shown by meta-analysis studies (Forey et al., 2011), but the pathogenesis remains unclear. Some studies have demonstrated that non-smokers may also develop COPD and an estimated 20-40% of COPD patients have never smoked tobacco (Kohansal et al., 2009). Second-hand smoking and population-attributable effects of smoking should also be considered (Vijayan, 2013).

Other environmental risk factors include both indoor and outdoor air pollution. Indoor pollution includes particulates, biomass smoke exposure, nitrogen dioxide, carbon monoxide, volatile organic compounds and biological allergens (Hu et al., 2010; Vijayan, 2013). Outdoor pollution includes ambient air pollution and pollutants from motor vehicles and industrial factories (Ko and Hui, 2012; (Salvi and Barnes, 2009).

In addition to pollutants, further COPD risk factors include exposure to dusts and fumes (including occupational risk), previous cases of tuberculosis, maternal smoking, as well as childhood conditions such as respiratory infections or asthma (Decramer et al., 2012).

Despite continued recent anti-smoking efforts in Western countries, the burden of COPD is going to increase in the future due to increased exposure to environmental risk factors. The global population is both increasing and aging, traffic density continues to rise, and certain developing countries and Asia still have high rates of air pollution and smoking (López-Campos et al., 2016).

1.3.2 Risk factors for COPD: Genetic

COPD also has complex genetic risk factors, which are likely to interact with environmental factors responsible for the disease. A severe deficiency in alpla1-antitrypsin (AAT) is one of the first proven and most established genetic risk factors, being responsible for around 1-2% of COPD cases (Silverman, 2020; Vijayan, 2013). AAT is mainly produced in the liver and acts as a plasma protease inhibitor of leukocyte elastase, an enzyme found in neutrophil granules. AAT is encoded by the *SERPINA1* gene (M allele) under normal conditions, but a mutation in *SERPINA1* (specifically a single base pair change leading to amino acid substitution) results in the Z allele, this mutant AAT polymerises in liver hepatocytes and leads to a reduction in the levels of circulating AAT. This substantially increases the risk for COPD as well as liver disease and is heritable, with 1 in 3000 people in the USA inheriting severe AAT deficiency (Silverman, 2020).

Further genetic risk factors have more recently been identified by genome-wide association studies (GWAS). The first GWAS of COPD identified the *CHRNA3/CHRNA5/IREB2* region on chromosome 15q25 as involved in COPD susceptibility (Pillai et al., 2009), with subsequent

studies identifying *HHIP* (Wilk et al., 2009), *FAM13A* (Hancock et al., 2010)*, RIN3, MMP12* and *TGFB2* (Cho et al., 2014). A number of interesting findings have emerged from COPD GWAS, such as: some genomic regions are also associated with fibrosis but in the inverse, where the risk allele for COPD protects from fibrosis, and vice versa; and that genetic determinants of COPD and lung function have a substantial overlap These insights give important clues, as well as identifying areas and targets for future study, but much of the heritability for COPD remains unexplained (Silverman, 2020).

1.3.3 Clinical features of COPD

COPD symptoms include breathlessness (dyspnoea), chronic cough, sputum production, low exercise capacity, wheezing, and long-lasting/more frequent bronchial infection. If one or more of these symptoms manifest and there are risk factors present (such as tobacco smoking), COPD is typically suspected. However, the early stages of COPD can be asymptomatic and often misdiagnosed, or COPD can be diagnosed at a late stage (Burkhardt and Pankow, 2014). Separating COPD patients based on clinical characteristics is difficult due to the wide range of phenotypes, age of onset, rate of progression and overlap with similar diseases such as asthma (Castaldi et al., 2014)

Breathlessness is often the most concerning early COPD symptom as it is persistent and progressive, worsening with physical exertion. The severity of breathlessness can be measured by the Medical Research Council breathlessness scale (Stenton, 2008), which ranges from Grade 1 (Not troubled by breathlessness except on strenuous exercise) to Grade 5 (Too breathless to leave the house, or breathless when undressing) and can be used to predict COPD mortality.

Chronic cough is one of the earliest COPD symptoms and can be productive or unproductive. The cough becomes more frequent as the disease progresses, but is often dismissed by patients as a sign of aging or lack of physical fitness (Putcha et al., 2014).

When mucus is expelled from the respiratory system, typically coughed up, it is referred to as phlegm or sputum. COPD patients typically produce excess sputum, if it is produced regularly in three or more months over two consecutive years it defines the presence of chronic bronchitis. However, this particular symptom in COPD typically varies in terms of quantity, colour and differing patient habits (as some patients will swallow the sputum), but a change in colour or volume is a sign of COPD exacerbation ("Global Initiative for Chronic Obstructive Lung Disease," 2020).

1.3.3.1 COPD diagnosis

A COPD diagnosis is considered when patients have one or more of the symptoms mentioned above, as well as a risk factor (typically smoking) and are over the age of 35 (NICE COPD Overview, 2010). The medical history and previous exposure to risk factors are also considered. At the time of diagnosis, airflow is typically measured with spirometry to obtain the following measures: FEV_1 (forced expiratory volume, the volume of air the patient can expel in the first second), and FVC (forced vital capacity, the total volume of air the patient can expel in one breath). Both FEV_1 and FVC are expressed as litres and as a percentage of the predicted value. If FEV_1/FVC is less than 0.7 it confirms the presence of COPD. The FEV_1 percentage value can then be used to further categorise the severity of COPD: >80% is GOLD stage 1/mild, 50-79% is GOLD stage 2/moderate, 30-49% is GOLD stage 3/severe, and <30% is GOLD stage 4/very severe (Burkhardt and Pankow, 2014).

The FEV_1 value is also part of the BODE index, measured with the Body mass index, Obstruction (using FEV_1 value), Dyspnoea (using MRC scale) and Exercise tolerance (using a six-minute walk test). This is a 10 point scoring system that NICE guidelines have recommended for assessment of potential COPD patients (NICE COPD Overview, 2010).

1.3.3.2 COPD exacerbations

While COPD is chronic and progressive it can be frequently aggravated by exacerbations, which are short periods (at least 48 hours) where symptoms worsen. These exacerbations can be mild (typically treated with increased doses of medication such as bronchodilators), moderate (requires treatment with corticosteroids and/or antibiotics) or severe (requires hospitalisation) (Decramer et al., 2012). The severity and frequency of exacerbations varies between COPD patients, but COPD severity has been linked to increased exacerbation frequency (Hoogendoorn et al., 2010).

When exacerbations occur they speed up COPD disease progression and increase the risk of death, which is why one aim of COPD treatment is to decrease the number of exacerbations (Decramer et al., 2012). Exacerbations are most frequently caused by viral or bacterial infection (60-80% of cases), with microbiology identifying several frequent species in sputum culture, including *H. influenzae, S. pneumoniae* and *M. catarrhalis* (Papi et al., 2006). Other causes of exacerbations include heart failure, pulmonary embolism and environmental factors such as cold air, pollutants, allergens and smoking (Decramer et al., 2012; Vijayan, 2013).

1.3.4 Pathophysiology of COPD

The persistent and progressive obstruction and airflow limitation in COPD is the result of two major pathological processes, the first involving remodelling and narrowing of small airways (chronic bronchitis), and the second involving destruction of the lung parenchyma and alveoli of these airways (emphysema). Both processes are typically the consequence of chronic inflammation, which increases in intensity as the disease progresses (Barnes, 2016).

1.3.4.1 Chronic Bronchitis

The foundation of chronic bronchitis is overproduction and hypersecretion of mucus from goblet cells. Epithelial cells that line the airway respond to toxic or infectious stimuli (typically smoking) by releasing inflammatory mediators such as TNF-α, IL-6 and IL-8, leading to ongoing inflammation of the bronchial tube. In addition, mucus hypersecretion can be activated by neutrophilic inflammation via neutrophil elastase secretion, which releases TGF- α and activates epithelial growth factor receptors (EGFRs) (Barnes, 2016). Along with these pro-inflammatory processes, there is decreased release of regulatory substances, such as angiotensin-converting enzyme and neutral endopeptidase (Widysanto and Mathew, 2020).

As part of the ongoing inflammatory response, neutrophils are released into the airway where they act in a pro-inflammatory manner. As well as releasing elastase and promoting mucus hypersecretion, neutrophils also alter the function of the cilial epithelium, compromising the ability to clear the excess mucus. This in turn makes the lungs more susceptible to infection, which again prompts an immune response and results in a vicious circle of intense chronic inflammation. In addition, neutrophils release other factors such as elastase, proteinase-3 and matrix metalloproteinases which can contribute to the destruction of bronchial elastin and other lung structures (Kim and Criner, 2013a; Y. Wang et al., 2018). Airway walls become

thickened due to a combination of fibrosis and oedema, further promoting the pooling of excess mucus. Thickening can persist to a stage where airways become narrowed to the extent that airway flow to and from the lungs is limited (**Fig.1.8**) (Barnes, 2016; Widysanto and Mathew, 2020)

In summary, the combination of mucus hyperreaction, decreased ciliary function, thickened airways and ineffective coughing leads to reduced expiration and shortness of breath. However, the inflammatory mechanisms responsible for this excess mucus production are poorly understood in humans, highlighting the need for further research and more effective pre-clinical work and model of the lung and COPD (Kim and Criner, 2013b).

1.3.4.2 Emphysema

Emphysema is defined as dilatation and destruction of distal airspaces, which includes the respiratory bronchioles, alveolar ducts and alveoli, also known as the pulmonary acinus (Gharib et al., 2018). This breakdown of alveolar structure affects gas exchange, meaning oxygen can no longer pass into the blood as effectively, leading to shortness of breath, coughing, and wheezing (Sharafkhaneh et al., 2008). Alveoli are optimally structured for gas exchange, but are delicate and easily damaged or destroyed.

After exposure to toxins and smoke, pro-inflammatory cells are recruited to the airways, including macrophages, neutrophils and T lymphocytes. These cells release proteinases and neutrophilic elastase and lead to mucus hypersecretion. Elastase and proteinase released from neutrophils act against elastin, an important component of lung ECM which maintains the integrity of the small airways. Increased levels of elastase and proteinase leads to destruction of small airway components and airspace enlargement. In addition, cytotoxic T cells release TNF-α and perforins, which leads to destruction of the alveolar epithelial cells

and rupture of the alveolar wall (Barnes, 2016; Pahal et al., 2020). This cell death can cause the release of further pro-inflammatory products from epithelial cells (Chen et al., 2010). The alveoli are damaged, and over time the inner walls of air sacs weaken and rupture, creating large air spaces instead of many small ones.

As well as activation of these pro-inflammatory pathways, smoking also inhibits anti-proteolytic enzymes and alveolar macrophages. Another factor is AAT, which typically inhibits neutrophil elastase, but in cases where the patient has an inherited AAT deficiency it can lead to emphysema (Pahal et al., 2020).

The loss of cells and elastin from ECM results in the destruction of alveolar walls, which can cause the lungs to expand within the chest, compressing small bronchi and leading to resistance to airflow. This makes it difficult for contraction to occur and reduces the passage of air through the airways. Reduced lung elasticity combined with limited expiration can lead to lung hyperinflation due to trapped air, both at rest or during exercise (Gagnon et al., 2014).

This can be worsened by air spaces in the lungs, some damaged alveoli can distend and form a large air space, otherwise known as a bullae. Bullous emphysema involves one or more of these large air spaces, and if these spaces rupture and leak air into the pleural space, the lung can collapse, known as pneumothorax (Siddiqui et al., 2020).

Emphysema has been subject to study with *in vivo* mouse models, but the overall mechanisms in the human disease is less clear (Goldklang and Stockley, 2016) Further study into human emphysema mechanisms is vital to limit the progression of the disease and to accelerate potential treatments and therapies.

1.3.5 Immunological Mechanisms of COPD

COPD features a characteristic pattern of inflammation, involving increased numbers of neutrophils, macrophages, and lymphocytes in the airways. There is a complex inflammatory response involving both innate and adaptive immune responses, but the role of these systems in COPD development is not completely understood (Barnes, 2008; Brusselle et al., 2011, Barnes, 2016).

The immune response is related to dendritic cell (DC) activation, but in general the function and distribution of DCs in COPD development is not well described. It is theorised that DCs can regulate effector CD8 T cell responses and might have a role in maintaining neutrophilic airway inflammation via proinflammatory chemokine release (Givi et al., 2012).

Numerous cell types are involved in the innate and adaptive immune responses in COPD and play key roles in disease progression, including macrophages, neutrophils, eosinophils, and lymphocytes (**Fig.1.9**).

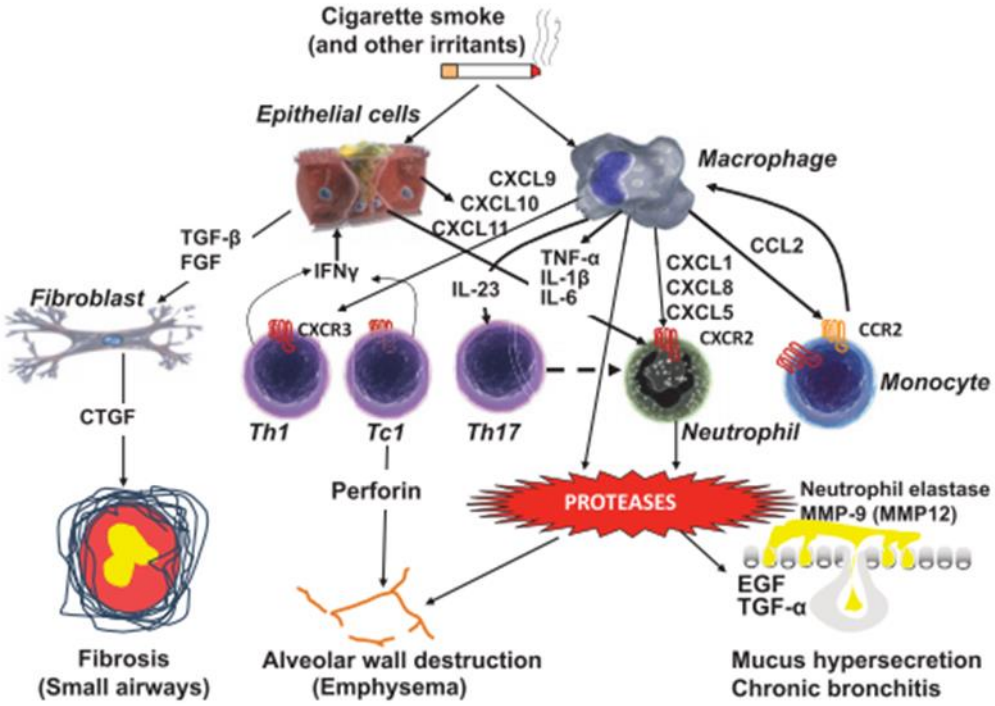

Figure 1.9: Inflammatory response to irritants that have a causative nature in COPD. Irritants first affect epithelial cells and macrophages, which start an inflammatory response by releasing several chemotactic factors in emphysema and chronic bronchitis. Interleukin (CXCL) 1, 8, 5, 9, 10 and 11 are produced by epithelial cells or macrophages to migrate neutrophils to an infected area. These cells also produce interleukins and interferons (IFN γ, IL-1B, IL-6, IL23), these factors then attract inflammatory cells (Th1, Tc1, Th17, helper cells) to the lungs and different responses occur. Emphysema can occur with affecting the pore-forming protein perforin or proteases, which both cause destruction of alveolar structure. Chronic bronchitis can occur by excess proteases in bronchitis causing mucus hypersecretion, it should be noted that fibrosis occurs through epithelial cell reaction only. Production of excess tissue growth factors (TGF-B and FGF) can cause excess production of CTGF (connective tissue growth factor), and this matricellular protein causes excess fibrous connective tissue growth (fibrosis). Image adapted from (Barnes, 2017).

1.3.5.1 Macrophages

Macrophages can be activated by toxins such as cigarette smoke to release inflammatory biochemicals including TNF-α, chemokines and reactive oxygen species (ROS), with alveolar macrophages also releasing matrix metalloproteases (MMPs), cathepsins and elastase (previously released by neutrophils and taken up by macrophages) (Barnes, 2016). In COPD there are many changes to macrophage activity, including: increased activation and secretion of the pro-inflammatory markers mentioned above; activation of the transcription factor NF-κB (inflammatory protein regulator); reduced phagocytic uptake of bacteria (50% of COPD patients have chronic colonization of lower airways) (Taylor et al., 2010) and apoptotic cells (resulting in continued inflammation); and increased numbers (5-10 times increased) of macrophages in the airways, parenchyma, and sputum due to increased release of monocyte-selective chemokines (CCL2 and CXCL1), resulting in recruitment of circulating monocytes (Barnes, 2019, 2016; Singh et al., 2014).

Continued smoking causes continued activation of these macrophages and chronic inflammation in the lungs as well as emphysema, with macrophages localised to sites of alveolar wall destruction (Barnes, 2019, 2016)

1.3.5.2 Neutrophils

Smoking, infection and oxidative stress can stimulate granulocyte (neutrophil, eosinophil, basophil) production and release from bone marrow, and secretion of granulocyte colony-stimulating factor (CSF) from macrophages can also promote neutrophil survival in the airways (Jasper et al., 2019). Neutrophils are recruited to the airways and adhere to endothelial cells via E-selectin, where they migrate further due to guiding chemical factors including CXCL1/5/8 chemokines (released by alveolar macrophages, epithelial cells or other

neutrophils). Both E-selectin and chemokines are upregulated in COPD, resulting in more neutrophils in the airways of COPD patients (Barnes, 2019, 2016). These neutrophils secrete elastase and proteinase (including MMPs), contributing to emphysema and breakdown of alveoli, as well as causing mucus hypersecretion (Fahy and Dickey, 2010). In addition, neutrophils in COPD have increased migration speed but reduced accuracy, meaning there is increased elastase release and damage throughout the airways, degrading lung ECM (Jasper et al., 2019). Studies have even shown that inhibition of neutrophil elastase can result in improved lung function and reduced airway inflammation (Thulborn et al., 2019). Overall, neutrophilic airway inflammation is a characteristic feature of COPD and can be used to measure disease severity (Barnes, 2019).

1.3.5.3 Eosinophils

While the increased numbers of macrophages and neutrophils in the airways and sputum are well studied, along with their immunological mechanisms in COPD, the role of eosinophils in COPD is less clear. Around 15% of patients have increased levels of eosinophils in the sputum and blood, and this may be linked to more frequent exacerbations, but mechanisms are uncertain (Barnes, 2019). The increased numbers of eosinophils may represent an overlap of COPD with asthma, while the two are distinct diseases there are cases where patients exhibit the features of both, known as asthma-COPD overlap (ACO) (Barnes, 2016). Asthma patients with severe asthma or who smoke often have increased neutrophils along with increased eosinophils (Barnes, 2019).

One potential mechanism for eosinophil inflammation in COPD involves the discovery of increased sputum IL-5 in eosinophilic COPD (Barnes, 2019). In response to smoking and/or infection, airway epithelial cells can release cytokines that recruit T helper-2 lymphocytes

(Th2) and type 2 innate lymphoid cells (ILC2). These cells may then secrete CCL5 chemokines to attract eosinophils to the airways, where they are maintained by IL-5 and CSF (Barnes, 2019; Possa et al., 2013). However, further research is needed in order to reveal the role of eosinophils in COPD or ACO.

1.3.5.4 Lymphocytes

The levels of T lymphocytes (Barnes, 2019, 2016), B lymphocytes (Seys et al., 2015), and innate lymphoid cells (ILCs) (De Grove et al., 2016) are all increased in the lungs of COPD patients. The levels of $CD8^+$ cytotoxic T cells (Tc1) are also greater than $CD4^+$ helper T cells (Th1, Th17), with the increased T cell numbers linked to increased COPD severity (both alveolar damage and airway blockage). Tc1 cells can release perforins and TNF-α resulting in apoptosis, this is linked to alveolar cell death in emphysema. (Barnes, 2016). These T cell types express chemokine receptors that can attract and recruit blood monocytes in COPD, further contributing towards increased numbers of macrophages and T cells in the lungs of COPD patients (Costa et al., 2016). In addition, ILCs may also have a role in the increased neutrophilic inflammation in COPD and the persistence of this inflammation after smoking cessation, due to secretion of interleukins by ILC3s (Barnes, 2019, 2016).

While there is no cure for COPD and the ongoing damage to the lungs cannot be repaired, COPD can be easily diagnosed and subsequently managed if identified early. The disease can be slowed by avoiding exposure to certain substances, and by using some treatments that can relieve symptoms.

1.3.6 Treatment and Management of COPD

COPD is a progressive lung disease which is preventable but irreversible. There is no treatment that can stop the ultimate failure in lung function, and available treatments are mainly aimed at increasing the quality of life of the patients, their functional status, and to reduce the risk of death (Mannino and Buist, 2007). The main management goals for COPD are to reduce the overproduction of mucus, improve mucus elimination mechanisms (ciliary transport, etc.), and controlling inflammation.

One of the best ways and likely first steps to improve the condition of a COPD patient should be education and the cessation of smoking. This cessation reduces the decline of FEV and lung function to the level of non-smokers, and quitters respond better to treatment (Jiménez-Ruiz et al., 2015). Studies have shown that smoking cessation can improve ciliary function and decrease goblet cell hyperplasia (Mullen et al., 1987), as well as decreasing mucus production and airway injury (Swann et al., 1992), and even alter the immune mechanisms that lead to inflammation due to the effects of tobacco smoke on epithelial gene expression (Burgel and Nadel, 2004). Despite this, 40% of COPD patients remain smokers, with some features of COPD making it harder to quit. COPD-smoking patients typically smoke far more than standard smokers, are more nicotine dependant, inhale a greater volume of smoke deeper into the lungs, and have little motivation to quit due to depression and self-esteem prevalence (Jiménez-Ruiz et al., 2015).

While smoking cessation remains one of the best COPD interventions, there are numerous commonly available COPD treatments, including bronchodilators, corticosteroids, antibiotics, oxygen therapy and lung volume reduction surgery.

1.3.6.1 Bronchodilators

Bronchodilators is a term used to describe the medications that increase lung function by changing airway smooth muscle tone, such as β2-agonists, anticholinergics, and methylxanthines. Metylxanthines and short-acting β-adrenergic agonists (SABAs such as salbutamol) promote mucus clearance by increasing the airway luminal diameter, ciliary beat frequency and mucus hydration (decreasing mucus viscosity) (Salathe, 2002).

As well as SABAs there are also long-acting β-adrenergic agonists (LABAs such as salmetreol), use of LABAs has been shown to increase mucociliary function, reduce hyperinflation and increase peak expiratory flow, leading to a more productive cough (van Noord et al., 2006).

Anticholinergics also act to increase luminal diameter and decrease mucus secretion, as well as facilitate mucus clearance through cough. However, anticholinergics can deplete airway surface liquid, making it more difficult to clear mucus (Kummer et al., 2008).

There are known side effects of bronchodilator treatments due to some non-specific effects on adrenergic receptors around the body, such as heart palpitations and headaches. These are controllable but unfortunately as most COPD patients are elderly, the side effects are more likely to occur (Almadhoun and Sharma, 2020).

1.3.6.2 Corticosteroids

Corticosteroids (generally referring to glucocorticosteroids) have a role in regulating inflammation and are very commonly used for inflammatory conditions such as COPD. These steroids act on the glucocorticoid receptor (GR), activation of GR leads to rapid translocation to the nucleus where it enhances or suppress specific gene expression, depending on the cell type (Ramamoorthy and Cidlowski, 2016). Generally, pro-inflammatory gene expression is suppressed by blocking NF-κB from entering the nucleus, and anti-inflammatory gene

expression is enhanced through binding of glucocorticoid-response elements (GREs). In addition, glucocorticoids also reduce expression of phospholipase A, which reduces levels of arachidonic acid, which in turn inhibits synthesis of several pro-inflammatory biochemical factors, including prostaglandins, leukotrienes and thromboxane, which leads to decreased macrophage action (Janahi et al., 2018).

In mouse models corticosteroids have been shown to reduce inflammation and mucus production (Innes et al., 2009), with dexamethasone shown to decrease mucin 5AC gene expression in human epithelial cells, and hasten mucociliary clearance (Chen et al., 2005a).

Both systemic and inhaled corticosteroids are used in COPD treatment, often over the long term as a maintenance therapy. Corticosteroids inhibit bronchoconstriction, suppress the immune response, have an anti-inflammatory effect, and lessen the effects of exacerbations (Janahi et al., 2018). In patients with GOLD 3-4 COPD (severe to very severe), inhaled corticosteroids (ICS) are used in combination with other therapies such as LABAs (Rabe et al., 2007).

While systemic corticosteroid use for COPD can reduce inflammation and the rate of exacerbations, they have also been linked to mortality in the over 65's, as well as significant toxicity (Falk et al., 2008). ICS have long been used to treat COPD but there remains controversy as to their effectiveness, with high ICS doses given that can result higher risk of pneumonia, cataracts, or diabetes (Sharon R Rosenberg and Kalhan, 2017; Suissa et al., 2013).

1.3.6.3 Antibiotics

As COPD patients are more likely to have bacterial colonization in their airways due to the dysfunctions in the mucocilliary system (Hodge et al., 2003), antibiotics can be used for COPD patients. While antibiotics may not have direct improvements for COPD management,

treatments with antibiotics such as erythromycin or azithromycin have been shown to result in fewer acute exacerbations and increased quality of life (Albert et al., 2011; Seemungal et al., 2008).

COPD exacerbations are a major contributor to morbidity, cost and mortality associated with COPD, and antibiotics are useful for reducing the frequency of these exacerbations. Neutrophil and eosinophil inflammation is present in COPD, this may be partly due to migration in response to bacterial/viral infections. Studies have shown that COPD exacerbations can be typically caused by certain bacteria (40-50%) or certain viruses (30-40%). Typical bacterial infections involved in COPD exacerbations include: *Haemophilus influenza* (30-50%)*, Streotococcus pneumoniae* (15-20%)*,* and *Moraxella catarrhalis* (15-20%)*,* and typical viral infections include: *Rhinovirus* (40-50%)*, Influenza* (10-20%) and *Coronavirus* (10-20%) (Papi et al., 2006; Siddiqi and Sethi, 2008; Vijayan, 2013).

1.3.6.4 Oxygen Therapy

In COPD there is impaired gas exchange, which can lead to insufficient oxygen levels. Oxygen therapy is defined as oxygen given at any concentration greater than air. Typical oxygen saturation in the blood is around 94-98%, and insufficient oxygen levels (hypoxemia) can be defined as <80-90%, as this is the level at which hypoxic tissue damage can occur (O'Driscoll et al., 2008).

Oxygen is typically delivered by a nasal cannula or oxygen mask, with long term oxygen therapy (LTOT) representing a life-extending therapy in COPD (Cranston et al., 2005) and reducing oxidative stress in diseased tissues (van Helvoort et al., 2006). Despite this, there are conflicting studies as to whether LTOT can improve patient quality of life (Tsolaki et al., 2011). Some alternative ways to deliver oxygen exist, including high flow oxygen therapy (HFOT),

where a preheated and moistened (to prevent airway dehydration) air-oxygen mix is delivered through the nose at high flow rates, this HFOT treatment has been shown to be safe and effective for COPD patients (Vogelsinger et al., 2017). In general, oxygen therapy delivered at moderate concentrations is sufficient to overcome hypoxia associated with COPD exacerbations (Calverley et al., 2003).

It should be noted that gas exchange in COPD is disrupted (particularly due to alveolar damage in emphysema) and blood can be poorly oxygenated (hypoxemia), or less carbon dioxide is eliminated leading to high CO_2 levels in the blood (hypercapnia). Hypercapnia can lead to chronic respiratory acidosis in COPD, where the excess carbon dioxide is hydrated to form carbonic acid and the kidneys compensate by storing bicarbonate (Brill and Wedzicha, 2014). Hypercapnia also affects alveolar epithelial cell function, proliferation and migration, (Shigemura et al., 2017).

1.3.7 Surgical approaches for COPD

Even with medical treatment, a number of COPD patients continue to deteriorate, leading to the use of surgery for management. This comes in two main forms, lung volume reduction surgery (LVRS) and/or lung transplantation. These treatments are typically only performed on patients with GOLD stage 3-4 COPD (severe or very severe), and even then very few procedures are carried out due to concerns about high levels of associated morbidity and mortality (Clark et al., 2014).

1.3.7.1 Lung volume reduction surgery

LVRS involves the removal of the most damaged areas of the lung. However, LVRS is only performed if patients meet several stages of inclusion criteria. High risk patients are excluded,

and patients with severely symptomatic COPD that are likely to recover with surgery are favoured. Some of the criteria include cessation of smoking, body-mass index below 30, good heart function, history of emphysema and no previous LVRS/lung surgeries (Minervini et al., 2018).

The aim of LVRS is to remove tissue affected with emphysema and/or hyperinflation, this decreases the dead air space in the lung and improves ventilation and perfusion (Aaron, 2014). After removing hyperinflated areas, a compressed lung will typically expand (Quezada and Make, 2016). The fragile lung tissue makes LVRS technically challenging and prone to complications, such as air leakage or total respiratory failure. Despite this, there is a general improvement in lung function for LVRS patients, both at rest and exercising (Minervini et al., 2018).

LVRS is rarely performed due to clinical concerns, in the UK there were only 96 procedures in 2009-10 and 90 in 2010-11, with studies showing that LVRS had a mortality rate of 5.5% 90 days post-surgery, and 24% of patients were still hospitalised (Clark et al., 2014). It is recommended that LVRS is undertaken with a multidisciplinary team after appropriate patient selection.

LVRS is typically only offered to patients with severe upper lobe emphysema (or heterogenous emphysema), where there are clear areas that can be resected. For severe homogenous emphysema LVRS is not suitable and alternatives are needed, especially when considering the morbidity and mortality risks of LVRS. Alternative techniques include endoscopic interventions, such as endobronchial valve (EBV) therapy and endoscopic lung volume reduction (ELVR), where endoscopes are used to access specific areas of the lung.

EBVs are one-way valves that are placed on hyperinflated lung regions, allowing air to escape but preventing air refilling the space, this can help reduce the volume of dead/trapped air and reduce pressure (Minervini et al., 2018). EBV in patients with severe homogeneous emphysema has been demonstrated to result in improved lung function, exercise tolerance, and quality of life (Valipour et al., 2016). This effect has also been tracked for 12 months post-surgery, resulting in improved gas transfer capacity, potentially explained by the distribution of air to other sites in the lung that are less affected by emphysema (Hsu et al., 2018). There has also been success with endoscopic placement of coils in the lungs of COPD patients (Herth et al., 2017).

Another example of ELVR includes thermal vapour ablation, where heated water is used to destroy specific emphysematous parts of the lung by inducing an inflammatory response, fibrosis, and scarring. Compared to standard medical treatments, thermal ablation has been shown to result in clinically meaningful and significant improvements in lung function and quality of life at 6 and 12 months (Herth et al., 2017).

Finally, biological sealants can be used, where expandable liquid-foam polymers (such as AeriSeal) are targeted via a bronchoscope to block small airways, promoting collapse and remodelling, with healthier lung tissue able to expand into the space (Herth et al., 2017). This can reduce hyperinflation over the course of several months, but is irreversible and must be used with care (Minervini et al., 2018).

1.3.7.2 Lung Transplantation

Lung transplantation offers an effective treatment for patients with end-stage COPD. LVRS is considered independent of lung transplantation, but one can follow the other, where in some

cases LVRS is merely delaying the need for a transplant. One option is to perform LVRS on one lung and transplant the other lung in order to reduce hyperinflation (Reece et al., 2008).

Lung transplantation is potentially considered if patients have a BODE score of 5-6, progressive disease, significant hypercapnia/hypoxemia, and a predicted FEV_1 of <25%. Patients are also recommended for transplant if they have had at least three severe COPD exacerbations in a year (or one severe exacerbation with acute hypercapnic respiratory failure), as they have a significant mortality risk (Weill et al., 2015). Negative points to consider when recommending patients for transplant include organ dysfunction, chronic infection (especially TB), spinal deformity, obesity, noncompliance, malnutrition, or previous extensive chest surgery (Kumar and Anjum, 2020).

There are a number of unclear factors when considering lung transplantation, including the timings for listing, surgical modalities, and single vs bilateral transplantation (Siddiqui and Diamond, 2018). COPD makes up a large portion of transplants, 36% of all transplants between 1995 and 2007 were for COPD out of more than 7000 transplants. While many of these transplants were for a single lung, bilateral transplants have become more frequent in recent years (Todd and Palmer, 2010).

There are a number of complications and drawbacks to lung transplantation. Some complications can occur immediately, such as acute rejection, donor-recipient mismatch, bleeding, and primary graft dysfunction (most common cause of mortality post-operation or rejection long-term). Any damage or complications to the donor lung itself have serious negative effects, such as lung collapse or air leaking. Over the longer term, other complications can arise such as infection, rejection, vascular or airway complications, and even a recurrence of COPD (Kumar and Anjum, 2020). Other conditions associated with

transplantation include acute native lung hyperinflation (single lung transplant only) and lung cancer after transplantation (Siddiqui and Diamond, 2018).

The chances of a COPD patient getting a lung transplant are low, and even if the operation goes ahead there are numerous risks and complications. Despite this, lung transplantation is still the ultimate treatment for end-stage lung disease. Transplant patients have good short-term survival, with <10% mortality after three months (Yusen et al., 2016), but it should be noted that whether or not lung transplantation provides an overall mortality benefit is still controversial (Siddiqui and Diamond, 2018). Demonstrating a survival advantage for COPD patients is difficult, and improvements in quality of life need further study.

In general, COPD patients are referred to lung transplant only once all other options have been exhausted, meaning that candidate selection is again performed strictly as the overall benefit of transplantation is not as clear as other treatments and the surgery is extremely risky. Further analysis of the benefits of lung transplantation are needed, but one issue is the lack of healthy lung tissue for transplant. Lungs suitable for transplantation are harvested from donors, but only a few of these donors are ideal for transplant and the lung tissue can deteriorate quickly in transportation due to its fragility (Kumar and Anjum, 2020). One option is the use of tissue engineering in order to generate more research and transplantable materials.

1.4 Tissue Engineering Approaches

Tissue engineering aims at developing functional substitutes for damaged tissues and organs, creating potential treatments of human diseases (including lung disease), with tissue engineered materials it may be possible to replace diseased organs and tissue (Carletti et al., 2011; O'Brien, 2011).

Tissue engineering involves growing, and often modifying, cells of specific types in order to engineer desired tissues. The cells of choice can be derived from a patient or model (autologous), another patient or model with sufficient similarity (allogeneic) or from an outside source such as cell lines from a different species (exogenous). Tissue engineering work with such cells is performed both *in vivo* and *in vitro* and can be broadly split into two categories, scaffold-free or scaffold-based.

The scaffold-free approach involves simply administering the cells directly, often with certain growth factors and other biochemical factors that regulate cell survival, proliferation and differentiation (Bakhshandeh et al., 2017).

Scaffold-based tissue engineering approaches involves loading cells onto a 3D scaffold as a growth matrix. The choice of scaffold material (natural, synthetic, derived from decellularized tissues, etc), morphology (porosity, stiffness, hydration, etc) and coating (adhesive, ECM components, etc) are vital to ensure good cell attachment, viability, proliferation and differentiation (Bakhshandeh et al., 2017), in addition, culturing cells in 3D is very different to 2D culture on tissue culture plastic, 3D culture is closer to the *in vivo* environment where the ECM acts as a scaffold (Mansouri and Bagheri, 2016).

Cell seeding densities are important to optimise to ensure sufficient cell-cell and cell-matrix interactions in 3D (Bakhshandeh et al., 2017). Typical choices of cell for scaffold-based tissue engineering are cell lines or primary cells. Cell lines are typically immortalised (can be derived from cancers or treated) cell cultures from different species and tissues, whereas primary cells are taken directly from a specific tissue and grown without many modifications. While primary cells are closer to the typical *in vivo* state and more biologically relevant as a model, they are fragile and can be difficult to culture as opposed to cell lines, which are immortalised

and will proliferate indefinitely. While they can be difficult to obtain, stem cells are also popular for tissue engineering, due to their ability to both self-renew and differentiate into other cell types. Endogenous adult stem cells (ASCs) are multipotent but have limited proliferation capacity, while embryonic stem cells (ESCs) are pluripotent and have much higher proliferation capacity. However, ESCs are subject to ethical concerns and are very difficult to obtain, making pluripotent alternatives like induced pluripotent stem cells (iPSCs) an attractive option (Bakhshandeh et al., 2017). iPSCs can be obtained from typical adult cells by direct reprogramming of just four genes (Myc, Oct3/4, Sox2, Klf4) and can differentiate into a wide variety of cell types (Takahashi and Yamanaka, 2006).

The scaffold can be implanted into a specific area of the body, where the physical and biochemical environment takes over growth and maintenance of the cells until a functional tissue has grown. Most tissues in the body demonstrate some form of endogenous regeneration, with tissue-specific stem cells located in niche environments regenerating any tissue damage (Miller and Kaplan, 2012; Wagers, 2012). An implanted scaffold often elicits an immune response depending on the core material and implantation methods. Implantation can result in triggering of a tissue injury or foreign material response, resulting in acute inflammation, recruitment of macrophages, and potentially encapsulation or degradation/reabsorption of the implant. Implant success is therefore influenced by scaffold material and cell-cell interactions, both vital when designing an *in vivo* tissue engineered scaffold (Crupi et al., 2015).

1.5 Tissue Engineering Approaches for Lung Diseases

Currently, lung diseases are a substantial health issue with only limited treatment options available. To find alternative treatments for respiratory disease, lung tissue engineering

approaches are required. With lung tissue engineering it might be possible to grow lung cells, tissues or organs in *in vitro* conditions and then replace the damaged lung tissue, allowing the body to repair itself or to replace the damaged lung entirely (Raredon et al., 2016). Lungs are capable of regenerating and repairing themselves at the microscopic, cellular level. Unfortunately, at the macroscopic level, damage by degeneration, infection or surgically resected lung tissue cannot repair itself *in vivo*. Lung tissue engineering approaches can investigate whether lung tissue can be generated *in vitro* (Calle et al., 2014).

Scaffolds are an essential structural support in all organs and tissues. For lung tissue engineering, scaffolds must allow cell adhesion, proliferation and survival. In lung tissue engineering hydrogels, decellularized tissue and porous polymeric scaffolds are commonly used. Therefore, using a combination of synthetic materials and porous natural materials can benefit from the synergy of natural cell-binding ligands and better synthetic mechanical properties. Initial studies include human tracheal transplants (Delaere et al., 2010; Elliott et al., 2012; Jungebluth et al., 2011; Macchiarini et al., 2008), leading to hope that the prospect of a tissue engineered tracheal replacement device and possibly even a whole-lung construct is not far off. Unfortunately, there are still many issues not yet resolved such as the need for airway stents.

There are *in vivo* studies involving the implantation of engineered scaffolds into model organisms. One study implanted an engineered lung into rats, these lungs were perfused with blood and inflated with air (but the level of inflation was less than the native lung) with gas exchange taking place, but there was clotting, bleeding into the engineered lung, a lack of surfactant production, and the lung did not survive long-term (Petersen et al., 2010a). Other studies have implanted scaffolds into mice (Ling et al., 2014). Despite this, robust schemes for

successful implantation and clinical use of synthetic lung scaffolds for COPD remains unknown (Wagner et al., 2013).

1.5.1 Tissue engineered models

Lungs have a unique 3D structure and it is quite challenging to manufacture lung-similar structures. There are many studies using different biomaterials to produce suitable scaffolds that support lung cells and allow them to grow and function (Dang-Tan et al., 2017).

Scaffolds composed of lung ECM component fibres such as collagen, fibronectin and laminin can be used to generate artificial scaffolds that mimic the native environment and 3D microstructure. These structures allow for binding and adsorbing of other proteins and growth factors and can be combined with endogenous/exogenous/induced stem cells for potential lung repair (Kruk et al., 2018).

Collagen scaffolds have been widely used in tissue regeneration (Santis et al., 2018; Wang et al., 2020), with collagen proteins being the major components of lung ECM (Wagner et al., 2013). Collagen is also present in all major structures, including airways, blood vessels, interstitium of the lung parenchyma, and basement membranes of epithelial and endothelial cells (Reis et al., 2008a; Zhang et al., 2011a). Collagen scaffolds are biocompatible, biodegradable, mechanically stable, and can guide cell growth, with studies making use of collagen-based hydrogen sponges and porous foams (Chen et al., 2005a; Reis et al., 2008a; Wang et al., 2020; Zhang et al., 2011a).

By using collagen-based scaffolds loaded with tissue-specific cells, it may be possible to promote lung repair and regeneration in lung diseases such as COPD, where such scaffolds can accelerate endogenous repair or act as a vehicle for regenerative stem cells.

The lung is a complex organ that contains many distinct cell types with different microenvironments, meaning that classification of active endogenous stem cells has been challenging, but it is likely that populations of stem cells maintain their specific anatomic regions of the lung. Studies in nonhuman primates (Plopper et al., 2007) and humans (Khoor et al., 1996) have shown populations of airway epithelial progenitor cells, including basal, Club and AT2 cells (Weiss et al., 2011). AT2 cells can function as tissue stem cells in the alveoli, but more robust models for studying human AT2 cells are needed (Yamamoto et al., 2017).

More study is needed for evaluating whether stem/progenitor cells, exogenous or endogenous, can form airway or alveolar-like structures when cultured on 3D scaffolds, either decellularised lungs or other scaffold materials. An example study involving an ECM-protein hydrogel seeded with lung mesenchymal cells from biopsies was tested both *in vitro* for cell attachment and *in vivo* during transplant into sheep lung (Ingenito et al., 2010). Scaffolds of this type will contribute to the development of cell-based therapies for patients with end-stage pulmonary diseases. Lung tissue bioengineering with stem cells on 3D scaffolds is likely to be an area of intense study due to the numerous benefits.

1.5.2 Decellularized lung tissue

Cells produce their own ECM *in vivo* with tissue-specific proteins that allow cells to grow on the structure and interact with other cells and tissues (Petersen et al., 2010b). Decellularisation is the process of isolating the ECM of a tissue from its inhabiting cells, typically using detergents such Triton-X, sodium dodecyl sulphate (SDS), sodium deoxycholate (SDC) or CHAPS to solubilise cell membranes, as well as detach cytoskeletal proteins and DNA (Balestrini and Niklason, 2015). The resulting decellularised tissue retains essential proteins

that were present in the original organ, in this case the lung. Decellularised lung tissue should aim to retain major basement membranes made up of collagen types I, III and IV, laminin, and fibronectin (DeQuach et al., 2011), as well as adhesive proteins and growth factors for cell survival, attachment, proliferation and differentiation (O'Neill et al., 2013a). Details on decellularisation and recellularisation of lung tissue can be seen in **Fig.1.10**.

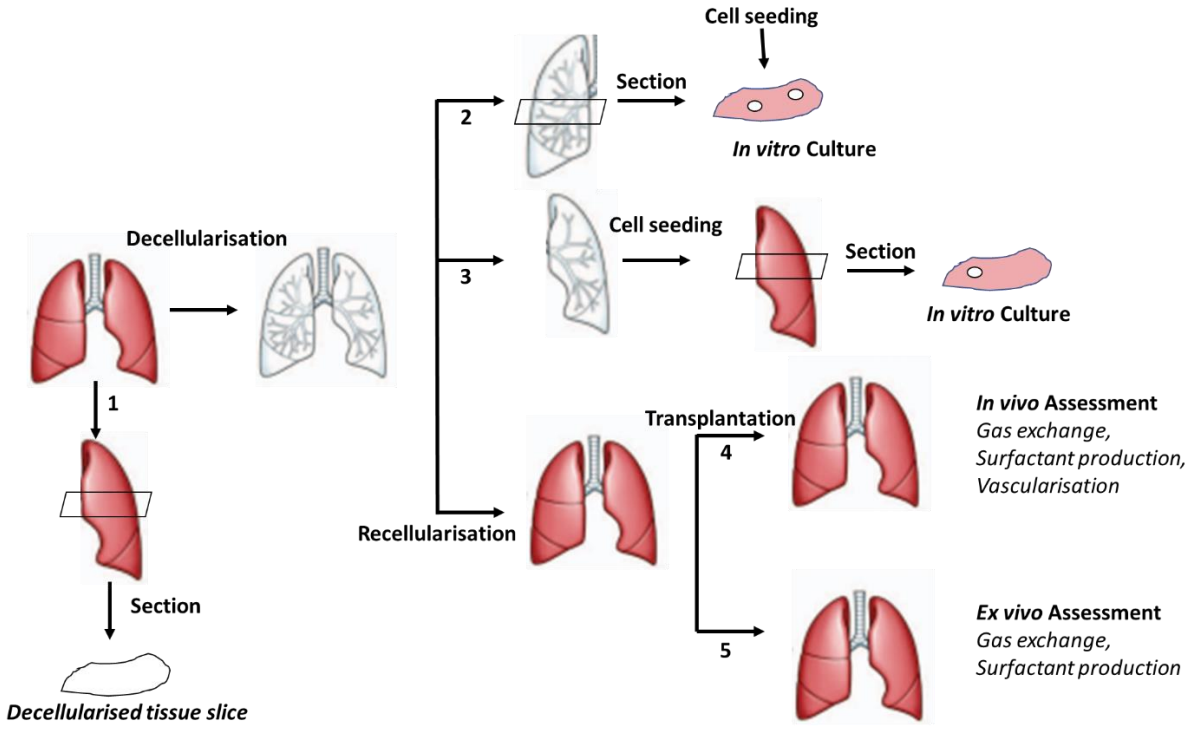

Figure 1.10: Different approaches to decellularisation/recellularisation of lung tissue. 1: Lung tissue can be sectioned and then decellularised to use as a decellularised tissue scaffold. 2: Decellularised lung tissue can be sectioned, then appropriate cells can be seeded onto slices for *in vitro* recellularisation. After recellularisation of the whole lung tissue, 4: recellularised tissue can be transplanted or 5: assessed *ex vivo* (Diagram made with Creative Commons license images).

While decellularized lung tissue presents a useful bioactive scaffold for lung tissue engineering due to the presence of lung ECM, there are issues with supply of clinical-grade scaffold material, particularly with suitable lungs being used for lung transplantation. When making a

decellularized lung scaffold the donor tissue does not have to be human in origin, porcine sources feature less limitations than human sources and are a more reliable source of donor material while remaining anatomically similar to human lungs (Santis et al., 2018).

1.6 Conclusion

COPD and other lung diseases are a huge burden on healthcare, society and the economy, only projected to increase over time due to an aging population and lack of preventative measures or effective cures. The lungs are a highly complex branching structure, composed of many different distinct cell types and hierarchical structures, and damage to parts of this structure can result in lung dysfunction and difficulty with respiration. While the lung can regenerate microstructure, tissue damage repair is much more difficult; clinical approaches to repair this damage are insufficient and damage tends to worsen with disease progression or smoking. New approaches are needed to tackle the issue of lung disease, requiring a better understanding of the lungs both structurally and functionally. One such approach is cell-based lung tissue engineering therapies, using *in vitro* pre-clinical models to accelerate and promote lung repair and regeneration. By using a 3D scaffold as a vehicle and for better cell attachment, these cell-based therapies can be improved by organising into alveolar-like structures.

1.7 Aims and Objectives

The aim of this project is to study a novel scaffold material as part of a cell-based lung tissue engineering approach for lung disease, specifically emphysema. The novel scaffold is composed of a commercially-available gelatine-based porous sponge named Surgispon®, which features a high level of porosity, elasticity and features a similar structure to alveoli of

the lung. By seeding cells typically found in the lung (epithelial cells and fibroblasts) onto the scaffold and performing various mechanical, structural and functional tests, Surgispon can be assessed for a role as a cell-based therapy or platform for study of lung pathogenesis and treatment.

The working hypothesis of this thesis is that Surgispon can be used as a scaffold for lung cells in order to study alveolar structure, and the potential use of Surgispon as a cell-based therapy for emphysema.

1.7.1 Key objectives

- Ensuring that Surgispon is a suitable scaffold cell culture, both mechanically and in terms of biocompatibility
- Testing the mechanical properties of Surgispon including pore size, ability to expand/contract, pore interconnectivity and gas porosity, and any similarities to alveoli *in vivo*
- Determining suitability of Surgispon with cell assays in order to assess cell attachment, viability and proliferation on the scaffold
- Testing the effectiveness of ECM-based chemical coatings on Surgispon in terms of cell attachment and proliferation
- Culturing both lung cell lines and lung primary cells on Surgispon scaffolds
- Culturing lung epithelial cells and lung fibroblasts on Surgispon scaffolds, both separately and together in co-culture
- Testing differentiation of primary lung cells cultured on Surgispon scaffolds
- Use of decellularised lung tissue slices as scaffolds for lung tissue engineering

- Use of Surgispon in combination with decellularised lung tissue slices in order to study cell migration as a proof-of-concept study for the use of Surgispon as a transplant *in vivo* for emphysema

Chapter 2

Materials and Methods

This chapter details the experimental methods used in this project, separated by type. Materials and equipment used in this project are listed in **Table 2.1** and **Table 2.2** respectively.

2.0 Materials

Table 2.1: Reagents and materials used in this project, along with supplier and item reference code.

Name	Supplier	Ref Number
Acetone	Fisher Scientific	A/0560/17
Adenine	Sigma-Aldrich	A2786
alamarBlue™ Cell Viability Reagent	Fisher Scientific	10161053
Bovine serum albumin (BSA)	Fisher Scientific	BP9703-100
Calcium magnesium salt (CaMg)	Sigma-Aldrich	C5149
Ciprofloxacin	Fisher Scientific	13541640
Collagen type I, high concentration, rat tail	Corning	354249
Collagen type IV, mouse	Corning	356233
4’,6-Diamidino-2-phenylindole (DAPI)	Sigma-Aldrich	D9542
Deoxycholic Acid Sodium Salt	Fisher Scientific	BP349-100
Dimethylsulphoxide (DMSO)	Sigma-Aldrich	D2650
Dulbecco's Modified Eagle Medium (DMEM) 4.5g/L, glucose w/ LG	Lonza	LZBE12-604F
Deoxyribonuclease (DNase) I	Roche	11284932001
DNeasy Blood and Tissue Kit	Qiagen	69504
Epidermal growth factor (EGF)	Preprotech	AF-100-15
Ethanol (absolute)	Fisher Scientific	E0650/17
Ethylene diamine tetra-acetic acid (EDTA)	Fisher Scientific	BP2482-1
Fibronectin	Sigma-Aldrich	F0895
Formalin	Sigma-Aldrich	F5554-4L

Foetal bovine serum (FBS)	Lonza	DE14-801F (Lot#1SB020)
Gentamicin sulphate 600 L/U/mg	Fisher Scientific	15435139
Glucose	Sigma-Aldrich	G7021
Glutaraldehyde (GTA) solution (25% in H_2O)	Sigma-Aldrich	G5882
Hank's Buffered Salt Solution	Lonza	10-547F
HistoGel	Fisher Scientific	HG-4000-012
Human Hepatocyte Growth Factor HGF	Peprotech	100-39H-100UG
Hydrochloric acid (HCl)	Sigma-Aldrich	320331
Hydrocortisone	Sigma-Aldrich	H0888
Industrial Methylated Spirit (IMS)	Genta Medical	I99050
Insulin, Transferrin, Selenium (ITS)	Sigma-Aldrich	I3146
L-glutamine (L-Glu)	Lonza	BE17-605E
LIVE/DEAD Viability/Cytotoxicity Kit	Invitrogen	10237012
Matrigel® Matrix	Corning	354234
Mitomycin C	Fisher Scientific	BP2531-2
MTT (Thiazolyl Blue Tetrazolium Bromide) cell viability assay	Sigma-Aldrich	M2128
Non-essential amino acids (NEAA)	Lonza	BE13-114E
Parafilm	Sigma-Aldrich	P7793
Penicillin/streptomycin/amphotericin B	Lonza	17-745E
Phosphate-buffered saline (PBS)	Lonza	LZBE17-516F
Pluronic F-127	Invitrogen	6866
PneumaCult ALI	Stemcell Technologies	05003
Proteinase K	Fisher Scientific	EO0491
Quant-iT™ PicoGreen™ dsDNA assay kit	Fisher Scientific	P11496
Red Blood Cell (RBC) lysis buffer	Roche	11814389001
Rho-associated protein kinase (ROCK) inhibitor	Stemcell Technologies	Y-27632

Sodium pyruvate	Sigma-Aldrich	S8636
Sodium deoxycholate (SDC)	Fisher Scientific	89904
Triiodothyronine	Sigma-Aldrich	T6397
Tris-buffered saline	Calbiochem	648314
Tris Acetate-EDTA buffer	Sigma-Aldrich	T9650-4L
Triton X-100	Sigma-Aldrich	X100-500ML
UltraPure DNase/RNase-Free Distilled Water	Fisher Scientific	10977049
Vybrant Multicolor Cell-Labeling Kit	Life technologies	V22889

Table 2.2: Equipment used in this project, along with supplier and item reference code.

Application	Product Name
Automated cell counter	Invitrogen Countess™ automated cell counter
Freeze Dryer	Akribis Scientific Ltd Edwards Modulyo Freeze Dryer
Laser scanning confocal microscope	Olympus FluoView 1200
Micro computed tomography (μCT) scanner	Scanco Medical μCT 40
Nanodrop (DNA quantification)	ThermoScientific Nanodrop 2000
Phase-contrast inverted microscope	Olympus CKX41
Plate reader	BioTek Synergy 2
UV Sterilisation Chamber	Bio-Rad GS Gene Linker UV Chamber

2.1 General cell culture

To maintain sterility all cell procedures were handled in a class II microbiology safety cabinet using disposable sterile equipment in order to maintain sterility. Except where stated, all cells and pellets were cultured and expanded in DMEM 4.5 g/L glucose supplemented with 10% FBS, 2 mM L-Glu, 1%, NEAA and 1% 100 U/ml penicillin, 100 µg/ml streptomycin, 0.25 µg/ml amphotericin B (PSA), referred to as **DMEM+ media**. All cells were expanded in a humidified incubator at 37°C in the presence of 5% CO_2 and 95% air. The cell lines and primary cells used for experiments are detailed in **Table 2.3**.

Table 2.3: Cell lines and primary cells used for experiments in this project

Cell type	Description	Origin
A549	Adenocarcinomic human alveolar basal epithelial cells	ATCC
35FLH	Human lung fibroblasts originating from a 35-year-old female lung. The cells have been retrovirally infected to express telomerase rendering the cells immortal.	Coriell Institute for Medical Research (AGO2603) (Forsyth et al., 2003)
PLEC	Primary porcine lung epithelial cells, obtained from porcine lung tissue dissection	Extracted from pig lungs provided by Staffordshire Meat Packers Ltd
PLF	Primary porcine lung fibroblasts, obtained from porcine lung tissue dissection	Extracted from pig lungs provided by Staffordshire Meat Packers Ltd

All cell types were cultured in standard DMEM+ media except PLECs, which were cultured in CFAD media. CFAD media refers to 1:4 Ham's F to DMEM 4.5 g/L glucose, supplemented with 10% FBS, 2 mM L-Glut, 1% NEAA, 1% PSA, 10 µg/ml Ciprofloxacin, 50 µg/ml Gentamicin, 0.13

µg/ml triiodothyronine, 10 ng/ml epidermal growth factor (EGF), 0.4 µg/ml hydrocortisone, 5 µg/ml insulin, 5 µg/ml transferrin, 24 µg/ml adenine and 1% sodium pyruvate.

CFAD+ indicates that 1 µg/ml Rho-associated protein kinase (ROCK) inhibitor Y-27632 (RI) was added freshly upon use, when needed. RI is used to promote expansion of PLECs in order to facilitate research (Dale et al., 2019a)

2.1.1 Trypsinisation and sub-culture

Cells were cultured in the relevant cell culture media to a necessary confluency between 70-90%, using either a T25 or T75 cell culture flask. T75/T25 flasks were washed with PBS to remove all traces of serum, then a solution of 0.05% trypsin and 0.02% EDTA (diluted 1 in 10 in PBS) was added (5 ml for T75, 2 ml for T25) and cells were incubated at 37°C until cells began to detach from the flask. Trypsinisation was checked under a microscope to confirm detachment before tapping the flasks to dislodge all cells. A similar volume of DMEM+ media was added to the flask to halt trypsin activity, and the cell suspension was removed into an appropriately-sized centrifuge tube and centrifuged at 1300 rpm for three minutes to form a pellet. The supernatant was removed and cells were re-suspended in the relevant cell culture media, and a small volume was taken for cell counting with a haemocytometer and/or in the automated cell counter Countess, along with trypan blue, to measure the cell number and viability. These counting methods are described in later sections. The appropriate cell concentrations were then seeded, with the media changed every 2-3 days.

2.1.2 Cell cryopreservation

For cryopreservation cells were resuspended in freezing medium, FBS supplemented with 10% (v/v) DMSO, 1 ml per $1x10^6$ cells. The cell suspension was immediately transferred into

cryovials and placed in an isopropanol-filled Mr Frosty to control temperate change at a rate of -1 °C per minute. Cells were placed in a -80 °C freezer for a minimum of 24 hours, and then moved to liquid nitrogen for long term storage.

When necessary, cryopreserved cells were recovered by removing the cryovial from liquid nitrogen and thawing in a water bath at 37 °C. Once thawed, cells were resuspended in cell culture medium in T75 flasks. The cells were incubated at 37°C for 24 hours after which the medium was replaced to remove any remaining DMSO.

2.1.3 Cell count with haemocytometer

For the count, 10 µL cell suspension was added to 10 µL trypan blue and mixed well with a pipette, and this cell suspension was used for cell counting. 10 µL of cell suspension was added under the adhered coverslip of a Neubauer haemocytometer and cells were counted under a brightfield microscope. Cells were counted within four 1 mm^2 corner regions to calculate the mean number of cells, which was multiplied by 10,000 to give cell number per ml. The addition of trypan blue was used in order to determine cell viability during a count, the dilution factor of this addition was taken into account in the calculation.

2.1.4 Cell count with Countess

Some counts did not use a Neubayer haemocytometer, instead adding the cell suspension (10 µl cells with 10 µl trypan blue) to a Countess automated cell counter (**Fig 2.1**), which can measure cell concentrations from $1x10^4$ to $1x10^7$ cells per ml. A cell suspension of 10 µL added to one side of a single-use Countess chamber slide, which was inserted into the Countess. When the image of the cells was appeared on the screen, the right dial on the machine would be used to focus the cells and cell count would be completed by pressing the start button.

After the cells were counted, the data appears on the screen including total count, live count, dead count, and mean diameter.

Figure 2.1: Countess automated cell counter. A: automated cell counter, B: single use Countess cell counting chamber slides (Image from Invitrogen).

2.1.5 Fibroblast deactivation

Fibroblasts were deactivated in order to form a feeder layer and promote epithelial cell growth, as well as improve the biological relevance of the model. Mitomycin C is an alkylating antibiotic isolated from *Streptomyces caespitosus* and can covalently bind to DNA and induce inter- and intrastrand crosslinks. The presence of such crosslinks results in inhibition of DNA synthesis primarily during late G1 and S phases, although it is not cell-cycle specific. Mitomycin C was used as it was freely available at low cost, easy to use, and other common deactivation methods (such as gamma irradiation) were not available (Llames et al., 2015).

Mitomycin C solution was prepared in a laminar flow cabinet, dissolving mitomycin C powder in dH_2O to a concentration of 0.25 mg/ml and sterilising using 0.20 µm filtration. Fibroblasts were cultured in T75 flasks as described in section 2.1. When cultured cells reached 80% confluency, the DMEM+ media was removed and 10 ml fresh DMEM+ media was added with 400 µl mitomycin C stock solution to achieve a final working concentration of 10 µg/ml mitomycin C. Cells were incubated with this solution for up to 3 hours. After incubation, the DMEM+ media with mitomycin C was removed and cells were washed twice with 10 ml PBS before adding 10 ml of DMEM+ media. After mitomycin C treatment, cells were incubated overnight in order to recover before experimentation.

2.2 Cell culture assays

A number of assays were applied to cells cultured on scaffolds, in order to characterise these cells and gather data about scaffold culture. These assays are detailed in the next sub-sections.

2.2.1 alamarBlue assay

The alamarBlue assay is designed to measure the metabolic activity of cells and indirectly determine viability. alamarBlue consists of resazurin, a non-toxic, cell permeable, non-fluorescent blue compound. Upon entering living cells, resazurin is reduced to resorufin, which is red in colour and highly fluorescent. The fluorescence intensity is proportional to the number of living and metabolising cells, meaning that alamarBlue is an indicator of cell metabolism, number and viability. The alamarBlue reagent was added to culture media at a 1:10 dilution, and this solution was added directly to the cells and left in culture for 2 hours in a 37 °C incubator and protected from light. 100 µl of alamarBlue solution was removed

from each sample in duplicate and pipetted directly into a 96 well plate. Fluorescence was measured on a plate reader at excitation wavelength of 530 nm.

2.2.2 MTT assay

The MTT cell metabolic assay was performed to estimate cell metabolic activity, as the reagent reduces to insoluble formazan through the action of an NADH-dependent oxidoreductase enzyme. Following the basic protocol, 500 µL of MTT reagent (5 mg/ml) was mixed with 5 ml of relevant cell culture media. Media was removed from well plates and 300 µL MTT-media solution was added to each well followed by incubation for 2 hours at 37 °C. MTT solution was then removed and 100 µL DMSO was added to each well and mixed thoroughly by pipetting before incubating again at 37 °C for a further 45 minutes. The absorption was measured with a plate reader at a wavelength of 570 nm with a reference wavelength reading at 650 nm.

2.2.3 Proteinase K digestion

Proteinase K is a broad range protease that digests proteins and is used to break down collagen/gelatine structures and lyse cells. Cells needed to be detached and digested for PicoGreen DNA quantification assay, as normal trypsinisation was not sufficient to remove the attached cells, proteinase K was used to digest the whole scaffold plus the attached cells, in order to extract the DNA. Acellular scaffolds were used as control.

Proteinase K solution is provided at a concentration of 20 mg/ml and was diluted with dH_2O to a stock concentration of 2.5 mg/ml, aliquoted and stored at -20°C. Once ready for use, the stock concentration is thawed at room temperature and diluted with dH_2O to a working concentration of 50 µg/ml. When proteinase K was used for cells in monolayers, relevant cell

culture media was aspirated from wells and 0.5 ml proteinase K working solution was pipetted directly onto cell monolayer in wells. To prepare the scaffold samples for proteinase K digestion, scaffolds were carefully placed into sterile microcentrifuge tubes by using sterile tweezers. A volume of 0.5 ml proteinase K working solution was directly added onto scaffolds and vortexed briefly. All proteinase K samples were placed in a 60 °C overnight. Following digestion, all samples were stored at -20°C until use.

2.2.4 Quant-iT PicoGreen DNA quantification assay

The PicoGreen DNA quantification assay allows for the quantification of DNA from cell lysate. Cell lysate from proteinase K digestion (**section 2.2.3**) was left to thaw on ice. DNA solution was diluted 1:50 in 1x TE buffer to prepare a working DNA solution and a standard curve was created using the working DNA solution, as shown in **Table 2.4**. The PicoGreen solution was prepared by diluting the PicoGreen stock solution 1:200 with 1x TE buffer. 50 µL of standard and cell lysate were pipetted into a 96 well plate in duplicate. Blanks were included which consisted of an acellular scaffold digested using the same proteinase K digestion method. 50 µL of PicoGreen working solution was then added to each sample. The samples were protected from light before measuring fluorescence at excitation 480 nm, emission 520 nm on a BioTek Synergy 2 plate reader. Concentrations were determined by plotting fluorescence emission intensity versus known DNA concentration using GraphPad Prism 7.0a, as seen in **Figure 2.2**.

Table 2.4: PicoGreen standard curve created to quantify DNA in unknown samples

Standard ()	Volume of 2µg/ml DNA working solution (µl)	Volume of 1xTE buffer (µl)
0	0	300
0.005	0.75	299.25
0.01	1.5	298.5
0.05	7.5	292.5
0.1	15	285
0.5	75	225
1.0	150	150
2.0	300	0

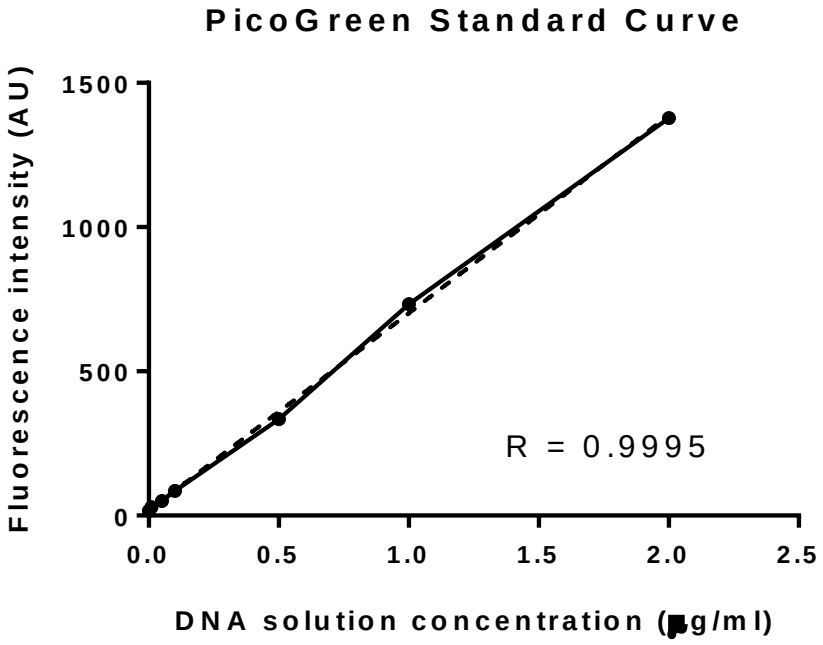

Figure 2.2: PicoGreen DNA standard curve. Serial dilutions of DNA were measured with PicoGreen in order to establish a standard curve. A linear relationship between DNA concentration and fluorescence intensity indicates that PicoGreen is viable for experimentation. A standard curve such as this was generated before every use of PicoGreen (R= 0.9995).

2.2.5 LIVE/DEAD viability/cytotoxicity assay

The LIVE/DEAD Viability/Cytotoxicity Kit (for mammalian cells) is a two-colour assay to determine cell viability. Calcein-AM (green fluorescence) stains cells with intracellular esterase activity, and ethidium homodimer-1 (EthD-1, red fluorescence) stains cells with a loss of plasma membrane integrity. This means that live cells appear green and dead cells appear red, allowing for easy assessment of cell viability.

Cells were prepared by removing the relevant cell culture media and washing samples twice with PBS. The staining solution was prepared by diluting 2 µL of 2mM EthD-1 stock solution and 0.5 µL of the 4 mM calcein AM stock solution into 1 ml of PBS. An appropriate volume of the staining solution was added to cover samples. The samples were left at 37°C for 30-45 minutes and protected from light. Before imaging on either a confocal microscope or a fluorescence microscopy, the staining solution was aspirated and samples were gently washed with PBS. A small volume of PBS was left on the samples to prevent samples drying out whilst imaging.

2.2.6 DNeasy Blood and Tissue Kit

The DNeasy Blood and Tissue Kit allows for purification of DNA from cells, and consists of a number of proprietary buffers along with proteinase K. Tissue samples were cut into small pieces and dried before weighing in a 1.5 ml microcentrifuge tube. 180 µl ATL buffer and 20 µl proteinase K were added to the tube and mixed by vortex before incubating the samples at 56 °C until completely lysed, usually left overnight. After incubation, samples were vortexed for 15 seconds and 200 µl AL buffer was added to samples, which were vortexed and incubated for a further 10 minutes at 56°C. A 95% ethanol mixture was pipetted into a DNeasy

mini spin column that was placed in a 2 ml collection tube and centrifuged at 6000g for 1 minute. Flow-through and the collection tube were discarded and placed in a new 2 ml collection tube. 500 µL AW1 buffer was added to the tubes and centrifuged for 1 minute at 6000g. 500 µL AW2 buffer was added to the tubes and centrifuged for 3 minutes at 20000g. DNA was eluted by adding 200 µL AE buffer to the centre of the spin column membrane. Samples were incubated for 1 minute at room temperature before centrifuging for one minute at 6000g.

2.2.7 DNA quantification with NanoDrop™ 2000

The NanoDrop 2000 is a UV-Vis spectrophotometer used to quantify DNA, RNA, protein and more from samples down to 0.5 µl in volume. Nucleic acids absorb light at 260 nm, meaning DNA concentration can be calculated from optical density measurements. Before measuring DNA, blank samples were measured by using buffer. A 2 µL drop of buffer was directly pipetted onto the optical measurement surface and the blank was read on the software. After taking the blank sample, the DNA solution was mixed with a pipette and 2 µL DNA solution was directly pipetted onto the optical measurement surface to measure the DNA quantity (**Fig 2.3**).

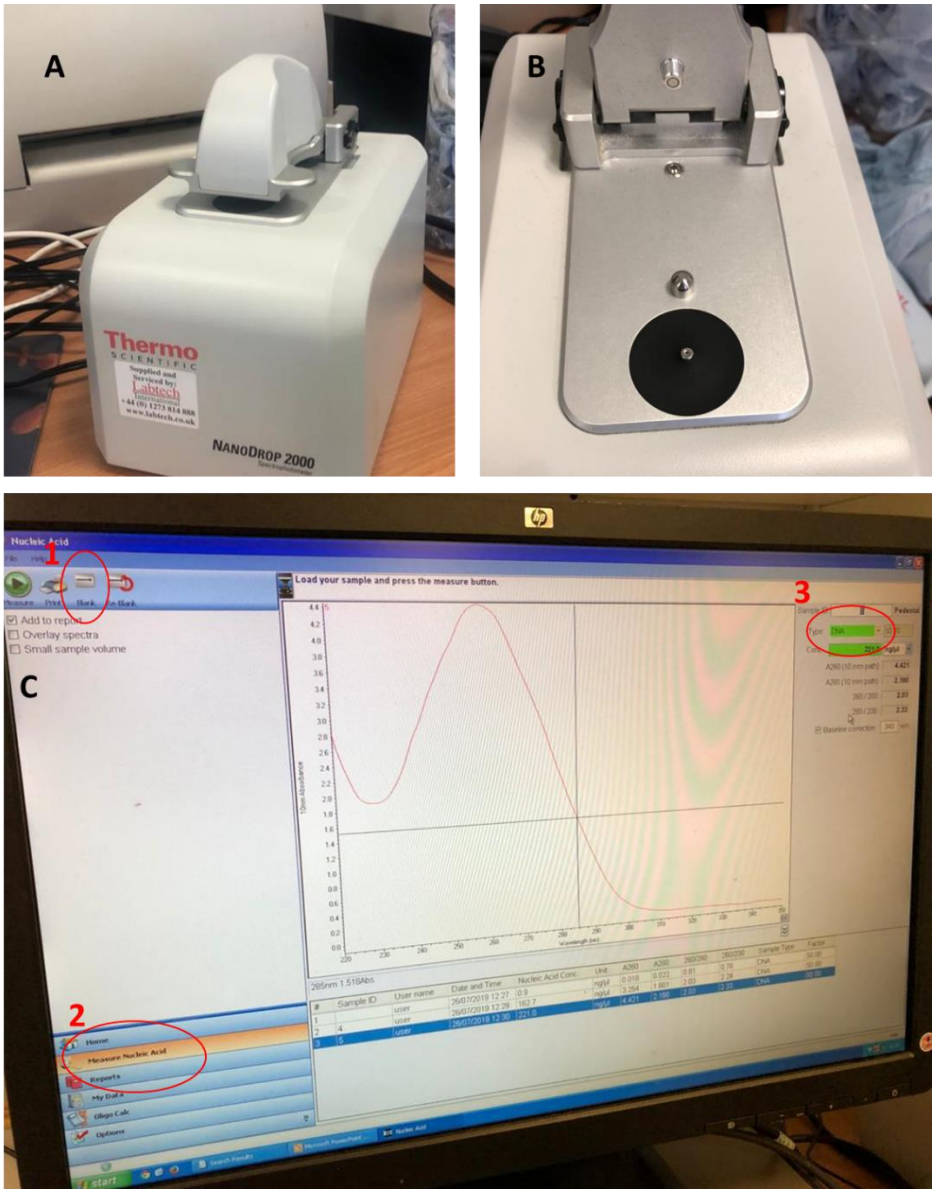

Figure 2.3: NanoDrop 2000 spectrophotometer. Thermo Scientific NanoDrop 2000 spectrophotometer (A) was used to measure DNA quantity of samples that was prepared by using DNeasy blood and tissue kit. NanoDrop 2000 software (C) was used, nucleic acid option was chosen to measure DNA. To take the measurement of blank, blank option (1) was clicked, measure nucleic acid (2) and DNA option (3) was chosen to set the system to DNA measurement.

2.3 Cell Imaging

Cells were imaged with microscopy in order to obtain qualitative images that could be analysed in order to learn more about cell morphology in 3D culture and cell-cell/cell-scaffold interactions.

2.3.1 DAPI staining

DAPI is a fluorescent dye that binds selectively to dsDNA and forms strongly fluorescent DNA-DAPI complexes with high specificity. Before applying DAPI staining to cells, samples were fixed using 10% formalin (approx. 4% formaldehyde) for 20 minutes at room temperature, washed with PBS and stored at 4°C until staining. DAPI powder was dissolved in dH_2O to a concentration of 10 mg/ml and stored at 4°C. Once ready for use, the stock concentration was diluted with dH_2O to a working concentration of 10 µg/ml. Samples were prepared by removing PBS and adding an appropriate volume of staining solution in order to cover samples. The samples were left at room temperature for 5 minutes and protected from light. Before imaging on a confocal microscope, the staining solution was aspirated and samples were gently washed with PBS. A small volume of PBS was left on the samples to prevent them drying out whilst imaging.

2.3.2 Vybrant™ multicolour cell-labelling kit

Using the Vybrant cell-labelling kit, cells were stained with either blue, green or red fluorescence using fluorescent di-alkyl dyes DiO, DiI and DiD. These dyes bind to cell membranes and fluoresce different colours, allowing for tracking of multiple cell types. Vybrant can be used either with cells in suspension or adherent cells but for these experiments, suspension cells were chosen for labelling. Cell suspension was prepared via

trypsinisation of cells as described in **section 2.1.1**. The cell density was set to $1x10^6$ cells/ml in serum-free relevant cell culture media and 5 µL cell labelling solution was added to 1 ml of cell suspension. The cell suspension was mixed well and incubated for 20 minutes at 37°C. After 20 minutes incubation, cell suspension was centrifuged at 1500rpm for 5 minutes. The supernatant was removed and the sample were re-suspended in relevant cell culture media and centrifuged/re-suspended twice more. Cell suspension was allowed 10 minutes recovery time before proceeding with imaging.

2.3.3 Immunocytochemical antibody staining

Primary antibody staining: Samples were fixed overnight in 10% formalin solution (approx. 4% formaldehyde) at 4°C and washed in PBS. PBS was removed from samples and 0.15% Triton X-100 in PBS was added to samples for permeabilization and samples were incubated for 15 minutes at room temperatures. After incubation, permeabilization solution was removed and blocking buffer consisting 1% BSA, 22.52mg/ml glycine, 0.1% Tween 20 in PBS was carefully added to each sample and incubated at room temperature for 1 hour. This blocking step involves using a protein mix (in this case BSA) to coat the cells and block non-specific antibody binding, this improves the signal-to-noise ratio and results in a clearer fluorescent image. Samples were then washed in PBS, and the primary antibody was diluted in PBS and then carefully added onto samples, which were incubated for overnight at 4°C.

The following primary antibodies were used in this project, as seen in **Table 2.5**.

Table 2.5: Primary antibody list

Antibody	Serial number	Target
Anti-podoplanin	ab10274	Alveolar type I cells
Anti-prosurfactant protein C (SPC)	ab211326	Alveolar type II cells
Anti-p63	ab124762	Basal cells
Anti-vimentin	ab92547	Fibroblasts
Anti-pan cytokeratin	ab86734	Epithelial cells
Anti-mucin 5AC	ab212636	Ciliated cells

Secondary antibody staining: Following primary antibody staining, slides were washed thoroughly with PBS three times and the appropriate biotinylated secondary antibody from either an anti-mouse or anti-rabbit staining system kit, diluted as directed by the manufacturer, was pipetted onto the sections and incubated at room temperature for 1 hour. After 1 hour incubation, samples were washed 3 times in PBS and then kept in PBS for imaging.

Staining experiments involved using pan-cytokeratin with vimentin and DAPI, in order to locate, count and distinguish between fibroblasts and epithelial cells. Another experiment involved using p63 and mucin 5AC with DAPI to identify differentiated or undifferentiated cells, as well as using SPC and podoplanin to identify any AT1/2 cells.

2.4 Surgispon® scaffold preparation

Commercially available sterile Surgispon was used as a scaffold. Surgispon is a gelatine-based porous sponge, similar in structure to lung alveoli. Scaffolds were cut into 5 x 5 x 2.5 mm^3 cubes for use as cell culture scaffolds in experiments. Native Surgispon dissolves in solution and requires crosslinking to maintain structural integrity in solution over the long term, as it was used to cell culture over several weeks. Glutaraldehyde (GTA) was used as a crosslinking agent in order to improve Surgispon structural integrity, where the free lysine/hydroxylysine amino acid groups in the gelatine polypeptide chains react with the aldehyde groups of GTA to form imine bonds. This results in increased structural integrity and stabilisation.

2.4.1 Vapour crosslinking (VCL)

Scaffolds were placed in a sealed desiccator containing 4 ml of 25% aqueous GTA solution in a petri dish. Scaffolds were placed onto another petri dish in the sealed desiccator and were crosslinked in the glutaraldehyde vapour at room temperature for 2h, 4h, 6h or 24h.

2.4.2 Liquid crosslinking (LCL)

Scaffolds were placed in a sealed desiccator containing 4 ml of 2.5% aqueous GTA solution in a glass 7 ml bijou. Scaffolds were placed directly into the bijou and the lid was sealed. The sealed bijou was then placed into a sealed desiccator and crosslinked at room temperature for 6h or 24h.

2.4.3 Scaffold Sterilization

After crosslinking, samples were exposed to air in a fume hood for three days and then washed with 50% acetone five times, with samples kept in acetone solution for 15 minutes

after each wash. After acetone washes, scaffolds were washed with PBS five times, with samples kept in PBS solution for 30 mins after each wash, and then left in PBS until required. When scaffolds were needed for experimentation, all sides of the scaffolds were exposed to 30 mJ UV light for 180 seconds.

2.5 Surgispon scaffold testing

2.5.1 Pore size analysis

Brightfield and confocal microscopy analysis of scaffolds was performed to investigate pore size and connectivity. Image J was used to measure pore size by taking the scale bar as a reference measurement in order to measure the diameter of 30 different pores and taking the average.

Brightfield images were taken with an integrated scale bar and analysed with Image J software. For analysis a replicate scale bar was superimposed onto the integrated scale bar (**Fig.2.4**).

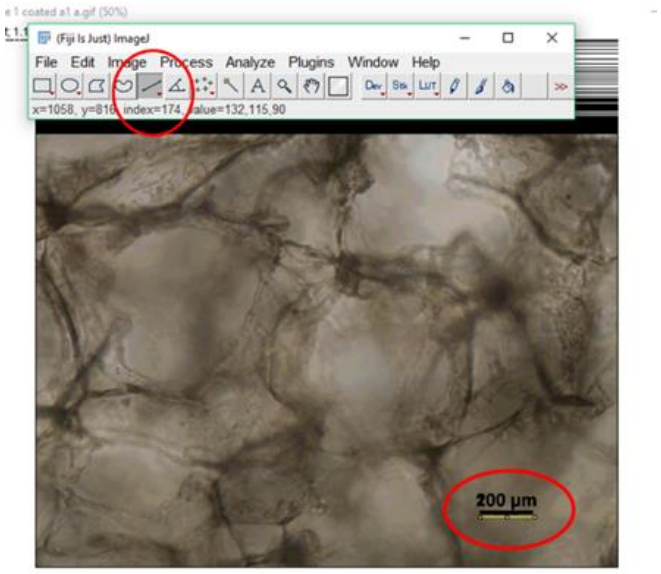

Figure 2.4: Replicating the integrated scale bar using the line tool on Image J software. The integrated scale bar allows for ImageJ analysis and quantitative measurements of length, converting from pixels to micrometres.

The superimposed scale bar was scaled to a known distance, the same unit of the length as the integrated scale bar (**Fig.2.5**).

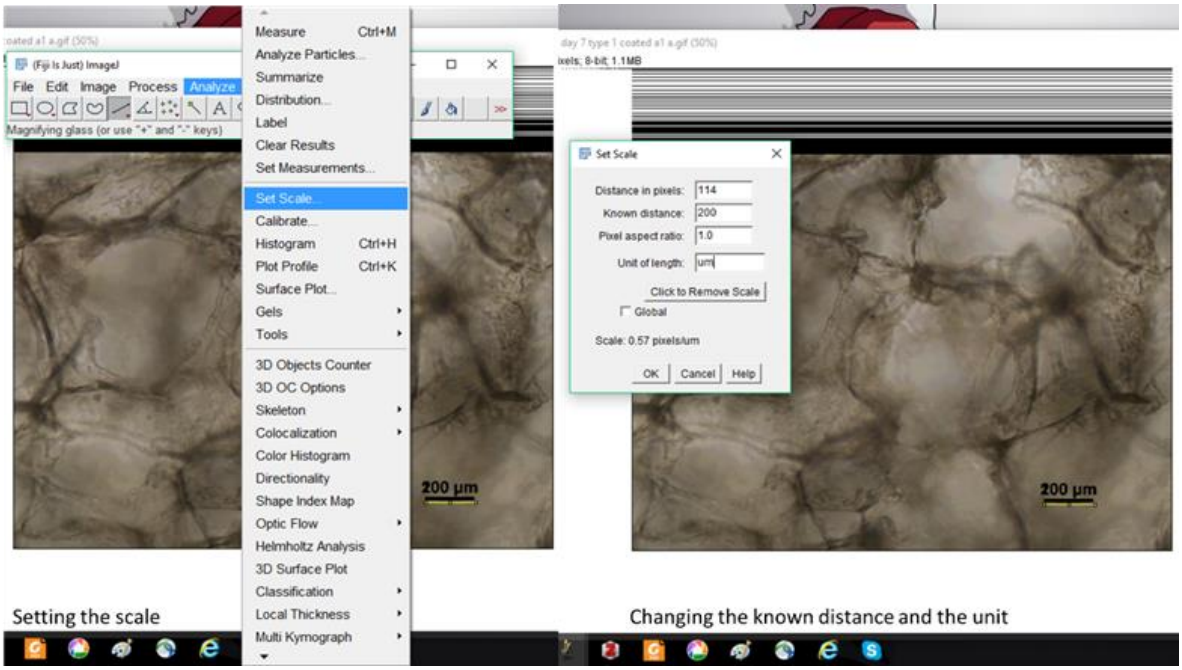

Figure 2.5: Matching the scale of the scale bars. On a set scale window, a known distance was changed to be the same as the scale bar (200) and the unit of length was changed (µm). This allows for measurement of features within the image in micrometres.

After setting the scale with the scale bars, the diagonal length was measured (CTRL+M) to get the measurement result. This measurement was repeated on at least 10 pores for each image, with at least 3 images for one type of scaffold, an average of 30 measurements. For each measurement the median was used (**Fig.2.6**).

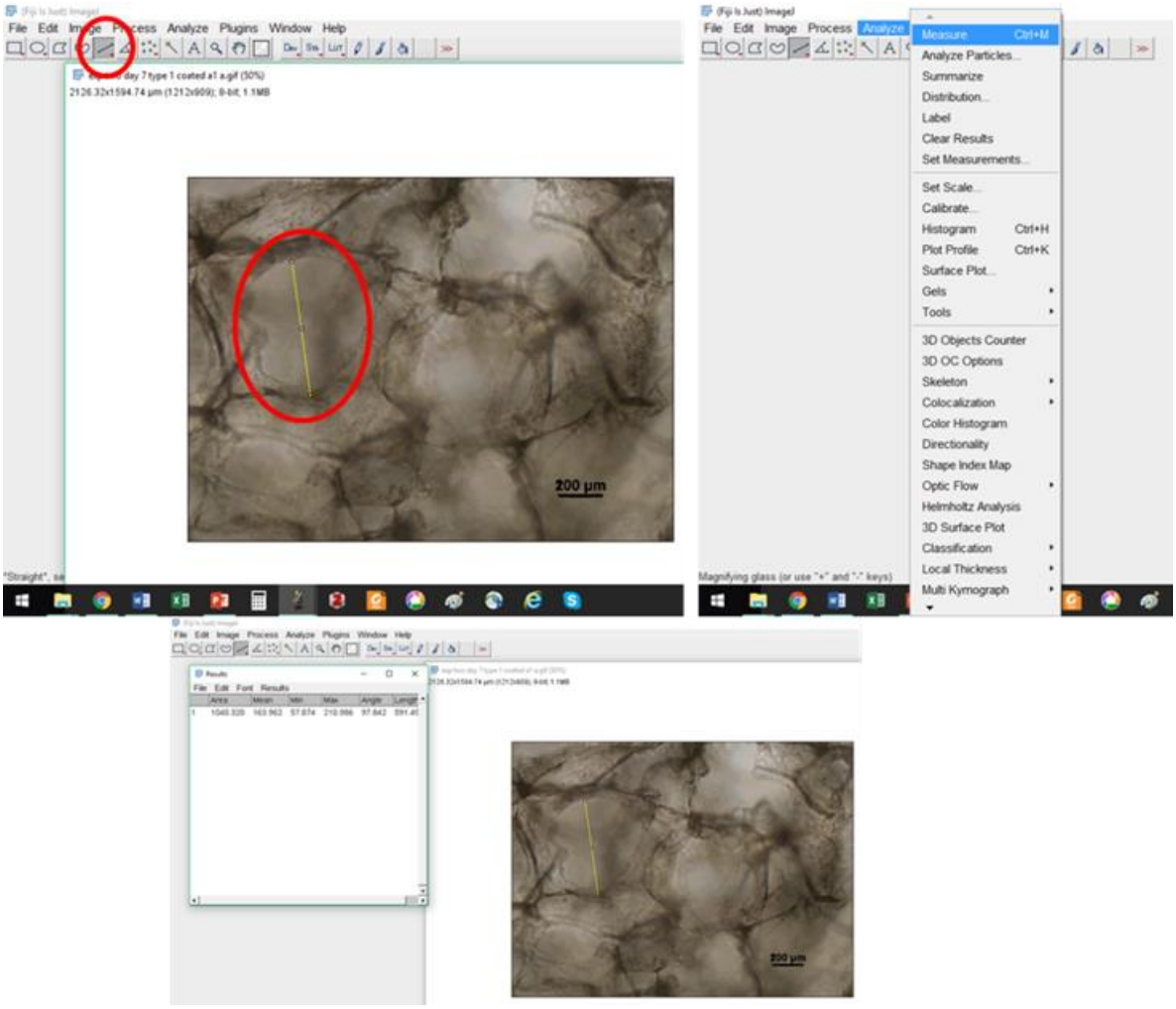

Figure 2.6: Measuring pore size. After setting a scale, a line was drawn on a pore as shown on the top left image and measured with CTRL+M). This measures the diameter of the pore in micrometres.

2.5.2 Micro computed tomography

Samples were stored in PBS prior to scanning. For scanning, samples were blotted briefly to remove excess liquid and placed on polystyrene packed into a 0.5 ml microcentrifuge tube. The microcentrifuge tube was slotted into the smallest sample holder provided with the micro computed tomography (µCT) scanner before being sealed with Parafilm. The sample holder was then slotted into position in the µCT scanner and the door sealed.

2.5.3 Mechanical durability testing

Untreated and crosslinked scaffolds were placed into various solutions and incubated at 37 °C in a cell culture incubator for the desired length of time (up to 60 days) in order to test the crosslinking process and the mechanical properties of the scaffolds in solution over the short and long term. Brightfield images of incubated scaffolds were taken every 24h, with untreated scaffolds used as a control to compare to crosslinked scaffolds (whether vapour or liquid crosslinked). Scaffold images were taken with brightfield and confocal microscopy to determine the pore diameter and to investigate the 3D structure before and after incubation. Image J were used to measure scaffolds pore size as mentioned above.

Dry scaffolds were weighed and then incubated in 20 ml of either DMEM+ media, DMEM only or distilled H_2O in order to test scaffold durability in solution. At set time points, scaffolds were removed, freeze-dried (as detailed in the next section) and then weighed and imaged again to investigate any differences in weight or size through the incubation process.

2.5.4 Freeze-drying

If samples were dry, 100 µl dH_2O was added, with scaffolds blotted to remove excess liquid. Samples were then placed directly into a -80°C freezer for one hour. After freezing, samples were either placed inside the freeze-drying chamber, the glass cover was closed and sealed, and the machine was turned on. Samples were left to freeze-dry overnight before being removed and stored in sterile 50 ml Falcon tubes.

2.6 Primary porcine lung cell extraction and culture

PLECs and PLFs were obtained from primary porcine lungs and used in experimentation as primary cell cultures.

2.6.1 Porcine lung dissection

Dissection tools were first sterilised at 121°C using an autoclave steriliser. These tools were as follows: large and small scissors, bracken forceps and Dumont forceps. The tools were cooled in a sterile container and left under a UV light.

Porcine lungs were supplied from Staffordshire Meat Packers Ltd. up to 6 hours after sacrifice (**Fig.2.7-1**). In a dissection hood, porcine lungs were washed with dH_2O and the pleural membrane was cut open and cleared from the lungs (**Fig.2.7-2**). Small samples (approximately 3 x 3 x 3 cm^3) were cut from lower respiratory portion of the tissue, and moved to a cell culture hood. These samples were placed into a washing solution (35 ml PBS, 10x PSA and 3x Gentamicin) for 5-10 minutes (**Fig.2.7-3**), the washing solution was replaced after this time until the washing solution was clear (**Fig.2.7-4**). Samples were moved into a buffer solution (HBSS, CaMg and 2x antibiotics) for three minutes and then placed into a pronase solution, shaken well and left on a tube roller in a cold room overnight (**Fig.2.7-5**). This process is displayed in **Figure 2.7**.

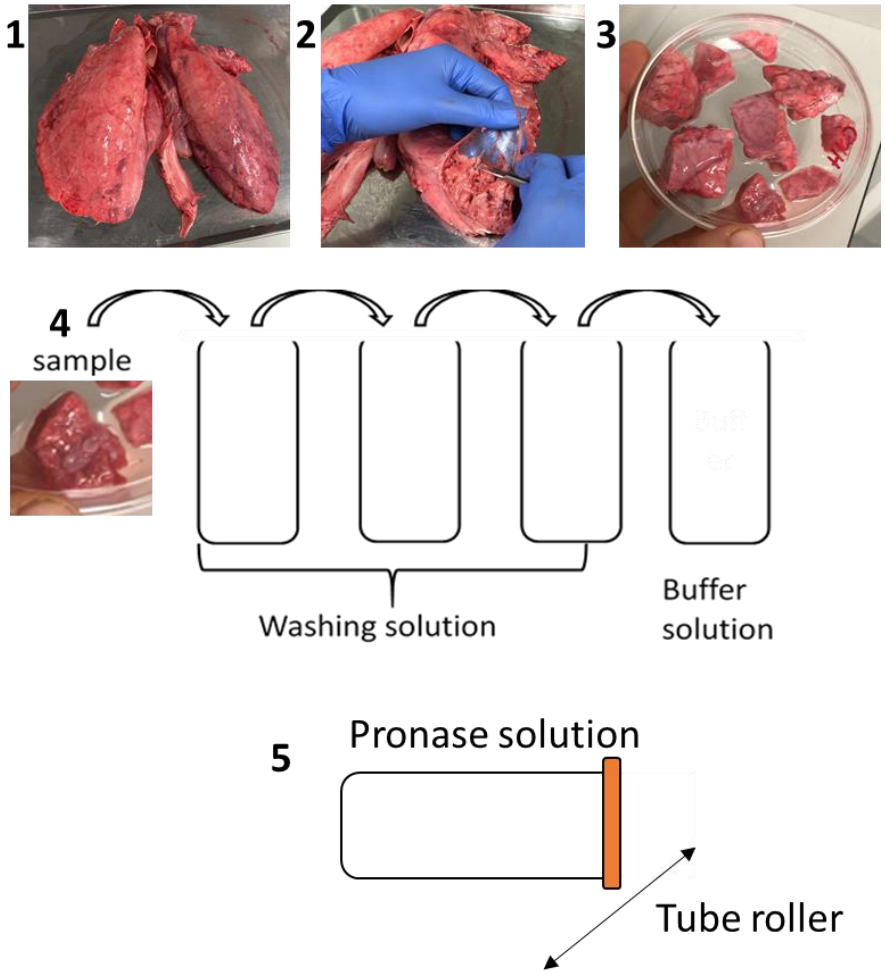

Figure 2.7: Dissection of porcine lungs. 1) Lungs were washed with dH_2O. 2) The pleural membrane was cut open and separated from the lungs. 3) Small pieces were cut from lower respiratory section. 4 Samples were washed in a washing solution until the washing solution was relatively clean, and then moved to buffer solution (all solutions kept on ice). 5) Samples were moved to 50 ml falcon tubes and topped with a pronase solution, then kept on a tube roller in a cold room overnight.

After overnight incubation in pronase, the tissue solution was filtered into an empty tube through an autoclaved gauze. The empty tubes were washed with HBSS and filtered again to collect any remaining material. The resulting solution was strained into a sterile 50 ml tube through a strainer. The strained solution was centrifuged for 20 min at 400G, the supernatant removed and a solution of 1 ml HBSS and 3 ml ready RBC lysis buffer was added to pellet. The

pellet was mixed well with solution and incubated at room temperature for 5-10 minutes. After incubation, 5 ml DMEM was added to the samples, which were centrifuged again for 10 minutes at 400G. The supernatant was removed and 3 ml of 10X HBSS (50 ml HBSS, 5 ml PSA, 500 µl gentamicin and 500 µl ciprofloxacin) solution was added, with samples centrifuged again for 5 minutes at 400G. After centrifuge, supernatant was removed and 3 ml 2X HBSS (50 ml HBSS, 1 ml PSA, 100 µl gentamicin and 100 µl ciprofloxacin) solution was added and the samples were centrifuged for 5 minutes at 400G. The supernatant was removed and the pellet was resuspended in the cell culture media, and a cell count was performed. Cells were seeded into T75 flasks at a density of 100,000 cells/cm^2. Cells isolated from this protocol include porcine lung epithelial cells (PLECs) and porcine lung fibroblasts (PLFs).

2.6.2 Porcine lung epithelial cell (PLEC) dfferentiation

This protocol was modified from a sphere culture method for differentiation of primary cells (Stemcell™ Technologies), using PneumaCult™-ALI (air-liquid interface) media and Matrigel® coating. PneumaCult-ALI is a serum-free media used for culture of airway epithelial cells at ALIs, encouraging these cells to undergo differentiation into an epithelium that bears resemblance to the *in vivo* airways (PneumaCult-ALI Medium STEMCELL Technologies). Matrigel is an ECM-based hydrogel containing many proteins and growth factors, and can be used for attachment and differentiation of certain epithelial cell types (Matrigel Extracellular Matrix, Corning). By coating Surgispon scaffolds with Matrigel and using PneumaCult-ALI media, PLEC differentiation on a 3D scaffold can be explored. PLECs were cultured on Surgispon as a co-culture with deactivated PLFs (D-PLFs).

Scaffolds were placed into 48 well plates and kept at 4 °C until required. Matrigel was diluted with the relevant cell culture media to 40% and the solution kept on ice. When ready, scaffolds were taken from fridge and placed on ice, with 50 µl 40% Matrigel solution added to each scaffold using refrigerated 200 µl pipette tips. Scaffolds were incubated at 37 °C in a humidified incubator for 30 minutes to allow for the Matrigel to solidify.

D-PLF cells were trypsinised and seeded onto Matrigel-coated scaffolds at a seeding concentration of $1.5x10^6$ cells/mL, with a seeding volume of 20 µl. D-PLFs were seeded directly onto scaffolds and incubated for 2 hours to allow for cell attachment. 200 µl DMEM+ media was added to each well to create an air-liquid interface. This volume of 200 µl was chosen based on the calculation that 230 µl of liquid would completely submerge the scaffolds (scaffolds were in a well plate, the base had an area of 0.95 cm^2 and scaffolds were 2.5 mm in height).

D-PLFs were cultured on Matrigel-coated scaffolds for a day and checked under brightfield microscope before PLECs were seeded onto scaffolds. A cell suspension of PLECS was prepared in relevant cell culture media with 5% Matrigel for cell seeding. The final cell seeding concentration was the same as D-PLFs, 1500 cells/µl in 20 µl volume, giving 30,000 cells/scaffold. The 200 µl of media was removed and PLECs were seeded directly onto Matrigel-coated scaffolds containing D-PLF cells. After cell seeding samples were kept in the incubator for 2 hours to allow for cell attachment, and 200 µl relevant cell culture media was added to each well to recreate the air-liquid interface. This process is further outlined in **Figure.2.8**.

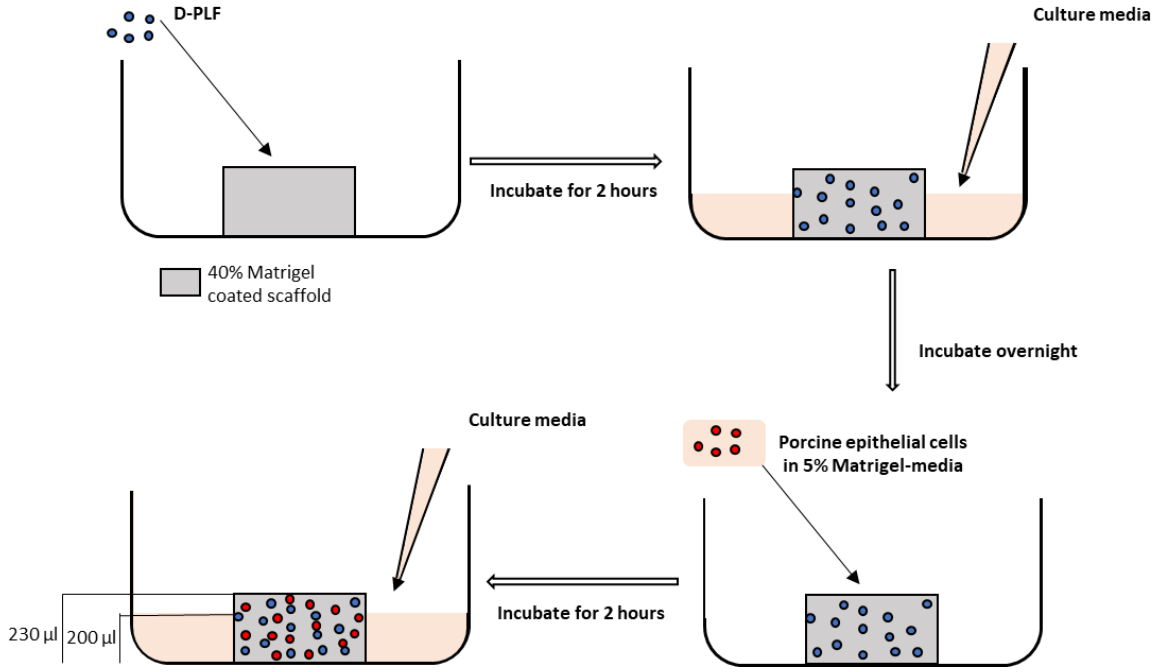

Figure 2.8: Preparing the co-culture of primary porcine cells for lung epithelial cell differentiation. 30000 D-PLF/scaffold was seeded onto 40% Matrigel coated scaffolds and incubated 2 hours before adding 200µl DMEM+ media. Samples were incubated over night before 30000 PLECs/scaffold were added onto them and after seeding these samples were incubated for further 2 hours to allow cell attachment and then 200 µl cell culture media added to create air liquid interface.

2.7 Decellularisation of lung tissue

Dissection tools were first sterilised at 121°C using an autoclave steriliser. These tools were as follows: large knife, bracken forceps and Dumont forceps. The tools were cooled in a sterile container and left under a UV light. While using 50 ml falcon tubes, all samples placed on ice.

Porcine lungs were supplied from Staffordshire Meat Packers Ltd. on the same day as sacrifice. Porcine lungs were washed with dH_2O and kept at -80°C for at least 4 hours until the whole lung was frozen thoroughly. Frozen lungs were taken to the dissection hood and sliced to 5 mm thickness. Lung slices were washed with dH_2O, dried on tissue paper and added to a

digestion solution. Digestion solution consisted of dH_2O, 1% triton X-100, sodium deoxycholate and 10mM tris buffer. 2M HCl was used to adjust the pH of the digestion solution to 7.6. Lung slices were kept in this digestion solution for three days, agitated using a magnetic stirrer and heated at 37 °C, with the digestion solution changed daily. Lung samples were then added to fresh digestion solution with 30 mg/L DNase and kept on a rocker at 4°C overnight (**Fig 2.9**). Lung slice samples were then mounted onto glass slides and freeze-dried as described in **section 2.5.4**.

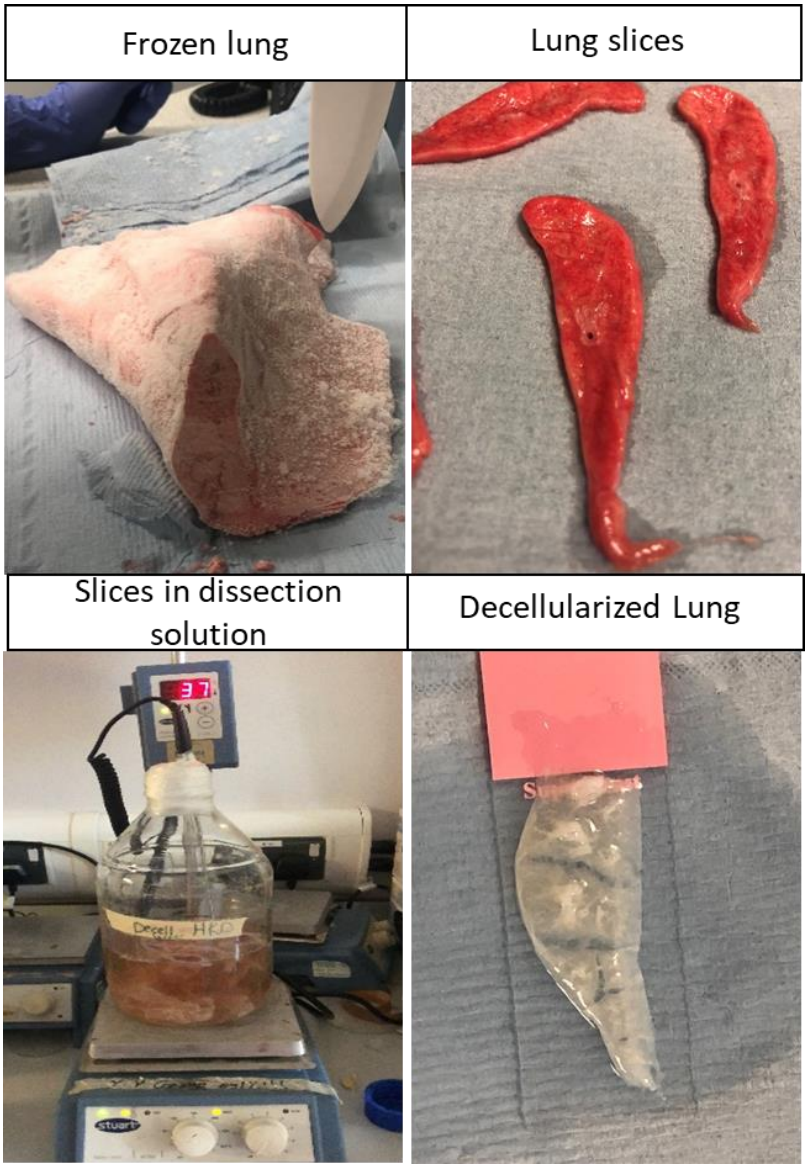

Figure 2.9: Decellularisation of porcine lungs. Fresh porcine lungs were obtained from Staffordshire Meat Packers Ltd and frozen at -80°C for minimum 4 hours. Frozen lungs were taken to dissection hood and sliced manually. Slices samples were placed in digestion solution on a magnetic stirrer and kept at 37°C for 3 days. Digestion solution was changed with fresh one every day and after 3 days, samples moved into DNase I solution for overnight. DNase I solution was kept on rocker and at 4°C. Decellularised lungs were placed on a glass slides before taking to freeze drier.

Chapter 3

Mechanical properties of Surgispon® scaffolds

3.1 Introduction

3.1.1 Pulmonary alveolus

Alveoli are made up of an epithelial layer which includes several cell types, mainly alveolar type I (AT1) and type II (AT2) pneumocytes, which are functional cells responsible for the action of alveoli such as gas exchange and surfactant production. AT1s are thin, flat cells that allow gas exchange at the alveoli membrane, and AT2s secrete surfactant into the alveolus to lower surface tension, preventing alveolar collapse or the inner alveolar walls sticking together upon compression. Each alveolus measures approximately ~200-500 µm in diameter, making them the smallest functional units in the pulmonary system (Schreiber et al., 2005a).

When these alveoli suffer structural damage, such as in emphysema, they lose their efficiency for gas exchange and this affects the respiration of the host organism. As such, the development of effective lung tissue engineering research for lung diseases is vital, such as the development of effective *in vitro* alveolar models for better pre-clinical research into lung disease (Cazzola et al., 2007).

3.1.2 Lung Tissue Engineering

With lung tissue engineering it can be possible to grow lung cells/tissues *in vitro* in order to replace damaged lung tissue, allowing the body to repair itself or to replace the damaged lung entirely (**Fig.3.1**) (Raredon et al., 2016). As outlined in **Chapter One (Section 1.4),** it is vital to be able to generate lung tissue *in vitro,* requiring the use of scaffolds in order to best mimic

the complex 3D environment of the alveolus, including the ability to support the growth of multiple cell types and the inclusion of pores ~200-500 µm in diameter.

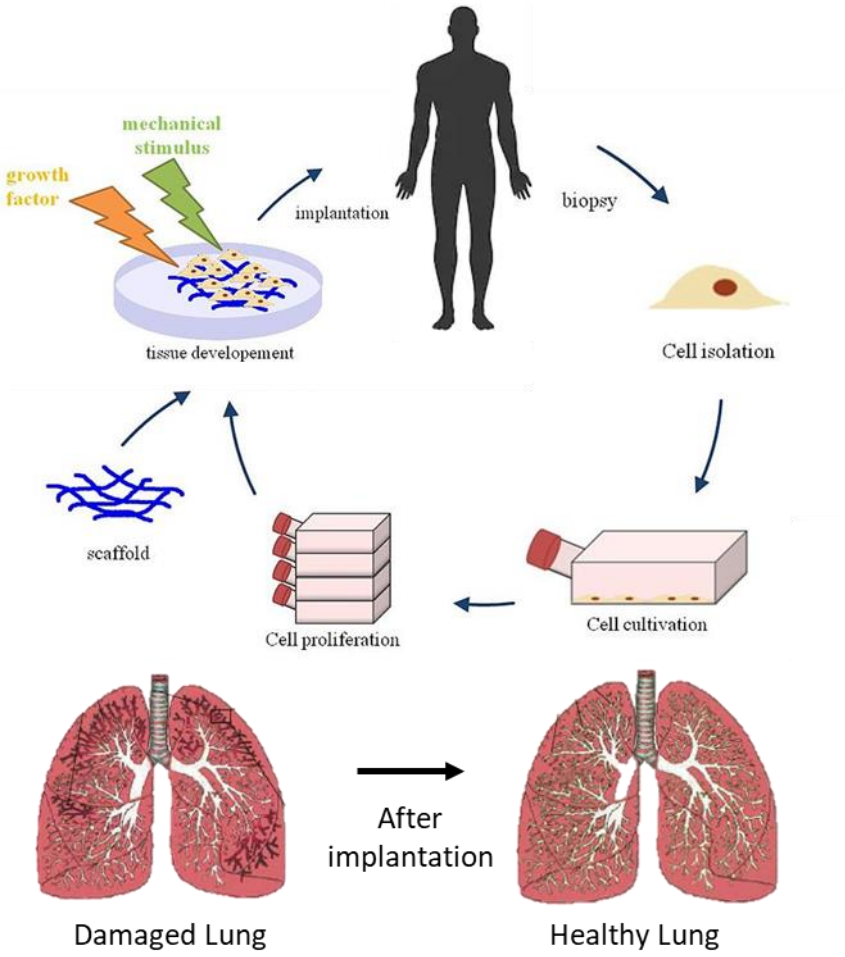

Figure 3.1: Lung tissue engineering approaches. Lung tissue engineering includes cell isolation, cultivation of cells in 2D and cell expansion and seeding cells onto 3D scaffolds. In this stage it is possible to use other chemicals such as growth factors or to stimulate with mechanical forces. After this stage *in vitro* cultured tissue can be transplanted for either to assist the damage tissue to self-repair or to replace the damaged tissue entirely (Images modified from Wikimedia Commons with Creative Commons Licence).

A number of lung tissue engineering studies *in vitro* have used sponges due to their inherently porous structure, with the pores often a similar diameter to individual alveoli. By culturing

epithelial or pneumocytic cells in these sponges, a clinically-relevant lung tissue model can be developed (Chen et al., 2005b; Reis et al., 2008b; Zhang et al., 2011b).

3.1.3 Scaffolds

Scaffolds are useful for *in vitro* lung tissue engineering as cells need a scaffold to provide structure and elasticity, a base for cells to proliferate on in 3D to promote cell-cell interaction, as well as help direct cells upon implantation. Scaffolds are a vital part of *in vitro* tissue engineering (Kubo, 2012). Several materials have had success as lung models, including naturally-occurring substances made up of lung ECM components, such as collagen- or gelatine-based scaffolds including Gelfoam® (gelatine) and Matrigel® (collagen, laminin).

Gelfoam is a gelatine sponge, featuring good flexibility and biocompatibility for *in vitro* lung osteosarcoma (Tome *et al*. 2014) and adipose stem cells (Damous et al., 2015), but most importantly supports pulmonary cell proliferation and features pore sizes similar to alveoli (Andrade et al., 2007a). Gelfoam has been in use for almost 30 years, with early studies culturing foetal rat lung cells on Gelfoam scaffolds, observing the development of alveolar-like structures lined with epithelial cells (Liu et al., 1992).

During long-term (40-60 days) *in vivo* engraftment into adult rat lungs rodents, Gelfoam formed alveolar-like structures at the border between the sponge and the lung tissue that expressed pulmonary markers, but these only formed at the implant border and not within the sponge itself, which degraded after several months. Furthermore, vascularisation was an issue with few capillaries or even endothelial cells growing into or within the Gelfoam (Bhatia, 2010).

Cell migration into Gelfoam implants was also observed to not be of sufficient magnitude to be useful for tissue regeneration, with Gelfoam implants needing to be exceedingly small in order for homogenous cell growth throughout the 3D structure (Andrade et al., 2007b).

Based on the success of naturally occurring sponge-like scaffolds for *in vitro* lung tissue engineering, alternatives to Gelfoam were sought in order to accelerate pre-clinical research. In this thesis, we use such an alternative, named Surgispon®.

3.1.4 Surgispon

Surgispon is a low-density gelatine sponge, originally designed as a haemostatic sponge, due to its ability to absorb 40-50x its own weight of liquid. Surgispon would adhere easily to the site of a wound or surgery, absorbing blood and preventing/stopping bleeding. Surgispon is used as a haemostatic in surgery of all kinds including dentistry, where it is applied to a bleeding site and absorbs blood. In addition, Surgispon has a porous structure which activates thrombocytes and promotes aggregation, catalysing fibrin formation and stopping the bleeding (Aegis Lifesciences)

Surgispon is made by lyophilizing (freeze-drying) hydrolysed porcine collagen, forming a highly purified gelatine sponge. These sponges feature uniform porosity and a low molecular structure, making them suitable as an alveolar model in a similar manner to Gelfoam. The use of Surgispon in dentistry and surgery has shown that the sponge is non-toxic, non-allergenic, non-immunogenic, non-pyrogenic, pH neutral, fully absorbed *in vivo* within 3-4 weeks, and liquefies in 2-5 days when immersed in liquid (Anser Medical). In this study, dental cubes of Surgispon are used, which measure 10x10x10 mm in X, Y and Z (a volume of 1000 mm^3).

This chapter details the characterisation of Surgispon for suitability as an *in vitro* lung tissue engineering approach to lung diseases, modelling the niche micro-environment of the alveoli.

3.2 Aim

The aims of this study are to evaluate the current candidate scaffold Surgispon for prospective future cell-based lung therapies and research:

a. Determine whether Surgispon has a structure similar to that of an alveolus
b. Determining if the mechanical stability of Surgispon can be increased through crosslinking, and if the scaffold is suitable for cell culture after crosslinking
c. Investigating the mechanical properties of Surgispon, namely the ability to expand and contract, range of pore sizes and gas porosity

3.3 Method

The diagram of the experiment is summarised in **Schematic 3.1** and all materials and methods are described in full in **Chapter 2**.

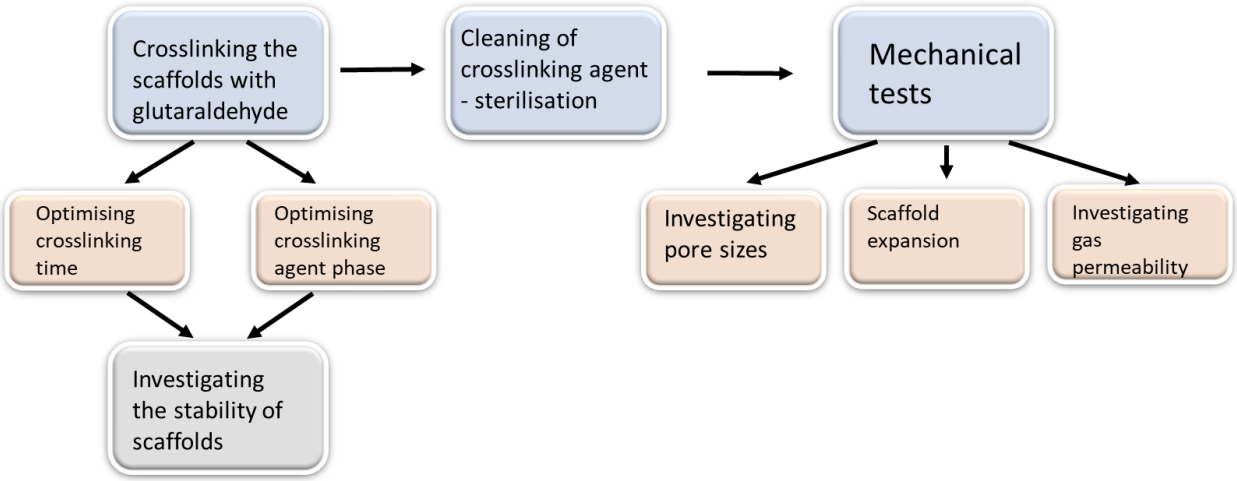

Schematic 3.1: A schematic to show the experimental design for chapter 3. These experimental steps involve the optimization of preparation, sterilisation and mechanical testing of Surgispon scaffolds. These optimised preparation procedures are then used throughout this project whenever Surgispon is used.

3.3.1 Optimising scaffold crosslinking

Commercially available sterile Surgispon was used as a scaffold. Surgispon is a gelatine-based porous structure that comes in sterile packaging as 10 x 10 x 10 mm^3 cubes. These cubes were cut into 5 x 5 x 2.5 mm^3 cubes crosslinked with vapour and liquid glutaraldehyde (GTA) as described in **section 2.4**. Samples were crosslinked for 2h, 4h, 6h and 24hand then left in the fume hood to remove the excess glutaraldehyde.

3.3.2 Investigating scaffold stability

To optimise crosslinking time and phase of crosslinking agent, crosslinked samples were tested for mechanical durability as described in **section 2.5.3**. Untreated samples were used as a control and incubated in DMEM+ media for seven days with crosslinked samples. Sample stability was checked under the brightfield microscope.

3.3.4 Pore size investigation

To investigate scaffold pore size, scaffolds were kept in DMEM+ media to mimic cell culture conditions. Scaffold images were taken with brightfield microscopy and scaffold pore size was calculated as described in **section 2.5.1**.

3.3.3 Sterilisation of scaffolds

After samples were sterilised as described in **section 2.4.3**, sample sterility was evaluated. A549 human lung epithelial cells were cultured and then trypsinised as described in **section 2.1 and 2.1.1**. Cells were seeded onto 48 well tissue culture plastic (TCP) and 100,000 cells/cm^2 were used per well. Cells were cultured for 3 days, maintaining 70-80% confluency before crosslinked scaffolds were placed on top of the confluent cell monolayer, with cell culture continued for 3 days as shown as in **Figure.3.2**. Cell-only wells and cells with untreated scaffolds were used as a control for normal cell growth. Cells were observed with brightfield microscopy and then the alamarBlue™ assay was applied to all samples as described in **section 2.2.1** to determine cell viability via metabolic activity.

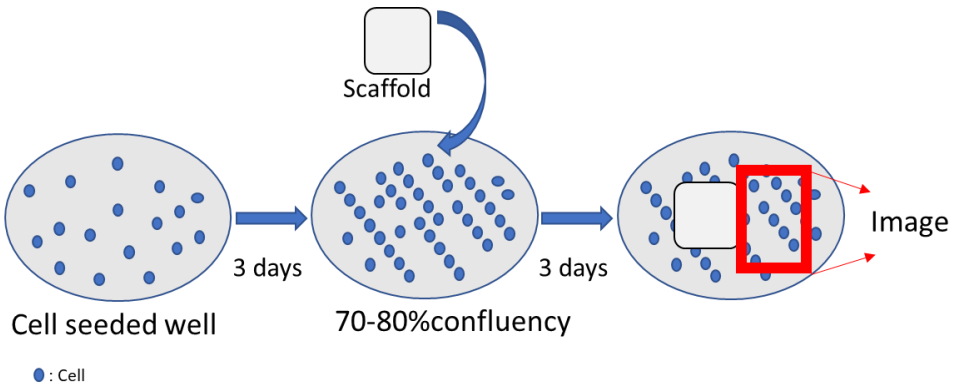

Figure 3.2: Cytotoxicity testing of crosslinked scaffolds. This cytotoxicity testing was designed to investigate the toxicity of any possible GTA residue by culturing cells in a standard 2D cell culture plate and placing a prepared and sterilised Surgispon scaffold onto the monolayer and observing any effects the scaffold had on the cell monolayer.

3.3.5 Expansion of scaffolds

To test scaffold expansion, scaffold dry weight was measured and scaffolds were transferred into one of three different solutions: DMEM with FBS and supplements (DMEM+ media), DMEM only and dH_2O. Scaffolds were placed into solution in 48 well plates and kept in the cell culture incubator for up to 60 days. Scaffolds were then freeze-dried as described in **section 2.5.4** in order to remove solution, and then scaffold weight was measured. Images of samples were taken on the same days as weighing in order to determine scaffold and pore size, with these data analysed in image J.

3.3.6 Gas porosity

To investigate the gas porosity of scaffolds, micro computed tomography (µCT) and confocal microscopy used in Z were used to create a porosity map of scaffolds structure as described in **section 2.5.2**. This was also used to determine pore interconnectivity.

3.3.7 Comparing Surgispon with lung tissue

24h VCL scaffolds were imaged with brightfield microscopy. In addition, after culturing A549 cells (60,000 cells/scaffold) on Surgispon scaffolds for 7 days (**section 2.1**) samples were stained with the LIVE/DEAD assay and imaged via confocal microscopy (**section 2.2.5**). These images were visually compared with fixed porcine lung slices which were stained with DAPI and imaged via fluorescence microscopy (**section 2.3.1**). Porcine lungs are widely used as an alternative to human tissue (O'Neill et al., 2013b).

3.4 Results

3.4.1 Surgispon structure analysis

Brightfield and confocal images of untreated Surgispon scaffolds were taken to investigate pore structure, size and connectivity (**Fig.3.3**). Inherent autofluorescence of gelatine allowed us to take 3D confocal images to investigate interconnectivity of pores. The 3D autofluorescence image is represented in 2D. Confocal 3D images were taken to demonstrate that untreated Surgispon scaffolds have an interconnected porous structure, but due to the complexity of the structure it wasn't initially possible to determine the interconnectivity of the pores from 3D images alone.

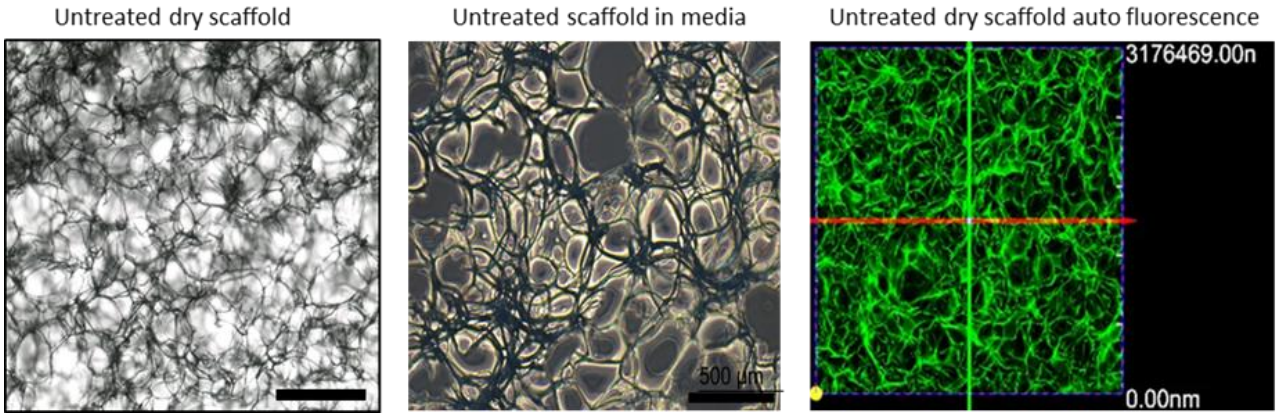

Figure 3.3: Untreated scaffold images. The left image shows a dry untreated scaffold, which resulted in poor image quality. Scaffolds were imaged again after 30 minutes in media, resulting in the middle image, a much clearer representation. The image on the right-hand side represents a 2D image of a 3D confocal microscopy auto fluorescence (gelatine) image (scale bars in all images are 500 µm).

Pore size of untreated scaffolds were measured via analysis of brightfield images with Image J. Each individual scaffold is unique in structure, with differences in pore location, pore size

and distribution of pore size. In order to determine the variation between scaffold pore sizes, three different scaffolds were imaged and measured. Pore size ranged from 44.83 µm to 493.97 µm with overall mean pore size being 223.92 µm (**Fig.3.4**). There was no significant difference in pore size distribution between the three scaffolds (p: 0.206).

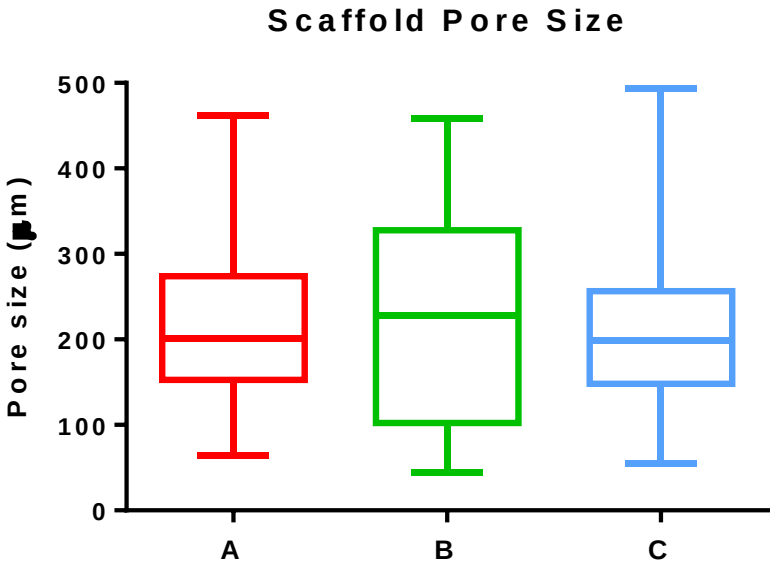

Figure 3.4: Pore sizes of three different untreated scaffolds. A box and whisker plot showing the distribution of pore sizes for three scaffolds, A (red), B (green) and C (blue). Minimum pore size 45-65 µm, average pore size: 220-231 µm, maximum pore size: 462-493 µm, n=28.

3.4.2 Surgispon crosslinking

As Surgispon is composed of a porous gelatine sponge, it is highly water-soluble and has a tendency to dissolve or disintegrate in liquid (Chae *et al.* 2018). Untreated Surgispon was kept in cell culture conditions (DMEM+ media and 37° C) for 5 days and brightfield images were taking to investigate the stability of Surgispon (**Fig.3.5**) Results showed that Surgispon was disintegrated/dissolved after 3 days in cell culture condition. Only small parts of disintegrated

Surgispon was viable on day 5. This makes untreated Surgispon unsuitable for cell culture beyond five days, but Surgispon can be crosslinked to increase stability. This crosslinking is done with glutaraldehyde (GTA) in either a gaseous or liquid form. In this section the effect of GTA crosslinking on Surgispon scaffolds is investigated.

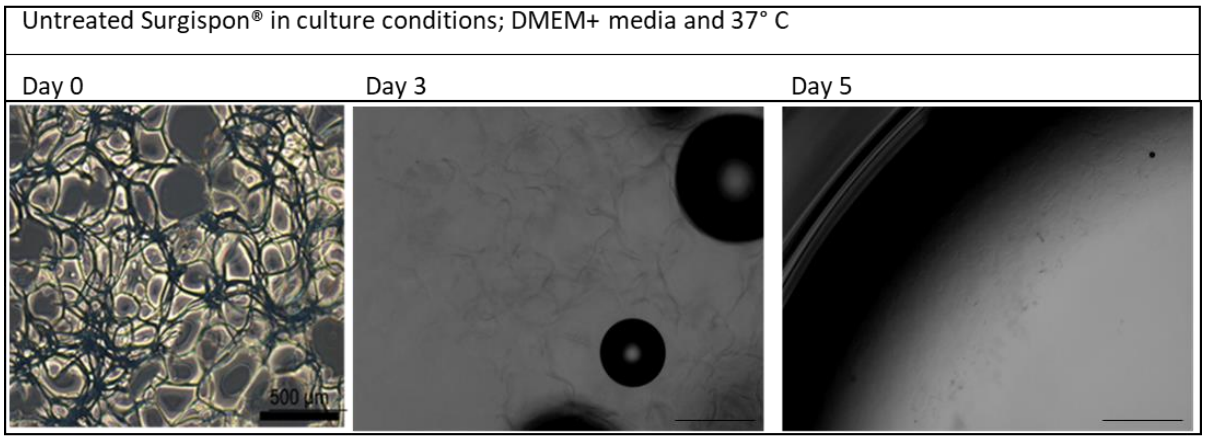

Figure 3.5: Untreated Surgispon in cell culture conditions over 5 days. Surgispon is viable on day 0 but started to lose structural integrity by day 3. Only disintegrated parts of Surgispon are visible by day 5.

3.4.2.1 Effect of crosslinking on mechanical stability in culture conditions

Surgispon scaffolds were crosslinked using GTA in vapour or liquid form. Free aldehyde groups react with the lysine/hydroxylysine residues of the gelatine and form GTA polymers (Olde Damink et al., 1995; Peng et al., 2017). Vapour crosslinked (VCL) scaffolds were crosslinked for 2, 4, 6, or 24 hours, while liquid crosslinked (LCL) scaffolds were crosslinked for 6 or 24 hours only, due to the GTA being at a lower concentration. Untreated, VCL and LCL scaffolds were incubated in DMEM+ media at 37°C for up to seven days, in order to test the scaffold mechanical stability as seen in **Figure 3.6**. After day 3, it became difficult to observe untreated scaffolds, 2h or 4h VCL scaffolds due to these scaffolds completely disintegrating in media.

This indicates that 2h and 4h VCL scaffolds were not mechanically stable and longer crosslinking is required. Greater stability was observed for scaffolds with 6h and 24h VCL and LCL scaffolds throughout incubation. For these reasons, effect of crosslinking was investigated on only 6h and 24h VCL and LCL scaffolds.

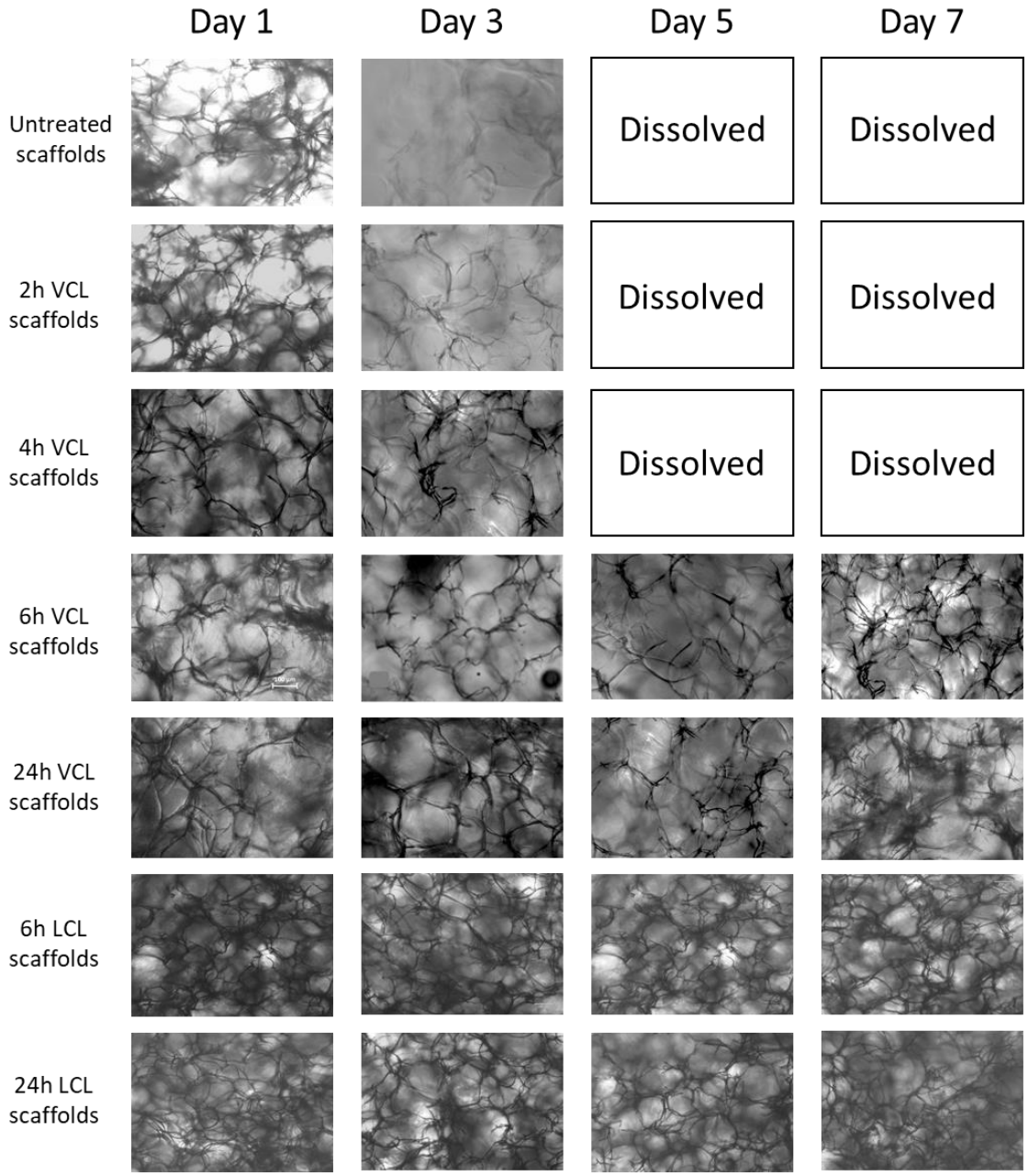

Figure 3.6: Brightfield images showing untreated (control) scaffolds and scaffolds VCL for various times, while incubating in media. Images were taken on day one, three, five and seven of incubation. Scale bars indicate 200 µm, n=9.

3.4.2.2 Effect of crosslinking on pore size

Difference in pore size between VCL and LCL was determined through brightfield imaging, shown in **Figure.3.7**. These images showed no visual difference between pore size of these scaffolds, after VCL or LCL the scaffolds were similar regardless of the length of crosslinking, or the type of crosslinking (liquid or vapour), this data is quantified in **Figure.3.8.**

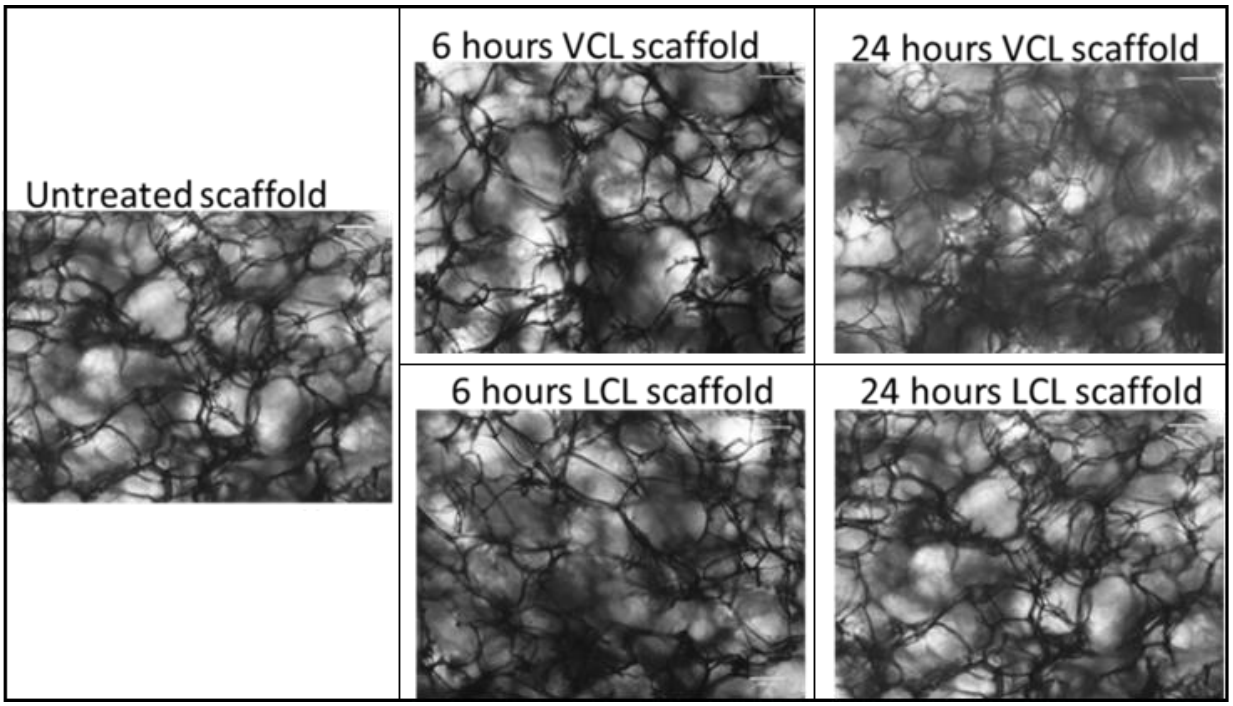

Figure 3.7: Brightfield images of scaffolds subject to different crosslinking treatments. Scaffolds shown are: untreated (control), 6h and 24h vapour crosslinked (VCL), and 6h and 12h liquid crosslinked (LCL). Images were taken after crosslinking and freeze-drying the scaffolds. Scale bar 200 µm, n=9.

Pore sizes of scaffolds from different lengths of VCL (6h and 24h) and LCL (6h and 24h) were quantified from images with Image J. There was no significant difference in scaffold pore size between crosslinking type and length of crosslinking when compared to the untreated control

(p: 0.78). This indicates that crosslinking may have no effect on pore size and the variation is retained.

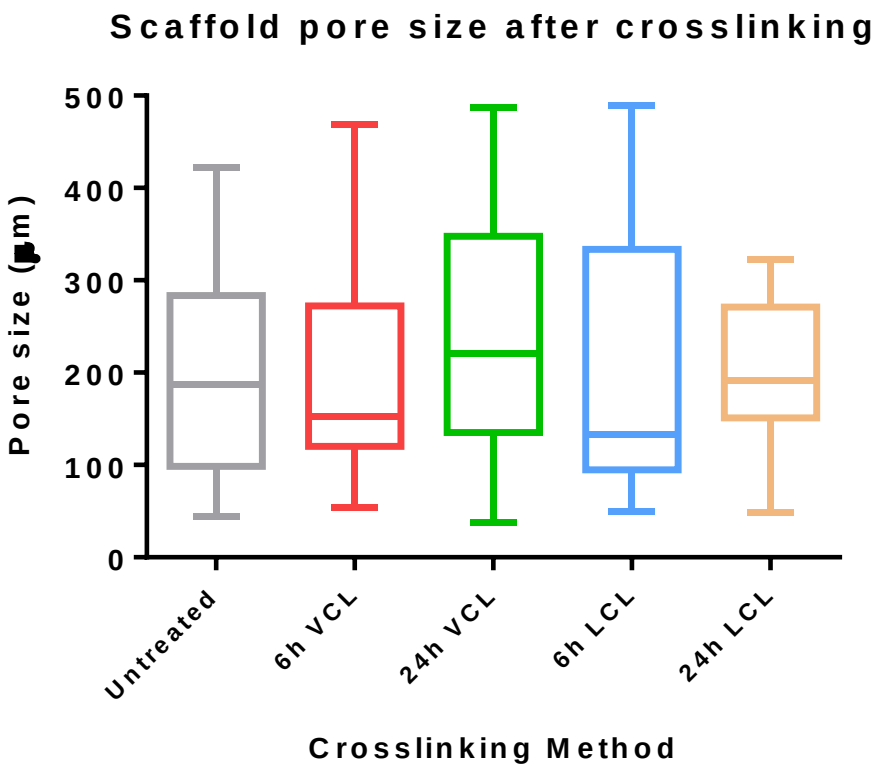

Figure 3.8: Pore sizes of scaffolds after different crosslinking methods. A box and whisker plot showing the distribution of pore sizes for scaffolds subject to VCL (6h and 24h) or LCL (6h and 24h), with an untreated scaffold serving as control. Average pore sizes: 200, 191, 232, 199, 200, n=24

3.4.3 Effect of crosslinking on cytotoxicity

Before any cell culture experiments, the cytotoxicity of VCL and LCL scaffolds was measured after crosslinking for 6 hours and 24 hours. To test scaffold cytotoxicity, scaffolds were placed onto confluent cell monolayers (previously cultured for three days) in a 48 well plate, and

incubated for two days with scaffolds and then imaged with brightfield microscopy. Untreated scaffolds and cells on TCP were also cultured as control groups (**Fig.3.9**).

Wells with LCL scaffolds had a large number of dead cells which detached from the culture surface, with other attached cells adopting a stressed rounded morphology. For VCL scaffolds, the majority of cells were still viable after three days, still attached and retained confluency.

The samples seen in **Figure 3.9** were tested with the alamarBlue cell viability assay to quantify any changes in cell viability. Results showed that there were changes in cell viability when exposed to LCL scaffolds, this data is shown in **Figure 3.10**. Cells exposed to LCL scaffolds (both 6h and 24h crosslinking) had significantly decreased viability than all other conditions (the two controls and VCL scaffolds), tested with two-way ANOVA ($p: <0.0001$). There was no significant change in cell viability when exposed to VCL scaffolds when compared to control ($p: >0.5$).

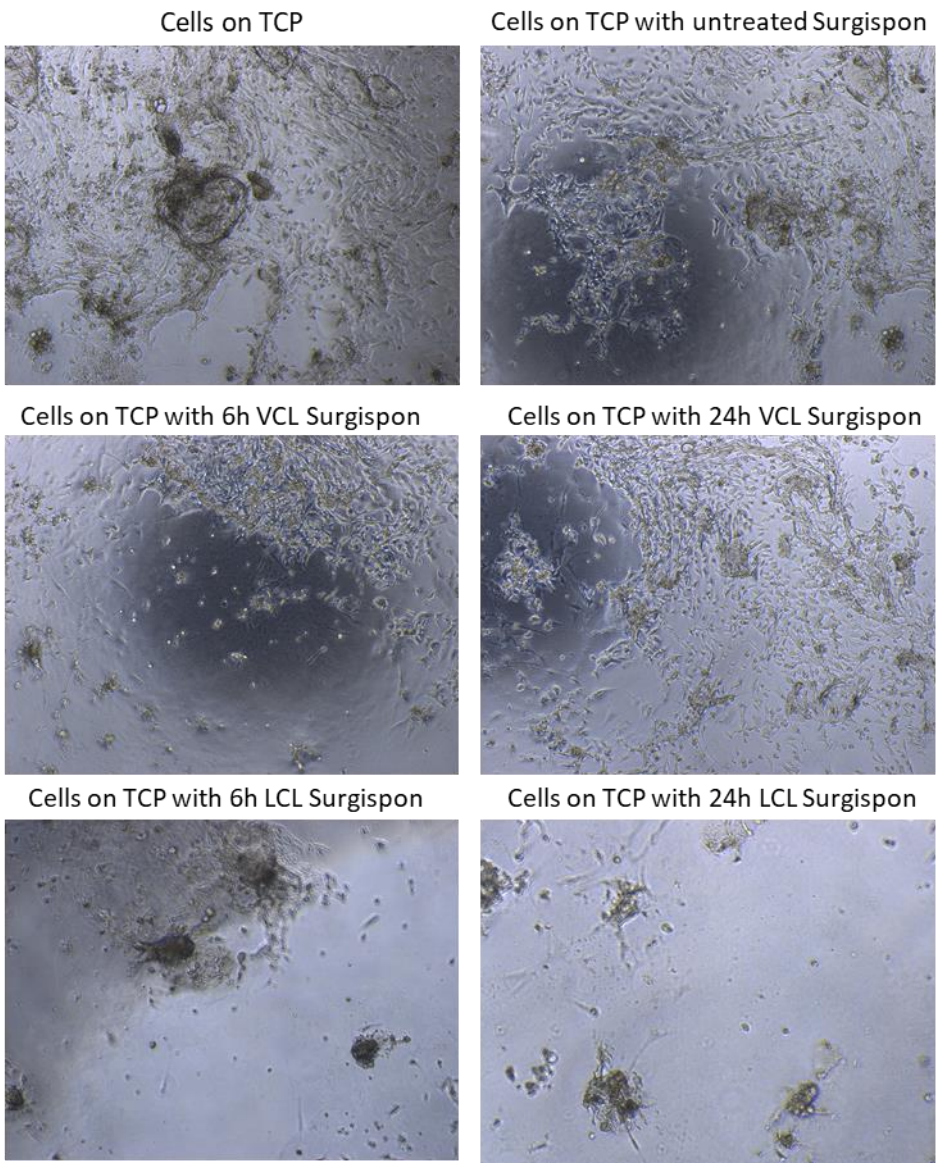

Figure 3.9: Cytotoxicity testing of VCL and LCL Surgispon scaffolds. To investigate the toxicity of any possible residual GTA, 6h and 12h VCL and LCL scaffolds were compared with TCP and untreated scaffolds used as control. After three days cell culture, scaffolds were placed onto cells and cells were cultured 2 more day and images were taken after scaffolds removed. (untreated scaffolds had dissolved), n=9.

Due to the high level of cytotoxicity of LCL scaffolds and the lack of a significant effect when using VCL scaffolds, VCL crosslinking was chosen as the prefereable Surgispon crosslinking method for the rest of the project.

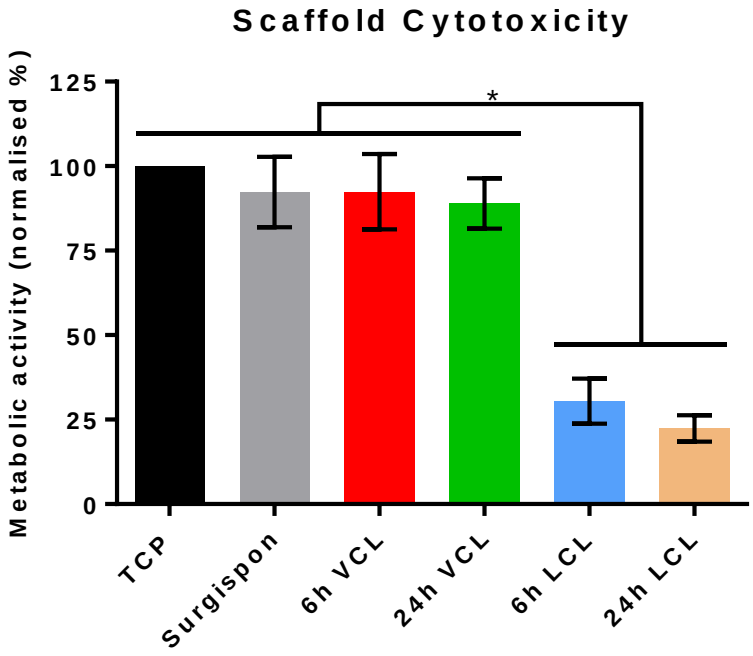

Figure 3.10: Effect of different scaffold crosslinking methods on cell viability activity. The viability data from alamarBlue assays was normalised, with crosslinking methods compared to tissue culture plastic (TCP, black bar) and untreated scaffold (grey bar) as controls. *: $p<0.0001$, n=9

3.4.4 Effect of VCL on scaffolds

3.4.4 1 Effect of crosslinking on relative scaffold weight

VCL scaffolds were crosslinked for 6h or 24h and were weighed before, during and after incubation in water (**Fig.3.11**) or standard cell culture media (DMEM+ media) (**Fig.3.12**) for 3, 5 and 10 days. Untreated scaffolds were used as a control group, but disintegrated after 3 days incubation.

In water, both 6h and 24h VCL scaffolds were stable over the 10 days incubation. This demonstrates significantly greater structural integrity than untreated scaffolds, which

dissolved into solution by day 3 (p: <0.0001). 6h and 24h VCL scaffolds initially decreased in weight by day 3, and then either gradually increased in weight (6h VCL) or stabilised (24h VCL), but this is a trend and overall, there was no significant weight change for 6h or 24h VCL scaffolds over the course of incubation (p: >0.5). However, 6h VCL scaffold weight was significantly lower on day 3 (p: <0.0001) compared to 24h VCL scaffolds, indicating that the 24h VCL protocol may exhibit improved structural integrity with the least change in weight over time.

Overall, VCL scaffolds demonstrated structural integrity in solution, as opposed to untreated scaffolds that dissolve within a few days. To test VCL scaffold suitability for cell culture these scaffolds were also incubated in DMEM+ media (**Fig.3.12**).

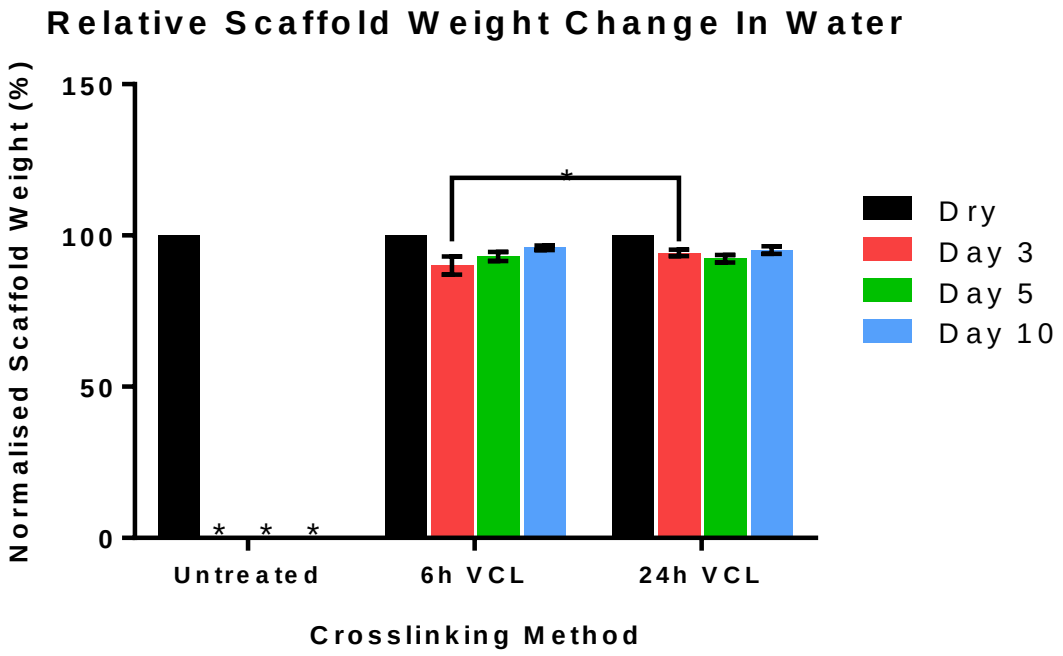

Figure 3.11: Change in VCL scaffold weight after incubation in water. Untreated scaffolds were used as a control group and dissolved into solution by day 3. 6h VCL and 24h VCL scaffolds are compared over days 3, 5 and 10 of incubation in water. *: p<0.0001, n=4.

Both 6h and 24h VCL scaffolds were stable in DMEM+ media conditions, unlike untreated scaffolds which again dissolved into solution by day 3. Both 6h and 24h VCL scaffolds increased in weight from day 3, potentially due to serum proteins adsorbing to the scaffolds.

24h VCL scaffolds displayed a significantly greater increase in weight when compared to 6h VCL scaffolds on day 10 (p: <0.0028). Both VCL conditions have demonstrated mechanical stability in DMEM+ media, the solution they will be incubated in across the long term in order for cell culture to occur, making this a relevant comparison.

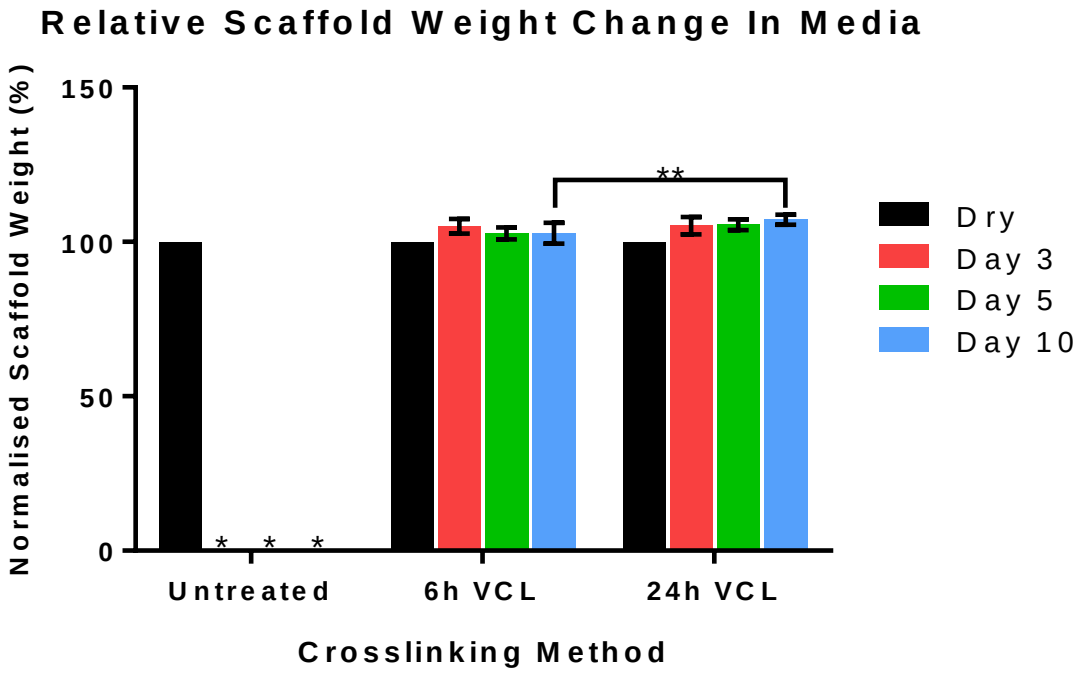

Figure 3.12: Change in VCL scaffold weight after incubation in DMEM+ media (containing serum). Untreated scaffolds were used as a control group and dissolved into solution by day 3. 6h VCL and 24h VCL scaffolds are compared over days 3, 5 and 10 of incubation in DMEM+ media. *: p<0.0001, **: p<0.01, n=4.

After 24 VCL crosslinking, Surgispon scaffolds maintained structural integrity for over 10 days in both water and serum-containing cell culture media. Longer incubation times, up to 60

days, were tested with 24h VCL scaffolds. This long-term mechanical stability experiment was tested with incubation of scaffolds in water (same conditions as **Fig.3.11**), DMEM or DMEM+ media (same conditions as **Fig.3.12**), as seen in **Figure.3.13**.

The 24h VCL scaffolds were stable in solution for the whole 60 days. In water scaffolds generally lost ~5% of their weight, but these changes were not significant (p: >0.1 for all comparisons) over the 60 days. In DMEM, scaffolds generally increased in weight by 2-4%, but again these changes were not significant and represented a trend over the 60 days (p: >0.1 for all comparisons). In DMEM+ (full cell culture media), scaffolds generally increased in weight by 5-9%, these increases in weight were significant from days 10-60 (p: <0.01 for these cases). This significant increase in DMEM+ is again most likely to serum proteins adsorbing to the scaffold.

Scaffolds incubated in either DMEM or DMEM+ solutions exhibited significant increases in weight when compared to scaffolds incubated in water, for days 1-60 (p: <0.001 for all comparisons). Scaffolds incubated in DMEM+ solutions exhibited significant increases in weight compared to DMEM-incubated scaffolds from days 10-60 (p: <0.05 for these cases). Overall, it is clear that the VCL protocol allows Surgispon scaffolds to maintain structural integrity over the long term (shown up to 60 days).

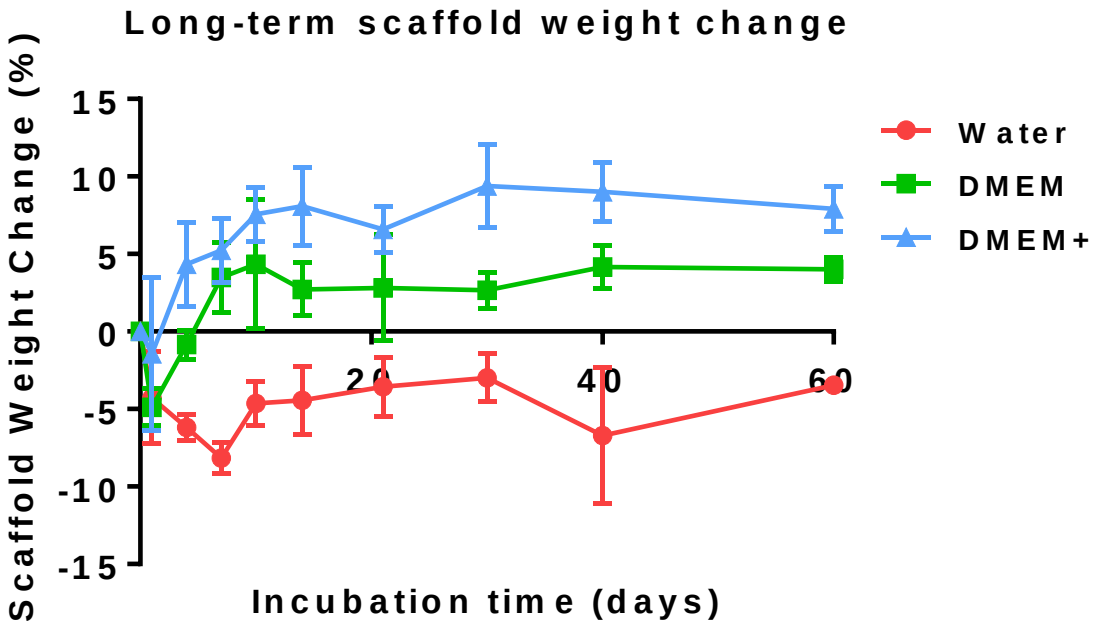

Figure 3.13: Effects of long-term scaffold incubation in water, DMEM or DMEM+ media (DMEM+FBS) over 60 days. 24h VCL scaffolds had previously been tested over 10 days, a longer time frame of 60 days is more realistic for potential future applications. The largest change in weight was observed in DMEM+ media conditions.

3.4.4.2 Effect of crosslinking on relative scaffold diagonal length

As well as scaffold weight, scaffold diagonal length was measured for both 6h and 24h VCL before, during, and after incubation in DMEM+ for 10 days to investigate the effect of crosslinking on scaffold expansion in solution **(Fig.3.14).** Both 6h and 24h VCL scaffolds decreased in size by day 1 and then increased in size thereafter (days 3, 5 and 10). There was no significant difference in scaffold diagonal length change between 6h and 24h VCL scaffolds (p: 0.164), but both scaffolds were significantly larger by days 5 and 10 when compared to day 0 (p: <0.0001 for all cases). 6h VCL scaffolds increased in size by 18.6% and 24h VCL scaffolds increased in size by 13.8%. This difference may be due to the longer crosslinking protocol leading to a tighter scaffold and more resistance to expansion in solution.

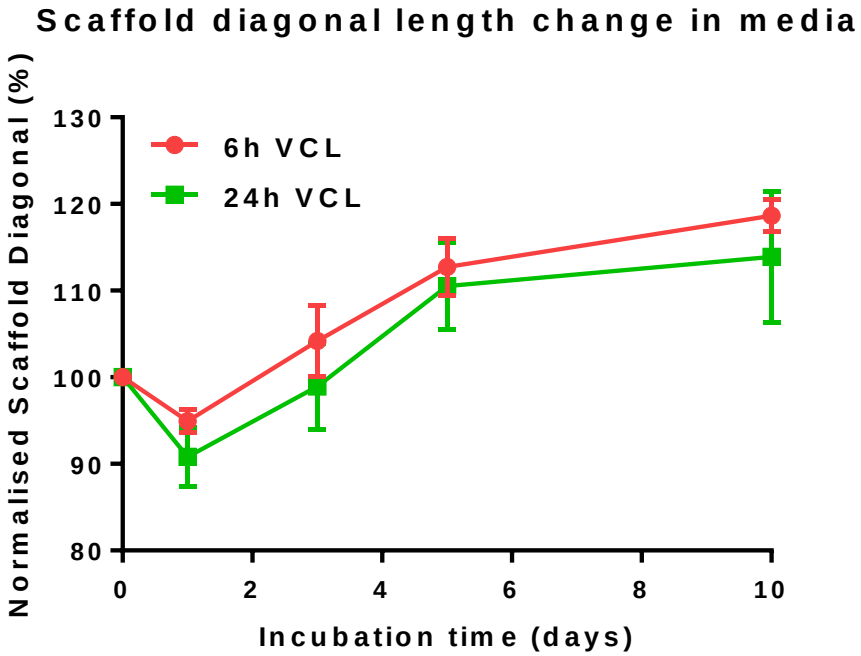

Figure 3.14: Change in diameter of 6h and 24h VCL scaffolds during incubation in DMEM+. Incubation time shown on x axis (days) and scaffold diameter is shown on y axis (mm). Both 6h (blue) and 24h (orange) VCL scaffolds showed a decrease first and then an increase in diameter but 6h scaffolds showed a larger end diameter size when compared to 24h scaffolds over 10 days.

3.4.4.3 Effect of crosslinking on scaffold pore diameter after incubation

Untreated scaffolds and 24h VCL were incubated in DMEM+ media for 24h, 36h or 48h, and the pore diameter was measured through analysis of brightfield images with ImageJ (**Fig.3.15**). A dry 24h VCL scaffold was included as a control. The effect of incubation time on the scaffold pore size was borderline not significant (p: 0.06), with the mean pore size across each condition as follows: 196 µm (untreated), 192 µm (24h VCL, dry), 197 µm (24h VCL, 24h DMEM+ incubation), 205 µm (24h VCL, 36h DMEM+ incubation), 219 µm (24h VCL, 48h

DMEM+ incubation). This data shows that untreated scaffold pore size is consistently ~200 µm (as in **Fig.3.4**), and 24h VCL does not significantly affect pore size (as in **Fig.3.8**).

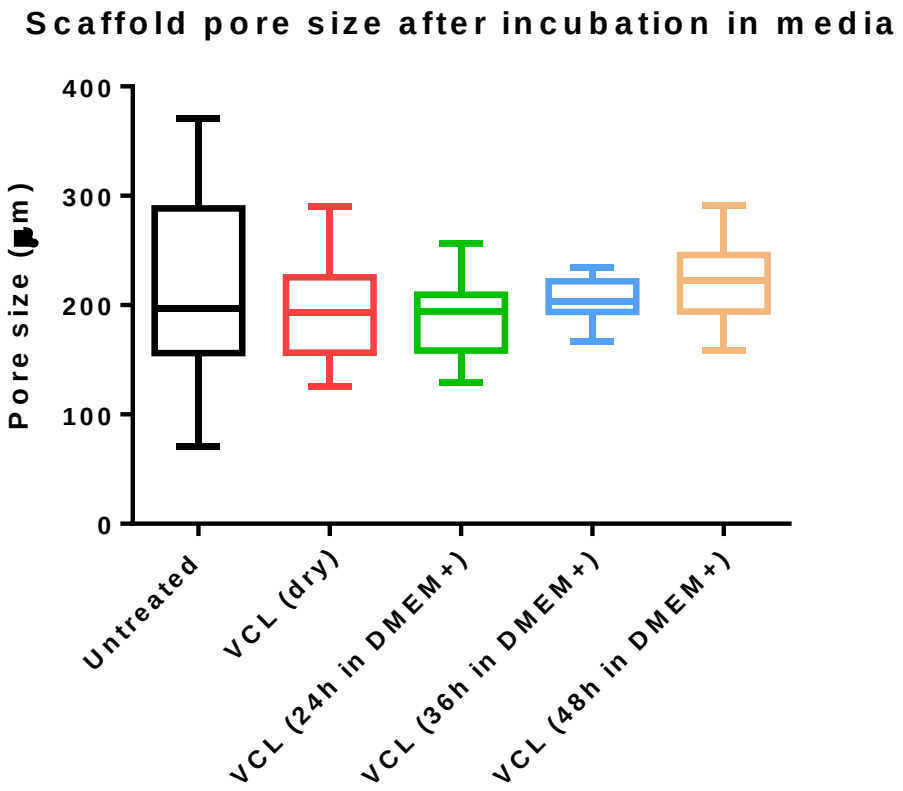

Figure 3.15: Scaffold pore size distribution after 24h VCL and different lengths of incubation (24-48h). Pore sizes ranged from 50 um to greater than 400 µm, with the frequency of these pore sizes shown for uncrosslinked, 24h VCL (dry), and 24h VCL after various lengths of incubation in media.

3.4.5 Surgispon pore interconnectivity/gas porosity analysis

The average pore size and the distribution of pore was analysed by applying direct 3D analysis with the Scanco µCT (micro computed tomography) package. This imaging package took many 2D slice images (tomographs) of a 3D Surgispon sample and produced 3D images, as seen in **Fig.3.16.**

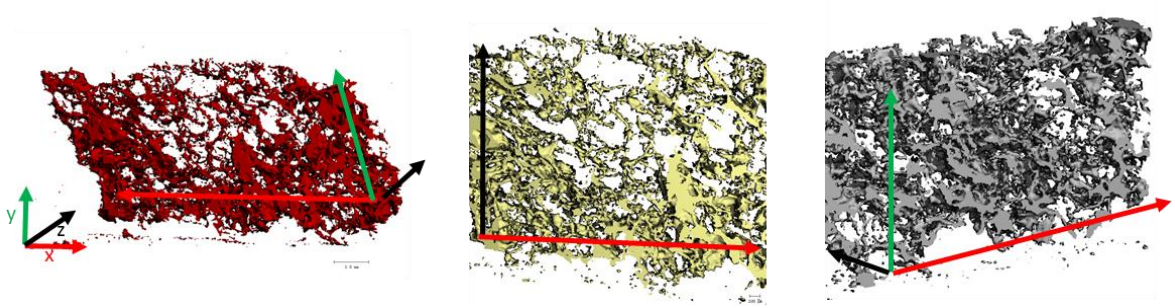

Figure 3.16: 3D µCT scan images of Surgispon scaffolds. Images were taken after 3D analysis was performed, showing the porosity and interconnectivity of pores.

The porosity of Surgispon was also calculated through the Scanco package. Firstly, the total volume (volume of Surgispon as a non-porous solid cube) and object volume (actual volume of Surgispon, not measuring the airspaces) were measured. The porosity of Surgipon was calculated by subtracting the object volume from the total volume, obtaining the unoccupied volume (the airspace), and dividing this unoccupied volume by the total volume. This analysis also calculated average pore size and whether or not pores are interconnected. Results from this analysis showed that Surgispon has a porosity of 93% and an average pore sizes were 231.35 µm, with these pores being interconnected.

Surgispon scaffolds were also imaged with confocal microscopy to investigate 3D structure and pore interconnectivity. No fluorescent labels were needed due to scaffold autofluorescence. Optical sections of Surgispon were taken and 3D images generated as seen in (**Fig 3.17**). These images show the high porosity of Surgispon.

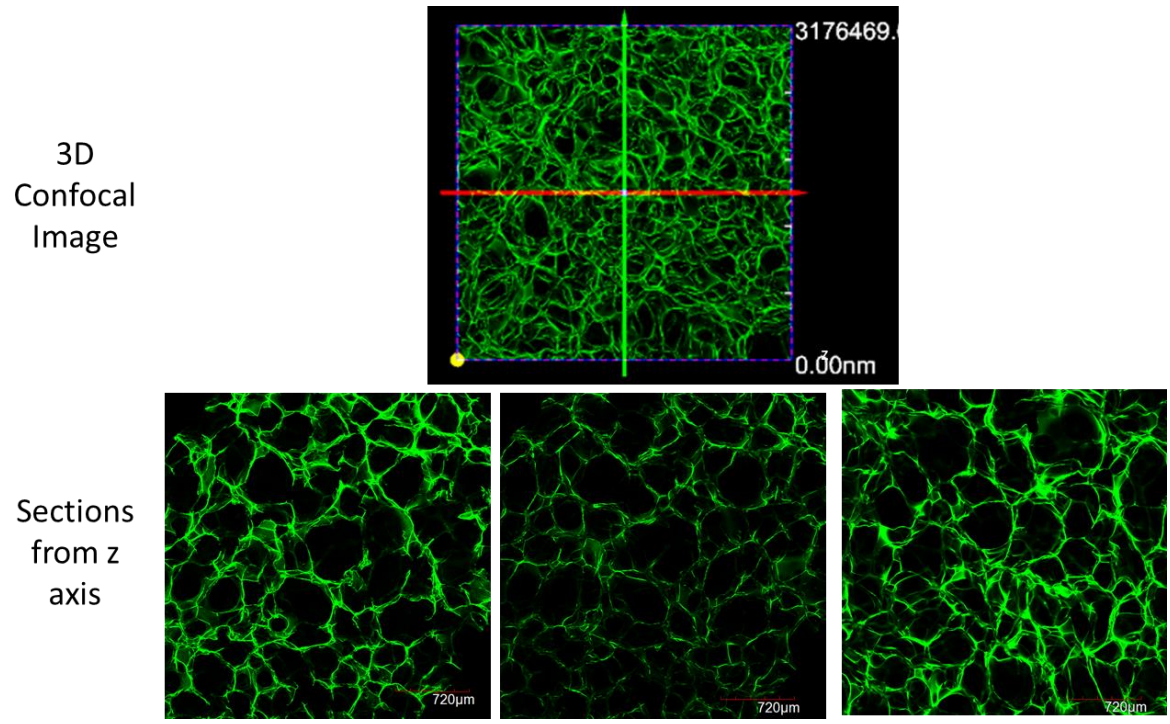

Figure 3.17: 3D confocal microscopy images of Surgispon scaffolds. Images show XYZ in different orientations and different optical sections from the z plane. Images clearly indicate a high level of porosity and pore interconnectivity.

3.4.5 Comparing Surgispon with primary lung tissue

24h VCL scaffolds were cultured with A549 cells for 7 days, and then stained with LIVE/DEAD assay. Scaffolds with cells were visually compared to porcine lung tissue slices, labelled with DAPI (**Fig 3.18**). This comparison showed visual similarity between Surgispon and lung tissue in terms of pore size and cell attachment around the pore perimeter in 3D.

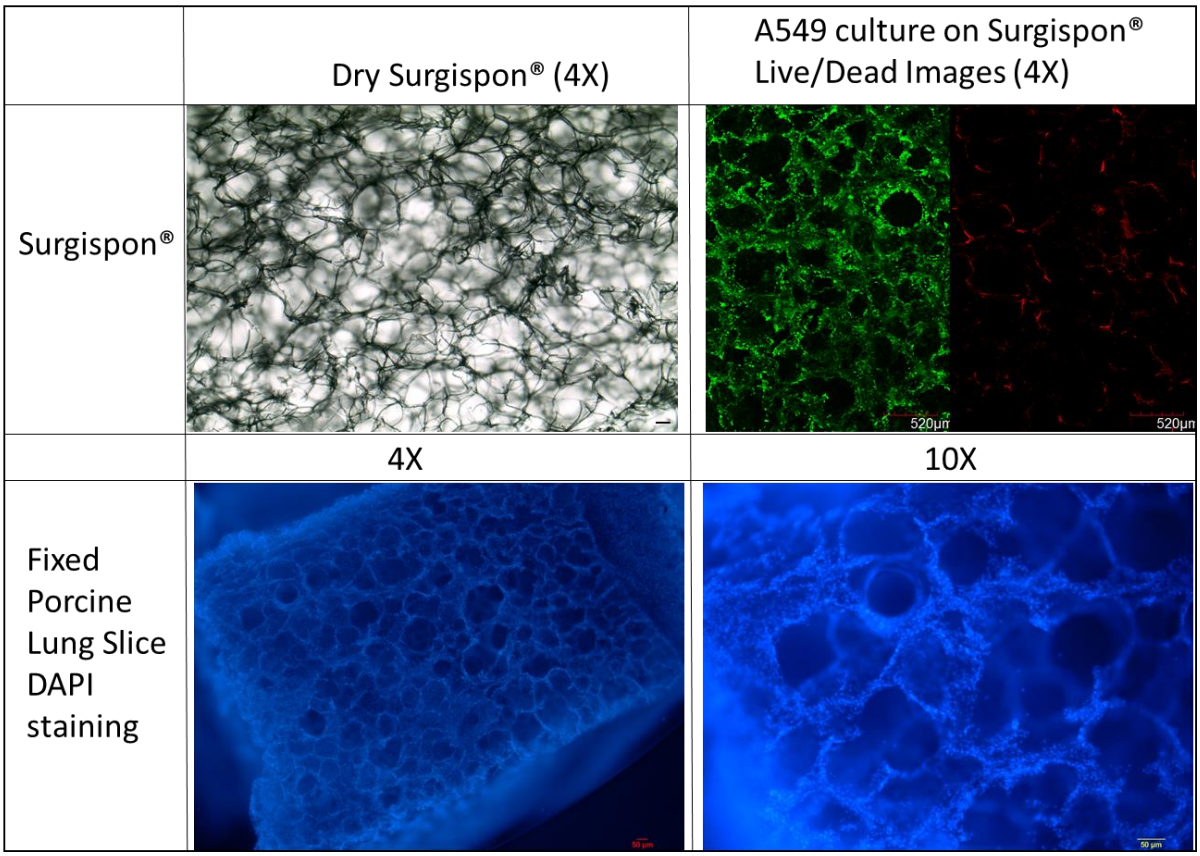

Figure 3.18: Images of Surgispon scaffolds vs fixed porcine lung slices Dry scaffold images and fluorescence images of scaffolds after 7 days of A549 cell culture are compared with fixed porcine lung tissue images to show the similarity between the scaffold and the lung tissue.

3.5 Discussion

The diameter of a single alveolus is ~200 µm on average (Ochs et al., 2004), pores in Surgispon scaffolds are similar in diameter to a single alveolus, measuring 223.92 µm on average. There is a range of pore sizes available in Surgispon, similar to the range of diameters (~200-500 µm) ("Berne & Levy Physiology) and range of alveolar geometric shapes (Hyde et al., 2004) *in vivo,* this supports the role of Surgispon as an alveolar mimic. These pores in Surgispon are also interconnected (**Figs 3.16 and 3.17**), meaning Surgispon could potentially create alveolar-like structures for lung cells. Previous studies using porous scaffolds have shown that pore size between 150-500 µm is preferable for cell attachment. However, 150-250 µm pore size showed higher tissue regeneration (Zhang et al., 2011a). The overall preference for pore size for a cell-based alveolar-like scaffold is therefore 150-250 µm, meaning that Surgispon scaffolds with the average pore size of ~223 µm has the potential to make an ideal model at this scale.

Native untreated Surgispon lacks stability, as seen in **Figure 3.5**. After three days of incubation in solution, it loses its structural integrity and dissolves/disintegrates, this period of time is not sufficient for cells to replace the scaffold with their extracellular matrix. Synthetic crosslinking improves the stability of the scaffold (Ahmed, 2015), and crosslinking Surgispon with GTA vapour resulted in much improved structural integrity (**Fig.3.6**), allowing incubation in solution for over 60 days. This crosslinking process is therefore performed on all subsequent scaffolds used in this project. Liquid crosslinking also displayed promising stability but cytotoxicity tests indicated the likely presence of residual GTA and its accompanying toxicity (**Figs 3.9 and 3.10**). GTA is widely used for crosslinking collagen-based materials such as gelatine sponges like Surgispon, but use of GTA as a liquid solution is linked to potential

cytotoxicity, and as scaffolds are absorbent some residual GTA solution (for LCL) may remain even after the washing stage. However, when using GTA in vapour phase for VCL, it is both easier to clear from the scaffolds, and more effective with working with structures such as sponges (Peng et al., 2017). Based on this, only vapour crosslinked scaffolds were used for future experiments.

The crosslinking process did not affect the average pore size, as seen in **Figure 3.8**, where the average pore size after VCL was 192-232 μm, similar to untreated scaffolds. Images from brightfield microscopy show that after crosslinking, the microstructure is the same as untreated scaffolds, and both conditions are still similar to the structure of the alveolus, as seen in **Figure 3.17**.

The minimum time for VCL was 6 hours, with crosslinking for less time resulting in degradation in solution (**Fig.3.6**). Crosslinking for 24 hours with GTA vapour allowed scaffolds to retain structural integrity over the long term, up to 60 days of incubation in cell culture conditions (**Fig.3.13**). During these incubations in cell culture media, an increase in weight was observed, this is most likely related to proteins contained within the FBS component of DMEM+ media adsorbing to the scaffold surface. This could be tested with some future work, by incubating the scaffolds in just FBS and measuring the weight gain over the long term compared to DMEM+. Alternatively, electron microscopy could be used to look for surface changes on the Surgispon before and after incubation, or the scaffolds could be broken down and tested via spectroscopy to determine the presence of different proteins (other than gelatine and collagen).

Surgispon is made from collagen-derived materials, with collagen shown to promote adhesion of serum proteins *in vitro*, potentially due to a similarity to the ECM *in vivo* (Koblinski et al.,

2005). Scaffolds incubated in serum-free DMEM also underwent a ~5% change in weight, the scaffolds weigh approx. 1-3 mg and this 5% corresponds to a change of 50-150 µg. It is possible that the salts, sugars, amino acids and other components of DMEM may contribute to this weight gain, but otherwise the reason is unknown. Degradation tests were also performed in water, and no weight gain was observed (**Figs 3.11 and 3.13**).

Scaffolds crosslinked for 24 hours had reduced levels of expansion than 6 hours (**Fig 3.14**, although an observed trend as this was non-significant). This is most likely due to increased crosslinking causing additional structural rigidity and less ability to expand/contract, as seen in previous studies (Hutchins et al., 2017). However, as this reduced expansion was not significantly different to 6h VCL scaffolds, and 24h crosslinking was used for future experiments due to the increased convenience for experimental design. Highly crosslinked sponges exhibit less swelling due to less water absorption, but also exhibit high material hardness, suitable for bone models but not for a soft tissue alveolar model. Further crosslinking of Surgispon would have led to less expansion during incubation in solution, but would have decreased the relevance of the scaffold as a lung model due to the stiffer matrix composition (Yang et al., 2018). In order to test the mechanical properties of Surgispon further, the Young's modulus and stiffness of the scaffold should also be measured and compared to the lung microenvironment, and also to see if there are any differences between 6 and 24 hour VCL in terms of Surgispon stiffness.

3.5.1 Limitations

GTA was chosen for crosslinking as it is easy to use and effective. Other options for crosslinking could have been investigated, gelatine sponges such as Surgispon could also be crosslinked using UV radiation, dehydrothermal methods, and using other chemicals as an

alternative to GTA such as genipin (GP, a planet-derived substance that crosslinks in a similar manner to GTA but stains scaffolds a dark blue pigment), 1-ethyl-3-(3-dimethyl aminopropyl) carbodiimide (EDC, free carboxylic and amine groups react to form amide bonds), and microbial transglutaminase (mTG, an enzyme that catalyses acyl transfer reactions and links glutamine and lysine residues) (Yang et al., 2018). GTA was chosen due to its widespread use, cost-effectiveness, previous use in the lab and general ease of use. However, exploring other crosslinking options may have been beneficial.

As crosslinking can increase the stiffness of scaffolds, more thorough mechanical testing of scaffolds would be advantageous in order to determine the Young's modulus of uncrosslinked scaffolds, and to see any changes in matrix stiffness with different crosslinking methods and durations. This would in turn be best linked to lung alveolar microenvironent stiffness *in vivo* to ensure that the Surgispon is a suitable mimic, as cells react to the stiffness of the growth surface (Liu et al., 2010; Melo et al., 2014)

Pore interconnectivity was investigated via uCT, however gas permeability assays were not explored on scaffolds. Gas permeability could be tested with devices such as a syringe pump in order to quantify the gas permeability through a layer of Surgispon (Kasai et al. 2016). Gas permeability is an important characteristic of porous scaffolds and is linked to pore size (Han et al., 2020), and should be investigated and quantified for Surgispon scaffolds.

Surgispon morphology should be investigated with scanning electron microscopy (SEM), especially visualising the pore size, area, morphology and distribution throughout each Surgispon scaffold in slices from top to bottom, in order to determine if the pores are uniform throughout each scaffold and how they can change throughout the 3D space. This could also be done to investigate the effects of different crosslinking methods, and the effect of

incubation in different solutions (water, DMEM, DMEM+) after crosslinking. However, it should be noted that Surgispon samples are challenging to slice in order to take images throughout the 3D structure, the Surgispon porosity is high and the gelatine walls are thin. When slicing was attempted in both frozen scaffolds on a microtome or wax embedded scaffolds, the scaffolds broke down, in addition the pressure of slicing would likely damage or change the pore structure. Access to SEM and other high-resolution imaging equipment was also limited during this project.

Other imaging techniques could be used to increase the contrast when imaging Surgispon scaffolds, such as phase contrast imaging or experimenting with different non-toxic contrast agents. Throughout this chapter most images were taken with a brightfield microscope and it can be challenging to see scaffold microstructure, cells, and different planes. When imaging in 3D without a confocal microscope, there is always the effect from out-of-focus light from above and below the imaging plane, this can affect image quality. Use of a confocal microscope would result in clearer images, but there was limited access and technical issues (such as filters and hardware reliability) with confocal microscopy throughout this project.

3.5.2 Conclusion

The main aim in tissue engineering is creating a scaffold that can mimic the body's own extracellular matrix (ECM) which would allow cells to attach, proliferate and function. Collagen-based porous scaffolds are used for regeneration of skin, cartilage, bone, nerve, liver, and lungs (Freyman et al., 2001). GTA crosslinking has been shown to increase the biostability of such collagen-based porous scaffolds, as collagen is a water-soluble material (Ma et al., 2003). GTA-treated scaffolds have shown good cytocompatibility, with effective cell attachment and cell proliferation on scaffolds. Further *in vivo* animal study also showed

that these scaffolds support and accelerate cell migration from the surrounding tissue (Ma et al., 2003).

We have demonstrated that the porous gelatine-based Surgispon is a good potential candidate for a tissue engineering scaffold for cell-based research into lung structure, function and disease (such as COPD). Surgispon scaffolds showed good response to crosslinking, with the 24h VCL protocol allowing for a robust scaffold for long-term cell culture experiments while remaining non-toxic and having high structural integrity in solution, along with the ability to expand in size over time in solution. This work highlights Surgispon as a candidate material for future tissue engineering work.

Chapter 4

Investigating 3D cell culture on Surgispon® scaffolds for lung tissue engineering

4.1 Introduction

4.1.1 Lung Anatomy

The lungs are the primary organs of respiration in the human body. They are responsible for taking oxygen into the blood and removing carbon dioxide. The lungs are situated on either side of the heart and other mediastinal contents (Abel et al., 2006). Each lung is free in its pleural cavity, except for its attachment to the heart and trachea at the hilum and pulmonary ligament respectively. When removed from the thorax, a fresh lung is spongy, can float in water, and crepitates when handled, because of the air within its alveoli. It is also highly elastic and so it retracts on removal from the thorax. Its surface is smooth and shiny and is separated by fine, dark lines into numerous small polyhedral domains, each crossed by numerous finer lines, indicating the areas of contact between its most peripheral lobules and the pleural surface (Mehta *et al.,* 2015).

4.1.2 Alveolar Structure

Alveoli are thin-walled respiratory surfaces that are distributed as isolated patches within the walls of respiratory bronchioles, as tube-like alveolar ducts and as groups of adjacent balloon-like alveolar sacs (Kurz *et al.,* 2015).

The alveoli provide the respiratory surface for gaseous exchange (**Fig. 4.1**). Their walls contain two types of epithelial cell (pneumocytes) and cover a delicate connective tissue within which a network of capillaries spreads out. Since the walls are extremely thin, they present a minimal barrier to gaseous exchange between the atmosphere and the blood in the capillaries. Adjacent alveoli are frequently in close contact, and the intervening connective tissue forms the central part of an interalveolar septum. The human respiratory tract contains

nearly 50 different cell types along its hierarchical structure (Breeze and Wheeldon, 1977) in distinct proximal (conducting) and distal (respiratory) zones (Klein et al., 2011).

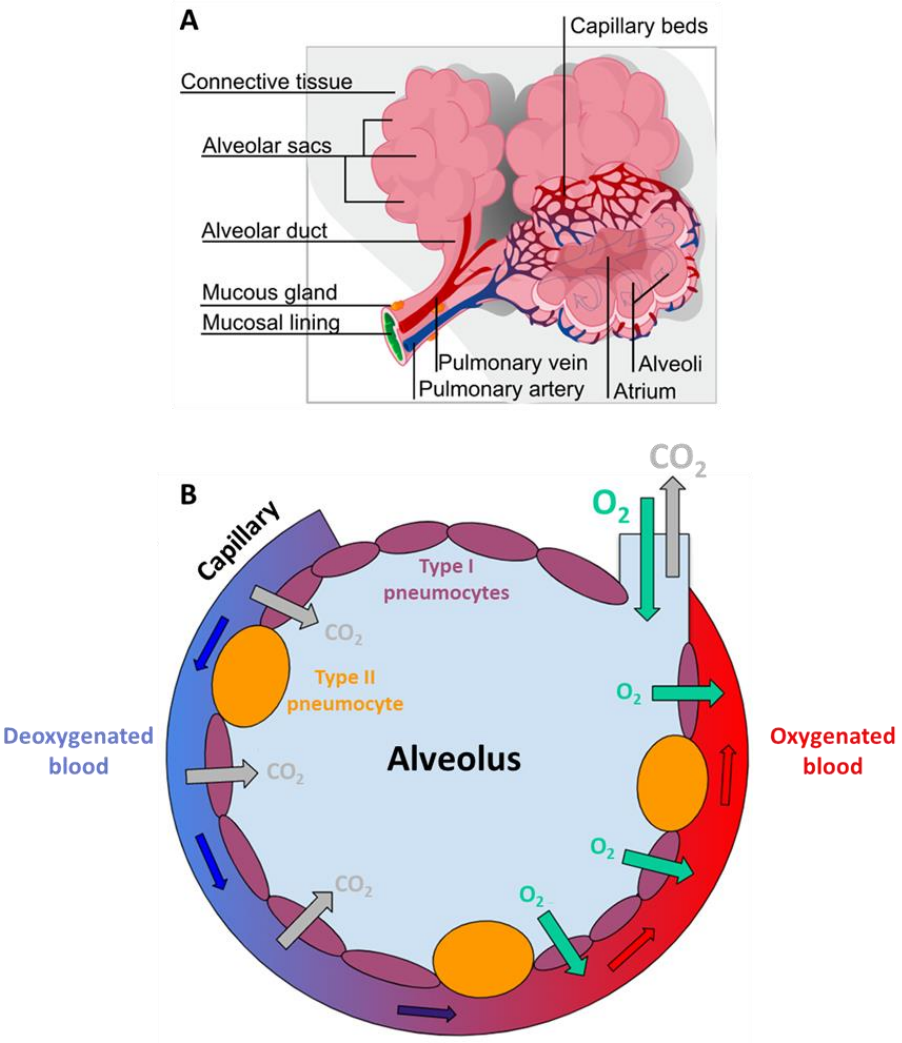

Figure 4.1: A diagram showing the lower respiratory system. A) A collection of alveoli, showing how each are surrounded by capillaries from the pulmonary system. B) A cross-section diagram of a single pulmonary alveolus. Alveoli are the site of gas exchange, giving oxygen and removing carbon dioxide from capillaries that surround each alveolus. These structures are made up of type I and II pneumocytes.

The alveolar epithelium is a mosaic of types I and II pneumocytes. Type I pneumocytes are simple squamous epithelial cells and form over 90% of the alveolar area (**Fig. 4.2**). Their basal laminae fuse with the basal laminae of the adjacent capillary endothelium to form the thin

portions of interalveolar septa. Their cytoplasm is thin (0.05–0.2 μm) which facilitates gaseous diffusion between the lumen of the alveolus and its capillaries. The edges of adjacent cells overlap; they are joined by tight junctions, creating a strict diffusion barrier between the alveolar surface and underlying tissues. Together with a similar endothelial barrier, this arrangement limits the movement of fluid from blood and interstitial spaces into the alveolar lumen (the blood–air barrier). If damaged, type I cells, which do not divide, are replaced by type II cells, which proliferate and differentiate into type I pneumocytes. The smaller type II cells are often more numerous than type I cells, but they contribute less than 10% of the alveolar surface area. They are rounded cells and protrude from the alveolar surface, particularly at the angles between alveolar profiles. In the human lung they are often associated with interalveolar pores of Kohn. Their cytoplasm contains numerous characteristic secretory lamellar bodies consisting of concentric whorls of phospholipid-rich membrane, the precursors of alveolar surfactant, which they can recycle (Schreiber et al., 2005b).

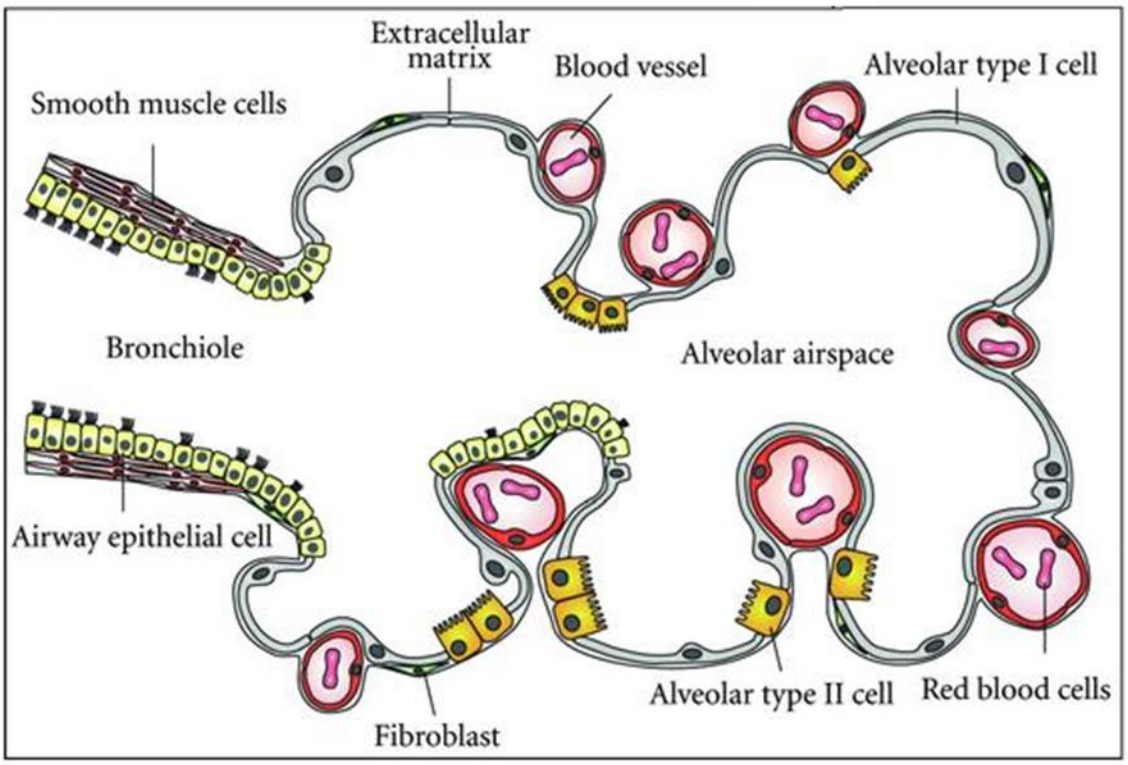

Figure 4.2: Cross-section of the alveolar region. Continuous layer of epithelial cells (type I and type II) form the alveolar surface. Fibroblasts are the main structural cells and produce the extracellular matrix (modified from (Hollenhorst et al., 2011).

The alveoli structure must be resistant to collapse, therefore alveoli feature inherent stabilizing factors such as surfactant, which protects alveoli structure and is the secretory product of type II alveolar epithelial cells. The other stabilizing mechanism is the connective tissue network system that consists of axial, peripheral and septal fibres (Knudsen and Ochs, 2018b). Cells, an extracellular network of elastic fibres, and bundles of banded collagen fibrils forming fibres are located in the bounded space between the capillary endothelial basal laminae and alveolar epithelial (Weibel, 1999). This space is called the interstitium and the main cell types that exist in this area are fibroblasts and myofibroblasts. While fibroblasts produce and maintain the extracellular matrix, myofibroblasts contain filaments oriented

across the interior of the alveolus, which not only connects the two epithelial walls of the alveolus, it also assists in bracing the interstitial space (Knudsen and Ochs, 2018b).

This intricate structure and balance of different cell types should be reflected and utilized in an *in vitro* model of the alveoli. This means that a successful *in vitro* therapy for alveolar replacement should involve multiple relevant cell types (including lung fibroblasts and epithelial cells) that can be cultured both in isolation and together; and a porous 3D structure that can serve as a scaffold for cells and is a physiologically relevant size to alveoli. In this chapter Surgispon® is used as such a scaffold, and is tested as a culture scaffold for lung epithelial and lung fibroblast cells.

Based on the work in **Chapter 3**, all Surgispon scaffolds in subsequent work are crosslinked for 24 hours with glutaraldehyde (GTA) vapour. These scaffolds showed no cytotoxicity towards A549 cells, and are stable in cell culture conditions for up to 60 days. These scaffolds are a promising material for cell-based lung tissue engineering studies as they have a similar pore size to alveoli. By culturing various biologically relevant cell types onto these Surgispon scaffolds, they can be further validated as a cell scaffold.

4.2 Aim

The aim of this study was to investigate 3D cell culture on Surgispon scaffolds, culturing lung epithelial A549 cells and lung fibroblast 35FLH cells in isolation and together as co-cultures.

a. Optimise cell seeding number on scaffold
b. Optimise cell metabolic activity assay(s) in order to determine cell attachment, proliferation and viability
c. Investigate possible chemical coatings that may affect cell attachment
d. Investigate co-culture of deactivated lung fibroblasts with lung epithelial cells

4.3 Method

The experiments in this chapter are summarised in **Schematic 4.1,** with all materials and methods for each experiment described in full in **Chapter 2**.

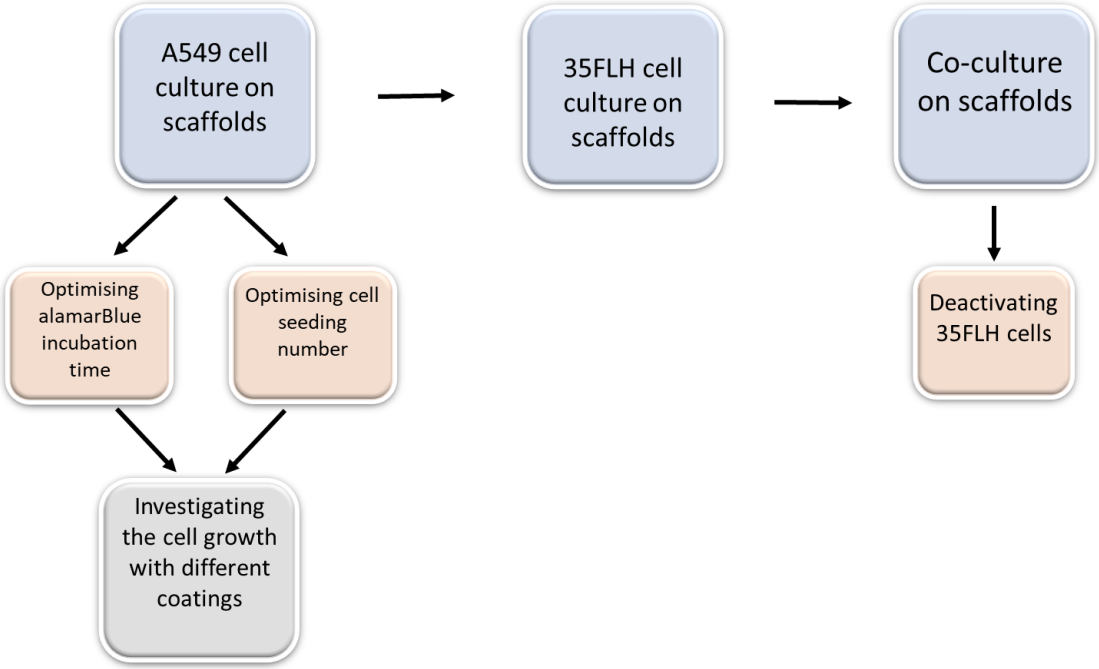

Schematic 4.1: A schematic to show the experimental design for chapter 4. This chapter involves culture of the A549 lung epithelial cell line and the 35FLH lung fibroblast cell line on Surgispon scaffolds, and the optimization of various cell metabolic activity assays in order to test cell growth and viability. Culture of A549 and 35FLH was done separately and as co-cultures in order to optimise cell seeding onto Surgispon scaffolds.

Unless otherwise stated, Surgispon scaffolds used in all cell culture experiments measured 5x5x2.5 mm^3, were crosslinked for 24 hours with GTA vapour and were sterilised. Crosslinking and sterilisation were done as described in **section 2.4**. Sterile scaffolds were placed into the wells of 48 well plates before seeding with cells.

4.3.1 alamarBlue™ standard curve

Before using alamarBlue in experiments, a standard curve was prepared. Cell suspensions of 600 cells/µl were prepared in DMEM+ media. Cells were seeded onto 48 well plates (tissue culture plastic or TCP) starting with 50 µl cell suspension in the first well and increasing by 50 µl until 500 µl, creating a range of cell numbers in different wells from 30,000-300,000 cells/cm^2. All samples were topped up to 500 µl DMEM+ media before incubation. After incubating the cells for 2 hours to allow cells to attach, the alamarBlue cell metabolic activity assay was applied to samples as previously described in **section 2.2.1** with suggested incubation time of 3 hours.

Another standard curve was also created, with cell numbers ranging from 1,500-150,000 cells/cm^2. After incubating the cells for 2 hours to allow cells to attach, alamarBlue cell metabolic activity assay applied to samples on day 0 and day 1 as previously described with suggested incubation time 3 hours.

4.3.2 Optimising cell seeding number for alamarBlue cell metabolic activity assay

In order to optimise the cell number for the alamarBlue assay a lower cell number range was prepared, from 1000-60,000 cells/cm^2. After seeding, all samples were topped up to 500 µl DMEM+ media and incubated for a minimum of 2 hours before starting any experiments to allow cells to attach. alamarBlue cell metabolic activity assay was applied to samples in triplicate every other day for up to seven days as previously described.

4.3.3 Optimising incubation time for alamarBlue cell metabolic activity assay

A cell suspension was prepared and cells were seeded as described in **section 4.3.1**. After cell seeding, cells were incubated for seven days. alamarBlue assays were applied to all samples on day seven. The first samples were incubated for 30 minutes, and every other sample was incubated for increasing time in 30 minute increments, with the longest incubation time being 3 hours.

4.3.4 Comparison of alamarBlue assay with MTT assay and trypsin cell count

To analyse the oversaturation of alamarBlue assays, samples were prepared as described in **section 4.3.2** and cultured for up to seven days. MTT assays were applied to samples on day 0 (seeding day), 1, 4 and 7 as described in **section 2.2.2**. These results were compared with alamarBlue assay results. Cell confluency was investigated by trypsinising the samples as described in **section 2.1.1,** and a cell count was performed by using the automated cell counter Countess™ (Invitrogen) as described in **section 2.1.4**.

4.3.5 Optimising cell seeding number for PicoGreen™ dsDNA assay

A cell suspension was prepared and cells were seeded as described in s**ection 4.3.1** and these samples were used to prepare a PicoGreen standard curve on the same day of cell seeding. Other samples were cultured for up to seven days. PicoGreen assays were applied to samples on day 0 (seeding day), 1, 4, and 7 as described in **section 2.2.4**.

4.3.6 A549 cell culture on scaffolds

A549 cells were cultured in T25 culture flasks, trypsinised and counted with haemocytometer as described in **section 2.1**. After cell count, cells were seeded directly onto each scaffold,

either at an initial cell density of 960 cells/mm^3 (60,000 cells per scaffold) or 32 cells/mm^3 (2000 cells per scaffold).

Before adding 500 µl DMEM+ media, all scaffolds were moved to empty sterile TCP to eliminate any seeding errors. Samples were incubated for up to 21 days in 500 µl media, with the media changed every three days. To determine cell attachment, viability and proliferation, scaffolds were moved to a new well with sterile tweezers, and alamarBlue, PicoGreen, LIVE/DEAD and DAPI assays were applied as described in **section 2.2, 2.2.5 and 2.3.1** every 7 days. 1 hour incubation time was used for alamarBlue assays, as previously optimised (**Fig.4.3**).

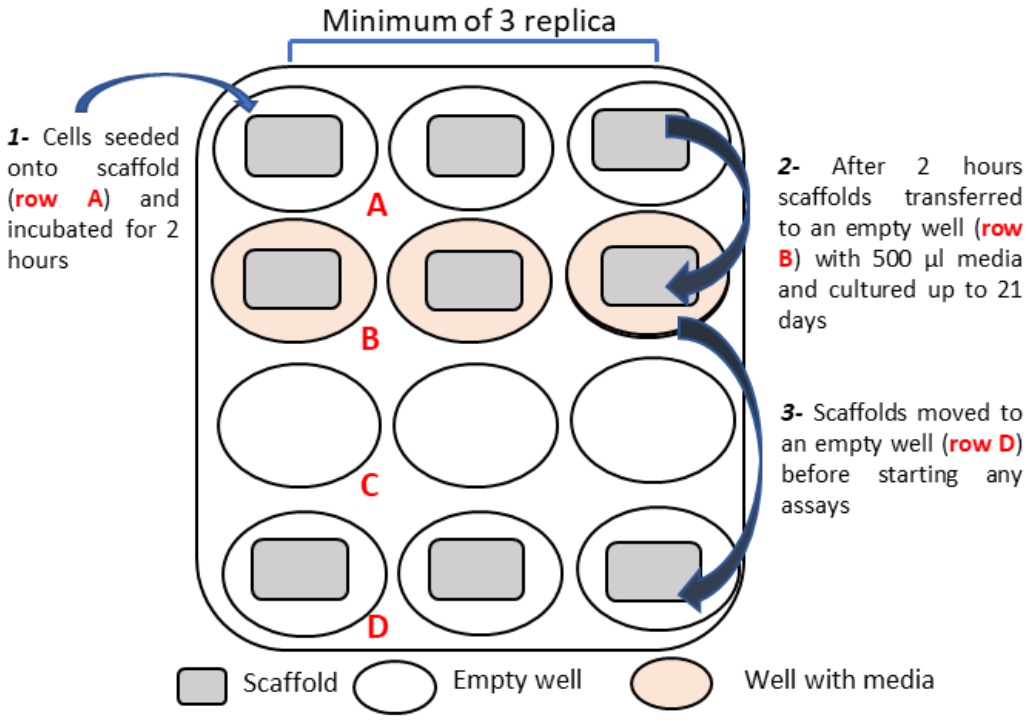

Figure 4.3: Cell seeding onto scaffolds along with cell analysis assays. Scaffolds were placed into a sterile well on row A and cells were seeded onto the scaffolds. These samples were incubated for 2 hours before being carefully relocated to empty wells on row B. Samples were cultured in these wells until further testing. Samples were then carefully relocated to empty wells on row D before applying any cell analysis assay.

4.3.7 Surgispon chemical coating

Surgispon scaffolds were coated with either 10 µg/ml collagen type I (COL), fibronectin (FIB) or collagen type I and fibronectin (COL+FIB) solutions to explore any impact on cell attachment to scaffolds. This concentration is based off previous work from our lab (Dale et al., 2019) but this is the first example of the protocol being used for Surgispon scaffold coating. Each type of collagen and fibronectin was diluted from its original concentration to the working concentration using PBS. Scaffolds were left in coating solution overnight, with a minimum of three replicates. Uncoated scaffolds were used as a control.

4.3.8 35FLH fibroblast cell culture on scaffolds

Cell seeding onto scaffolds was performed as described in **section 4.3.6** and 35FLH cells were seeded onto chemically-coated (or uncoated control) scaffolds with an initial seeding density of 32 cells/mm^3 (2000 cells per scaffold). Before adding 500 µl DMEM+ media, all samples were moved to an empty sterile TCP to eliminate the seeding mistakes. Samples were incubated for 21 days in 500 µl media and every three days media was changed. To determine cell viability alamarBlue and PicoGreen were applied on days 7, 14 and 21, while LIVE/DEAD and DAPI assays were applied on day 7 and 21 as described in **section 2.2, 2.2.5 and 2.3.1** and 1 hour incubation time was used for alamarBlue assays as previously optimised in **section 4.3.3**.

4.3.9 Deactivating 35FLH fibroblast cells

35FLH cells were deactivated as described in **section 2.1.5,** this was done in order to create a feeder layer on the scaffold for the epithelial cells, and in order to make the model more

biologically relevant. To investigate the mitomycin C deactivation process, deactivated 35FLH (D-35FLH) cells were seeded onto TCP as described in **section 4.3.6** (60,000 cells/cm^2), with alamarBlue and PicoGreen assays applied to measure cell metabolic activity over 7 days. D-35FLH cells were imaged using brightfield microscopy, stained with LIVE/DEAD assay for imaging with fluorescence microscopy, on days 1 and 7.

4.3.10 Co-culture of A549 and D-35FLH fibroblast cells on scaffold

35FLH fibroblasts were deactivated before seeding onto uncoated scaffolds for co-culture. D 35FLH cells were labelled with blue Vybrant™ cell tracker as described in **section 2.3.2**. D-35FLH cells were seeded onto scaffolds at an initial seeding density of 32 cells/mm^3 (2000 cells per scaffold) and incubated for 2 hours for cell attachment. After incubation, A549 cells were seeded onto the same scaffolds at an initial seeding density of 32 cells/mm^3 (2000 cells per scaffold) to create a co-culture, which was further incubated for 2 hours for cell attachment (**Fig.4.4**), with 500 µl DMEM+ media added to each well. These co-cultures on scaffolds were imaged using the LIVE/DEAD assay and Vybrant-labelled cells for fluorescence microscopy.

As well as co-culture on scaffolds, co-cultures and isolated cell cultures were also seeded onto TCP at an initial cell density of 2000 cells/cm^2. Brightfield images of TCP and scaffolds were taken on days 1 and 7 for analysis of A549, D-35FLH and co-culture cell proliferation.

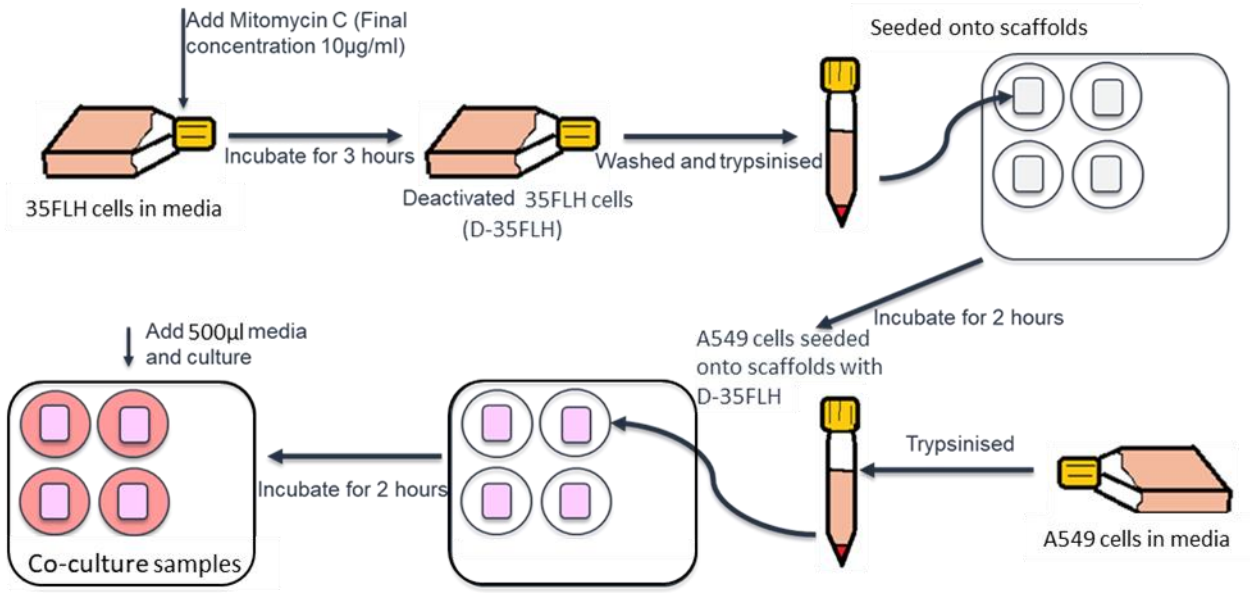

Figure 4.4: Cell seeding onto scaffolds to prepare a co-culture. 35FLH cells were deactivated (D-35FLH) by adding mitomycin C to DMEM+ media (final concentration of 10 µg/ml) and incubated for 3 hours at 37°C with 5% CO_2. After the deactivation process, cells were prepared for culture and D-35FLH cells were seeded onto scaffolds. Samples were incubated for 2 hours to allow cell attachment. After incubation, A549 cells were prepared and seeded onto the same scaffolds with D-35FLH cells. Samples were incubated for another 2 hours, before adding 500 µl DMEM+ media to each well.

4.3.11 Imaging with CellTracker™ Blue CMAC Dye

CellTracker Blue CMAC (7-amino-4-chloromethylcourmarin) is a fluorescent dye designed for monitoring cell movement and location, as it penetrates the membrane and is converted to a membrane-impermanent intracellular probe. D-PLF cells were labelled with CellTracker and seeded onto a scaffold for co-culture with A549 cells. After 21 days co-culture, the LIVE/DEAD assay was applied to samples, with the blue fluorescent channel used to image CellTracker, localising and tracking D-35FLH samples (**Fig.4.28**).

4.4 Results

4.4.1 Optimising alamarBlue metabolic assay

An alamarBlue standard curve was prepared by seeding between 0-300,000 A549 cells/cm^2 onto TCP. The alamarBlue assay was applied to samples 2 hours after cell seeding (**Fig.4.5**) with a 3 hour incubation time. The alamarBlue assay showed oversaturation when cell numbers were in excess of 90,000 cell/cm^2 initial seeding density, meaning that cell numbers above this could not have their metabolism readily quantified as different, and their viability determined. The correlation coefficient is 0.66, a standard curve should have a strong linear relationship, meaning this curve is insufficient.

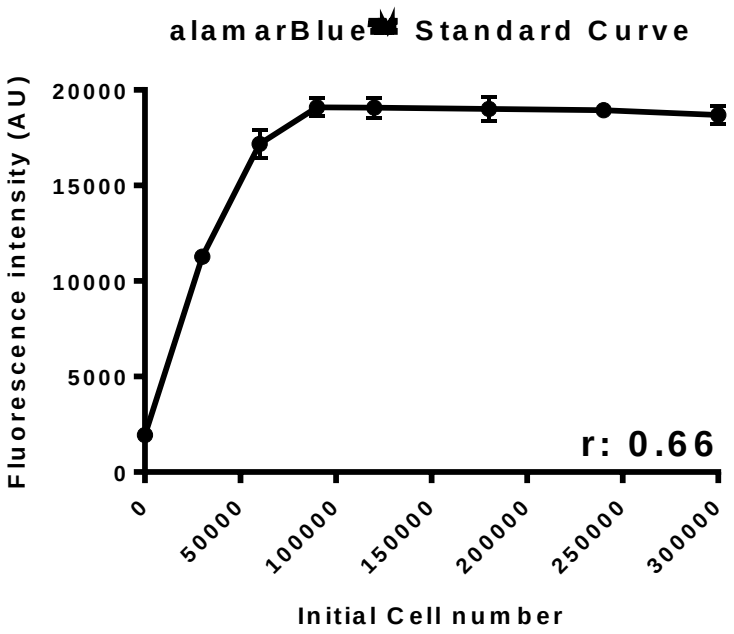

Figure 4.5: alamarBlue standard curve (0-300,000 cells/cm^2). A549 cells were seeded onto 48 well plates for the alamarBlue standard curve, which showed oversaturation when the initial cell seeding density was over 90,000 cells/cm^2, (n=6).

Based on these results, a second alamarBlue standard curve was prepared with a lower cell concentration, ranging from 0-150,000 cells/cm^2. alamarBlue reagent was applied to the

samples on the seeding day (day 0) and after overnight culture (day 1) to observe the effects of cell proliferation on the standard curve (**Fig.4.6**). Similarly to the original higher cell density standard curve (**Fig.4.5**), there is oversaturation at higher cell numbers.

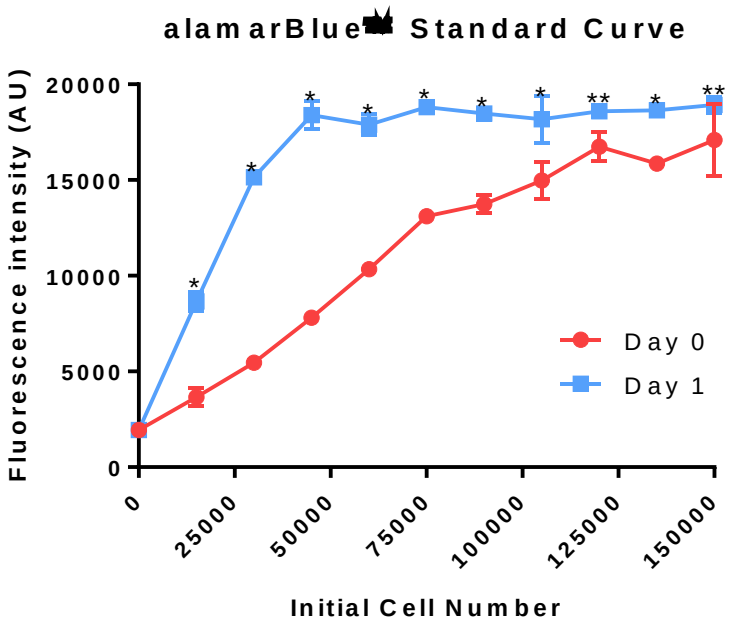

Figure 4.6: alamarBlue standard curve (0-150,000 cells/cm^2). These standard curves show the metabolic activity of A549 cells on day 0 and day 1. By day 1, alamarBlue showed oversaturation from 45,000 cells/cm^2 initial seeding density and above. *: $p<0.0001$, **: $p<0.001$, n=4, some error bars are negligible and not visible.

The day 0 standard curve showed increased metabolic activity from 0-115,000 cells/cm^2. The correlation coefficient for day 0 is 0.97, showing strong positive correlation and a useful standard curve at this lower cell number. However, day 1 results showed oversaturation after 45,000 cells/cm^2 initial seeding density, most likely due to cell proliferation overnight, resulting in a reduced correlation coefficient of 0.74. This shows that using a high initial cell seeding number limits the effectiveness of alamarBlue at quantifying cell metabolic activity, and therefore inferring cell viability and proliferation. Cell growth overnight had a significant

effect on the fluorescence intensity (p: <0.0001), and at each cell seeding number (except 0), there was significantly more fluorescence intensity by day 1 (p: <0.001 for all comparisons). As cells are expected to be cultured for far longer than one day, the alamarBlue assay needed optimisation in order to stop oversaturation and be effective for weeks of cell culture.

4.4.2 Optimising cell seeding number for alamarBlue cell metabolic activity assay

alamarBlue standard curves were prepared using lower cell densities, from 0-60,000 cells/cm^2, to investigate the effect of the initial cell seeding density on alamarBlue assays after up to 7 days of cell culture. Cells were cultured on TCP and the alamarBlue assay was applied to samples every other day including the seeding day (day 0) until day 7. For each measurement, new samples were used to avoid any effect of previous alamarBlue assay. These results can be seen in **Fig.4.7**.

Correlation coefficients decreased as the cells proliferated in culture, with day 0 having near-perfect 0.99 correlation and decreasing to 0.31 by day 7, showing how limited this would be as a standard curve.

From days 0-1 the standard curve did not oversaturate, but oversaturation was observed from day 3. The day 3 results showed oversaturation from 10,000 cells/cm^2 initial seeding density and above, day 5 from 5000 cells/cm^2.initial seeding density and day 7 across all samples (**Fig 4.7**). The cell culture time had a significant effect on the fluorescence intensity ($p<0.0001$), with days 3-7 having significantly greater fluorescence intensity from 10000-60000 cells/cm^2 when compared to days 0-1 ($p<0.01$ for all comparisons).

These alamarBlue standard curves show that this assay can only be used with less than 60,000 cells/cm^2 initial seeding density if cells are going to be cultured for more than three days. In addition to optimising the cell number, the alamarBlue incubation time was also optimised, as seen in **Figure 4.8**.

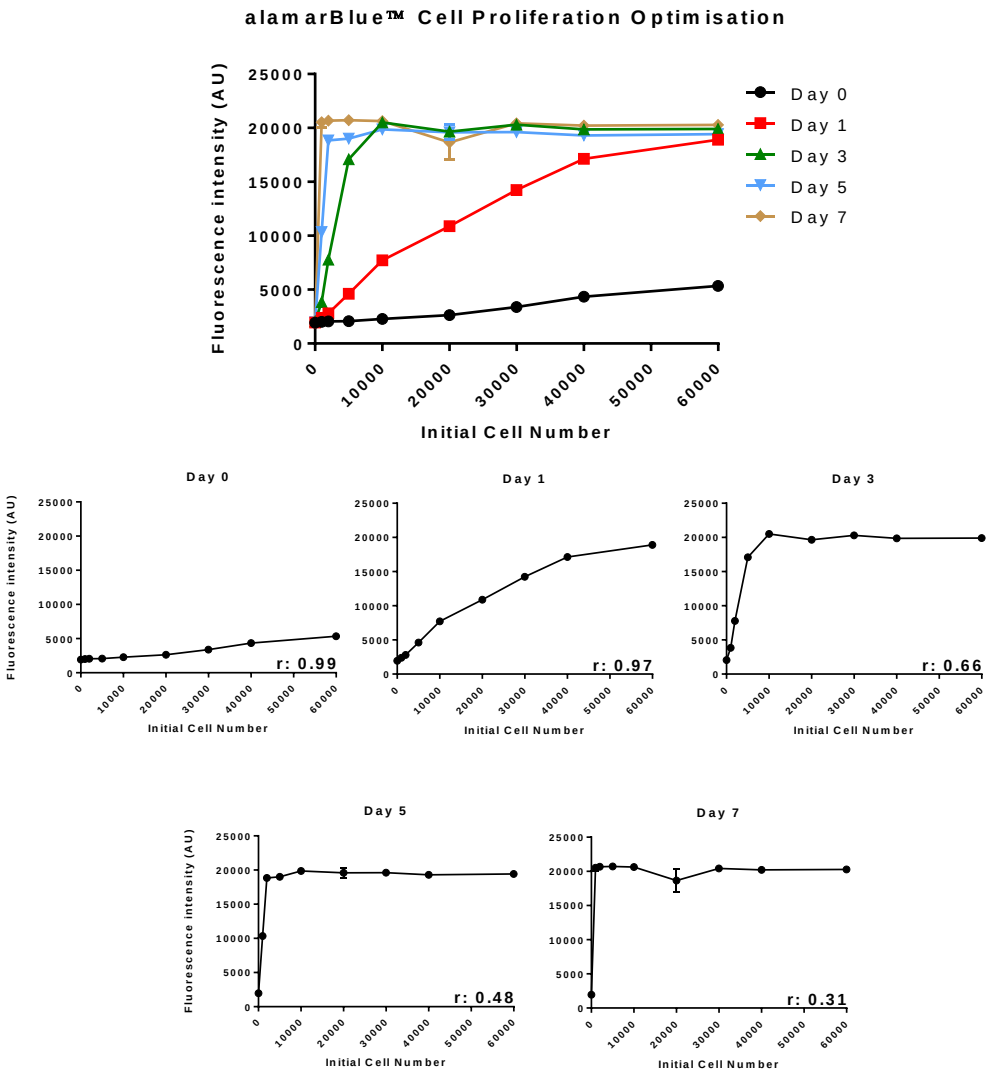

Figure 4.7: The effect of cell proliferation on alamarBlue standard curves. The alamarBlue standard curves show an increase in metabolic activity with increased cell number, and this increased further as cells were incubated. With cell culture lasting over 14 days in experimental conditions, it is important to optimise this assay and avoid oversaturation. Some error bars are negligible and not visible, n=4.

4.4.3 Optimising incubation time for alamarBlue cell metabolic activity assay

As well as the initial cell seeding number, the alamarBlue incubation time was another variable to optimise, as all previous assays had used the standard 3 hours incubation time, and this may be responsible for oversaturation.

A standard curve was prepared by using between 0-60,000 cells/cm^2 initial cell seeding density to investigate the effect of alamarBlue incubation time. For this test, cells were incubated for 7 days before applying the assay in order to achieve higher confluency, which is the main cause of oversaturation. When the alamarBlue assay was applied, the first sample was incubated for 30 minutes and incubation time was increased by in 30 minute increments to 3 hours maximum incubation time, as shown in **Fig.4.8**.

The correlation coefficient decreased with longer incubation times, starting at 0.63 with 0.5 hours and decreasing to 0.3 for >2 hours. Any incubation time beyond 1 hour resulted in an unreliable standard curve.

With 30 minute alamarBlue incubation, oversaturation was observed beyond 10,000 cells/cm^2 initial cell seeding density. At longer incubation times, oversaturation was observed at lower initial cell densities: 5000 cells/cm^2 for 1 hour and 2000 cells/cm^2 for 1.5 hours and beyond. The alamarBlue incubation time had a significant effect on the fluorescence intensity ($p<0.0001$), with 1.5-3 hour incubation having significantly greater fluorescence intensity when compared to 0.5-1 hour incubation ($p<0.001$ for all comparisons).

The overall results show that the alamarBlue assay should be used with an initial cell seeding density of 2000 cells/cm^2, along with a 1 hour incubation time. These variables will stop oversaturation over longer (up to 21 day) cell culture experiments on both 2D tissue culture

plastic and 3D Surgispon scaffolds, and allow for alamarBlue to be used as a measure for cell viability and proliferation.

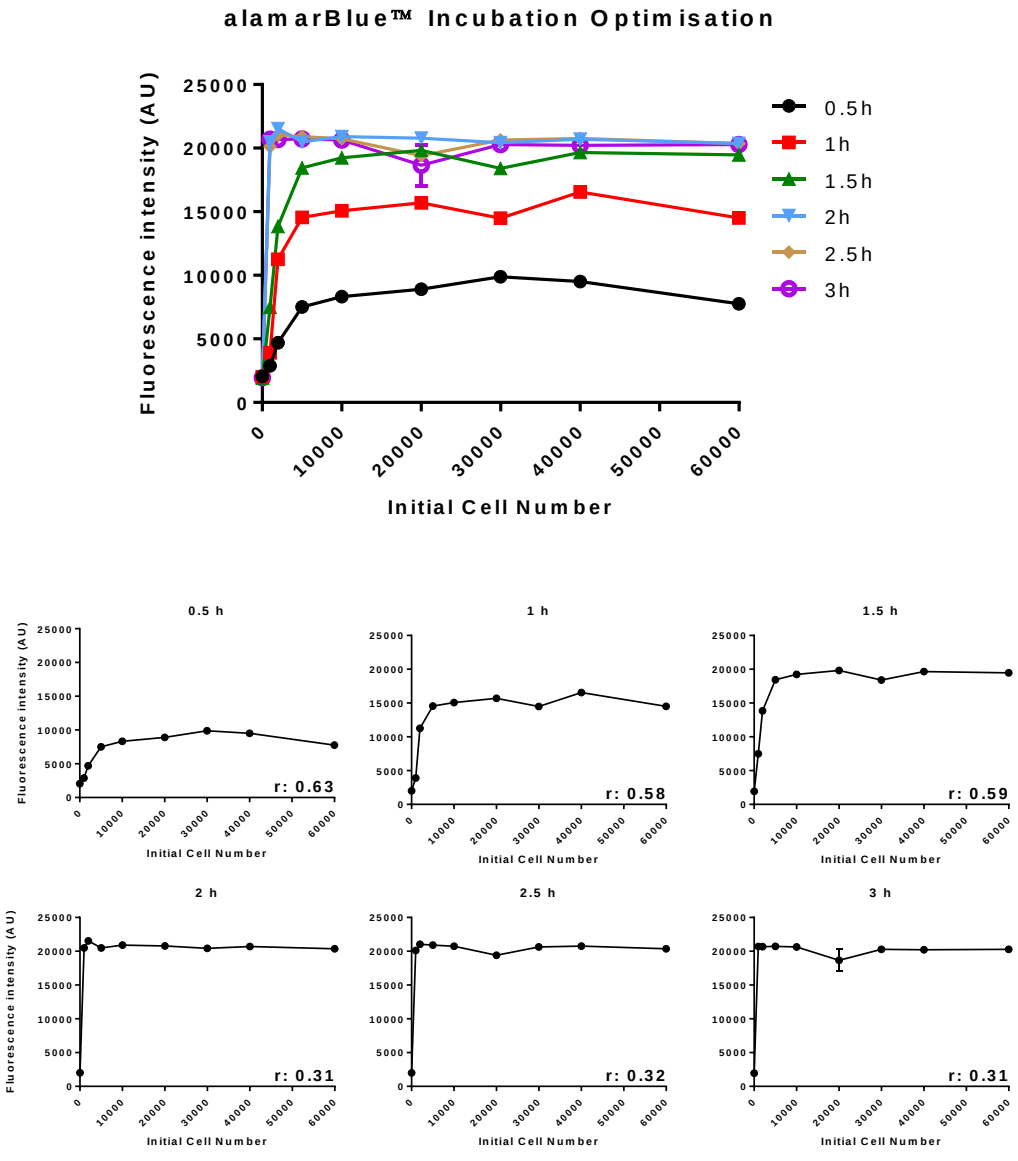

Figure 4.8: The effect of alamarBlue incubation on standard curves. Increased alamarBlue incubation results in increased fluorescence intensity with increased cell number. Some error bars are negligible and not visible, n=4.

4.4.4 Comparison of alamarBlue assay with MTT assay and trypsin cell count

As a potential alternative to alamarBlue, the MTT cell metabolic assay was explored, as well as a trypsinization method to remove cells from the scaffold and stain with trypan blue in order to determine the viability and number of cells.

A MTT standard curve was prepared by using between 2,000-60,000 cells/cm^2 initial cell seeding density. Cells were incubated for up to 7 days and the MTT assay was applied on days 0, 1, 4 and 7, with results shown in **Figure 4.9**.

The correlation coefficient decreased as the cells proliferated, with perfect positive correlation at day 0 (r: 1.0) and less correlation by day 7 (r: 0.57). Only the standard curves from day 0-1 would be suitable for experimentation.

MTT graphs showed oversaturation by day 1 at 20,000 cells/cm^2 initial cell seeding density, similarly on day 4 and reduced to 5000 cells/cm^2 initial cell seeding density by day 7. The effect of cell proliferation on the MTT assay was significant ($p<0.0001$), with days 4-7 being unsuitable for determining cell viability and proliferation through quantifying cell metabolic activity.

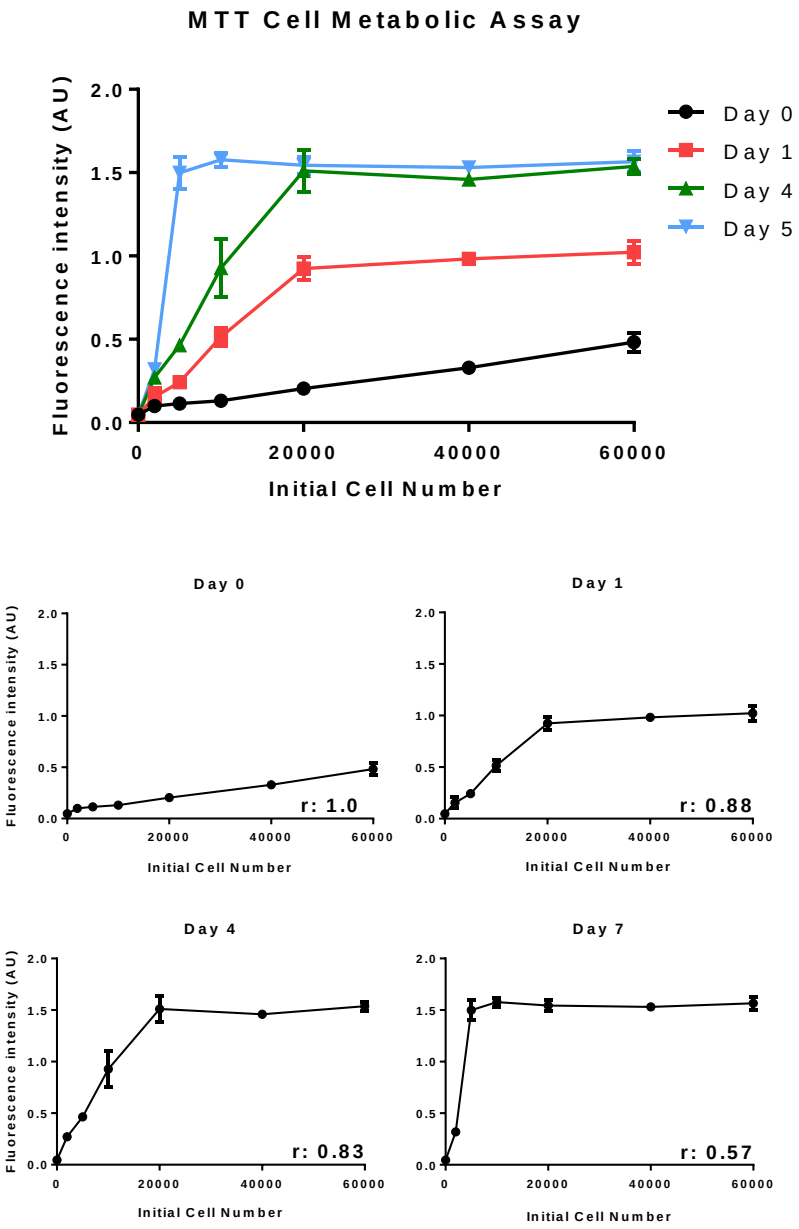

Figure 4.9: Effect of cell proliferation on MTT metabolic assay standard curves. Similarly to alamarBlue, increased culture times lead to oversaturation. (n=4).

This experiment was repeated with alamarBlue in order to more directly compare with MTT, these results are shown in **Figure.4.10**. As previously optimized, alamarBlue samples were incubated for 1 hour.

MTT and alamarBlue standard curves both showed oversaturation on day 7 at around 5000 cells/cm^2 initial cell seeding density. Correlation analysis for the alamarBlue results on days 0, 1, 4 and 7 give r values of 0.99, 0.97, 0.75 and 0.53 respectively, showing that the cell number was significantly positively correlated to the alamarBlue fluorescence intensity for days 0-1, with decreasing correlation to day 7 as the plateau forms.

It should be noted that MTT assay samples cannot be used after assay due to MTT requiring DMSO which is cytotoxic, while alamarBlue samples can be successfully cultured after analysis. Due to this, the alamarBlue assay was used to measure cell metabolic activity and cell proliferation on scaffolds, due to alamarBlue and MTT otherwise showing similar results (**Fig.4.10**).

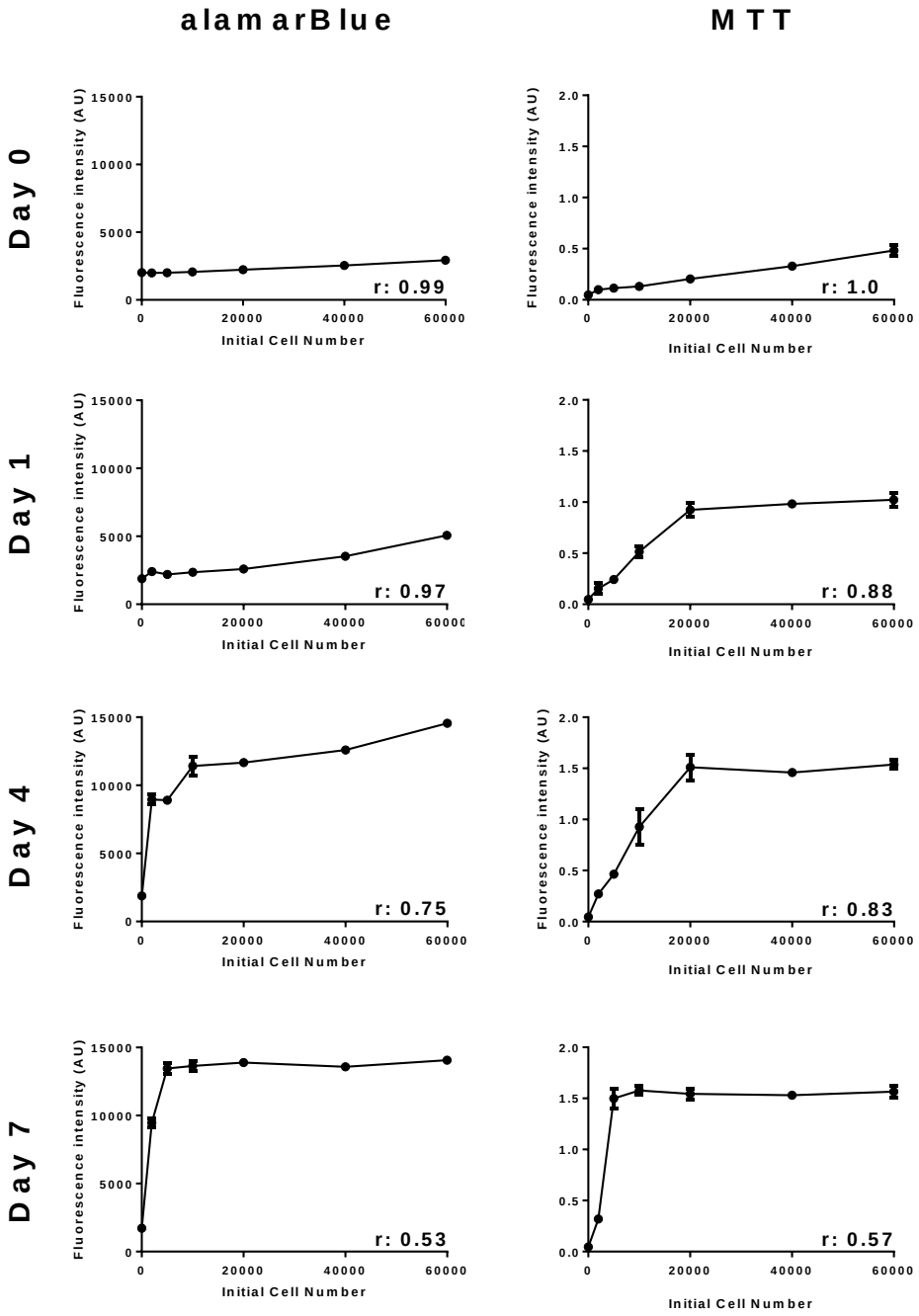

Figure 4.10: MTT and alamarBlue standard curves over 7 days culture period. MTT standard curve shows oversaturation similarly to alamarBlue samples on D 7. On D 1 and D 4, MTT samples showed oversaturation with smaller cell numbers than alamarBlue™ samples (20,000 cells). alamarBlue (n=7).

Cell counting was also investigated alongside MTT. Cell confluency was investigated by trypsinisation and then counting cells using the automated cell counter Countess. Samples

ranged from 2,000-60,000 cells/cm^2 initial cell seeding density (**Fig.4.11**), and counts were done on days 0, 1, 4 and 7.

Cell counts performed on days 0-4 resulted in perfect positive correlation (coefficients shown on **Fig.4.11**), showing that cell counts were accurate and changed with cell number seeded. However, by day 7 cells had reached confluency and could not proliferate at the same rate, resulting in a plateau. Cells seeded at an initial density greater than 10,000 cells/cm^2 could not be accurately counted due to confluence.

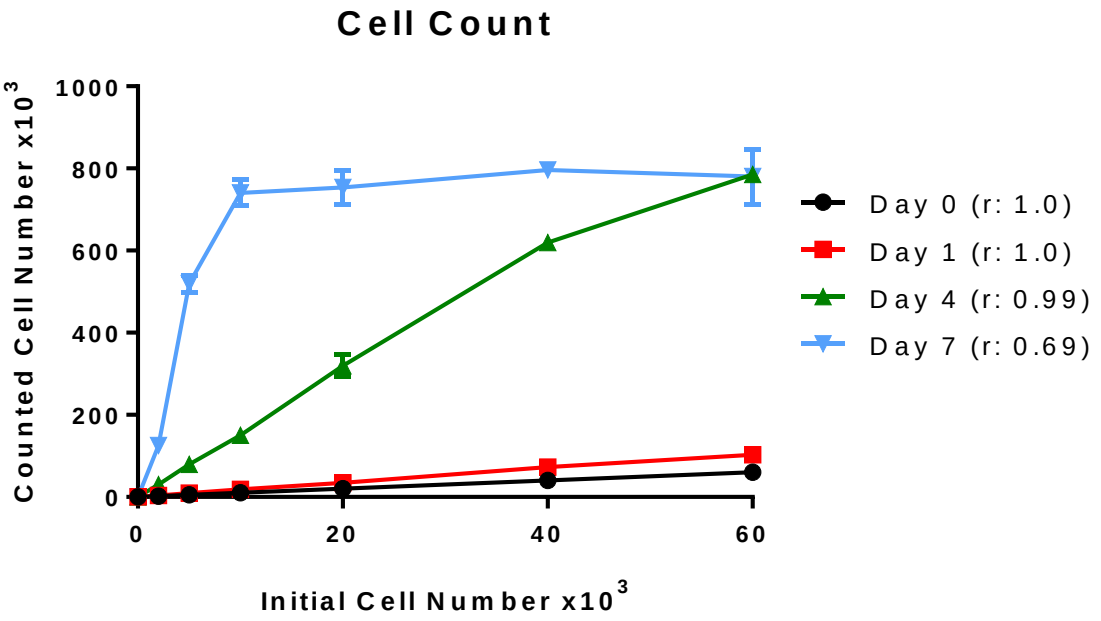

Figure 4.11: Cell number count over 7 days culture period. Cell counting graphs showed that when 10,000 or greater number of cells was seeded onto a 48 well plate, samples reach confluency by day 7. When 60,000 cell seeding number was used, confluency was reached on D4 and the cell number on the plate did not change after D4.(n=4).

4.4.5 Optimising cell seeding number for PicoGreen dsDNA assay

A complementary cell analysis assay to alamarBlue is the double stranded DNA (dsDNA) quantification assay, PicoGreen. A standard curve was prepared with initial cell seeding

densities from 2000-60,000 cell/cm^2. Cells were incubated for up to 7 days and the PicoGreen assay was applied on days 0, 1, 4 and 7, results shown on **Fig.4.12**.

PicoGreen results showed significantly increased fluorescence intensity with increasing cell number from days 0-4 ($p<0.0001$). However, day 7 results show oversaturation from 10,000 cell/cm^2 initial cell seeding density and greater. Correlation analysis of this data showed that at days 0, 1, 4 and 7 the r values were 0.99, 0.97, 0.89, 0.57, indicating that the correlation drops off as the plateau forms at day 7.

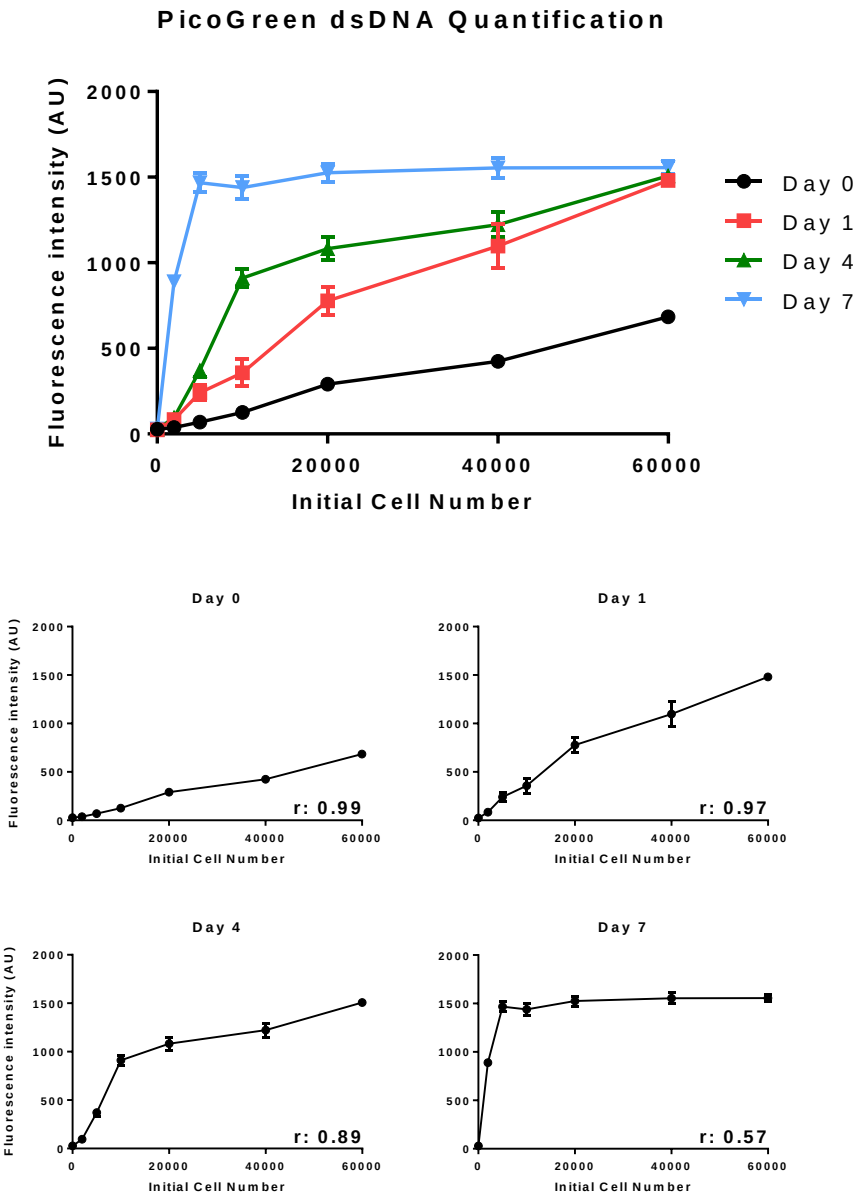

Figure 4.12: PicoGreen standard curves over 7 days culture period. PicoGreen standard curve shows increase in fluorescence intensity with increased cell number until day 7. By day 7 >10,000 cell/cm^2 initial cell seeding showed oversaturation which also states that those samples have same number of cells on the wells, (n=8).

From these experiments the optimized A549 cell seeding number was determined to be 2000 cells per scaffold in order to not oversaturate cell metabolic assays and to achieve an

accurate measure of cell culture and proliferation rate on Surgispon scaffolds. These Surgispon scaffolds were vapour crosslinked (VCL) for 24 hours as optimised in **Chapter 3**.

4.4.6 A549 cell culture on scaffolds

A549 cells were cultured on Surgispon scaffolds in 48 well plates, and brightfield images of cells seeded on these scaffolds were taken in order to perform preliminary investigations of cell attachment at days 7, 14 and 21 (**Fig.4.13**). 960 cells/cm^3 (60,000 cells per scaffolds) were seeded onto each scaffold. Brightfield images showed A549 cell attachment and growth on scaffolds at all three time points.

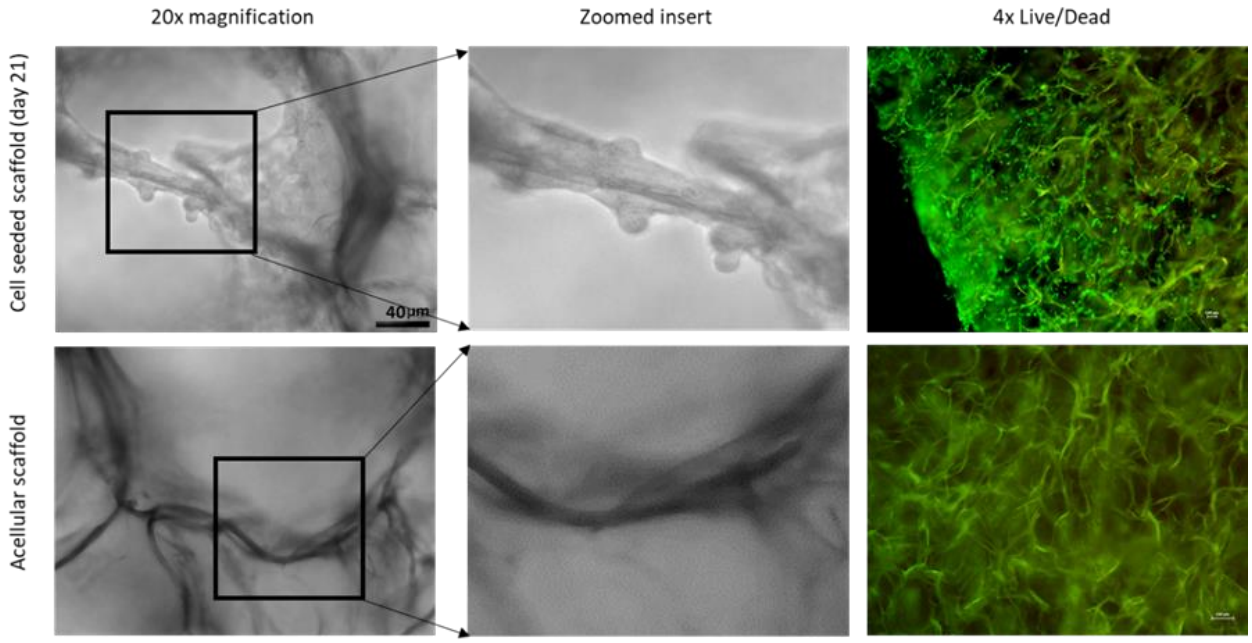

Figure 4.13: A549 cell culture on Surgispon scaffolds. Brightfield images of A549 cells on scaffolds were taken after 21 days of culture at different magnifications, and compared with acellular scaffolds. Fluorescent LIVE/DEAD stain is also used, green indicates live cells but is also subject to autofluorescence.

Brightfield images were also taken of A549 cells on the TCP well plate underneath and near the scaffolds to determine whether A549 cells continued to grow on TCP after being seeded onto the scaffold (**Fig.4.14**). Cell growth under the scaffolds on the TCP was observed, which suggests cell migration from scaffolds or a lack of attachment during the initial seeding stage. Based on this population of cells growing under scaffolds, for accurate cell culture analysis scaffolds were always moved to new wells before applying assays, to ensure that only cells attached to scaffolds were being analysed.

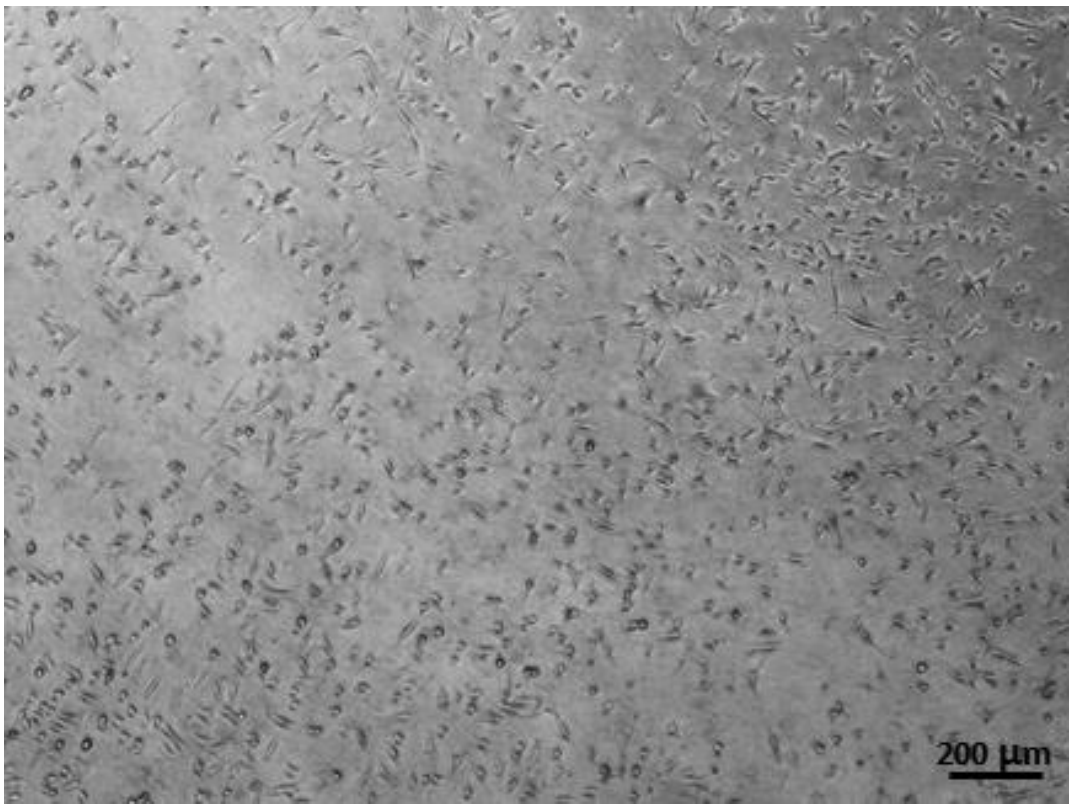

Figure 4.14: A549 cell culture on 2D TCP. Image shows cells on TCP, these cells grew underneath a scaffold for 7 days of culture, and the scaffold was removed prior to taking the image for clarity.

4.4.7 A549 cell metabolic activity

The alamarBlue cell metabolic activity assay was applied to scaffolds seeded with either 2000 or 60,000 A549 cells (32 vs 960 cells/mm^3 respectively) in order to investigate cell growth on scaffolds over a 21 day period (**Fig.4.15**).

For scaffolds seeded with 2000 cells, the cell proliferation over time had a significant effect on the fluorescence intensity, with both the 7-14 and 14-21 increases in fluorescence intensity being significant ($p<0.0001$). These increases indicate that A549 cells attached, metabolised and proliferated on uncoated VCL Surgispon scaffolds.

Scaffolds seeded with 60,000 cells showed a significant change in fluorescence intensity from days 7-14 ($p<0.001$) due to cell proliferation, but the change from days 14-21 was not significant (p: 0.27) due to alamarBlue™ saturation by day 14 due to cell proliferation.

These experiments show that for scaffolds, 2000 cells should be the initial cell seeding number in order for alamarBlue to measure cell metabolism over longer cell culture experiments.

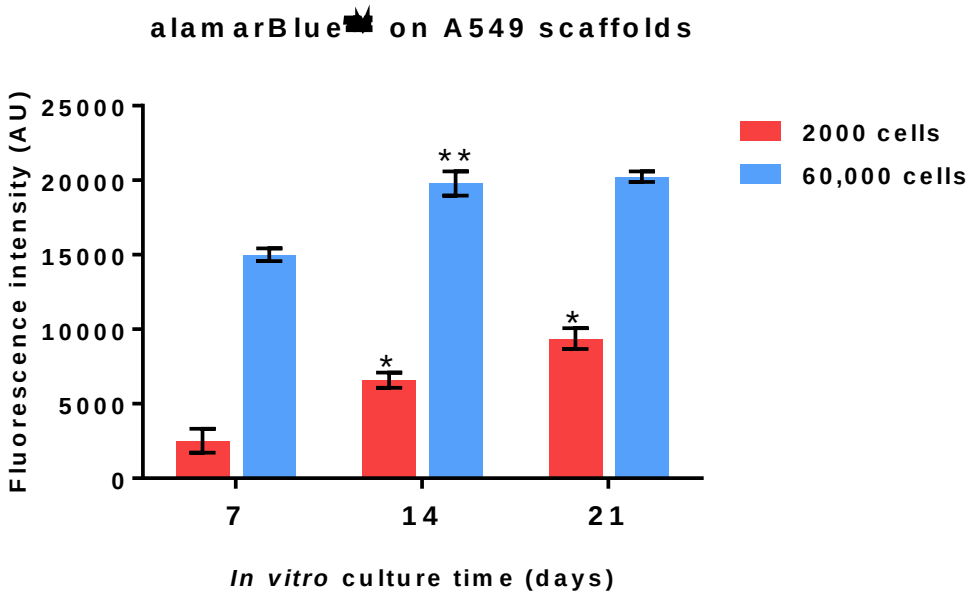

Figure 4.15: Metabolic activity of A549 cells seeded onto scaffolds Cell metabolic activity was monitored by measuring with alamarBlue assay over a 21 day period. Significiance is displayed with regards to the previous data point (14 compared to 7, 21 compared to 14). *: $p<0.0001$, **: $p<0.001$, (n=4).

4.4.8 Effect of scaffold chemical coating on A549 cell culture.

Surgispon scaffolds were coated either 10 µg/ml collagen type I (COL), fibronectin (FIB) or collagen and fibronectin (COL+FIB) solution to investigate the effect of scaffold coating on cell attachment.

In order to determine the success of the coating protocol and the binding of chemicals to the Surgispon, scaffolds were weighed after coating with 100 µg/ml solution (as 10 µg/ml change was too small to observe with scales) and compared to an uncoated control, in order to demonstrate a weight gain after coating. This data is shown in **Fig. 4.16.**

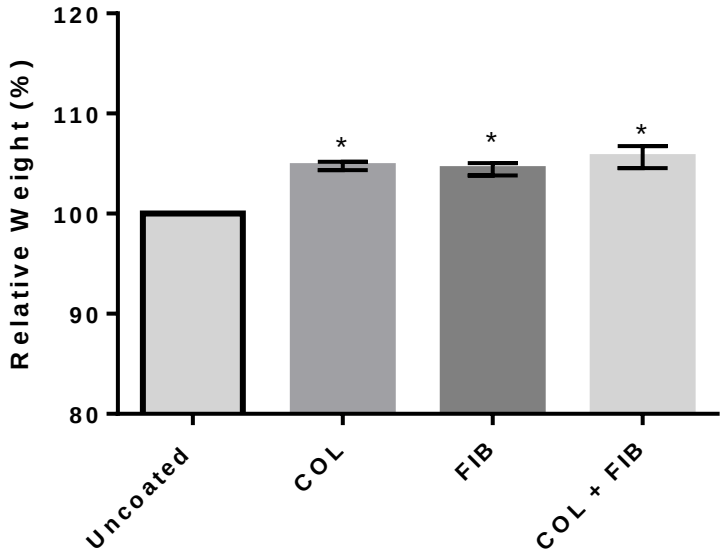

Figure 4.16: Scaffold weight after chemical coating. Scaffolds coated with 100 ug/ml collagen type I, fibronectin, or both, are compared in weight to an uncoated scaffold. Significance is shown compared to the uncoated control, *: $p<0.0001$

Cell attachment on the coated scaffolds was compared to cell attachment on uncoated control scaffolds to determine the effect of coating. 2000 A549 cells (32 cells/mm^3) were seeded onto each scaffold and cultured for up to 21 days. alamarBlue and PicoGreen assays were applied to samples on days 7, 14 and 21, as seen in **Figure.4.16**.

Both assays significantly increased in fluorescence intensity from days 7-14 and 14-21 due to A549 proliferation ($p<0.0001$ for all cases). There was no significant effect of chemical coating on either alamarBlue or PicoGreen results ($p>0.05$), COL, FIB and COL+FIB scaffolds did not have significantly different assay results when compared to uncoated scaffolds (p: 0.12 for alamarBlue, p: 0.19 for PicoGreen).

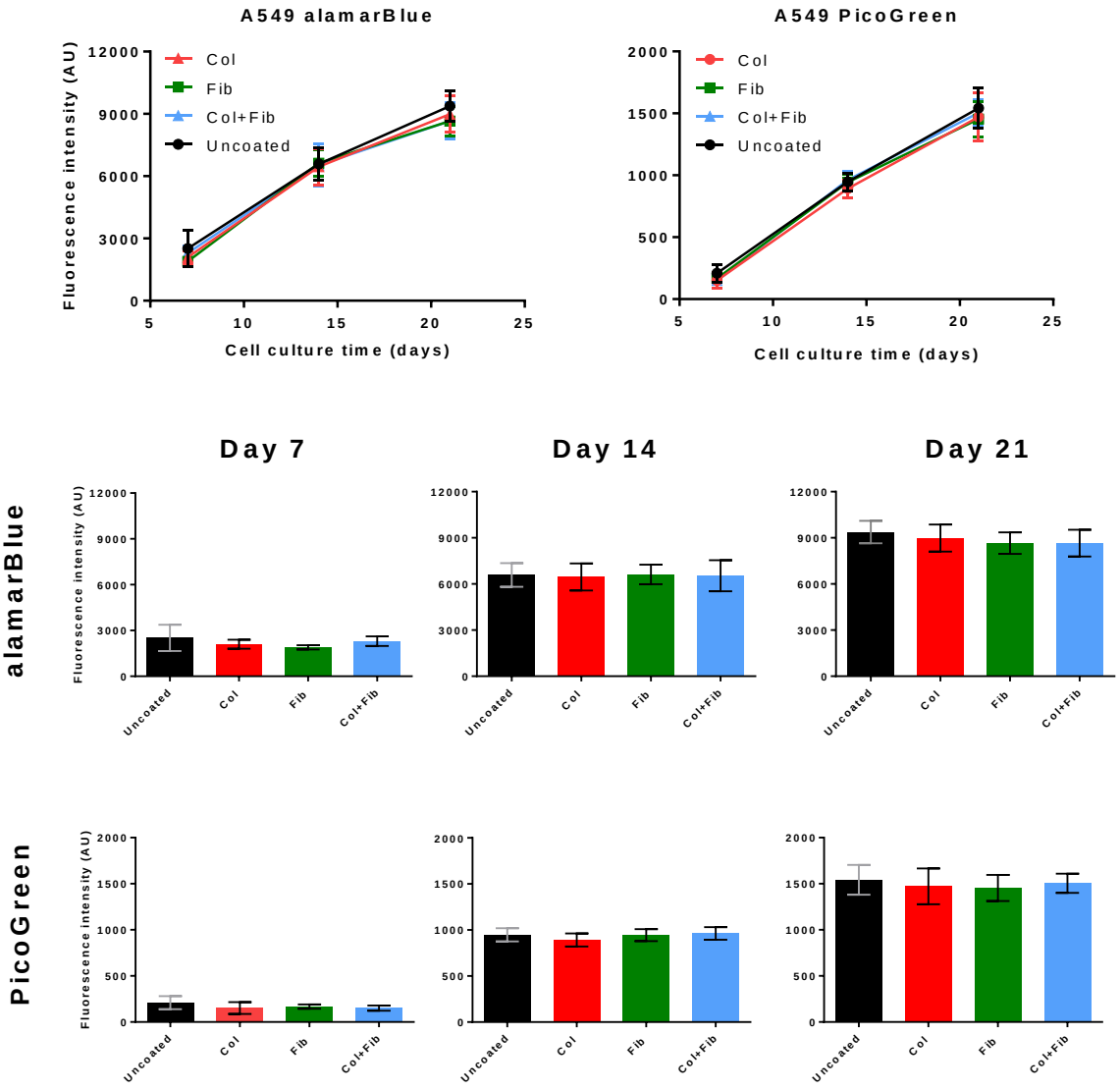

Figure 4.17: The effect of chemical coating on A549 cells cultured on Surgispon scaffolds. Scaffolds were coated with either collagen type I (COL), fibronectin (FIB), collagen and fibronectin solution (COL+FIB) or uncoated. Assays were applied on day 7, day 14 and day 21. (n=9).

4.4.9 Fluorescent imaging of scaffolds and A549 cell culture

Uncoated acellular Surgispon scaffolds were imaged in the blue, green and red fluorescent channels on a fluorescence microscope, and demonstrated autofluorescence in every

emission channel, as seen in **Figure 4.17**. This natural autofluorescence of Surgispon gelatine sponges is a limiting factor for fluorescent imaging as it generates substantial image background and could interfere with signal from cells, this should be taken into account for future fluorescence imaging of any condition (coating, presence of cells) on these scaffolds.

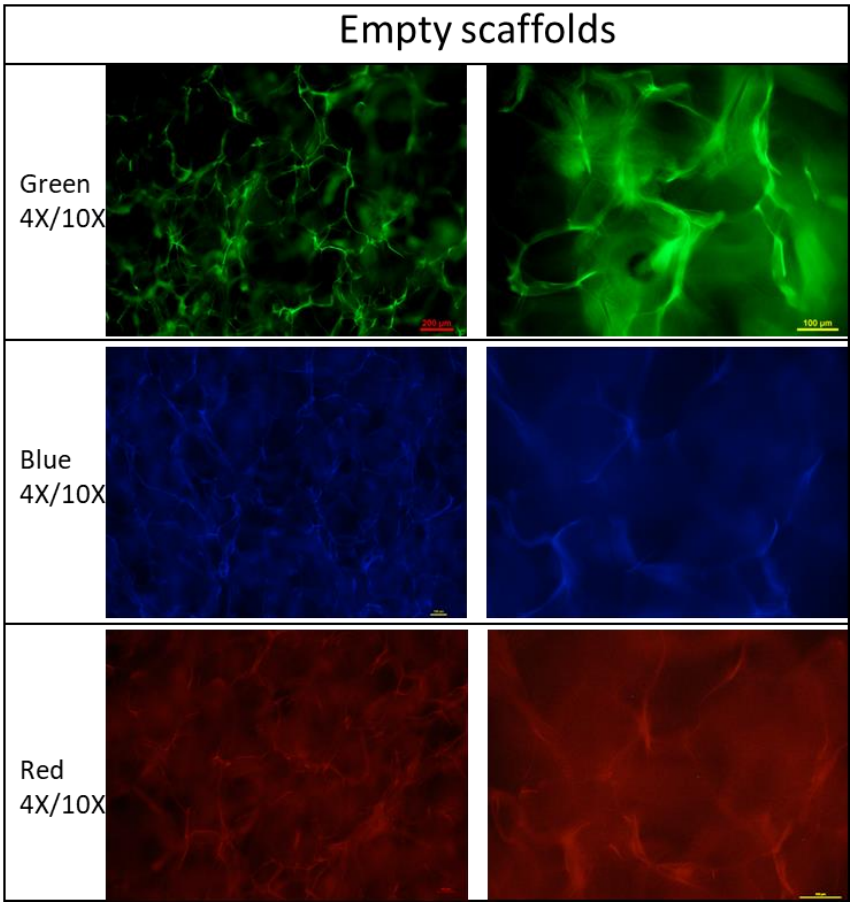

Figure 4.18: Fluorescent imaging of uncoated, acellular Surgispon scaffolds. These scaffolds were not stained with any fluorescent markers, all fluorescence observed is from gelatine autofluorescence.

The same scaffolds from **Figure 4.17** were also fluorescently imaged using DAPI and the LIVE/DEAD fluorescent viability assay. Acellular uncoated scaffolds were imaged in the blue (DAPI, $358_{ex}/461_{em}$ nm), green (calcein AM live, $494_{ex}/517_{em}$ nm) and red (ethidium homodimer dead, $528_{ex}/617_{em}$ nm) spectra. DAPI images are shown in **Figure 4.18**, with LIVE/DEAD images shown in **Figure 4.19**.

Day 7 DAPI and LIVE/DEAD images showed cells attached to scaffolds, with increased cell numbers observed by day 21. Across all chemical coatings, attachment was observed, this is supported by A549 cell proliferation as shown in alamarBlue and PicoGreen graphs from the previous experiment with these same scaffolds (see **Figure 4.16**). No cells were noted in the red DEAD channel, potentially due to dead cells detaching from the scaffold and not being available for imaging, or due to more intense autofluorescence in the red channel.

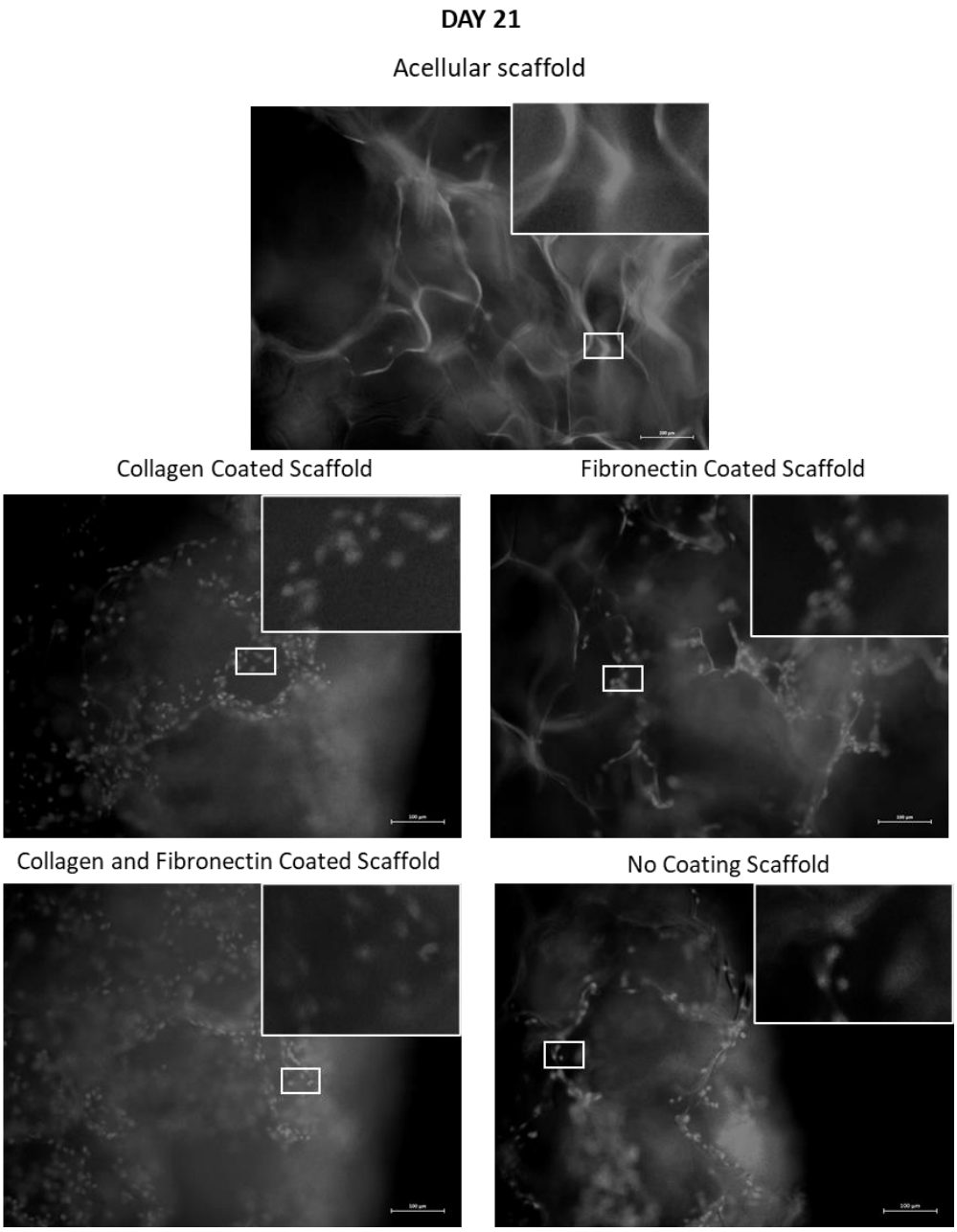

Figure 4.19: Monochrome images of Surgispon scaffolds seeded with A549 cells and labelled with DAPI. Scaffolds were coated with COL, FIB, COL+FIB or uncoated, and imaged with DAPI stain. Cells can be observed growing on the scaffolds across all conditions.

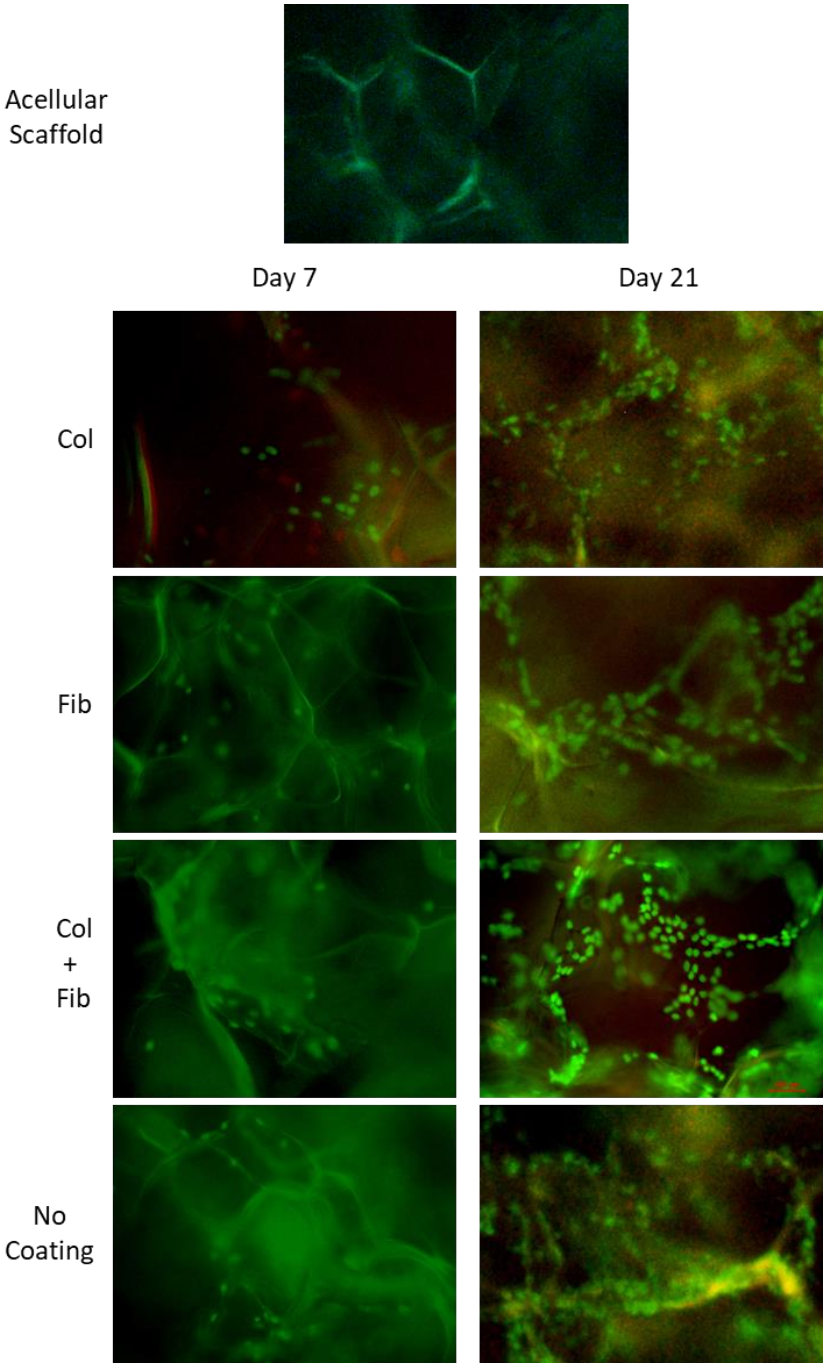

Figure 4.20: Images of Surgispon scaffolds seeded with A549 cells and labelled with LIVE/DEAD assay. Scaffolds were coated with COL, FIB, COL+FIB or uncoated, and imaged using LIVE/DEAD stains. Cells can be observed growing on the scaffolds across all conditions.

4.4.10 35FLH fibroblast cell culture on scaffolds

As well as epithelial cells, fibroblasts were also tested with Surgispon scaffolds. 2000 35FLH cells were seeded onto coated and uncoated Surgispon scaffolds, an initial cell density of 32 cells/mm^3, (**see 4.3.7**) and cultured for up to 21 days. alamarBlue and PicoGreen assays were applied to samples on day 7, 14 and 21 (**Fig.4.20**).

Similarly to results from A529 cells (**Fig.4.16**), there were significant increases in fluorescent intensity due to cell proliferation from days 7-14 and 14-21 ($p<0.0001$). Also similarly to A549 results, there was no significant effect of chemical coating on either alamarBlue or PicoGreen results: COL, FIB and COL+FIB scaffolds did not have significantly different assay results when compared to uncoated scaffolds (p: 0.66 for alamarBlue, p: 0.34 for PicoGreen).

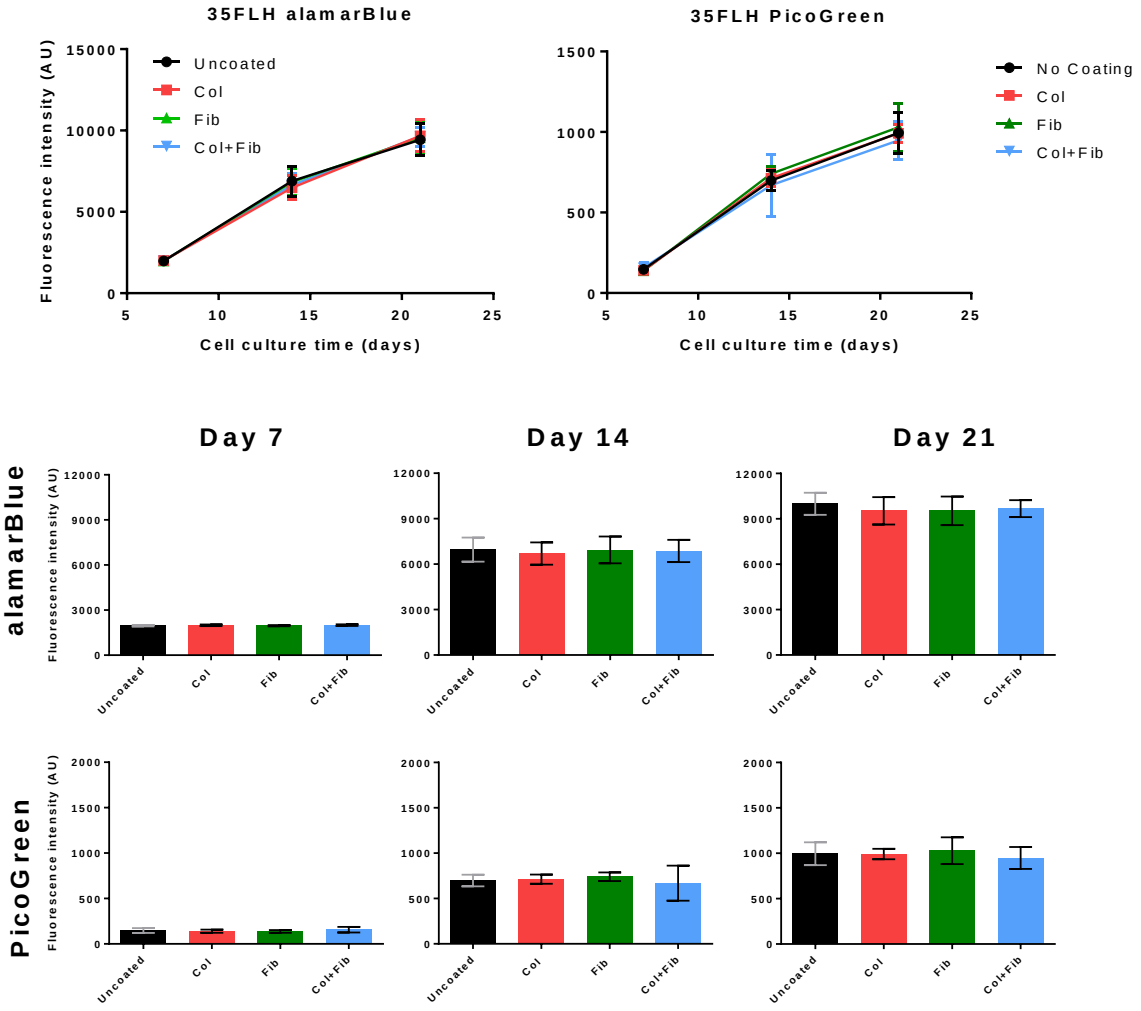

Figure 4.21: The effect of chemical coating on 35FLH cells cultured on Surgispon scaffolds. Scaffolds were coated with either collagen type I (COL), fibronectin (FIB), collagen and fibronectin solution (COL+FIB) or uncoated. Assays were applied on day 7, day 14 and day 21. (n=9).

Surgispon scaffolds were seeded with 2000 35FLH cells (an initial cell density of 32 cells/mm^3) and were fluorescently imaged with DAPI and LIVE/DEAD as seen in **Figures 4.21** and **4.22**.

Day 7 DAPI and LIVE/DEAD images showed cell attachment on scaffolds from all conditions. Day 21 DAPI and LIVE/DEAD images showed more cells attached to scaffolds than day 7 whether scaffolds were coated or not, this all supports 35FLH cell proliferation as shown in alamarBlue and PicoGreen results (**Fig.4.20**). These experiments have demonstrated successful epithelial and fibroblast cell attachment and proliferation on scaffolds, and both showed that there is no significant difference between coating types or between coated scaffolds and uncoated scaffolds.

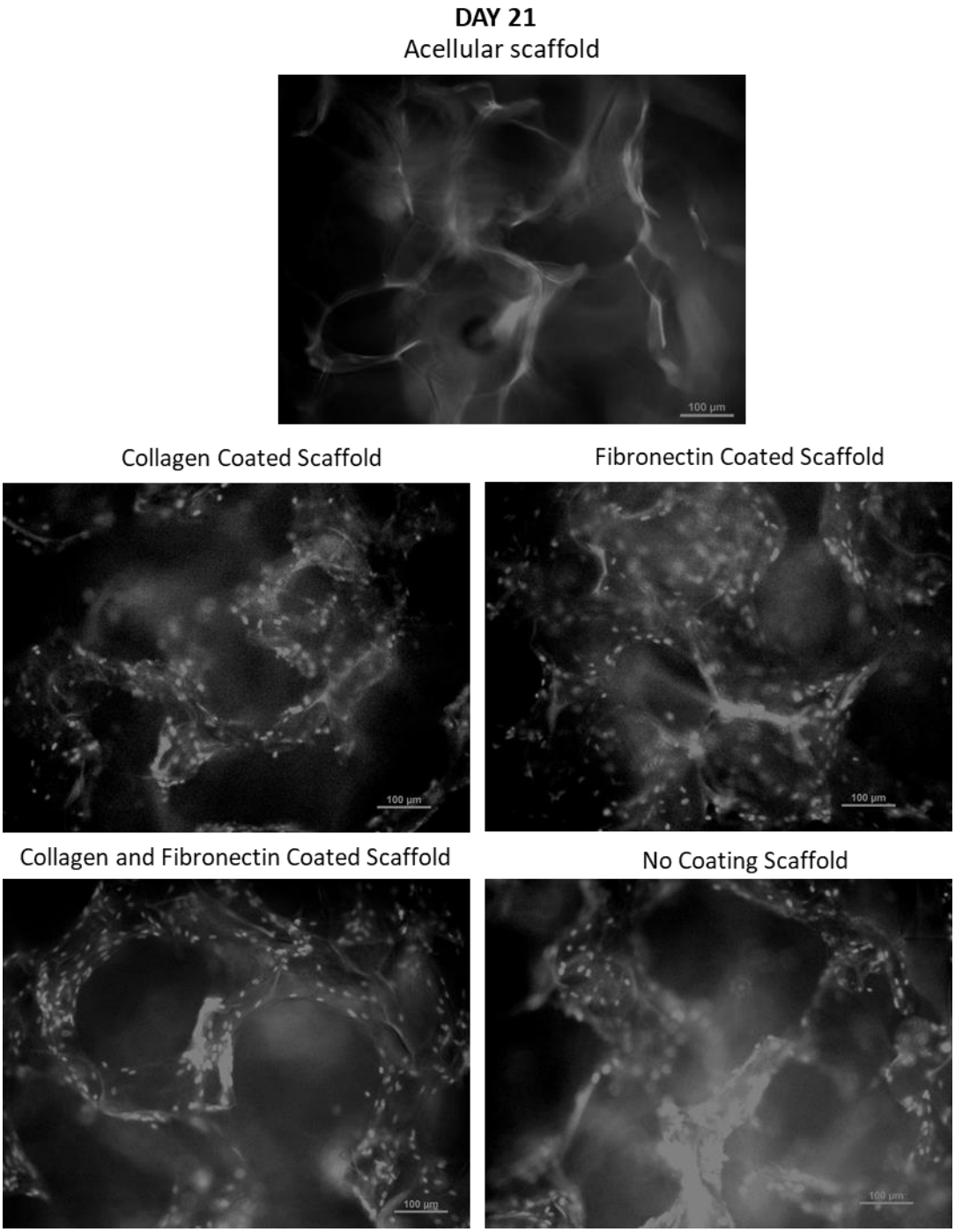

Figure 4.22: Monochrome images of Surgispon scaffolds seeded with 35FLH cells and labelled with DAPI. Scaffolds were coated with COL, FIB, COL+FIB or uncoated, and imaged with DAPI stain. Cells can be observed growing on the scaffolds across all conditions.

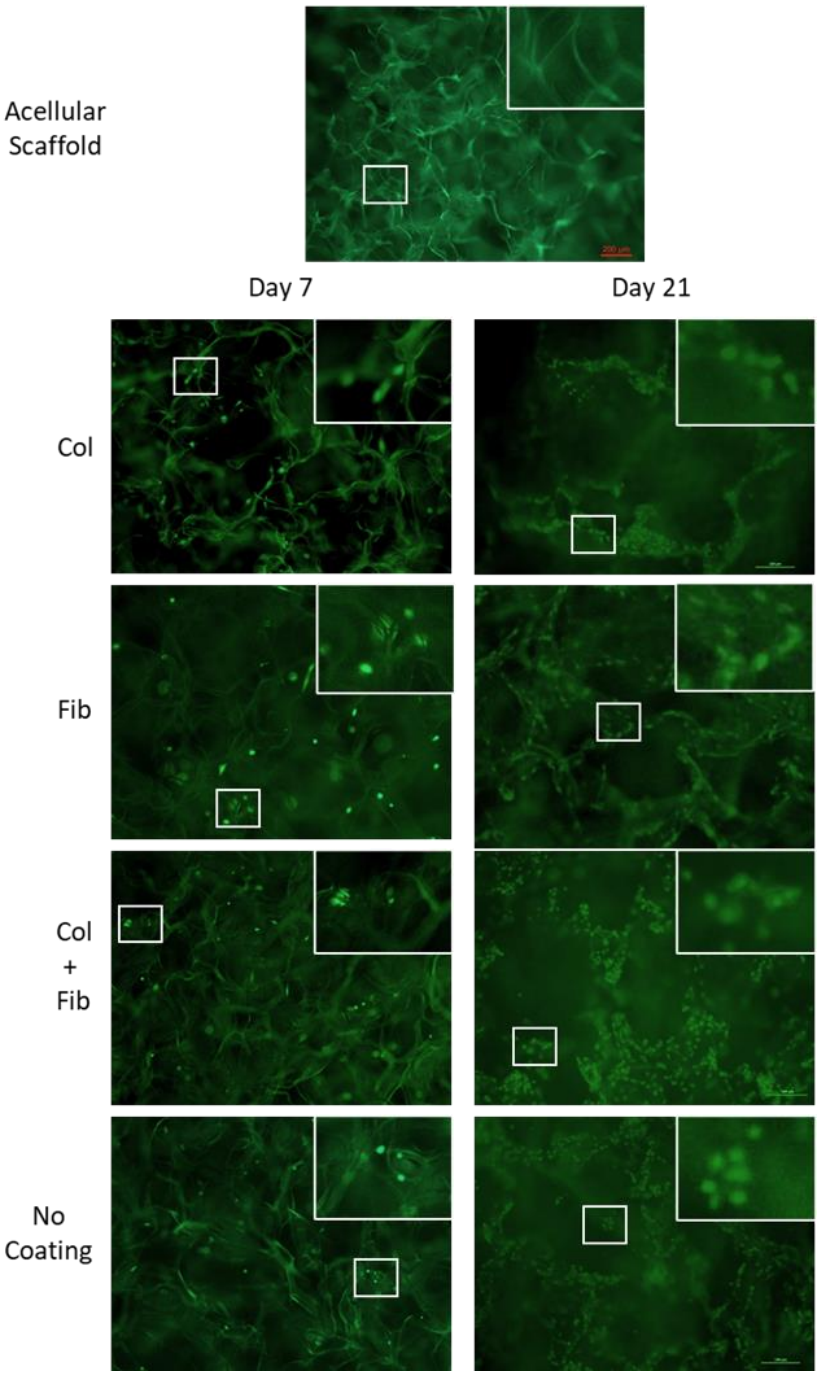

Figure 4.23: Images of Surgispon scaffolds seeded with 35FLH cells and labelled with LIVE/DEAD assay. Scaffolds were coated with COL, FIB, COL+FIB or uncoated, and imaged using LIVE/DEAD stains. Cells can be observed growing on the scaffolds across all conditions.

Based on these experiments, it was clear that chemical coating of the Surgispon scaffolds with collagen type I, fibronectin, or a combination of the two, had no significant effect when

compared to an uncoated scaffold. Having optimised the chemical coating, future experimentation was performed on uncoated scaffolds.

4.4.11 Deactivating 35FLH fibroblast cells

Before co-culturing epithelial (A549) and fibroblast (35FLH) cells, fibroblast cells were deactivated with mitomycin C as described in **section 2.1.5**. Fibroblasts were deactivated (halting of proliferation) in order to create a feeder layer for epithelial cells. The feeder layer is used to increase epithelial cell attachment and proliferation, as well as increasing the similarity to the *in vivo* lung microstructure where basal layers are present (Dale et al., 2019; Hynds et al., 2018).

Deactivating fibroblasts is necessary in order to maintain cultures over a long period of time, with deactivation halting proliferation without impairing the ability of fibroblast to produce ECM and act as a feeder layer and support epithelial cell growth. Without deactivation, excess proliferation would lead to overcrowding and apoptotic cell death (Hegab et al., 2015). The method of deactivation was use of the antibiotic mitomycin C, as this is a proven, reliable and economical method. An alternative would have been the use of x-ray or gamma irradiation, but we did not have access to these sources (Jiang et al., 2016).

Deactivated 35FLH (D-35FLH) cells were seeded onto TCP (60,000 cells/cm^2) and cultured up to 7 days. alamarBlue and PicoGreen assays were applied on samples on days 0, 1, 4 and 7 and untreated 35FLH cells were used as a control. While 35FLH cells showed increased metabolic activity over time, D-35FLH cells showed no change in either alamarBlue or PicoGreen assays, which confirmed the mitomycin C deactivation process (**Fig.4.23**).

It is clear that deactivation has a significant effect on proliferation of 35FLH cells ($p<0.0001$ for alamarBlue and PicoGreen). At days 1, 4 and 7 there is significantly more cell proliferation in 35FLH cultures than D-35FLH cultures, for both alamarBlue or PicoGreen.

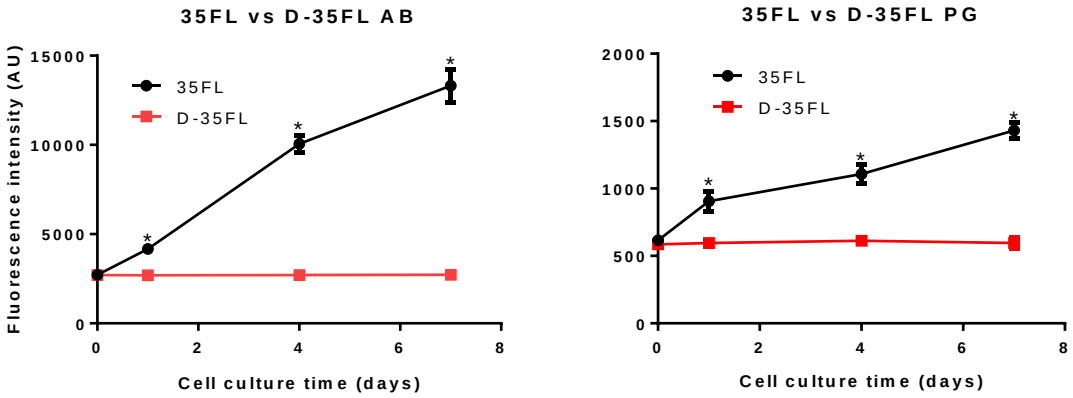

Figure 4.24: Metabolic analysis of 35FLH and D-35FLH cells. alamarBlue and PicoGreen assays were applied on samples to investigate the cell proliferation of active and deactivated cells. Both alamarBlue and PicoGreen assays showed increased activity with 35FLH cells and none with D-35FLH. $p < 0.0001$ (*), (n=4).

Brightfield and fluorescent images of D-35FLH showed similar cell concentrations both on day 1 and day 7 (**Fig.4.24**). LIVE/DEAD images of D-35FLH and 35FLH showed that D-35FLH cells were alive and but did not proliferate, unlike 35FLH cells. Both imaging and metabolic assays showed no increased cell number for D-35FLH.

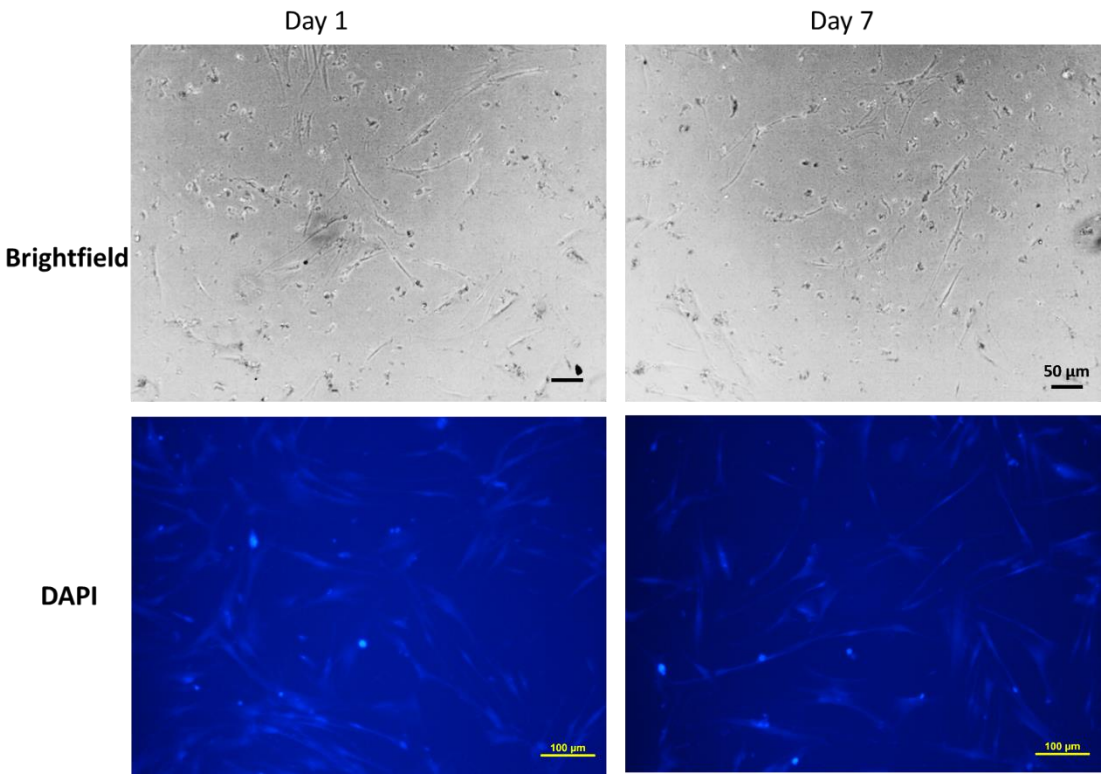

Figure 4.25: DAPI Imaging D-35FLH cells. Brightfield images of D-35FLH cells on day 1 and day 7 did not show cell proliferation on wells. DAPI images also did not show difference between day 1 and day7. Red arrowheads indicate the locations of cells.

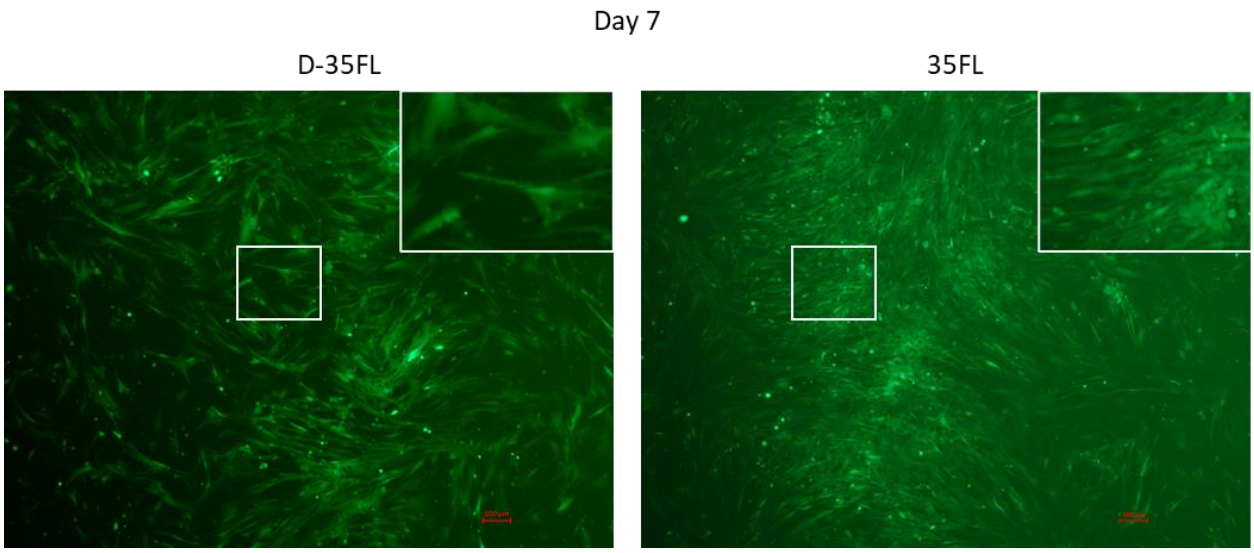

Figure 4.26: LIVE/DEAD imaging of D-35FLH cells and 35FLH cells. Live images of D-35 FL showed that deactivated cells did not proliferate meanwhile 35FLH cells proliferated and became confluent on the wells. Magnified insert contains 15 cells for D35FLH vs 100 cells for 35FLH.

4.4.12 Co-culture of A549 and D-35FLH cells on scaffold

A549 cells and D-35FLH cells were co-cultured on uncoated scaffolds. A549 cells, 35FLH cells and D-35FLH cells were also separately seeded onto additional uncoated scaffolds for control. alamarBlue and PicoGreen assays were applied to samples on days 7, 14 and 21 (**Fig.4.26**).

Firstly, A549, 35FLH and A549 from co-cultures all significantly increased in fluorescence intensity from days 7-14 and 14-21 for either alamarBlue or PicoGreen ($p<0.001$ for all comparisons). D-35FLH did not significantly increase at any stage ($p>0.9$ for both), showing that the deactivation protocol was successful.

Secondly, for alamarBlue results, co-culturing the cells had a significant effect on the cell proliferation over time ($p<0.0001$), with A549 + D-35FLH co-cultures having a significantly greater cell proliferation for days 7, 14 and 21 compared to other conditions. A549 also had

significantly greater proliferation over time compared to 35FLH ($p<0.001$) from alamarBlue results.

Lastly, for PicoGreen, conditions containing A549 cells (A549 and A549+D-35FLH) had significantly greater cell proliferation than 35-FLH cells ($p<0.001$). However, there was no significant difference between the cell proliferation of A549 and the co-culture A549+D-35FLH from PicoGreen results of days 14-21 ($p>0.05$).

A549 cells on uncoated scaffolds showed similar results to **section 4.3.7** and 35FLH cells showed similar results to **section 4.3.8** as expected.

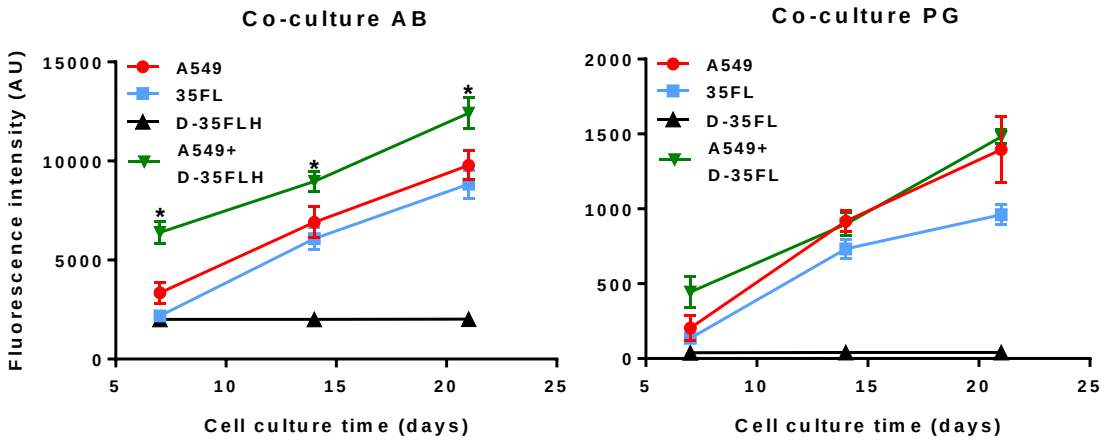

Figure 4.27: Viability analysis of cultures and co-cultures on uncoated Surgispon scaffolds. Single cell type cultures of A549 cells, 35FLH cells and D-35FLH cells on uncoated scaffolds were used as control. *: $p<0.001$, n=6.

D-35FLH cells were labelled with CellTracker Blue CMAC Dye, which penetrates the membrane and is converted to a membrane-impermanent fluorescent probe inside the cell. The process of conversion is detailed in **4.3.11**. These labelled cells were seeded onto a scaffold for co-culture with A549 cells. After 21 days co-culture, the LIVE/DEAD assay was

applied to samples, with the blue fluorescent channel used to localise and track D-35FLH samples (**Fig.4.28**).

Fluorescence images show D-35FLH cells in blue and viable, proliferating A549 cells in green. Tracking the deactivated cells in this manner shows that fibroblast and epithelial cells are localised and attached together on the scaffolds, as they are in the alveoli.

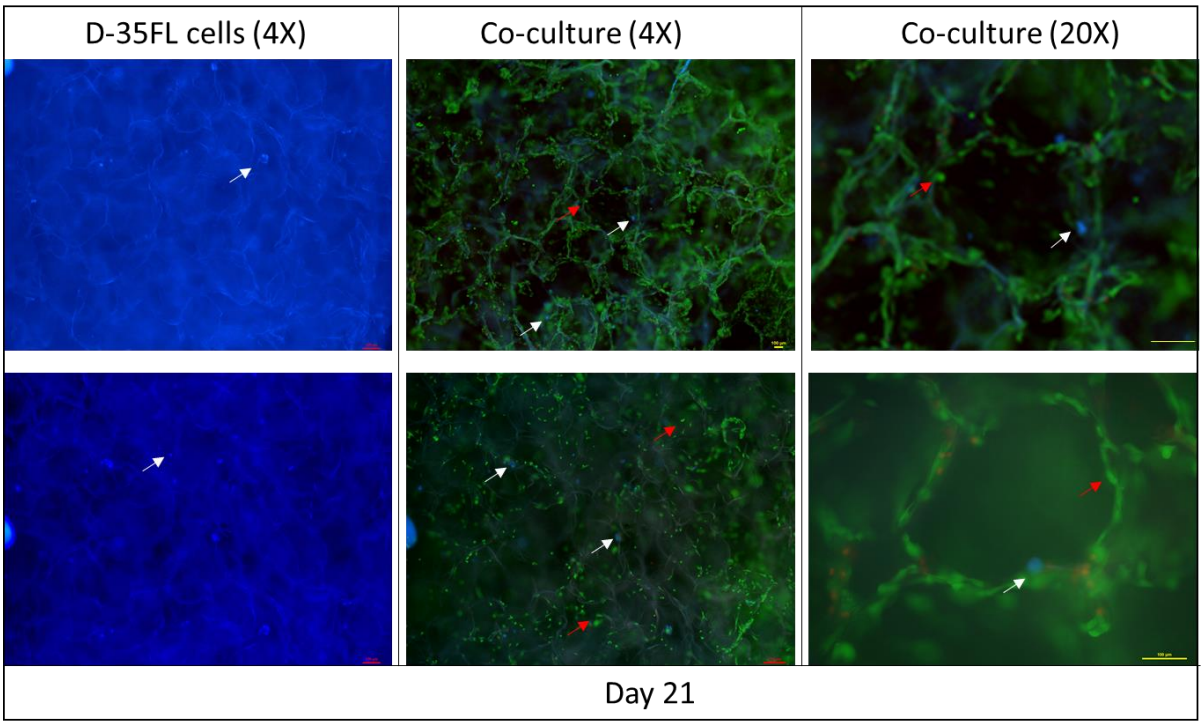

Figure 4.28: Tracking D-35FLH in co-cultures on scaffolds. Blue fluorescence shows D-35FLH, green fluorescence from LIVE/DEAD shows A549. Both cells can be seen attached around the perimeter and localised to each other. Red arrowheads indicate the locations of A549 cells and white arrowheads indicate the location of D-35FLH cells. Scale bars shown.

4.5 Discussion

In this chapter Surgispon scaffolds were shown to support the culture of human lung epithelial (A549) and lung fibroblast (35FLH) cell lines, both separate and together as co-cultures. These cells attach to scaffolds and proliferate over the long term (up to 21 days), and are shown to remain viable throughout (**Figs 4.15, 4.18, 4.19, 4.21, 4.22, 4.26, 4.28**). This is an important step for Surgispon as a scaffold as part of a cell-based approach for lung tissue engineering. Deactivated fibroblasts (D-35FLH) had an effect on the metabolic activity and proliferation of epithelial cells in co-culture. For epithelial and fibroblast co-culture, fibroblasts were deactivated in order to halt their proliferation (the fibroblasts are rendered mitotically inactive) and create a feeder layer for epithelial cells. The feeder layer is used to increase epithelial cell attachment and proliferation, as well as increasing the similarity to the in vivo lung microstructure where basal layers are present (Dale et al., 2019; Hynds et al., 2018). Deactivating fibroblasts is necessary in order to maintain cultures over a long period of time, with deactivation halting proliferation without impairing the ability of fibroblast to produce ECM and act as a feeder layer and support epithelial cell growth. Without deactivation, excess proliferation would lead to overcrowding and apoptotic cell death (Hegab et al., 2015).

The addition of a feeder layer of D-35FLH cells affected the proliferation of A549 cells, this may be due to fibroblasts producing extracellular matrix (ECM) proteins and creating a better microenvironment for the lung epithelial cells. This could be investigated in more detail with additional experiments imaging scaffolds with EM before and after fibroblast seeding to observe any protein deposition. Scaffold mechanical properties after fibroblast culture could also be investigated, looking at stiffness and elasticity through the Young's modulus.

This model is also a better mimic of the *in vivo* alveoli (seen in **Fig.4.2**), which features co-localization of both fibroblasts and epithelial cells, as shown in **Figure 4.28**. Cell analysis assays alamarBlue and PicoGreen have successfully been applied to 3D cell cultures on scaffolds but required optimisation in order to be effective over the long term (**Figs.4.5-4.12**).

Fluorescent assays such as LIVE/DEAD, Vybrant cell tracker or DAPI labelling can be effective but are limited due to the native Surgispon autofluorescence in most channels (**Fig.4.17**). This autofluorescence is an issue across most visible wavelengths, with collagen exhibiting fluorescence from approximately 370-700 nm (Yova et al., 2001), most of the visible spectrum and covering all fluorescent dyes used in this project, from DAPI to LIVE/DEAD. There are some potential solutions to lessen the effects of autofluorescence, including: using a fluorophore beyond 700 nm in wavelength such as a far red/infrared probe such as Cy5/Cy7, bleaching the scaffold of autofluorescence using long exposures to a high powered light source (ideally a laser), or using non-fluorescent imaging such as brightfield or EM. The most feasible solution would be to test with some far-red dyes for future experiments. Bleaching scaffolds would require regular and long-term access to a high-powered light source for every scaffold experiment, there is limited access to these both in terms of power and booking time, and it may affect the structure of the scaffold. The last option of EM is also limited in terms of access, brightfield imaging was done but lacked contrast, it would be useful to try phase-contrast imaging in order to introduce contrast and avoid fluorescence. However, both EM and brightfield would be challenging to use with fluorescent probes in order to characterise live cells and look at specific proteins, but could at least observe morphology and compare different experimental conditions.

As a gelatine sponge, Surgispon did not require any chemical coating in order to be effective as a 3D cell culture scaffold, this is another advantage for Surgispon as little processing is needed to prepare them for experimentation with cells. Surgispon is composed of gelatin, which is derived from collagen. With collagen being the most abundant protein in ECM, Surgispon already presents an ECM-like microenvironment to cells. By coating with additional ECM proteins such as fibronectin and elastin the biological relevance may increase, but experiments with fibronectin coating did not show any increased in cell viability or proliferation for A549 or 35FLH cells (Fig.4.16 and Fig.4.20), despite the microenvironment being closer to in vivo ECM. It may be that the presence of collagen has the most effect, it would be challenging to test these scaffolds in the absence of collagen as they are composed of gelatin, if a similar non-collagen-based scaffold could be identified it would work well to test how the presence of collagen in native Surgispon assists cell attachment, viability and proliferation.

The alamarBlue cell metabolic activity assay was chosen to track cell proliferation and viability through their metabolic activity. This assay is a resazurin base, photosensitive solution that can quantitatively measure cell viability based on use of the indicator by healthy cells. This assay has been used to determine cell viability for many cell types, but it requires optimising for each application and cell model (Rampersad, 2012).

The initial alamarBlue standard curve in **Figure.4.5** showed strong linear correlation from 0 to 90,000 cells/cm^2, indicating increased cell metabolic activity in association with increased cell number. However, when the cell number was higher than 90,000 cells/cm^2, the alamarBlue assay reached a plateau due to equalised reduction level of resazurin. Resazurin reduction increases with increased cell metabolic activity, which can increase with increased cell

number (Borra et al., 2009). When the same experiment was repeated after culturing cells for a day, the alamarBlue assay reached plateau with an initial cell seeding number of 45,000 cells/cm^2, even lower than the previous result (**Fig.4.6**). This shows that the cell number increased due to overnight proliferation, and the standard curve plateaued (saturated) even earlier. If this occurred after just one day, cell culture experiments over several weeks would most likely only show saturated results, limiting the use of the assay in displaying how cells have proliferated on the scaffold.

With a smaller initial cell seeding density, the alamarBlue standard curve showed increased metabolic activity strongly correlating with increased cell number at day 0 (r:0.99, **Fig.4.7**). However, when these samples were cultured, the graphs started to plateau by day 3, and by on day 7 a plateau had been reached for all samples. Due to this oversaturation, results indicate that to be able to assess cell proliferation in cultures that have been cultured for longer than 7 days, it will be necessary to optimise the initial cell seeding number and the alamarBlue™ incubation time (Al-Nasiry et al., 2007).

alamarBlue is a non-toxic solution for cells even with a long incubation time. However, increased incubation time allows cells to reduce resazurin to highly fluorescent resorufin (Mikus and Steverding, 2000). When 1000-60,000 cells/cm^2 were seeded onto TCP and cultured for 7 days, 3 hour alamarBlue incubation time still showed oversaturation due to cell proliferation. However, when this incubation time was reduced, the level of saturation changed. However, as this was done at day 7, most results were oversaturated and had low linear associations. Based on the cell number and incubation time optimization, 2000 cells was chosen as the initial seeding number for scaffolds in order to investigate cell proliferation

on 3D cell culture over the long term without assay saturation, if the assay was incubated for 1 hour or less.

The MTT cell metabolic assay determines the mitochondrial activity of living cells by the conversion of MTT into formazan crystals. The MTT assay is broadly used for measuring cell viability thanks to the correlation between cell population and total cell metabolic activity, similarly to alamarBlue (Hamid et al., 2004). MTT results showed a similar linear increase in fluorescence intensity with increased cell number during early days of cell culture, but MTT reached a plateau on day 1, earlier than alamarBlue. Detached but not fragmented cells would continue transforming MTT to formazan which would result in false positives and overestimation. It is suggested that both alamarBlue and MTT assays are effective to measure cell viability (Hamid et al., 2004), but based on these results, the alamarBlue assay was chosen to determine cell proliferation on scaffolds. Another reason the MTT assay was not desirable was the fact that the formazan crystals need to be dissolved in a strong organic solvent, DMSO, in order to take the fluorescence reading. DMSO is highly cytotoxic and not suitable for repeated use, unlike the alamarBlue assay which does not affect cell viability when applied. The alamarBlue assay is simple, rapid, efficient, reliable, sensitive, safe and cost-effective cell viability assay (O'Brien et al., 2000).

PicoGreen™ is a very sensitive double stranded DNA (dsDNA) quantification assay that can detect as little as 25 pg/ml of dsDNA in the presence of single stranded DNA (ssDNA), RNA, and free nucleotides (Ikeda et al., 2009). When cell proliferation was assessed with the alamarBlue assay, it is possible to compare the results with DNA quantification assays such as PicoGreen (Quent et al., 2010). Before cell cultures reached confluency on day 4, PicoGreen results showed increased dsDNA quantity with increased initial cell seeding density, based on

these results the PicoGreen assay was chosen for study of cell proliferation on scaffolds as well as the alamarBlue assays. Using two assays that complement each other allows for more robust data and tracking of cell proliferation and viability.

While cell culture is commonly done on 2D surfaces, it gives insufficient data for direct clinical applications on 3D samples, such as the complex 3D structure of the alveoli and lung. 3D scaffolds provide a similar structure to *in vivo* natural systems (Ravi et al., 2015). In order to support cell growth on 3D structures, scaffolds must offer a similar surface to native *in vivo* ECM (Carletti et al., 2011)). Microscopy and cell assay results together showed that Surgispon scaffolds support cell growth. However, brightfield images show cells growing on the scaffold as well as the TCP underneath the scaffold, suggesting possible cell migration from scaffolds to the plate, or poor initial attachment (**Figs.4.13-4.14**). This suggested that Surgispon scaffolds may benefit from a coating that improves cell attachment.

The nature of the Surgispon scaffold surface has an important role for cell attachment, proliferation and function. Cells are more likely to attach and proliferate on surfaces similar to extracellular matrix (ECM), and the main protein types in the ECM are fibronectin, collagen and laminin (Kleinman et al., 1987). Collagens are the major proteins in the lung and create the base membrane for epithelial and endothelial cells (Lang et al., 1994), with collagen type I being one of the major types of collagens in lung alveolar wall (Seyer et al., 1976). By coating the Surgispon scaffolds with collagen and/or fibronectin, improvements in cell attachment and viability were expected as the microenvironment would be more similar to that of the lung. However, no significant difference in cell proliferation or metabolic activity was observed between scaffold coating types or uncoated scaffolds (**Figs.4.16 and 4.20**). Surgispon scaffolds are made of pure pharmaceutical gelatine foam. This gelatine is

hydrolysed collagen, being derived from collagen means Surgispon is itself a good structure for mimicking the lung microenvironment and the ECM. Gelatine-based scaffolds have been used as 3D scaffolds for cell culture and supported good cell proliferation (Li and Wang, 2012). This feature of Surgispon means that additional chemical coatings are unnecessary, and future experiments involve uncoated scaffolds.

Alveolar fibroblasts produce ECM proteins that supports the lung alveolar structure which is critical for gas exchange, cell proliferation and metabolic functions (Herzog et al., 2008). 35FLH fibroblasts were successfully cultured on scaffolds for 21 days, with LIVE/DEAD (**Fig.4.22**) and DAPI (**Fig.4.21**) images showing cell attachment, and alamarBlue and PicoGreen assays showing cell proliferation over time up to 21 days (**Fig.4.20**). Surgispon scaffolds can support fibroblast cell growth with or without chemical coating.

Although fibroblast cells produce ECM proteins, when they differentiate to myofibroblasts these cells are the major contributor to the fibrotic lung disease (Hinz et al., 2007). Fibroblast cells are therefore deactivated before culturing with epithelial cells in a co-culture that is a good *in vitro* mimic of the *in vivo* alveoli. Deactivation of cells were checked by using alamarBlue and PicoGreen assays. Both assays showed no increase in cell metabolic activity nor dsDNA quantity over 7 days (**Fig.4.23**). Images of samples also showed higher cell concentration on fibroblast samples then deactivated samples which also confirms deactivation of fibroblast cells (**Fig.4.25**). These deactivated cells are now a good feeder layer for the epithelial cells, the fibroblasts can put down ECM and prepare the scaffold surface without any risk of fibrosis.

Epithelial cells (type I and type II) are the main and major cells in lung alveoli as well as fibroblast cells for the structure of the alveolus (Pottier et al., 2009). A549 epithelial cells were

cultured on uncoated Surgispon scaffolds with deactivated 35FLH (D-35FLH) fibroblast cells for 21 days. The combination of these two cells types represents a rudimentary alveolus. By combining them and co-localizing on the same scaffold, a better model of the alveoli is produced *in vitro.* alamarBlue and PicoGreen graphs showed cell proliferation on scaffolds while there is no increase for D-35FLH only samples on scaffolds (**Fig.4.26**). Cell proliferation was observed for A549 cells or 35FLH cells in separate cultures on scaffolds, as well as for A549+D-35FLH co-cultures, based on metabolic analysis. Fluorescent imaging also showed viable cell attachment (**Fig.4.28**).

When specifically labelling and tracking D-35FLH cells, they were shown to be localized with A549 cells on the scaffold (**Fig.4.28**), similarly to the structure of the alveoli *in vivo.* Interaction between epithelial cells and fibroblast cell plays a critical role in lung tissues. 3D co-culture systems represent a more accurate *in vivo* mimic, demonstrating the architecture of the alveolus and cell-to-cell communication as well as cell to ECM interaction (Horie et al., 2012).

We have demonstrated that porous Surgispon scaffolds are an excellent candidate material for lung cell culture, having been shown to support attachment and proliferation of both lung epithelial and lung fibroblast cell lines, either separately or together in co-cultures. This is promising for the next stage of primary lung cell culture in order to create a more clinically relevant model of the alveoli for COPD pre-clinical research.

Chapter 5

Examining the Surgispon® scaffolds for primary cell culture and proof of concept study

5.1 Introduction

5.1.1 Porcine Lung Models

Porcine lung models have been used in many studies and have made a significant contribution to lung research over the decades. Porcine lung models have been used as disease models to help increase the understanding of pathogenesis and to develop novel treatment strategies. For example, Bruun and colleagues studied emphysema using a porcine model, revealing the role of metalloproteinases in the pathogenesis of emphysema, showing that the porcine model is comparable to human emphysema patients in both morphology and functionality (Bruun et al., 2013). Other examples used porcine lung models to study cystic fibrosis (Rogers et al., 2008), bile aspiration (Porembka et al., 1993) and infection with *Pseudomonas aeruginosa* (Harrison et al., 2014).

Porcine lungs are similar in size and anatomy to human lungs, with similar immunology (Pabst, 2020) and showed that they can be used as successful lung models, particularly for translational research (Judge et al., 2014; Lu et al. 2020; Ohata and Ott, 2020). Rodents are not preferred as, unlike pigs, rodents do not have lobe division on the left lung, their lungs are far smaller, and their respiratory rate is approximately 5x than an adult human (Perinel et al., 2017). In addition, some disease models showed a higher similarity comparing pigs to humans than mouse to humans. However, scientific literature related to porcine lungs is still limited (Judge et al., 2014).

5.1.2 Importance of Cell Attachment

In tissues, cell attachment is important for repair, organisation and maintenance (Khalili and Ahmad, 2015). Tissue repair is even more important within the perspective of lung disease,

especially in chronic obstructive pulmonary disease (COPD) and related conditions, as the lung cells of COPD patients are not able to complete repair functions. The first step of epithelium repair requires cell migration and proliferation followed by de-differentiation of epithelial cells, it has been shown that cell attachment and proliferation play a key role in COPD (Perotin et al., 2014).

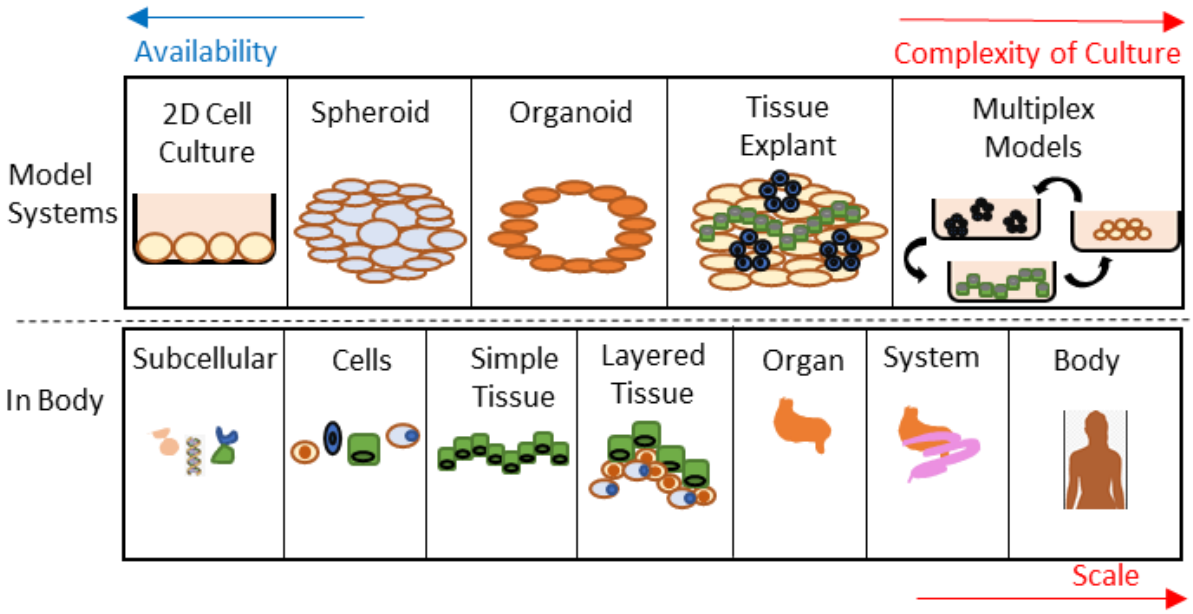

Figure 5.1: Model systems in life science vs organisations of the body. In life science many models start with simple 2D monolayer cell culture, then complexity and scale increases while availability decreases due to the need for tools and biochemical compounds. When compared to tissue explants, organoid systems can mimic similar cell-cell and cell-matrix interactions.

The lung epithelium has a complex structure with numerous functions and different cell types. These cells include basal, secretory and ciliated cells in the conducting airways, and type I/II pneumocytes lining the alveoli. These lung epithelial cells can be cultured in 3D structures and in the right conditions they can self-organise into structures knows as organoids (**Fig 5.1**) (Barkauskas et al., 2017). Recent studies showed that air-liquid interface (ALI) cultures most

closely resemble the microenvironment of the in vivo lung epithelia (**Fig 5.2**) (Pezzulo et al., 2010).

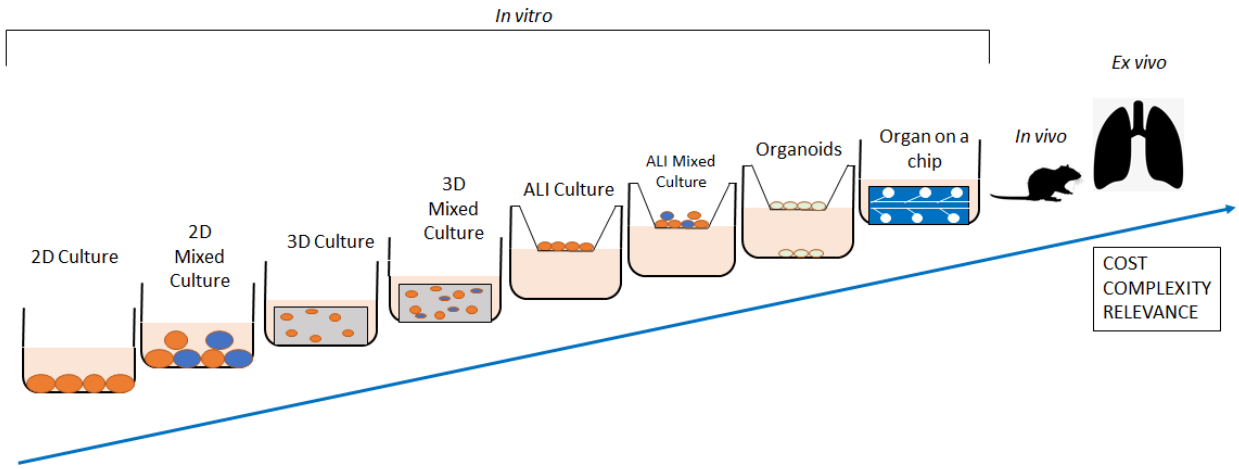

Figure 5.2: Models for respiratory research. Some available respiratory models are shown, increasing in cost, complexity and relevance from left to right. Models range from 2D cell culture of one cell type to full *in vivo* animal models and *ex vivo* organs.

5.1.3 Decellularised Lung Tissue

Decellularised tissues present an opportunity to perform more research into ex vivo organ generation and in vitro lung extracellular matrix (ECM), particularly cell-ECM interactions (Wagner et al., 2014). Decellularised tissues can be used as an implantable organ graft that can be transplanted via surgeries in rodent models. Using decellularised tissues as an implantable acellular scaffold can increase the potential number of treatments for end stage lung disease. Unfortunately, lung transplantation is still the only potential cure for end-stage lung diseases patients, and this option is very limited due to organ shortage (Zhou et al., 2018). Increased research into ex vivo lung models and 3D lung tissue engineering can result in many benefits for COPD patients and those who need transplants.

The ECM plays an important role for cell attachment, proliferation and differentiation. After decellularisation of a tissue, the ECM is the main structure remaining and has a crucial effect on the recellularisation process (Brown and Badylak, 2014). The decellularisation process can be very harsh for the ECM due to the use of detergent, and this process can result in poor decellularised tissues that can have negative outcomes when attempting to culture cells on them, such as reduced cell attachment, increased cell death and increased inflammation (Reing et al., 2010). Successful decellularisation would allow for cell attachment and proliferation on decellularised tissues (Balestrini et al., 2015), resulting in recellularised tissues that can be powerful models for the lung.

Successful decellularisation of small lung segments or slices has been successfully established (Bonvillain et al., 2012). Alongside this, recellularisation of decellularised lung tissues with epithelial and endothelial cells has shown that it is possible to achieve bioengineered lungs that are capable of gas exchange in rodents (Petersen et al., 2010b), this is a huge opportunity for lung tissue engineering research. Scaling this work to human cells and grafts is the next important step for clinically relevant studies. Using porcine lungs represents a great chance to increase our knowledge in this area and to create human-like lung models, due to porcine lung tissue having such anatomical similarity to human lungs.

Some research has used acellular ECM-like scaffolds that can act as a tissue-specific template and help constructive remodelling of the lung (Brown and Badylak, 2014). Tissue-specific 3D scaffolds are capable of control and directing cell migration in order to help cell organisation (Ovsianikov et al., 2010). Cell migration has an important role in lung injuries as the epithelium must be repaired to restore lung function (Lesur et al., 1996). As well as repair, airway epithelial cell migration is responsible of lung development and growth. Several lung diseases

such as COPD, characterised with absent of repair of damaged respiratory tissue, lowered epithelial migration to the site (Xiao et al., 2012).

As previous chapter results have shown, 3D porous gelatine sponge Surgispon® can provide a 3D scaffold that is suitable for cell culture and contains pores that can mimic the structure of alveoli. This cell culture was performed on epithelial and fibroblast human lung cell lines, in order to establish a more biologically relevant model, human lung primary cells would be a desirable cell type to culture on our scaffold, but due to the lack of human tissue and the previously explained similarity between porcine and human lung anatomy and functionality, porcine lung primary cells are a suitable substitute.

In this chapter, primary porcine lung cells are cultured on 3D Surgispon scaffolds in order to establish an alveolar model. These scaffolds are also used in combination with decellularised primary porcine lung tissue, in order to study migration and the use of Surgispon as a transplant in vivo, as a platform for lung tissue engineering.

5.2 Aim

The aim of this chapter was to investigate 3D cell culture of primary porcine lung epithelial and fibroblast cells on Surgispon scaffolds and decellularised porcine lung tissue. Migration of lung cells from scaffolds to tissue and vice versa was also tested to determine Surgispon scaffold suitability for in vivo studies.

5.3 Method

The diagram of the experiment is summarised in **Schematic 5.1** and all materials and methods are described in full in **Chapter 2.**

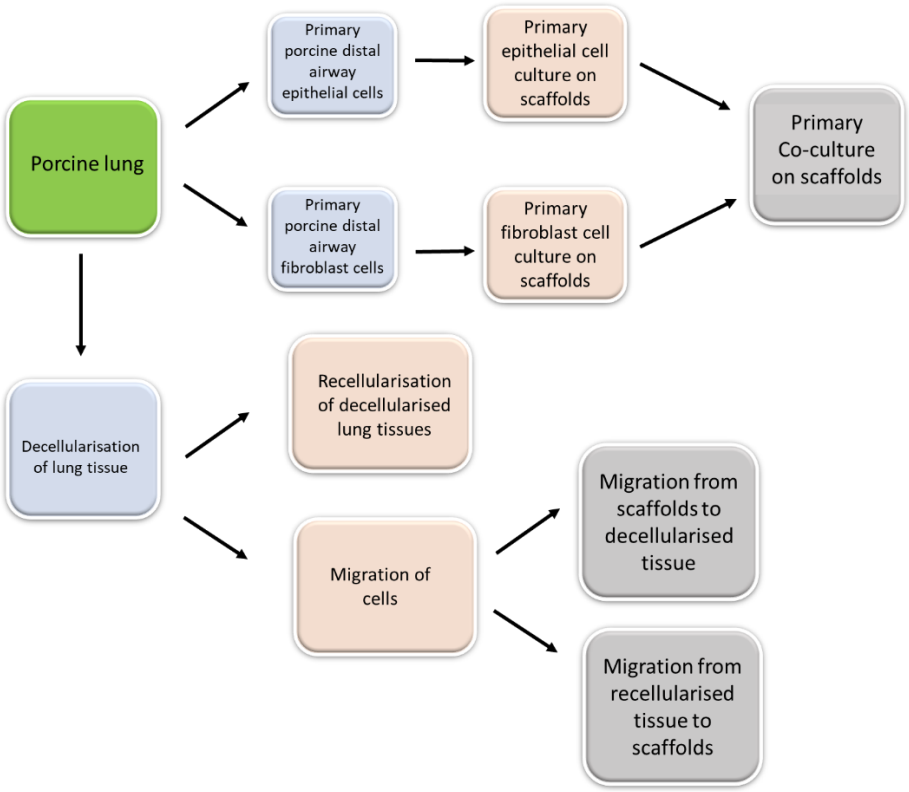

Schematic 5.1: A schematic to show the flow of experimental design for chapter 5. Porcine lung primary cells and decellularised porcine lung tissue is used in combination with Surgispon scaffolds in order to study 3D cell culture on different materials and migration between these materials.

5.3.1 Primary porcine lung cell culture on scaffolds

Porcine lungs were dissected and processed as described in **section 2.6.1** in order to isolate lung distal airway cells, these cells were cultured in specific conditions in order to isolate porcine lung epithelial cells (PLECs) or porcine lung fibroblasts (PLFs). For PLECs, the cell suspension was seeded onto collagen coated (10 µg/cm^2) T75 flasks and cultured with cFAD+ media to confluency (as described in **section 2.6**). For PLFs, cell suspension was seeded into uncoated T75s and cultured with DMEM+. A high antibiotic (50 ml ready media, 50 µl gentamycin, and 50 µl ciprofloxacin) concentration was used in all media until cells were passaged up to three times in order to prevent any possible contamination.

For all Surgispon scaffold culture experiments, cells with passage numbers 3-6 were used. Cells were trypsinised as described in **section 2.1.1** and prepared for seeding onto uncoated scaffolds. 2000 cells were seeded onto each scaffold at an initial seeding density of 32 cells/mm^3 as described in **section 4.3.6** and cultured in 48 well plates up to 21 days. To determine primary cell growth and viability on scaffolds, alamarBlue™, PicoGreen™, LIVE/DEAD and DAPI assays were applied on as described in **section 2.2**. Scaffolds were carefully moved to sterile 48 well plates using sterile tweezers. alamarBlue and PicoGreen assays were applied to samples on days 7, 14 and 21. LIVE/DEAD and DAPI assays were applied to samples on days 7 and 21 to confirm cell viability and proliferation.

5.3.2 Deactivating porcine lung fibroblasts

When PLFs reached 80% confluency in T75 flasks, cells were deactivated using mitomycin C as described in **section 2.1.5**. Deactivated PLFs (D-PLFs) were trypsinised and 2000 cells/cm^2 were and seeded onto 48-well plates. Cells were cultured up to 7 days and alamarBlue and PicoGreen assays were applied on days 0, 1, 4 and 7 to investigate the deactivation process. The same density of active PLF cells were used as a control. LIVE/DEAD cell viability staining was applied to both D-PLF and PLF samples on day 1 and 7 to observe the difference in cell numbers between D-PLF and PLF cells over time.

5.3.3 Differentiation of primary lung epithelial cells

D-PLFs and PLECs were seeded onto scaffolds coated with 40% Matrigel® as described in **section 2.6.2**, based on the sphere culture differentiation protocol from StemCell technologies which uses PneumaCult-ALI medium (STEMCELL Technologies, 2019). As well as using PneumaCult-ALI medium, we also used our in-house medium cFAD (Dale et al., 2019b)

to determine if it would also support cell growth and differentiation. The following supplements were used:

Table 5.1: Different media used for PLEC differentiation.

Name of media	Contents (further described in section 2.1)
CFAD+	CFAD media with ROCK inhibitor (1 µg/ml) added fresh.
CFAD+++	CFAD media with ROCK inhibitor (1 µg/ml), FGF (0.05 ug/ml), HGF (0.03 ug/ml) and EGF (10 ng/ml) added fresh.
Pneumacult+	Pneumacult-ALI media with hydrocortisone (0.32 µl/ml) and heparin (2 µl/ml) added fresh.
Pneumacult +++	Pneumacult-ALI media with hydrocortisone (0.32 µl/ml), heparin (2 µl/ml), FGF (0.05 ug/ml), HGF (0.03 ug/ml) and EGF (10 ng/ml) added fresh.

ROCK inhibitor was added to CFAD to promote epithelial growth based on work in (Dale et al., 2019b), and hydrocortisone/heparin were added to Pneumacult media in line with the protocol from StemCell. Growth factor supplements HGF, EGF and FGF were added based on work by our collaborators in China, (Wang et al., 2019)). All samples were cultured for 14 days and the morphology of cells were observed using brightfield microscopy.

5.3.4 Immunohistochemical staining

PLECs and D-PLFs were co-cultured on 40% Matrigel coated scaffolds and cultured in cFAD+ media for 21 days. After 21 days samples were fixed with 10% formalin solution (approx. 4% formaldehyde) overnight and washed with PBS. Washed samples were first imaged under a brightfield microscope and then stained with DAPI and imaged with a fluorescence microscope.

To characterise each cell type, PLECs were stained with antibodies for pan-Cytokeratin and PLFs were stained with antibodies for vimentin. In order to confirm the presence of stem cells,

antibodies for p63 were used as a keratinocyte stem cell marker. To determine the differentiation of cells on scaffolds, samples were stained with podoplanin (AT1 marker), anti-prosurfactant protein C (SPC) (AT2 marker) and mucin 5AC (ciliated cell marker). Details of primary and secondary antibodies and dilutions are given in **table 5.1**. All of the stainings were accompanied with DAPI (**section 2.2**).

Table 5.2 Primary and secondary antibodies and dilutions for immunocytochemical staining

Primary Antibody	Secondary	Dilution for primary	Dilution for secondary
Pan Cytokeratin	Mouse Mono - Alexa Fluor 594	1:100	1:250
Vimentin	Rabbit Mono - Alexa Fluor 488	1:100	1:500
Podoplanin	Rabbit Mono - Alexa Fluor 488	1:100	1:250
SPC	Rabbit Mono - Alexa Fluor 488	1:100	1:500
p63	Rabbit Mono – Alexa Fluor 488	1:300	1:300
Mucin 5AC	Mouse Mono – Alexa Fluor 594	1:100	1:500

5.3.5 Decellularisation of lung tissue

Porcine lungs were sliced and decellularised as described in **section 2.7**. Decellularised tissues were stained with DAPI to investigate for any possible residual nuclei or cells. Sliced lung samples were also fixed and stained with DAPI as described in **section 2.3.1** and used as a control group. DAPI stained samples were imaged with a fluorescence microscope.

After DAPI staining, decellularised tissues were prepared for DNA analysis by using DNeasy blood and tissue kit as described in **section 2.2.6**. DNeasy was used to extract DNA from samples. Extracted DNA solutions were quantified with a NanoDrop™ spectrophotometer as described in **section 2.2.7**. As well measuring DNA quantity with the NanoDrop, samples were also prepared for PicoGreen DNA assay with proteinase K digestion of samples as described in **section 2.2.3**.

5.3.6 Recellularisation of decellularised lung tissues

Decellularised lung tissues slices were prepared for recellularisation by washing with PBS three times and cut to create pieces with a 1 cm^2 surface area. Decellularised lung tissues were reseeded with either A549 cells or PLECs to investigate the structure of decellularised tissue structure.

Cells were fluorescently tagged with Vybrant™ multicolour cell-labelling kit as described in **section 2.3.2**. A549 cells were stained with red and primary porcine lung epithelial cells were stained with green fluorescence before seeding onto decellularised tissues. Cells were prepared for cell culture as described in **section 2.1** and 100,000 cells were seeded onto each decellularised tissue sample with 20 µl of the appropriate media. After cell seeding all samples were incubated in cell culture incubator for 2 hours before adding 200 µl of appropriate cell

culture media. Samples were cultured for 3 days and imaged with a fluorescence microscope to investigate cell attachment. Fixed and DAPI stained lung tissue slices were used as a control.

5.3.7 Cell migration in decellularised lung tissue

A549/35FLH cell lines or PLF/PLEC primary cells were prepared and 30,000 cells were seeded either onto uncoated scaffolds (initial seeding density of 480 cells/mm^3) or decellularised lung tissue pieces (initial seeding density of 30,000 cells/cm^2) as described in **section 2.1**. Cells were cultured for 7 days to investigate cell migration.

Scaffolds and decellularised lung tissues were stained with LIVE/DEAD and imaged with a fluorescence microscope to investigate cell viability, attachment onto scaffolds/decellularised tissue and migration to/from scaffolds/decellularised lung tissue. PicoGreen was applied to scaffolds (cells seeded onto), decellularised tissue (scaffolds with cells cultured on). recellularised tissue (cells seeded onto) and empty scaffolds (cultured on recellularised tissue) as described in **section 2.2.4**. The format of the migration assay experiments is highlighted in **Schematic 5.2**.

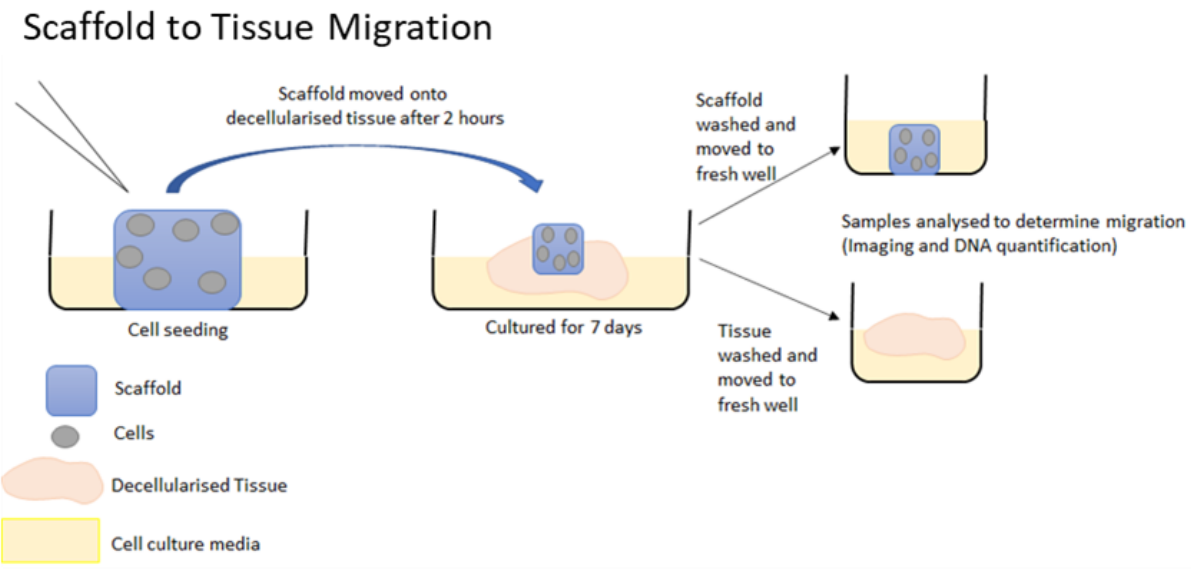

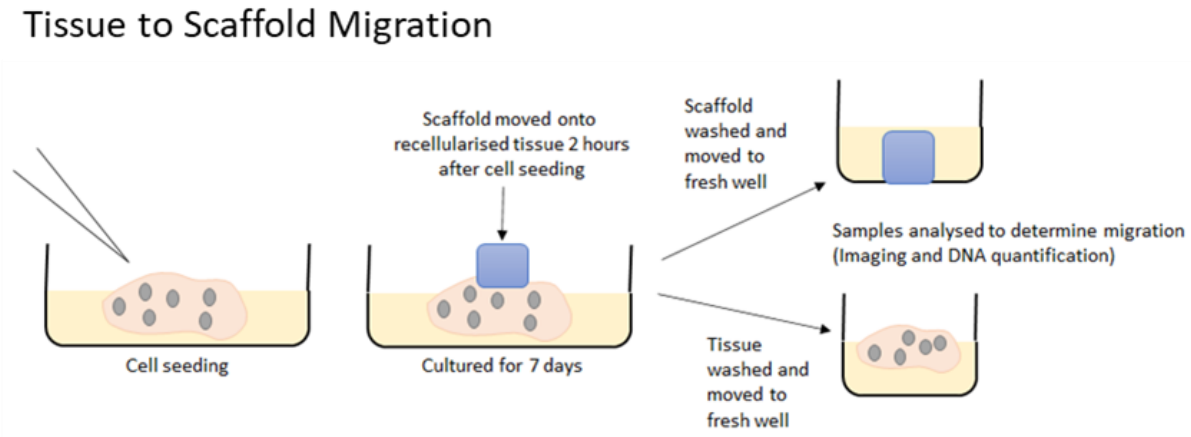

Schematic 5.2: Viability and proliferation analysis of PLECs cultured on uncoated scaffolds. Both graphs showed significant increases in assay results from days 7-14 and 14-21, as shown by asterisks, (*): $p < 0.05$, n=7.

Cells seeded onto scaffolds/standard lung tissue cultured alone in 48 well plates were used as positive controls while decellularised tissue and sterile uncoated scaffolds were used as negative controls. As well as PicoGreen, samples were also treated DNeasy Blood and Tissue Kit as described in **section 2.2.6** and DNA quantity measure by using NanoDrop as in **section 2.2.7**.

5.3.8 Primary cell co-culture migration

D-PLFs were stained with Vybrant for green fluorescence as described in **section 2.3.2** and 30,000 cells were seeded onto either scaffolds (initial seeding density of 480 cells/mm^3) or decellularised lung tissue pieces (initial seeding density of 30,000 cells/cm^2). Before PLECs were seeded onto samples, PLECs were stained with Vybrant for red fluorescence as described in **section** 2.3.2, and 30,000 PLECS were seeded onto D-PLF scaffolds/tissue pieces. These Co-culture samples were cultured for 7 days and fluorescence images were taken to investigate cell migration. PicoGreen and NanoDrop was applied to the same group of samples as described in **section 2.2.4 and 2.2.5**.

5.4 Results

5.4.1 Assessment of PLEC culture on scaffolds

Porcine lung epithelial cells (PLECs) were cultured on uncoated Surgispon scaffolds and the cells were assessed with alamarBlue and PicoGreen assays, as shown in **Figure 5.3.** Both assays showed significantly greater fluorescence intensity over time ($p<0.0001$ for both), with a significant increase from days 7-14 and 14-21 ($p<0.05$ for all), suggesting PLEC attachment and proliferation on uncoated scaffolds over a 21 day culture period.

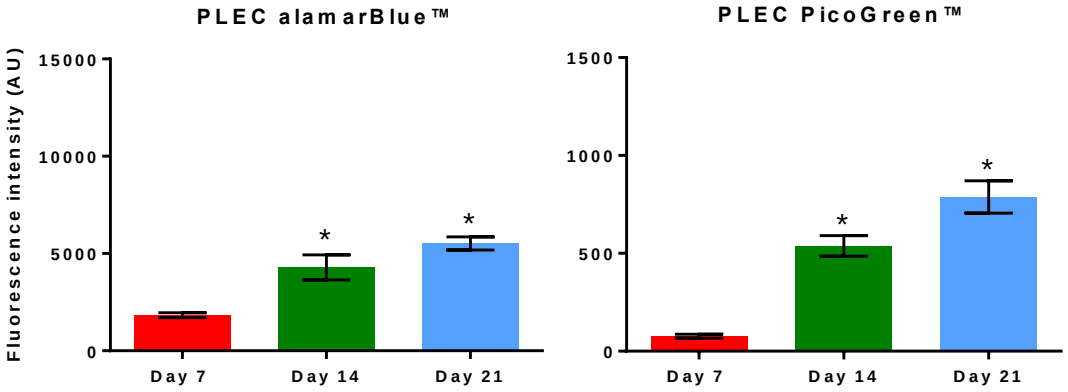

Figure 5.3: Viability and proliferation analysis of PLECs cultured on uncoated scaffolds. Both graphs showed significant increases in assay results from days 7-14 and 14-21, as shown by asterisks, (*): $p< 0.05$, n=7.

LIVE/DEAD and DAPI assays were applied to samples on days 7 and 21 to investigate cell attachment onto scaffolds and cell viability. Images from these assays are shown in **Figure 5.4**. All fluorescent channels are subject to autofluorescence from Surgispon, empty scaffolds were imaged as a control group.

The images show that the attached cells are viable and proliferated on the scaffolds. No dead cells were observed, which could indicate either a lack of cell death during culture time or that dead cells did not remain attached to scaffolds. This indicates that only live cells were attached to scaffolds and confirms that PicoGreen detected dsDNA from live cells and not from dead cells on scaffolds.

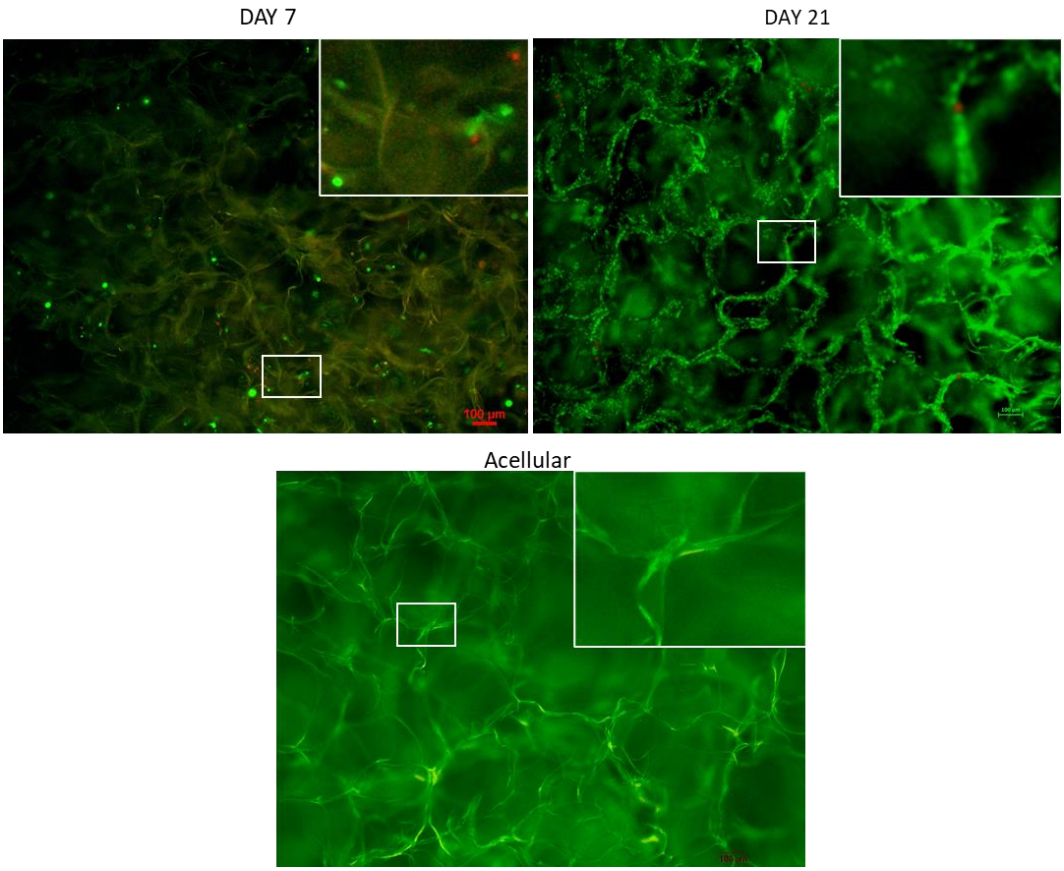

Figure 5.4: Fluorescent image analysis of PLECs cultured on scaffolds. The LIVE/DEAD assay showed living, attached cells on scaffolds, both on day 7 and 21 with increased cell density by day 21. Few dead cells were observed. Acellular scaffolds were imaged as a control group.

5.4.2 Assessment of PLF cell culture on scaffolds

PLFs were cultured onto uncoated scaffolds and assessed with alamarBlue and PicoGreen, as seen in **Figure 5.5**. Both results showed significantly greater fluorescence intensity over time ($p<0.0001$), with significant increases from day 7-14 and 14-21 ($p<0.05$ for all cases). Both results confirm that PLFs attached, were viable and proliferate on uncoated scaffolds over a 21 day culture period.

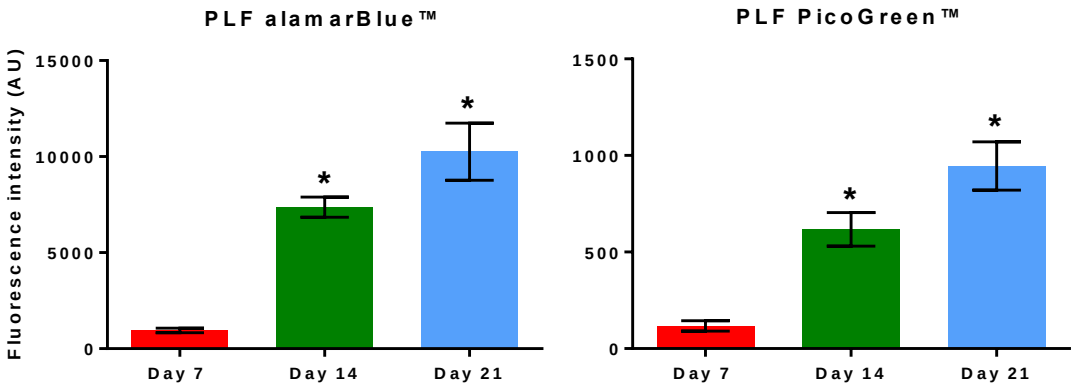

Figure 5.5: Viability and proliferation analysis of PLFs cultured on uncoated scaffolds. Both graphs showed significant increases in assay results from days 7-14 and 14-21, as shown by asterisks, (*): $p< 0.05$, n=7.

LIVE/DEAD and DAPI assays were also applied to samples on day 7 and day 21 to investigate cell attachment onto scaffolds and cell viability. Images from these assays are shown in **Figure 5.6**.

LIVE/DEAD and DAPI imaging showed cell attachment to scaffolds, these attached cells stained for LIVE, reinforcing the results received from the previous assays. For DEAD, there were no dead cells on scaffolds, which could indicate either a lack of cell death during culture

time or that dead cells did not remain attached to scaffolds. All fluorescent channels are subject to autofluorescence from Surgispon.

While DAPI stains all the nuclei on scaffolds, when applied with LIVE/DEAD viability assay, it gives the opportunity to see all the cells on scaffolds. LIVE and DAPI images both showed cells on scaffolds, these cells are attached and from days 7-21 have proliferated on the scaffolds. Both alamarBlue and PicoGreen results are supported by LIVE and DAPI images. DEAD images did not show cells on scaffolds, indicating that only live cells are attached on scaffolds, confirming that PicoGreen detected DNA from live cells and not from dead cells on scaffolds.

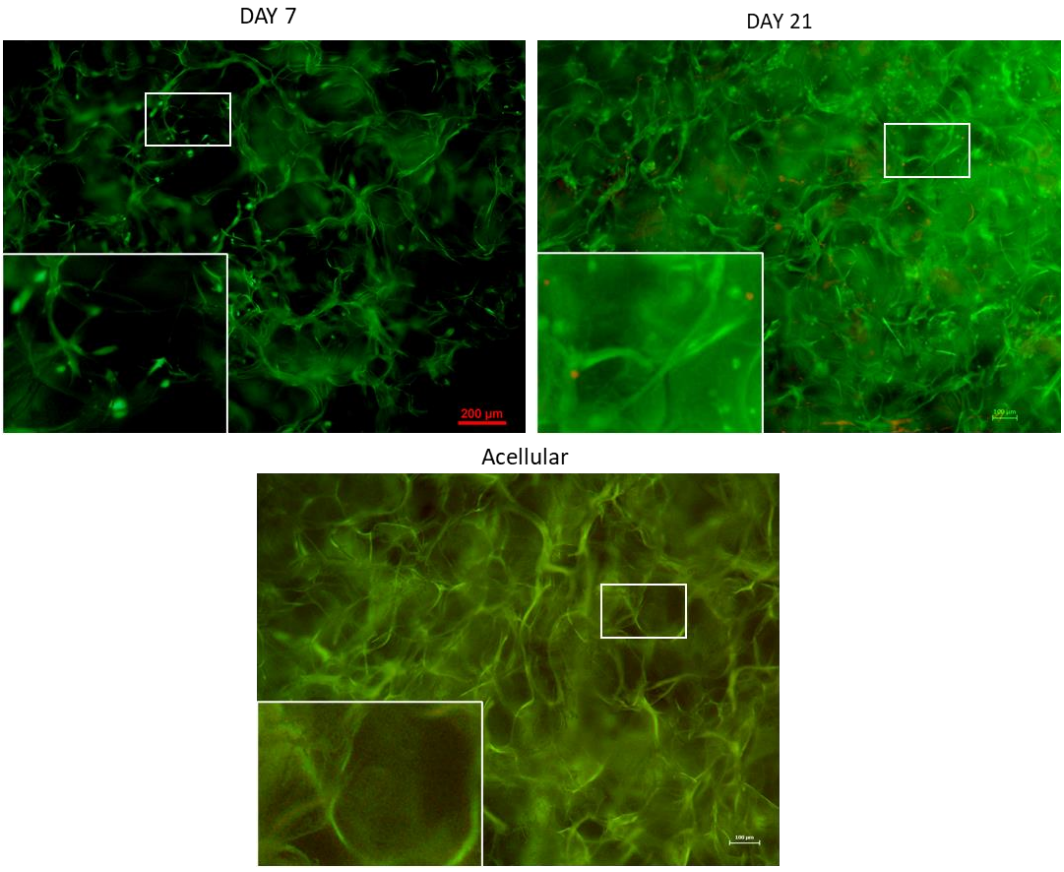

Figure 5.6: Fluorescent image analysis of PLFs cultured on scaffolds. Similar to PLEC results, the LIVE/DEAD assay showed living, attached cells on scaffolds, both on day 7 and 21 with increased cell density by day 21. Few dead cells were observed. Acellular scaffolds imaged as control group.

5.4.3 PLF Deactivation

PLFs were deactivated in order to prepare for co-culture with PLECs. D-PLFs were cultured for 7 days and alamarBlue/PicoGreen assays were applied to samples on days 0, 1, 4 and 7, with untreated PLFs used as a control, as seen in **Figure 5.7**. While PLFs showed increased metabolic activity over time as cells proliferated, D-PLF cells showed significantly less fluorescence intensity over time ($p<0.0001$ for both assays). Both assays indicate that deactivation had a significant effect on PLF cells, and the protocol is robust.

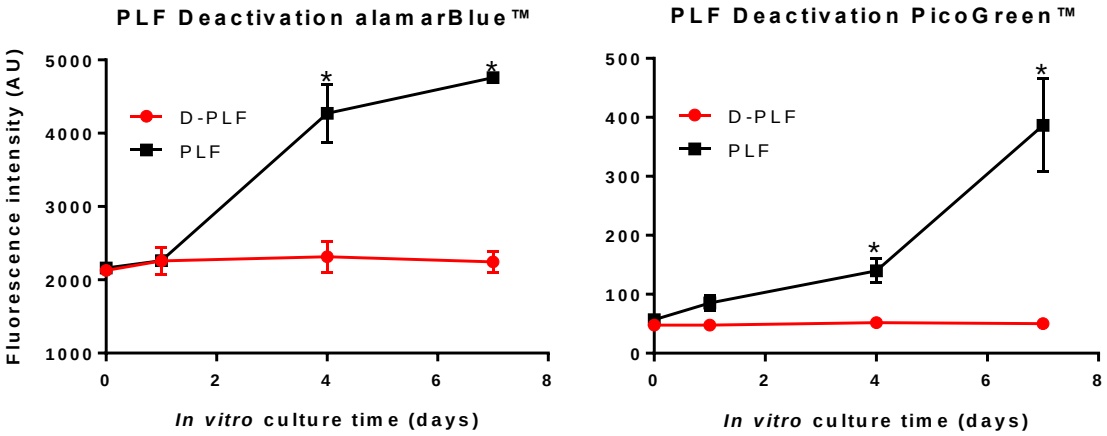

Figure 5.7: Viability and DNA quantity analysis of PLF cells vs D-PLF cells. alamarBlue and PicoGreen were applied to samples to investigate the cell proliferation of active and deactivated cells. There is a clear effect from deactivation seen on the graph. (*): $p<0.001$, n=11.

Fluorescence images of PLF and D-PLF cultures were taken on day 1 and 7 after the LIVE/DEAD cell viability assay was applied, with the resulting images shown in **Figure 5.8**. On day 1, PLFs were viable and attached onto cell culture plates, after 7 days culture the cells continued to proliferate and were imaged in increased cell concentrations on the plate. D-PLFs showed similar cell concentrations on day 1 and 7, indicating that the deactivation process stopped

cells proliferating. This confirms the results from the assays, with all results supporting the deactivation process.

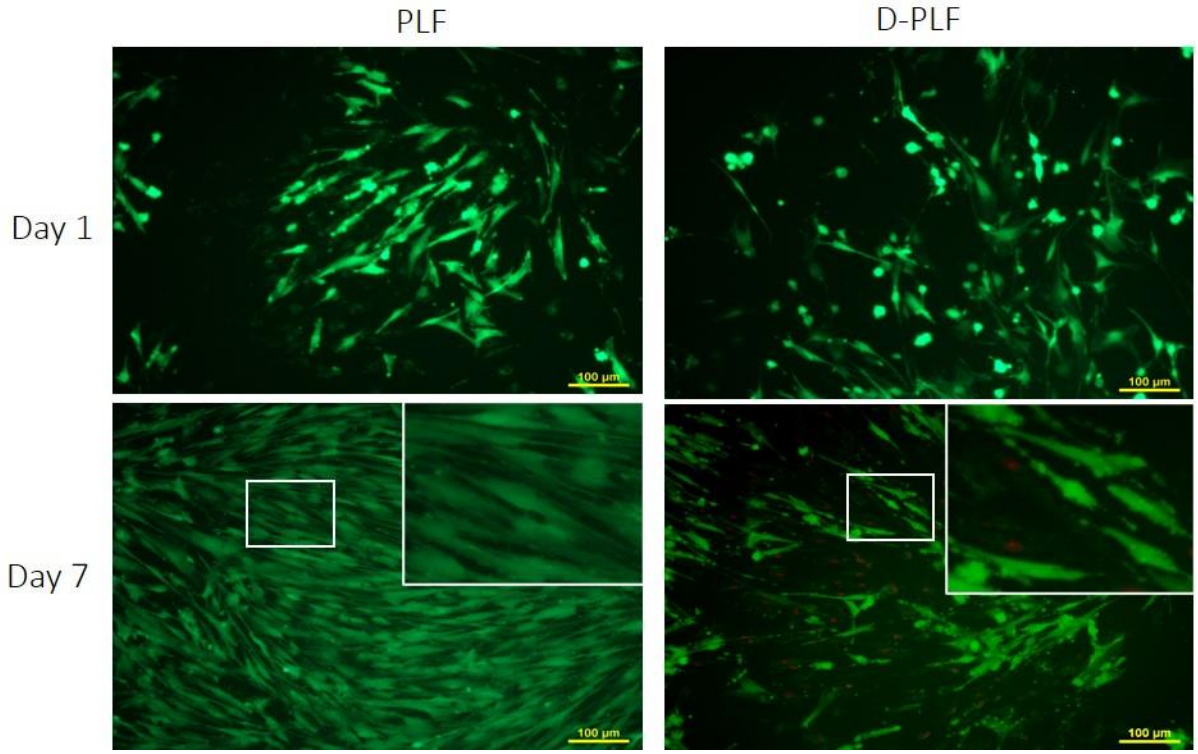

Figure 5.8: Comparing PLFs and D-PLFs on TCP. PLF images show increased cell concentration from day 1-7, the attached cells continued to proliferate, while D-PLFs did not proliferate. D-PLF insert contains 7 cells, PLF insert contains 24 cells.`

5.4.4 Differentiation of PLECs

Here, D-PLFs and PLECs were seeded onto 40% Matrigel-coated Surgispon scaffolds as a co-culture in order to test differentiation of PLECs into bronchospheres. While the previous protocol suggested the use of PneumaCult-ALI media, in-house CFAD media were also tested to determine the effect of different cell culture media on the differentiation process.

PLEC cell morphology was investigated through brightfield images taken on days 1, 2, 4, 7 and 14. Images of samples cultured with CFAD+, CFAD+++, PneumaCult-ALI+ and PneumaCult-

ALI+++ are shown in **Figure 5.9**. On day 1, cells were small and rounded, organising into small spherical morphologies by day 2. From day 4 cells were showing both bronchosphere and small organoid morphologies, and by day 14 the bronchospheres were bigger and an increased number of spheres were observed on scaffolds. Organoid merging was also observed, decreasing the number of organoids overall but increasing the range and maximum sizes seen.

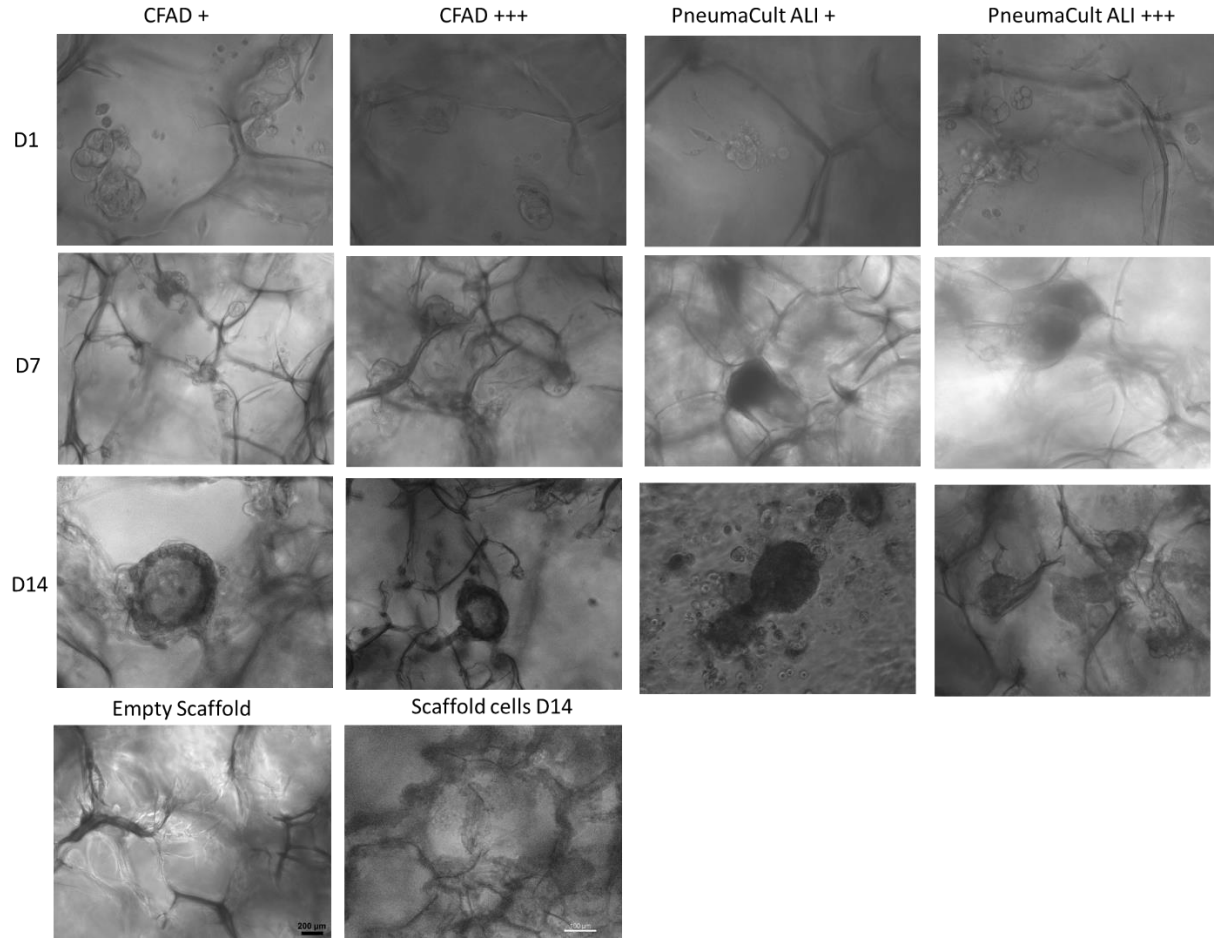

Figure 5.9: Imaging PLEC differentiation on Surgispon scaffolds. Brightfield images of PLEC differentiation on scaffolds are shown at days 1, 7 and 21 of culture. Scaffolds were incubated with one of four media types: CFAD+, CFAD+++, PneumaCult-ALI+ and PneumaCult-ALI+++, and are shown alongside an empty scaffold (cell control) and a scaffold seeded with the same cell concentration but with no sphere culture protocol (differentiation protocol). The presence of organoids when using sphere culture indicates some effect from PLEC differentiation.

Organoid diameters over time for each media type is shown in **Figure 5.10**. The effect of time on organoid diameter was significant ($p<0.0001$), but the effect of different media types was not significant (p: 0.48). Looking at average organoid diameter, organoids were 103-130 µm on day 2, 162-202 µm on day 4, 134-169 µm on day 7 and 140-224 µm on day 14. While average organoid size did not increase beyond ~250 µm, it is clear from **Figure 5.9** that the range of organoid sizes increased markedly. This is due to there being many smaller organoids around day 2, which grow in size by day 4 either by proliferation or potentially by combining, with lung organoid and bronchosphere fusion being previously documented (Hild and Jaffe, 2016; Sachs et al., 2019), but the mechanism remaining a mystery.

If these organoids are combining, the organoid number would drop but the average size would increase. However, by days 7-14, there are many larger organoids and new smaller organoids are forming, hence the large range in organoid sizes from 100-400 µm. The standard deviation of organoid sizes increases with culture time, from ~50 to ~140, indicating the change in organoid size range. Despite these changes in organoid size over time, the different media used did not have a significant effect on these changes.

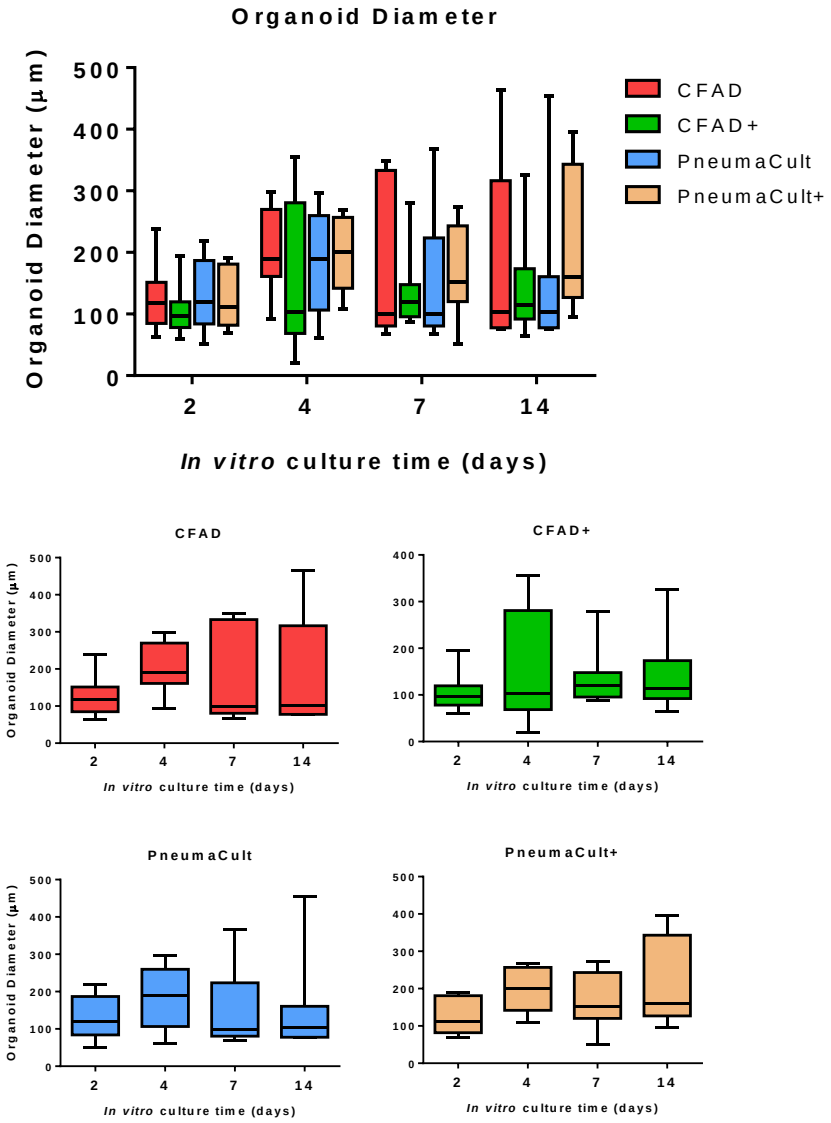

Figure 5.10: Organoid diameter from PLEC differentiation over time in different media. Organoids formed from the differentiation of PLECs on a Matrigel-coated scaffolds were measured in diameter from days 2-14, in CFAD, CFAD+, PneumaCult and PneumaCult+ medias, where + indicates the use of supplements. The box and whisker plots show the range of organoid sizes measured at each stage, n=11.

Due to the lack of a significant difference between media types, CFAD in-house was chosen for future experiments rather than PneumaCult-ALI. There were high levels of variation in

CFAD organoids diameters over time, demonstrating a dynamic system where differentiation and proliferation are occurring.

The differentiation experiment was repeated with a D-PLF/PLEC co-culture on 40% Matrigel-coated Surgispon scaffolds for 21 days in CFAD+ media. Brightfield and DAPI images were taken and are shown in **Figure 5.11**. Both brightfield and DAPI images show cells on scaffolds that had self-organised into organoid structures.

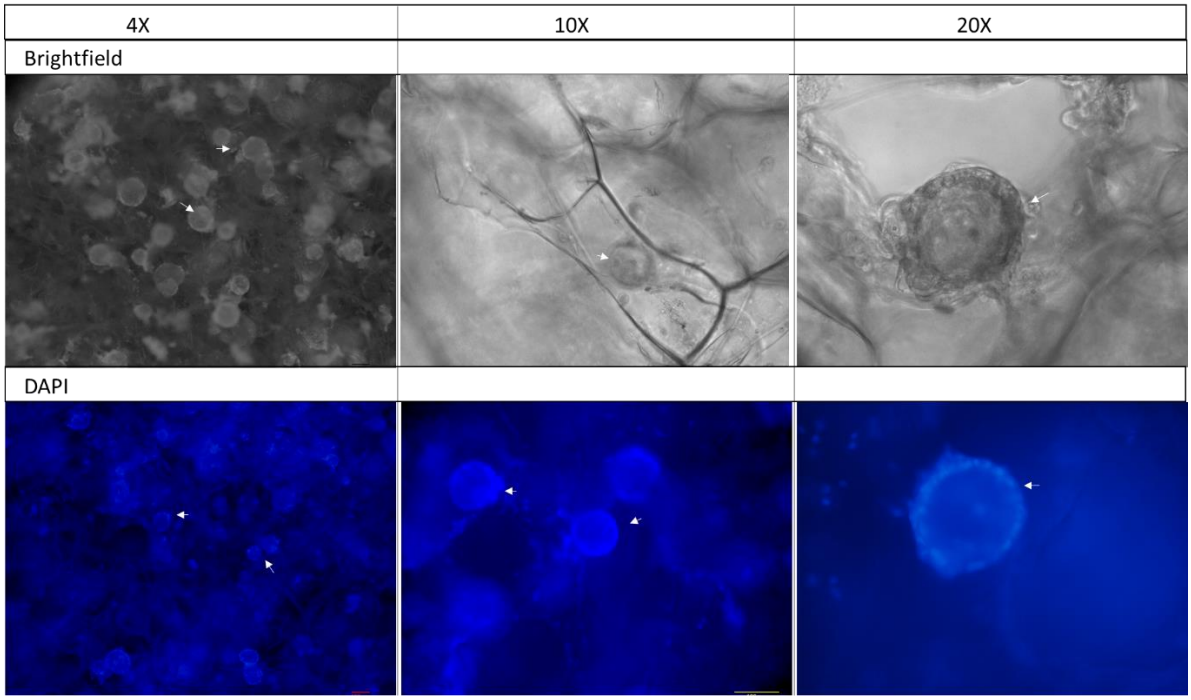

Figure 5.11: Imaging D-PLF and PLEC co-cultures on Surgispon scaffolds. Many organoids and surrounding attached cells were observed on scaffolds. 4X showed multiple organoids on scaffolds, 10X focused on attached cells on organoids and 20X showed individual cells on organoids and surrounding cells. DAPI images confirm what is seen in brightfield and shows individual cells on organoids as well as cells on multiple organoid structures.

The changes in spheroid and organoid-like structures changes throughout culture, as shown in **Figure 5.12.** From days 1-2 the cell aggregates are spheroid-like in structure, where the entire spherical mass is composed of cells. These spheroids typically gather together, as seen

in the example from day 2. By day 3 a more complex structure is forming, where the cells make a perimeter around an empty air space within the structure, this can be more clearly seen in day 4, where cells form around an empty central space. By days 5-6, these organoids can be seen merging into larger organoids, by day 6 especially there are many observable organoids in the Surgispon scaffolds.

Experiments in this section show that scaffolds with a 40% Matrigel coating can be suitable for PLEC differentiation into organoid-like bronchospheres. This differentiation process may only be possible due to the combination of Matrigel coating and culturing the scaffolds half-submerged in media, forming an air-liquid interface (ALI), indicating that Surgispon may be a suitable environment to support an ALI in 3D. Cells are exposed to both air and liquid (culture media), the oxygenation of the media could be tested, otherwise Surgispon appears similar in function to transwell and other related ALI models (Cao et al., 2020).

5.4.5 Immunocytochemical staining

Antibody staining was performed, both to characterise PLFs and PLECs (confirming the accuracy of cell isolation from the dissection protocol) and to investigate PLEC differentiation on Surgsipon scaffolds.

For characterisation, scaffolds were stained with Pan-Cytokeratin (an epithelial marker for PLECs, red), Vimentin (a fibroblast marker for PLFs, green) and DAPI (general cell marker, blue) (**Fig 5.12)**. Staining showed D-PLFs and PLECs attached to scaffolds and staining positive for their respective markers, confirming the accuracy of cell isolation during porcine lung dissection, as the cell types stain as expected.

In addition, DAPI staining mostly highlights organoids, the lack of co-staining indicates that these cells in organoid structures are no longer epithelial cells and have most likely differentiated.

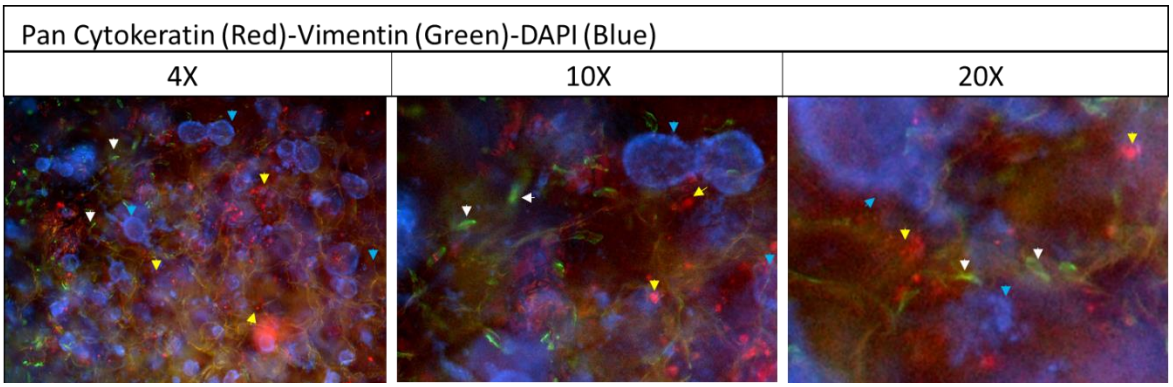

Figure 5.12: Characterization and differentiation staining of D-PLF and PLECs on Surgispon scaffold. Primary antibody staining showed red epithelial cells (yellow arrowhead) and green D-PLFs (white arrowhead) on scaffolds. DAPI stained nuclei and showed cells that had organised into organoid structures (blue arrowhead) on scaffolds.

In order to further investigate the identity of differentiated cells, samples were further stained with additional antibody markers. D-PLF and PLEC co-cultures on scaffolds were stained with mucin 5AC (mucus cell/airway ciliated cell marker), p63 (transcription factor expressed in airway stem/progenitor cells), podoplanin (stromal cell AT1) and prosurfactant protein C (SPC, hydrophobic surfactant protein secreted by AT2). All primary antibody staining was accompanied with DAPI staining.

The results of this staining are seen in **Figure 5.13**, which indicates positive staining results for mucin 5AC and p63, suggesting that PLECs had populations of stem/progenitor cells that had potentially differentiated into airway ciliated cells. Cells stained negative for SPC and

podoplanin, indicating that they did not differentiate into pneumocyte type cells, or these cells were not present in these cultures from the start.

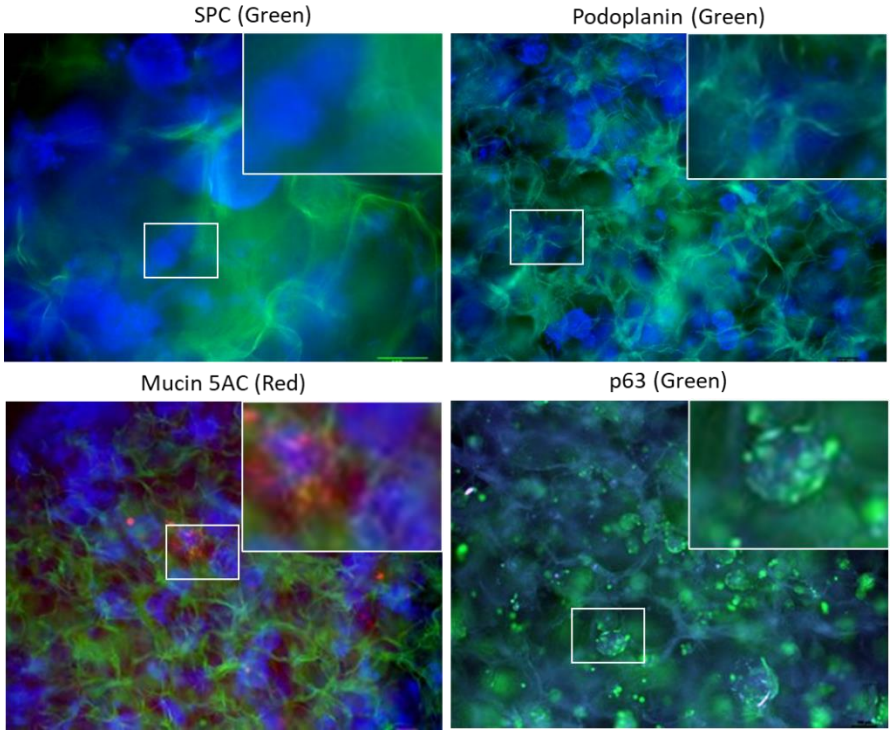

Figure 5.13: PLEC differentiation antibody staining. PLEC cultures were stained with SPC (pneumocyte type II marker), podoplanin (pneumocyte type I marker), mucin 5AC (ciliated cell marker) and p63 (basal cell marker). SPC and podoplanin had negative staining, while mucin 5AC and p63 had positive staining.

Based on these positive mucin 5AC and p63 results, this staining was repeated with both stains used at once: differentiated PLECs were stained for mucin 5AC (red), p63 (green) and DAPI (blue). In addition, PLECs were grown on tissue culture plastic (TCP) and also stained with mucin 5AC and p63, in order to determine if these populations were present in PLECs without a differentiation protocol. Fluorescent images from these staining is seen in **Figure 5.14.**

Mucin 5AC and p63 again stain positively, indicating that after the differentiation protocol on Matrigel-coated Surgispon scaffolds a population of PLEC stem/progenitor cells have potentially differentiated into ciliated airway cells. The TCP experiment indicates that there is a p63-postive population of stem/progenitor cells in PLEC cultures, but there were no mucin 5AC-positive cells, suggesting that it may only be through the successful differentiation on Surgispon scaffolds that ciliated cells were produced.

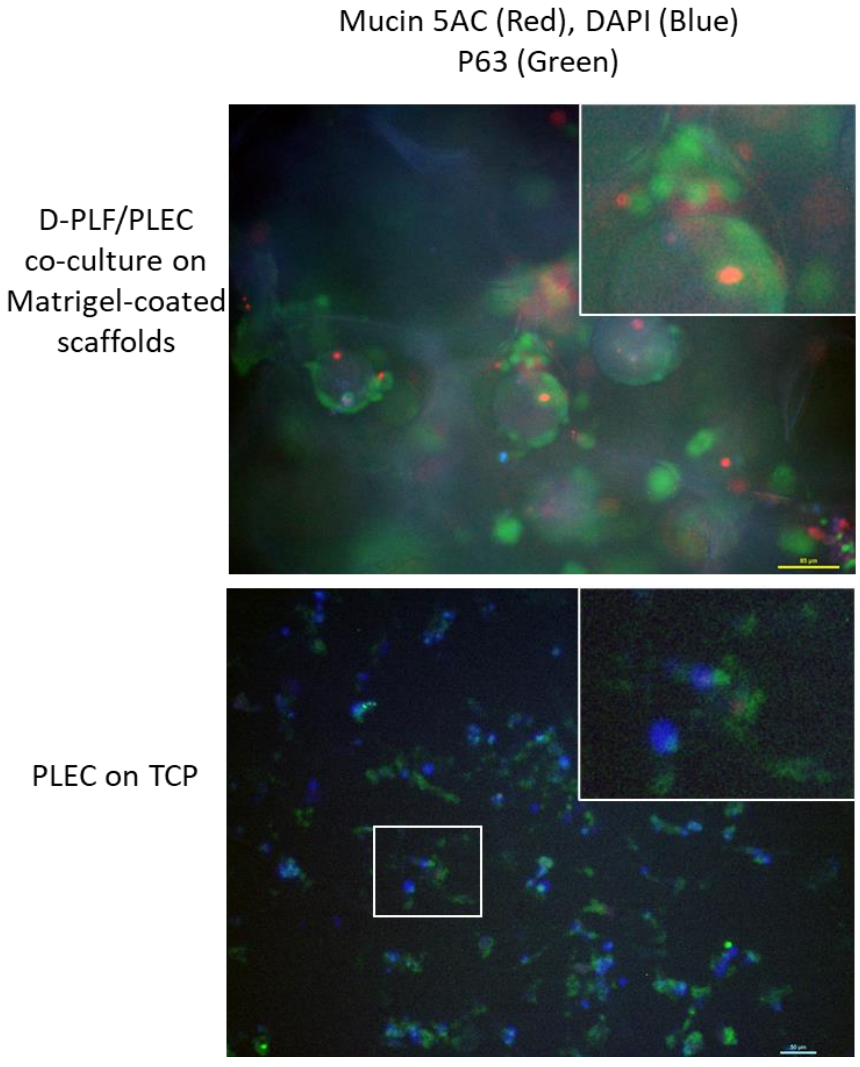

Figure 5.14: PLEC differentiation on scaffold vs TCP. Fluorescence images show mucin 5AC (red, ciliated cell marker), p63 (green, stem/progenitor cell marker) and DAPI (blue, nuclei) stains on 21 day co-cultures of PLECs with D-PLFs, using CFAD+++ media. While scaffold culture results in positive mucin-5AC staining (red), TCP culture does not.

5.4.6 Decellularised porcine lung tissue

Decellularised and untreated lung tissue samples were imaged with DAPI to determine if all cells (and therefore genetic material) had been removed through the decellularisation process (**Fig 5.15**). While untreated lung slices featured alveolar structures and clear pores from DAPI-stained cell nuclei, these structures and DAPI-stained nuclei were absent in the decellularised tissue, showing that the decellularisation protocol had successfully removed cells from the lung tissue, with no residual nuclei remaining. Photographs of both untreated and decellularised lung slices are also shown in **Figure 5.15**.

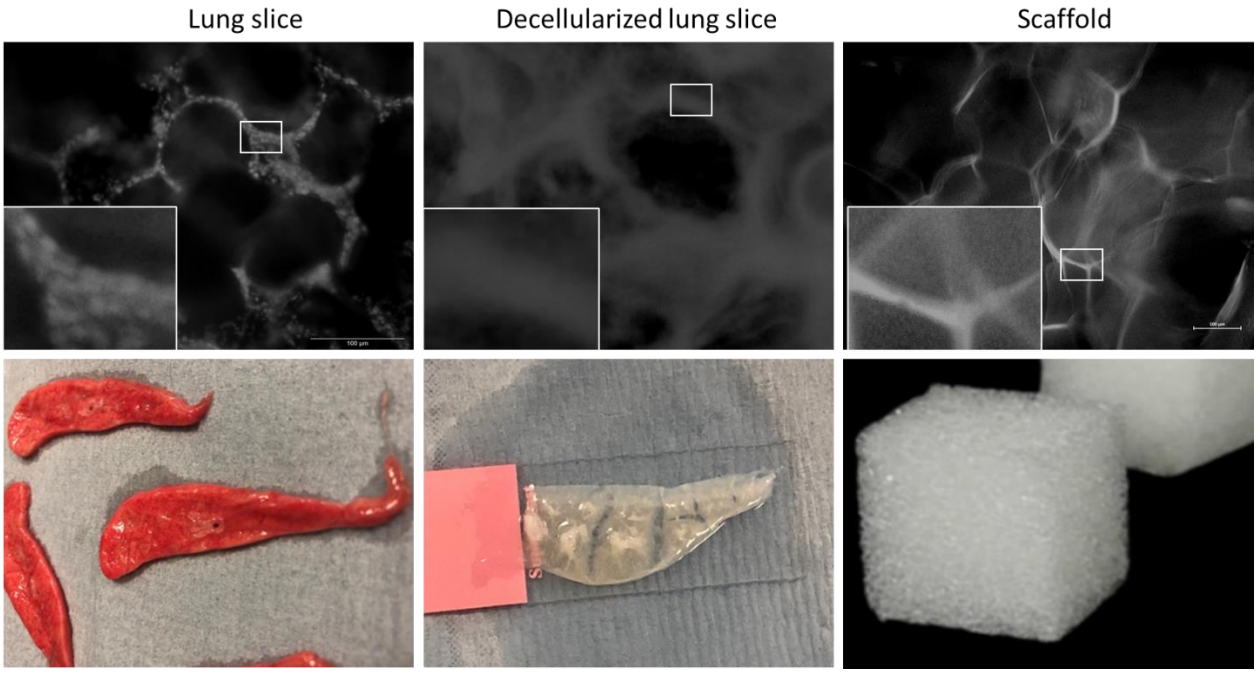

Figure 5.15: Native lung tissue vs decellularised lung tissue vs Surgispon scaffold. All three conditions stained with DAPI (monochrome for clarity). Cells observed on native tissue, but only autofluorescence from the ECM observed for decellularised tissue and scaffolds.

In order to quantify the extent of decellularisation, lung slices were prepared and used for DNA quantification with NanoDrop and PicoGreen, as shown in **Fig 5.16**. Both DNA quantity assays showed a significant decrease in genetic material between untreated lung tissue and decellularised lung tissue ($p<0.0001$), showing that the decellularisation process successfully removed cells, residual nuclei, and free genetic material from lung slices. NanoDrop and PicoGreen showed a 98.47% and 96.56% reduction in DNA concentration from native to decellularised tissue slices respectively. These decellularised tissue slices were used for cell migration experiments and recellularisation in combination with Surgispon scaffolds.

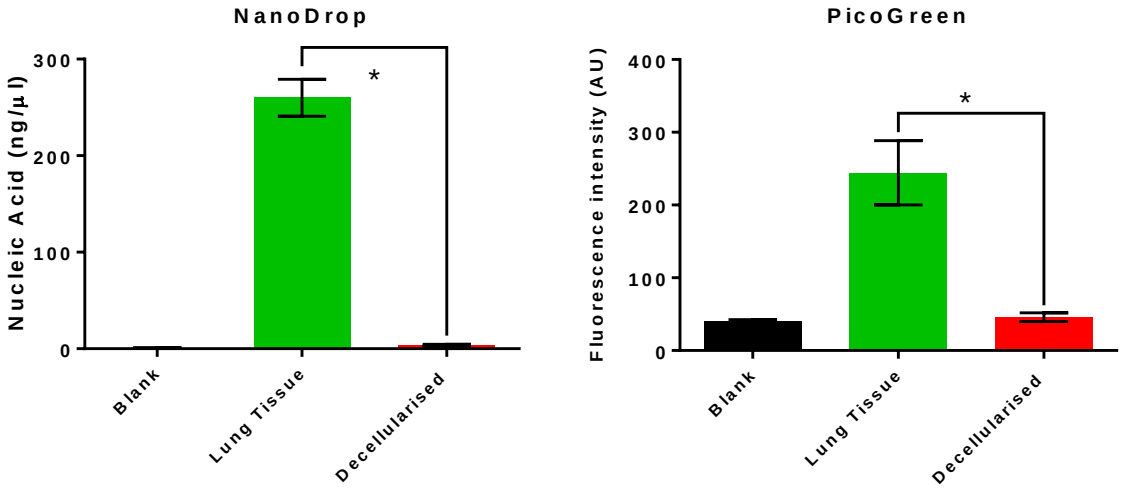

Figure 5.16: DNA quantification analysis of decellularised lung tissues. Both NanoDrop and PicoGreen assays were used to test native lung tissue slices and decellularised lung tissue slices, in order to see if the decellularisation process was functional. (*): $p<0.0001$, n=9.

5.4.6.1 Recellularisation of lung tissues with epithelial cells

With successful decellularisation, recellularisation of lung slices with epithelial cells was explored in order to test the viability of the remaining ECM for cell attachment and proliferation. A549 epithelial cell line and PLECs were fluorescently tagged using Vybrant cell

labelling kit, red for A549 or green for PLECs, before seeding separately onto decellularised tissues. Samples were cultured for 3 days and imaged with untreated lung tissue slices as a control (**Fig 5.17**).

Fluorescence images showed a high level of A549 and PLEC attachment on decellularised tissues, these A549-/PLEC-recellularised tissues showed a similar structure to the DAPI-stained untreated lung tissues, indicating that the lung ECM was likely not damaged by the decellularisation protocol. This result means that decellularised porcine lung tissue can support cell culture and is suitable for experimentation in combination with Surgsipon scaffolds.

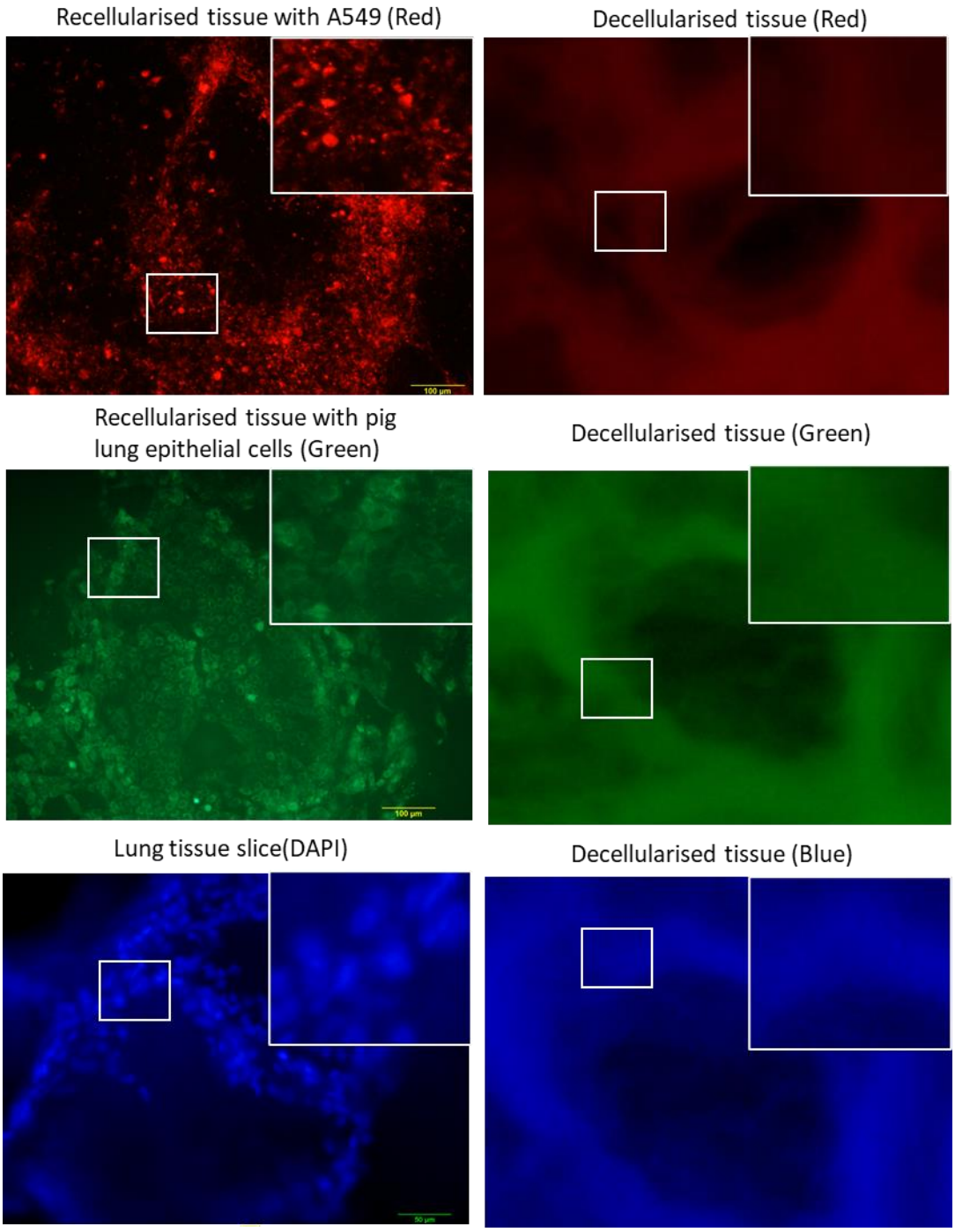

Figure 5.17: Recellularisation of decellularised porcine lung tissue slices. A549s or PLECs were seeded onto decellularised lung slices and compared to native lung tissue (positive control, stained with DAPI) and decellularised tissues (negative control).

5.4.7 Cell migration: scaffold to tissue

In order to test Surgispon scaffolds suitability for potential *in vivo* implantation, migration assays were performed with decellularised tissue slices. Cells were seeded onto scaffolds, and these scaffolds were placed onto decellularised porcine lung tissue in order to determine if cells would migrate from the scaffold to the tissue. This was done with all available cell types: A549 epithelial cell line, 35FLH fibroblast cell line, PLECs, PLFs and a D-PLF/PLEC co-culture.

5.4.7.1 A549

30,000 A549 cells were seeded onto scaffolds and cultured for 7 days, then stained with LIVE/DEAD to investigate cell migration from the scaffold into decellularised lung tissue **(Fig 5.18).**

LIVE/DEAD staining showed that A549 cells on scaffolds were attached and viable. The decellularised tissue in contact with the scaffolds also showed attached and viable cells after 7 days, showing that A549 cells migrated from the scaffold into the tissue and attached, and proliferated in the tissue successfully after attachment. As well as live cells, dead cells were also observed on the decellularised tissue, suggesting that either A549s had died on scaffolds, become detached and relocated to decellularised tissue, or that A549s had migrated into tissue and then died. However, there were only a small proportion of dead cells on the decellularised tissue.

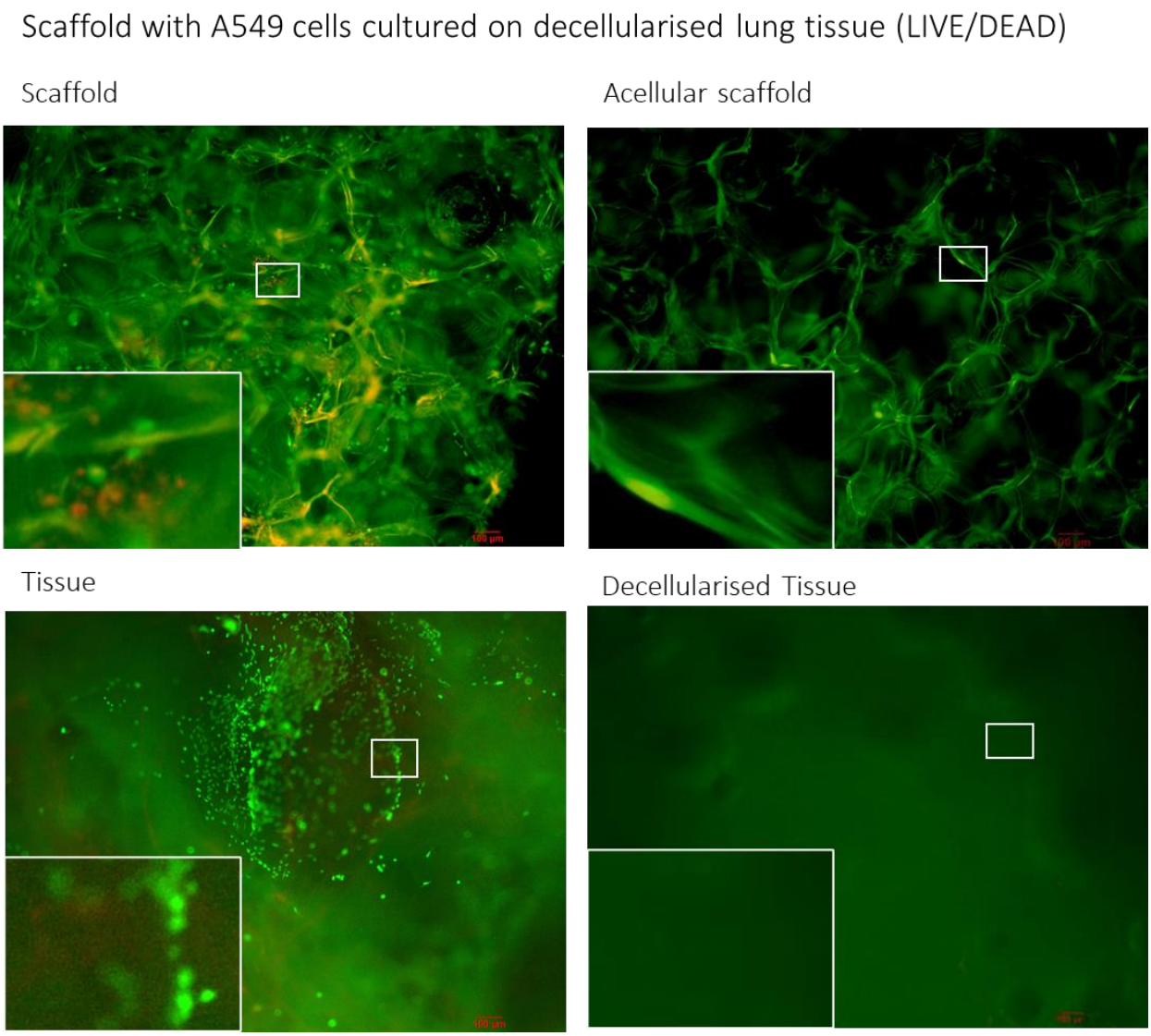

Figure 5.18: Assessing A549 migration from scaffold to tissue. LIVE/DEAD images show viable cells on both scaffolds and tissue, indicating migration from scaffold to tissue after 7 days of culture. Acellular scaffolds and decellularised tissue used as negative controls.

Alongside LIVE/DEAD images, DNA quantification assays NanoDrop and PicoGreen were also used on the same scaffolds in order to quantify DNA in both Surgispon scaffolds and lung tissue (**Fig 5.19**). For both assays, seeded scaffolds had a significant increase in DNA quantity compared to control empty scaffolds ($p < 0.001$ for both), and lung tissues had a significant increase in DNA quantity compared to control decellularised lung tissue ($p<0.001$ for both).

The latter result shows that cells had migrated into lung tissue from Surgispon scaffolds in significant numbers.

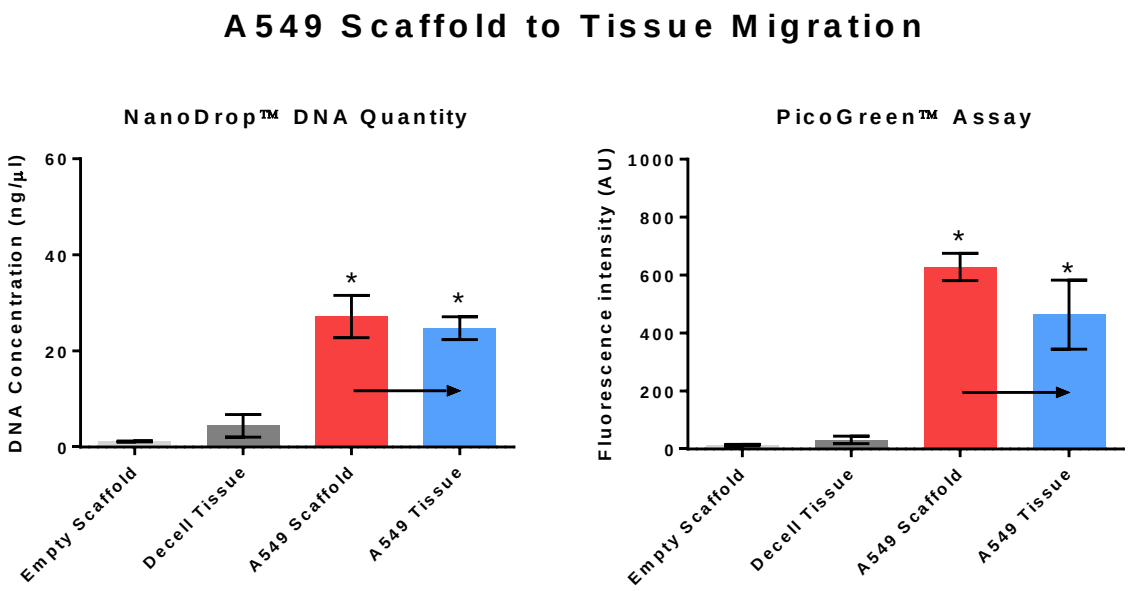

Figure 5.19: A549 migration from seeded scaffolds to decellularised tissue. NanoDrop and PicoGreen assays used on negative controls (empty scaffolds and decellularised tissue), on A549 scaffolds placed on tissues (RED), and on the tissues themselves to see if cells migrated (BLUE). (*): $p<0.001$

5.4.7.2 35FLH

30,000 35FLH cells were seeded onto scaffolds and cultured for 7 days, then stained with LIVE/DEAD® to investigate cell migration from the scaffold into decellularised lung tissue **(Fig 5.20).**

LIVE/DEAD staining showed that 35FLH cells on scaffolds were attached and viable. Decellularised tissue in contact with scaffolds showed a very low number of attached and viable cells after 7 days, suggesting that only small number of 35FLH cells migrated from the scaffold into the tissue and attached.

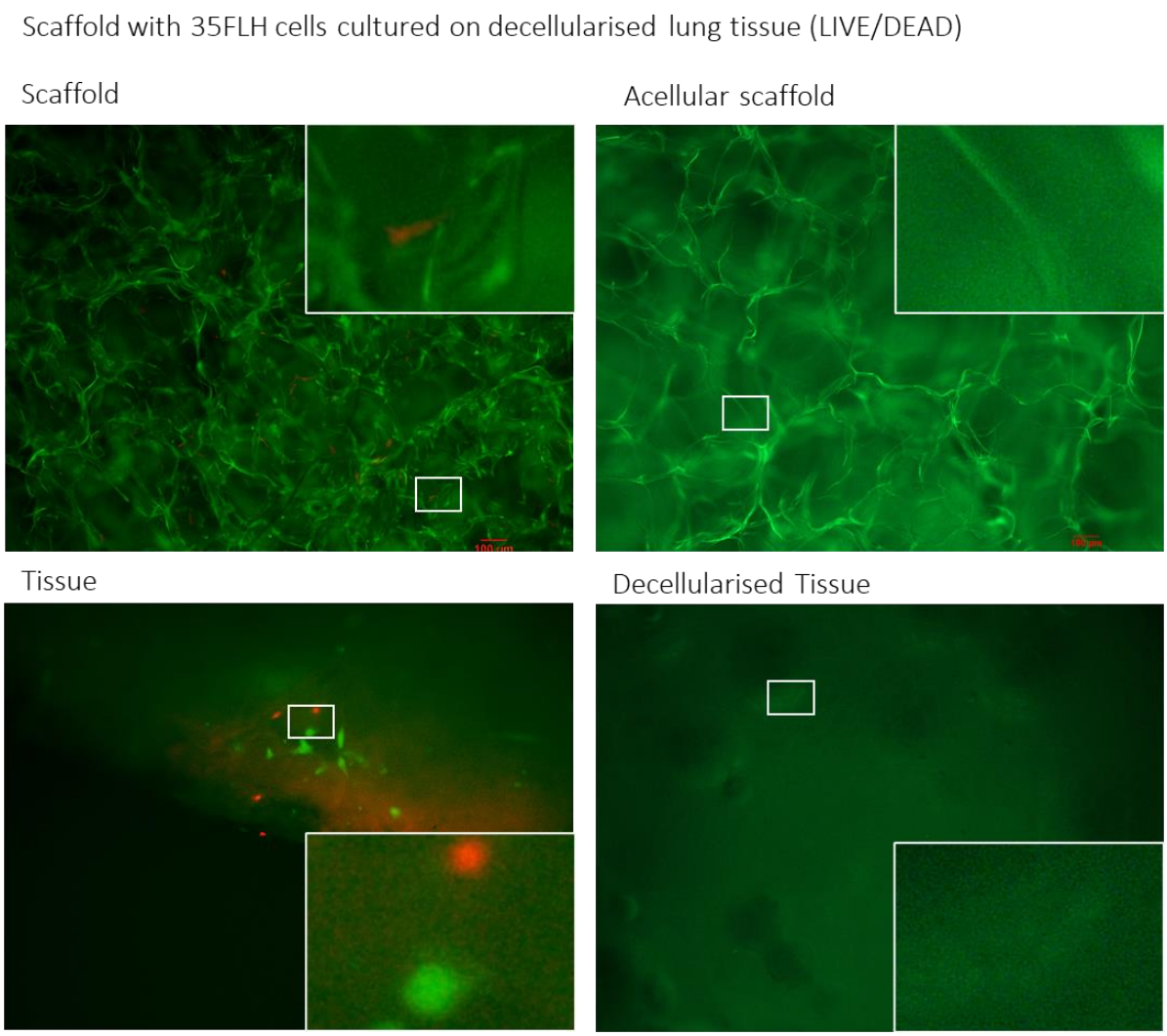

Figure 5.20: Assessing 35FLH migration from scaffold to tissue. LIVE/DEAD images show viable cells on both scaffolds and tissue, indicating migration from scaffold to tissue after 7 days of culture. Acellular scaffolds and decellularised tissue used as negative controls.

DNA quantification assays showed that seeded scaffolds had a significant increase in DNA quantity compared to control empty scaffolds ($p < 0.0001$ for both), but only PicoGreen data showed a significant increase in DNA quantity compared to control decellularised lung tissue (**Fig 5.21**) ($p<0.01$). 35FLH migration was not as extensive as A549 migration.

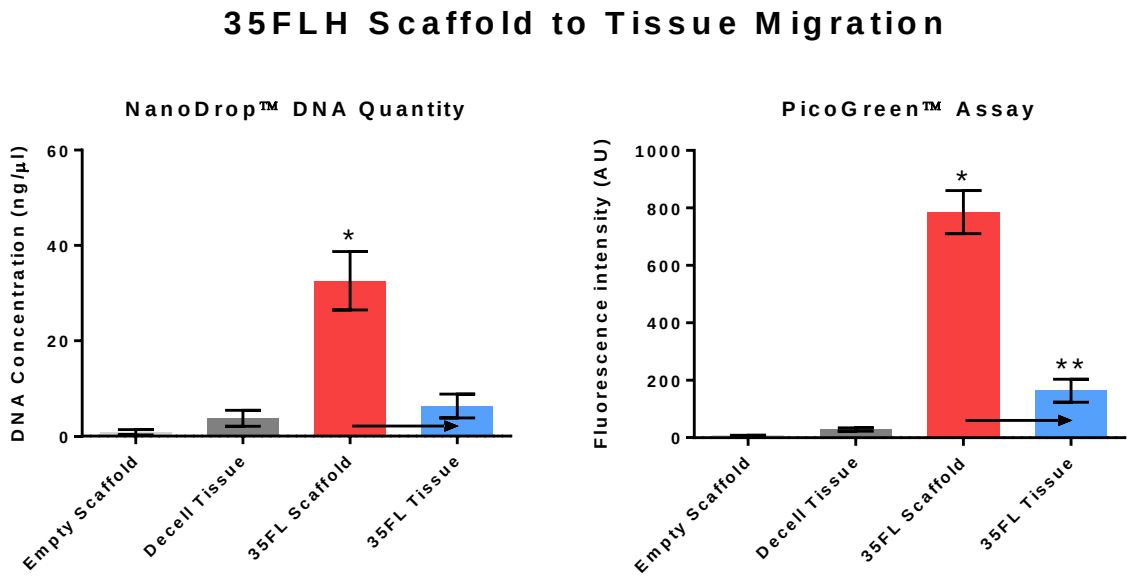

Figure 2.21: 35FLH migration from seeded scaffolds to decellularised tissue. NanoDrop and PicoGreen assays ran on controls (empty scaffolds and decellularised tissue), on 35FLH scaffolds placed on tissues (RED), and on the tissues themselves to see if cells migrated (BLUE). (*): $p<0.0001$, (**): $p<0.01$

5.4.7.3 PLECs

30,000 PLECs were seeded onto scaffolds and cultured for 7 days, then stained with LIVE/DEAD to investigate cell migration from the scaffold into decellularised lung tissue **(Fig 5.22).**

LIVE/DEAD staining showed that PLECs on scaffolds were attached and viable. The decellularised tissue in contact with the scaffolds also showed attached and viable cells on after 7 days, showing migration of PLECs from the scaffold into the tissue and attached, and were cultured there successfully after attachment.

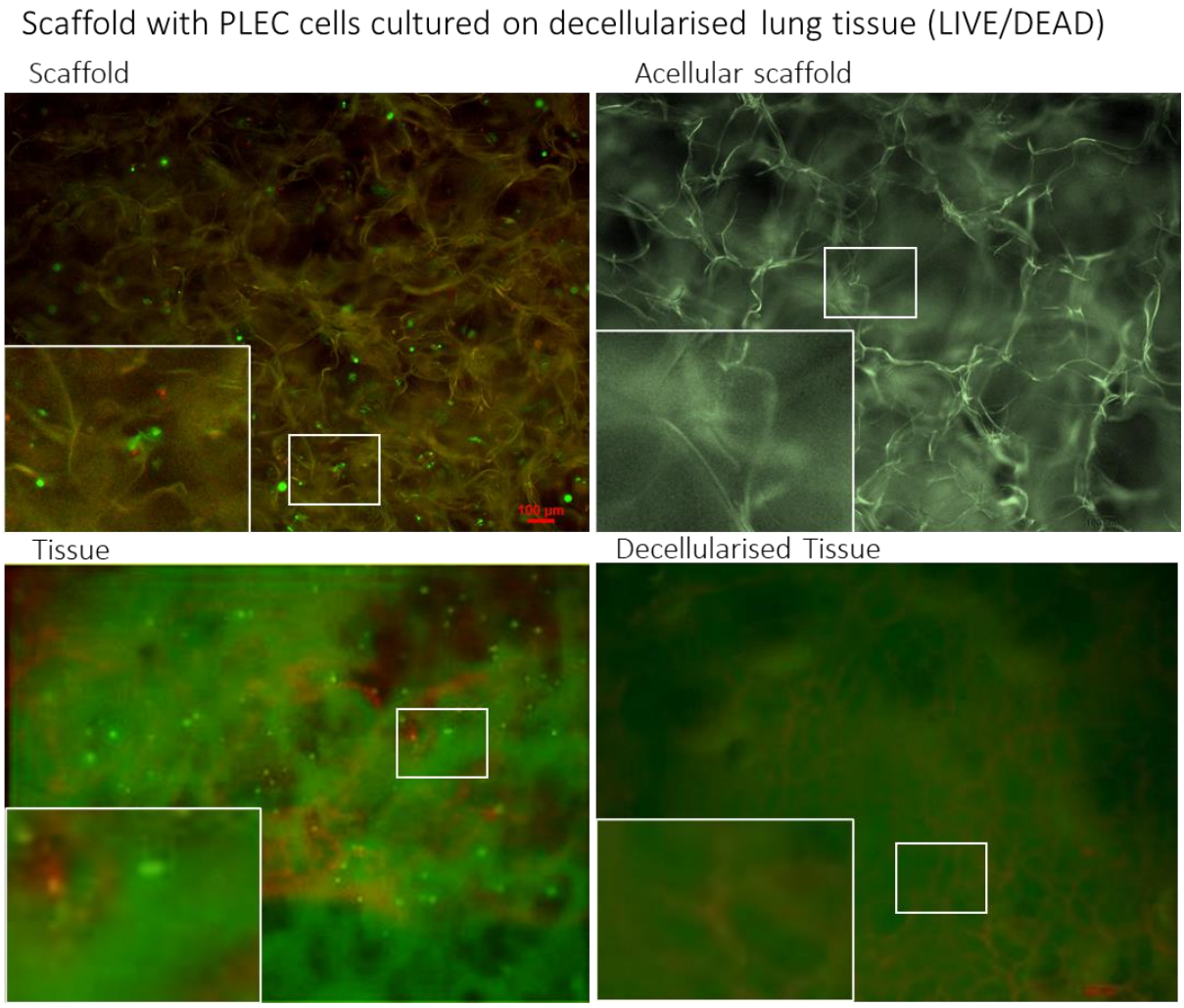

Figure 5.22: Assessing PLEC migration from scaffold to tissue. LIVE/DEAD images show viable cells on both scaffolds and tissue, indicating migration from scaffold to tissue after 7 days of culture. Acellular scaffolds and decellularised tissue used as negative controls.

DNA quantification assays showed that seeded scaffolds had a significant increase in DNA quantity compared to control empty scaffolds ($p < 0.0001$ for both), and a significant increase in DNA quantity compared to control decellularised lung tissue ($p<0.01$ for PicoGreen, $p<0.001$ for NanoDrop) (**Fig 5.23**). These results show that a significant number of PLECs migrated into decellularised lung tissue from Surgispon scaffolds.

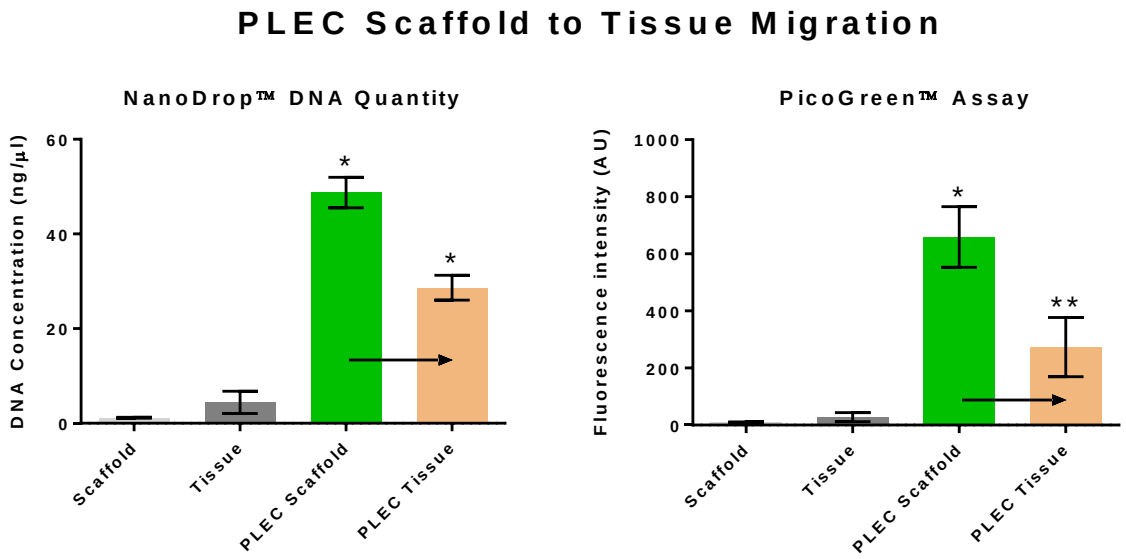

Figure 5.23: PLEC migration from seeded scaffolds to decellularised tissue. NanoDrop and PicoGreen assays ran on controls (empty scaffolds and decellularised tissue), on PLEC scaffolds placed on tissues (GREEN), and on the tissues themselves to see if cells migrated (ORANGE).

5.4.7.4 PLFs

30,000 PLFs were seeded onto Surgispon scaffolds and scaffolds were placed onto decellularised lung tissue, this was cultured for 7 days. After 7 days of cell culture samples were stained with the LIVE/DEAD to investigate cell migration from the scaffold into decellularised lung tissue (**Fig 5.24**).

LIVE/DEAD staining showed that PLFs on scaffolds were attached and viable. However, the decellularised tissue in contact with the scaffolds showed only small number of cells attached and viable cells on after 7 days, showing possible migration of PLFs from the scaffold into the tissue and attached. However, attached cells would be expected to proliferate and there was not enough evidence of cell proliferation of migrated cells on decellularised tissues. This is similar to data seen from 35FLH fibroblasts, which also did not migrate to a great extent.

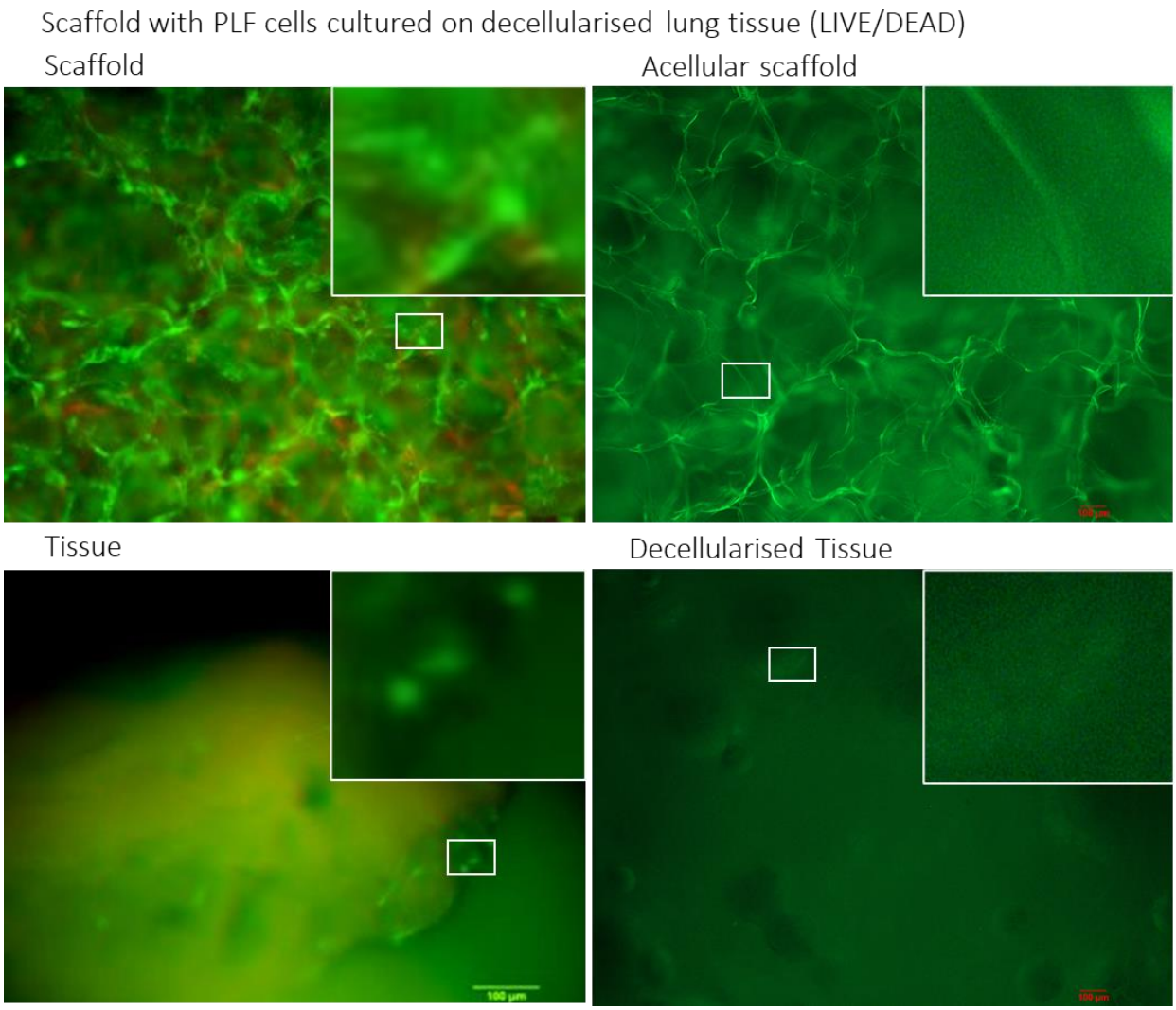

Figure 5.24: Assessing PLF migration from scaffold to tissue. LIVE/DEAD images show viable cells on both scaffolds and tissue, indicating migration from scaffold to tissue after 7 days of culture. Acellular scaffolds and decellularised tissue used as negative controls.

DNA quantification assays showed that seeded scaffolds had a significant increase in DNA quantity compared to control empty scaffolds ($p < 0.0001$ for both), but there was not a significant difference in DNA quantity compared to control decellularised lung tissue ($p > 0.05$ for both) (**Fig 5.25**). These results show that PLFs migrated least out of the four cell types, despite growing well on Surgispon scaffolds.

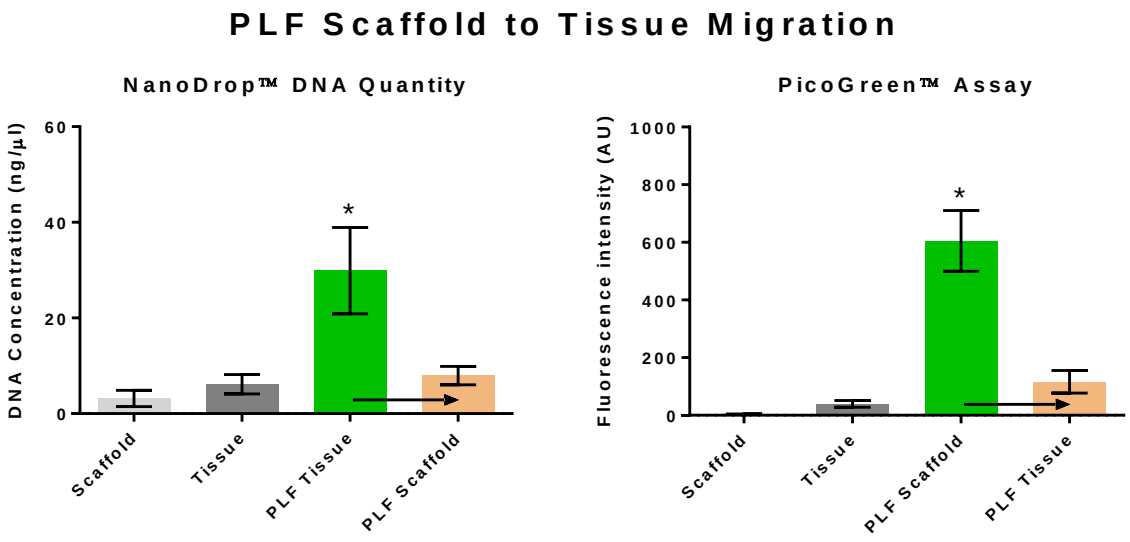

Figure 5.25: PLF migration from seeded scaffolds to decellularised tissue. NanoDrop and PicoGreen assays were performed on controls (empty scaffolds and decellularised tissue), on PLF scaffolds placed on tissues (GREEN), and on the tissues themselves to see if cells migrated (ORANGE).

5.4.7.5 D-PLF/PLEC co-cultures

30,000 D-PLFs were seeded onto Surgispon scaffolds followed by 30,000 PLECs, these cells were fluorescently labelled: PLECs with red fluorescence and D-PLFs with green fluorescence. After 7 days of cell culture, scaffolds were imaged in order to investigate cell migration from scaffold into decellularised lung tissue **(Fig 5.26).**

Fluorescent images showed that both PLECs and D-PLFs were attached to scaffolds and featured a healthy morphology. A higher number of PLECs were observed on the scaffolds when compared to D-PLFs, this is most likely due to D-PLFs no longer proliferating. Decellularised tissue in contact with the scaffolds also showed PLECs with a healthy morphology after 7 days, showing migration of PLECs from the scaffold into the tissue and

successful proliferation after migration. However, no D-PLFs were observed on decellularised tissue.

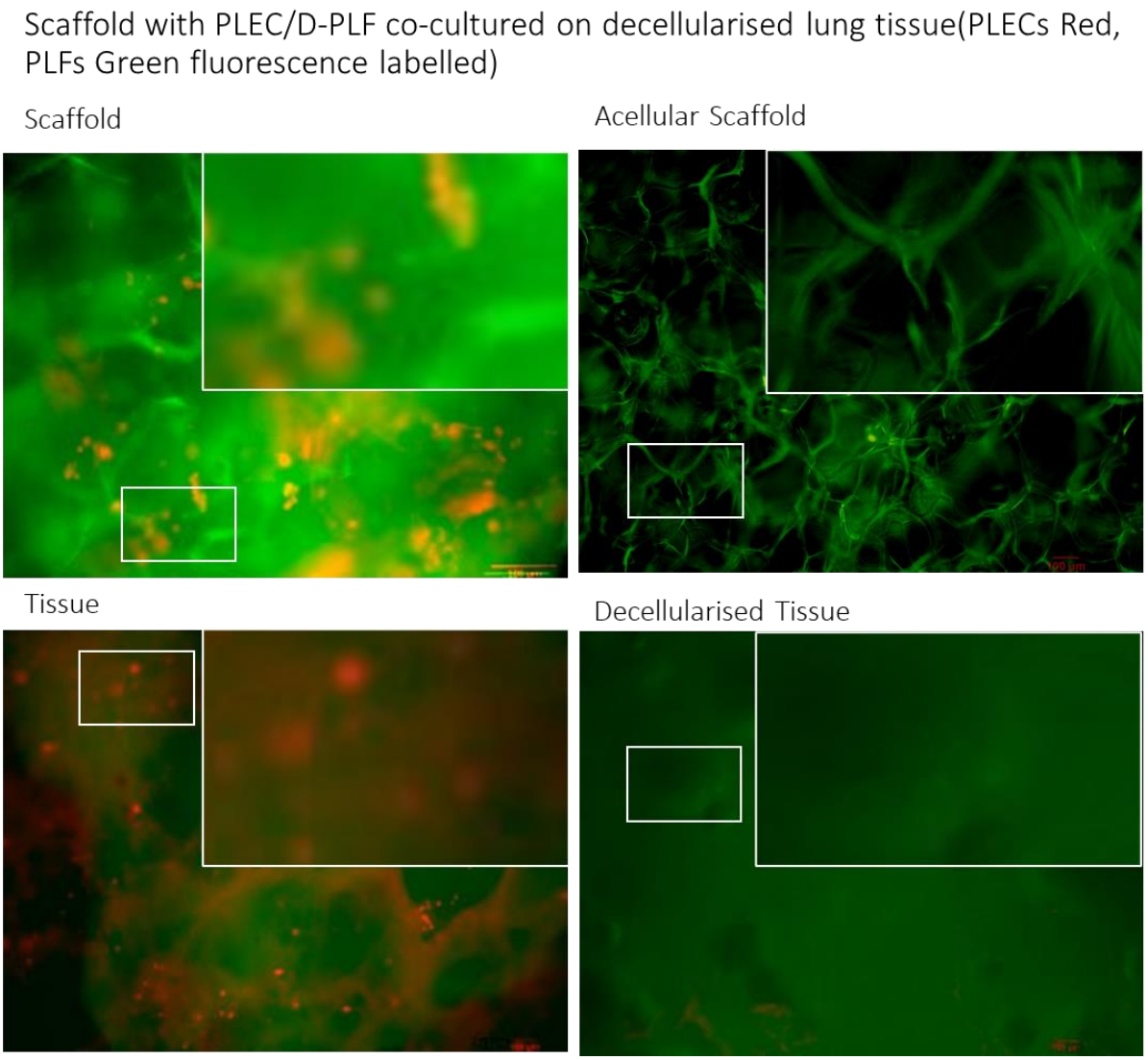

Figure 5.26: Assessing PLEC/D-PLF co-culture migration from scaffold to tissue. Cells are fluorescently labelled, PLECs in red, D-PLFs in green. Fluorescent images show PLEC and D-PLF successfully cultured on scaffolds, with PLECs migrating to tissue, no migration seen for D-PLFs.

The NanoDrop and PicoGreen assays could only quantify the amount of DNA on tissues and scaffolds, showing migration (**Fig 5.27**). They could not characterize the cell type that had

migrated, but from observing the images in **Figure 5.26**, it is clear that any migration seen can be attributed to PLECs. A significant increase in DNA quantity was seen from the empty scaffold control when compared to D-PLF/PLEC co-culture scaffolds ($p<0.0001$ for both), and a significant increase was also seen from decellularised tissue control when compared to tissue next to seeded Surgispon scaffold ($p<0.0001$ for both), indicating that migration had occurred.

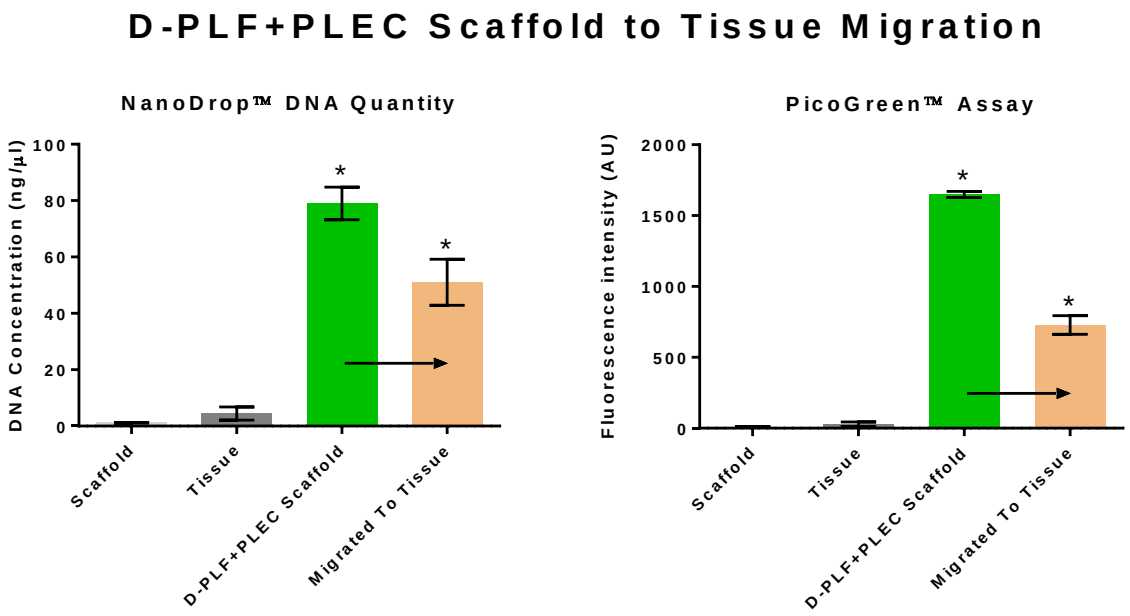

Figure 5.27: D-PLF+PLEC co-culture migration from seeded scaffolds to decellularised tissue. NanoDrop and PicoGreen assays ran on controls (empty scaffolds and decellularised tissue), on D-PLF+PLEC scaffolds placed on tissues (ORANGE/GREEN), and on the tissues themselves to see if cells migrated (ORANGE).

5.4.8 Cell migration: tissue to scaffold

These migration experiments are inverse of the previous section, cells were seeded onto decellularised lung tissue slices and empty acellular Surgispon scaffolds were placed onto these recellularised tissues, in order to determine if cells would migrate from porcine lung tissue into the Surgispon scaffold, the reverse direction to the experiments above. This was done with all available cell types: A549 epithelial cell line, 35FLH fibroblast cell line, PLECs, PLFs and a D-PLF/PLEC co-culture.

5.4.8.1 A549

30,000 A549 cells were seeded onto decellularised porcine lung tissue slices and an empty Surgispon scaffold was placed onto the seeding site. At the end of 7 days culture, samples were stained with LIVE/DEAD kit (**Fig 5.28**).

LIVE/DEAD staining showed that A549 cells on recellularised lung tissue were attached, viable and proliferating. By comparing images to the previous scaffold to tissue migration, it appeared as though a smaller number of cells attached to tissue compare to scaffolds.

A549 cells were observed on the Surgispon scaffolds placed onto the recellularised tissue, these cells were viable and attached, indicating that A549 cells migrated from the recellularised tissue into the scaffold and attached. Unlike the previous experiment, these cells were migrating against gravity, meaning that they were unlikely to end up growing on the scaffold unless deliberate migration had taken place. As well as live cells, dead cells were also observed on the scaffold, suggesting that some cells migrated cells then died. Compared to this, there were only a small number of dead cells on the decellularised tissue.

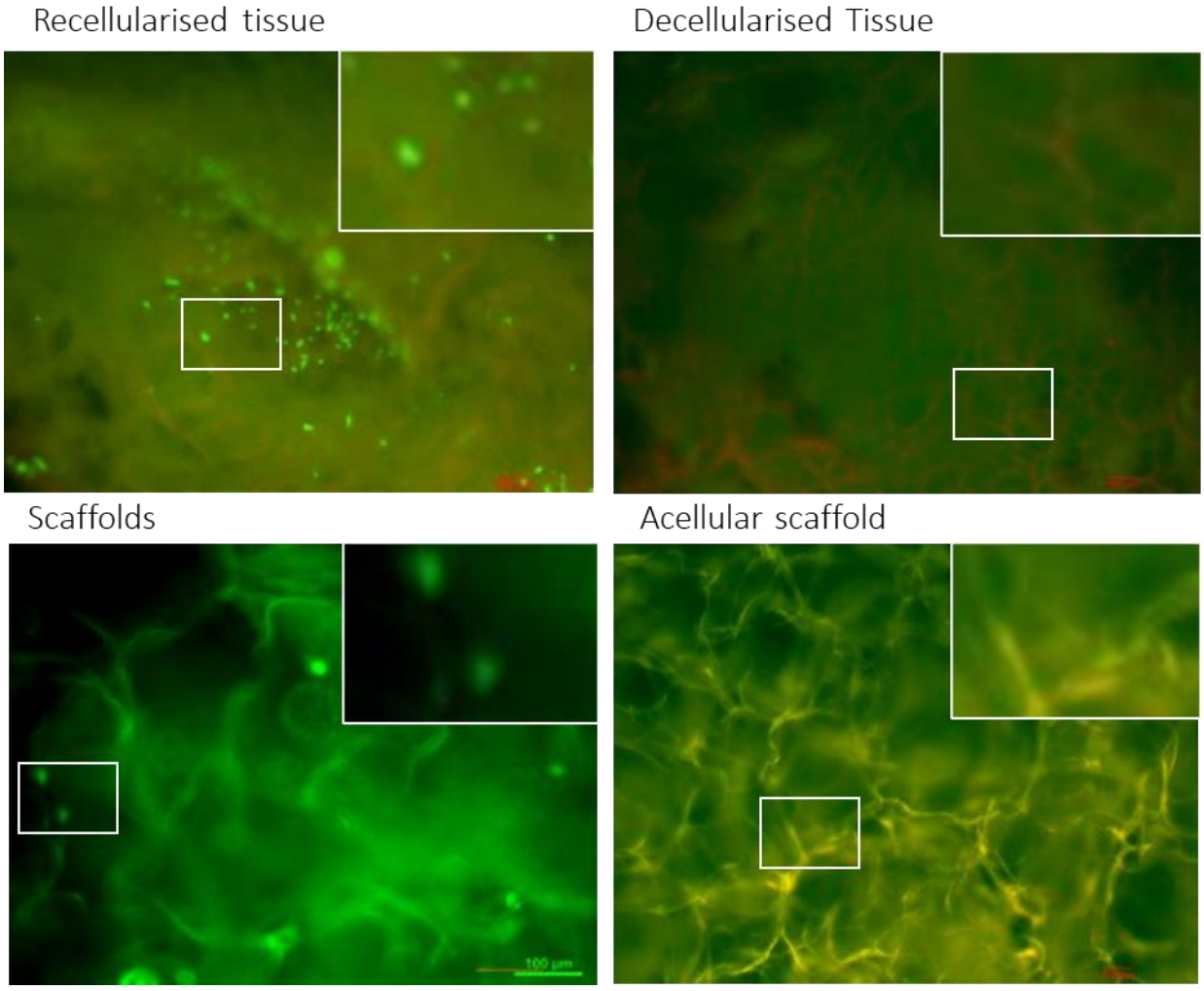

Figure 5.28: Assessing A549 migration from tissue to scaffold. LIVE/DEAD images show viable cells on both recellularised tissue and scaffold, indicating migration from tissue to scaffold after 7 days of culture. Decellularised tissue and acellular scaffolds used as negative controls.

DNA quantification assays NanoDrop and PicoGreen were used on the same scaffolds in order to quantify DNA in both Surgispon scaffolds and lung tissue (**Fig 5.29**). For both assays, recellularised tissues had a significant increase in DNA quantity compared to control decellularised tissues ($p < 0.001$ for both), and scaffolds placed on tissues had a significant increase in DNA quantity compared to control empty scaffolds ($p<0.001$ for PicoGreen, $p<0.01$

for NanoDrop). The latter results show that A549s had migrated into Surgispon scaffolds from lung tissue in significant numbers.

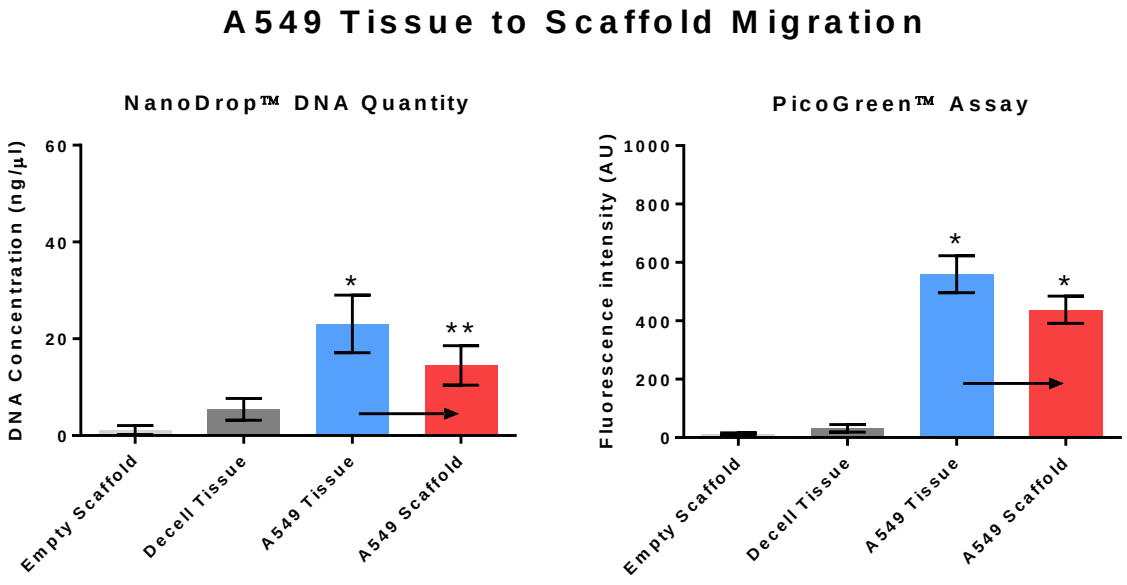

Figure 5.29: A549 migration from recellularised tissue to empty scaffolds. NanoDrop and PicoGreen assays ran on controls (empty scaffolds and decellularised tissue), on tissue recellularised with A549 cells (BLUE), and on empty scaffolds placed on these tissues (RED). (*): $p<0.001$, (**): $p<0.01$.

5.4.8.2 35FLH

30,000 35FLH cells were seeded onto decellularised porcine lung tissue slices and an empty Surgispon scaffold was placed onto the seeding site. At the end of 7 days culture, samples were stained with LIVE/DEAD® kit (**Fig 5.30**).

LIVE/DEAD staining showed large numbers of attached, viable 35FLHs on recellularised lung tissue. However, the scaffold in contact with the recellularised tissue showed a very low number of viable attached cells after the 7 days. Migrated and attached cells would be expected to proliferate on scaffold and no sign of cell culture on scaffolds was observed. The

similar lack of red staining shows that these cells did not migrate and then die, but more likely did not migrate at all.

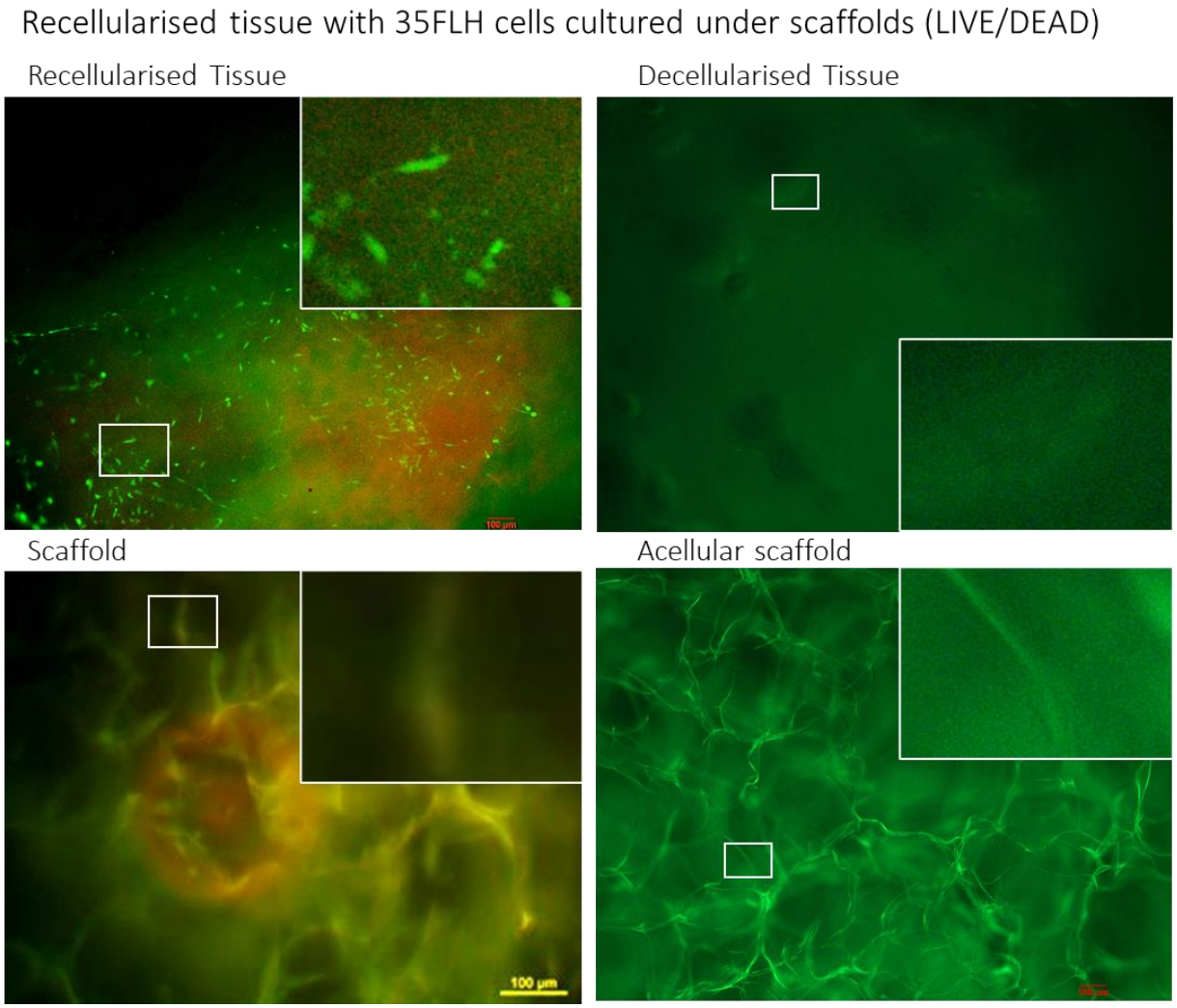

Figure 5.30: Assessing 35FLH migration from tissue to scaffold. LIVE/DEAD images show viable cells on recellularised tissues, but none on scaffolds, suggesting a lack of migration. Decellularised tissue and acellular scaffolds were used as negative controls.

NanoDrop and PicoGreen results show that recellularised tissues had a significant increase in DNA quantity compared to control decellularised tissues ($p < 0.0001$ for both), greater than that for A549 cells (**Fig 5.31**). However, scaffolds placed on tissues had no significant increase in DNA quantity compared to control empty scaffolds ($p > 0.05$ for both). This indicates that 35FLH cells did not migrate from lung tissue to Surgispon, but grew well on lung tissues.

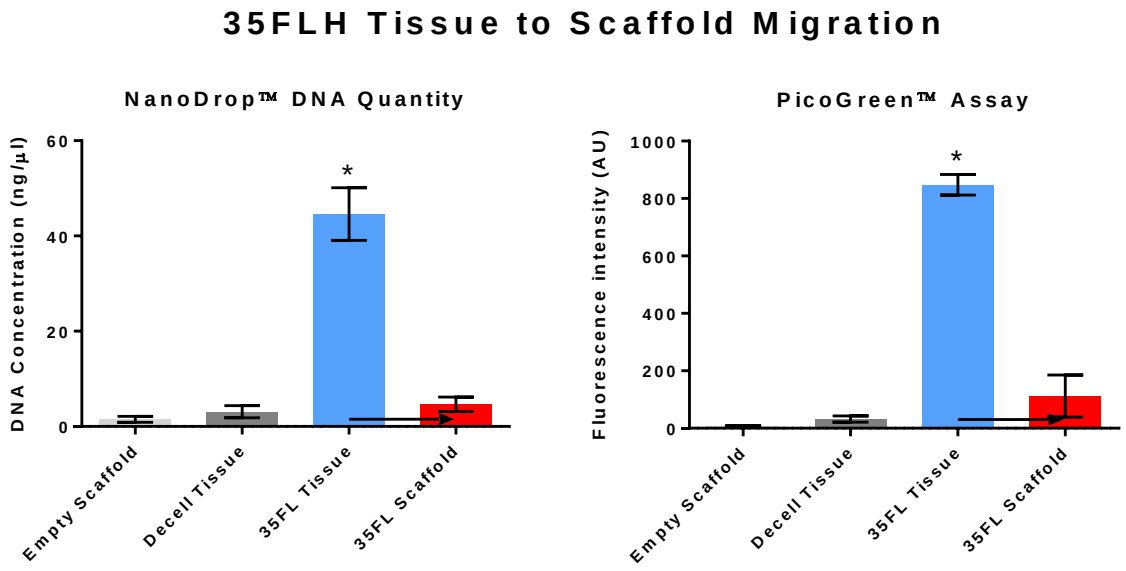

Figure 5.31: 35FLH migration from recellularised tissue to empty scaffolds. NanoDrop and PicoGreen assays ran on controls (empty scaffolds and decellularised tissue), on tissue recellularised with 35FLH cells (BLUE), and on empty scaffolds placed on these tissues (RED).

5.4.8.3 PLECs

30,000 PLECs were seeded onto decellularised porcine lung tissue slices and an empty Surgispon scaffold was placed onto the seeding site. At the end of 7 days culture, samples were stained with LIVE/DEAD kit (**Fig 5.32**).

LIVE/DEAD staining showed that PLECs on decellularised lung tissue were attached and viable. Similarly to A549 results, Surgispon scaffolds in contact with the recellularised tissue showed attached and viable cells on after 7 days, showing that PLECs cells migrated from the recellularised tissue into the scaffold and attached. Dead cells were also observed on the scaffold, but only in low numbers.

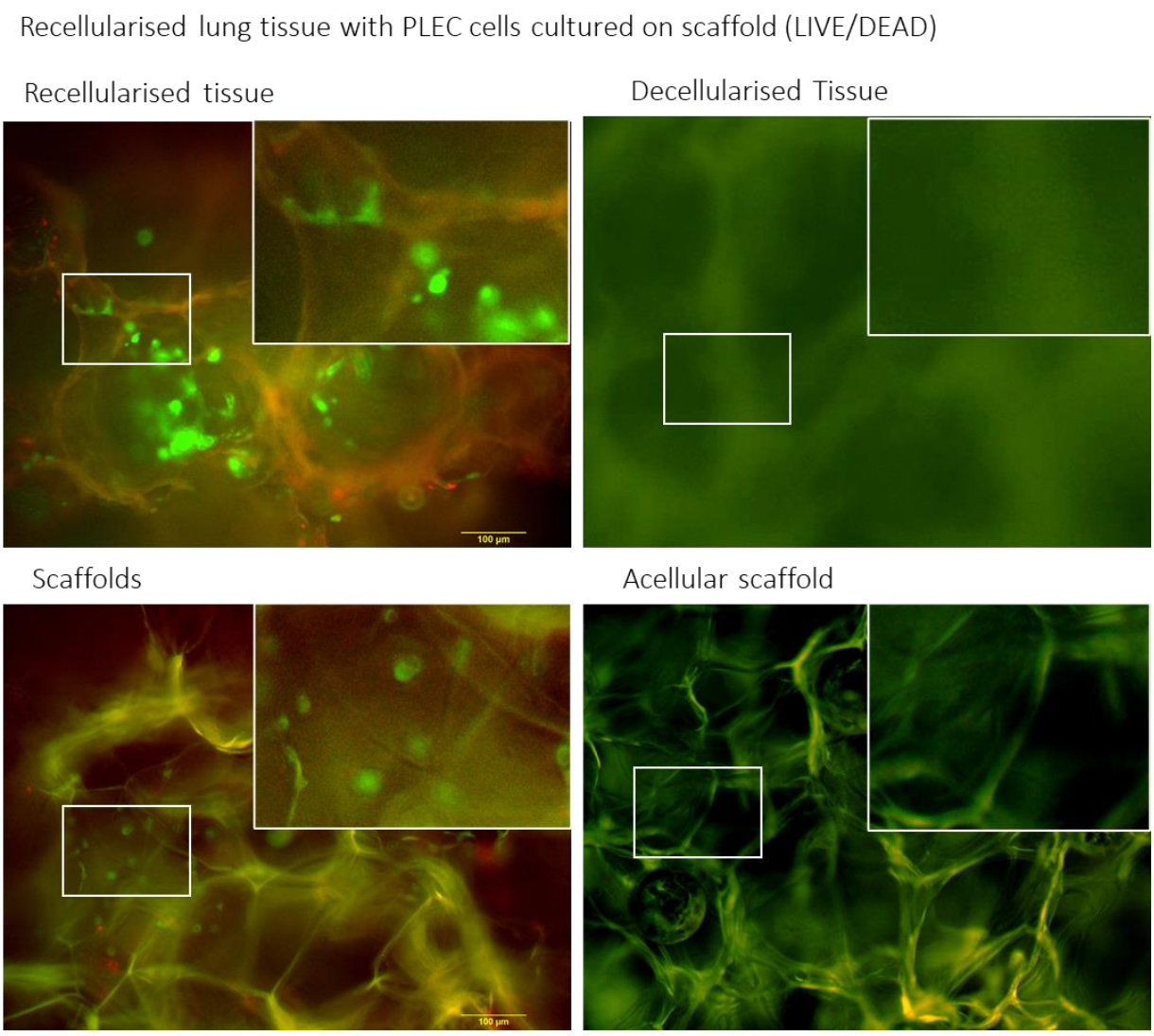

Figure 5.32: Assessing PLEC migration from tissue to scaffold. LIVE/DEAD images show viable cells on both recellularised tissue and scaffold, indicating migration from tissue to scaffold after 7 days of culture. Decellularised tissue and acellular scaffolds used as negative controls.

NanoDrop and PicoGreen results show that recellularised tissues had a significant increase in DNA quantity compared to control decellularised tissues ($p < 0.001$ for both), and scaffolds placed on tissues had a significant increase in DNA quantity compared to control empty scaffolds ($p<0.001$ for NanoDrop, $p<0.01$ for PicoGreen) (**Fig 5.33**). This indicates that PLECs successfully migrated from lung tissue to Surgispon® scaffolds.

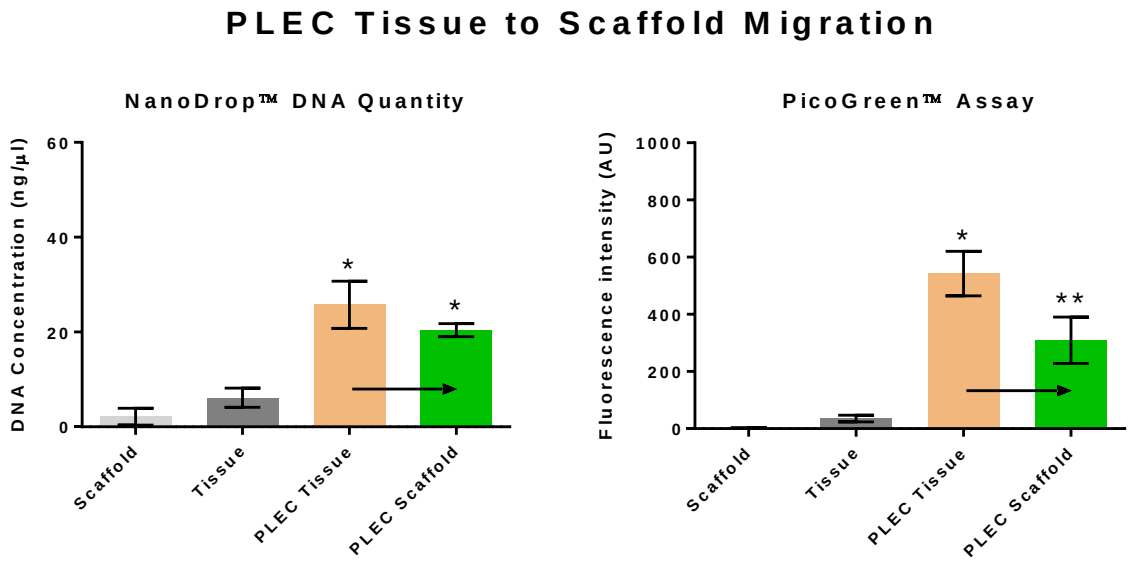

Figure 5.33: PLEC migration from recellularised tissue to empty scaffolds. NanoDrop and PicoGreen assays ran on controls (empty scaffolds and decellularised tissue), on tissue recellularised with PLEC cells (ORANGE), and on empty scaffolds placed on these tissues (GREEN).

5.4.8.5 PLFs

30,000 PLFs were seeded onto decellularised porcine lung tissue slices and an empty Surgispon scaffold was placed onto the seeding site. At the end of 7 days culture, samples were stained with LIVE/DEAD kit (**Fig 5.34**).

LIVE/DEAD staining showed that PLFs on recellularised lung tissue were attached and viable. However, the Surgispon scaffold in contact with the recellularised tissue did not show enough evidence of cell migration from recellularised tissue into the scaffold. Similar to live cells, dead cells were also not observed on the scaffold. Similarly to 35FLH cells, there was a lack of migration.

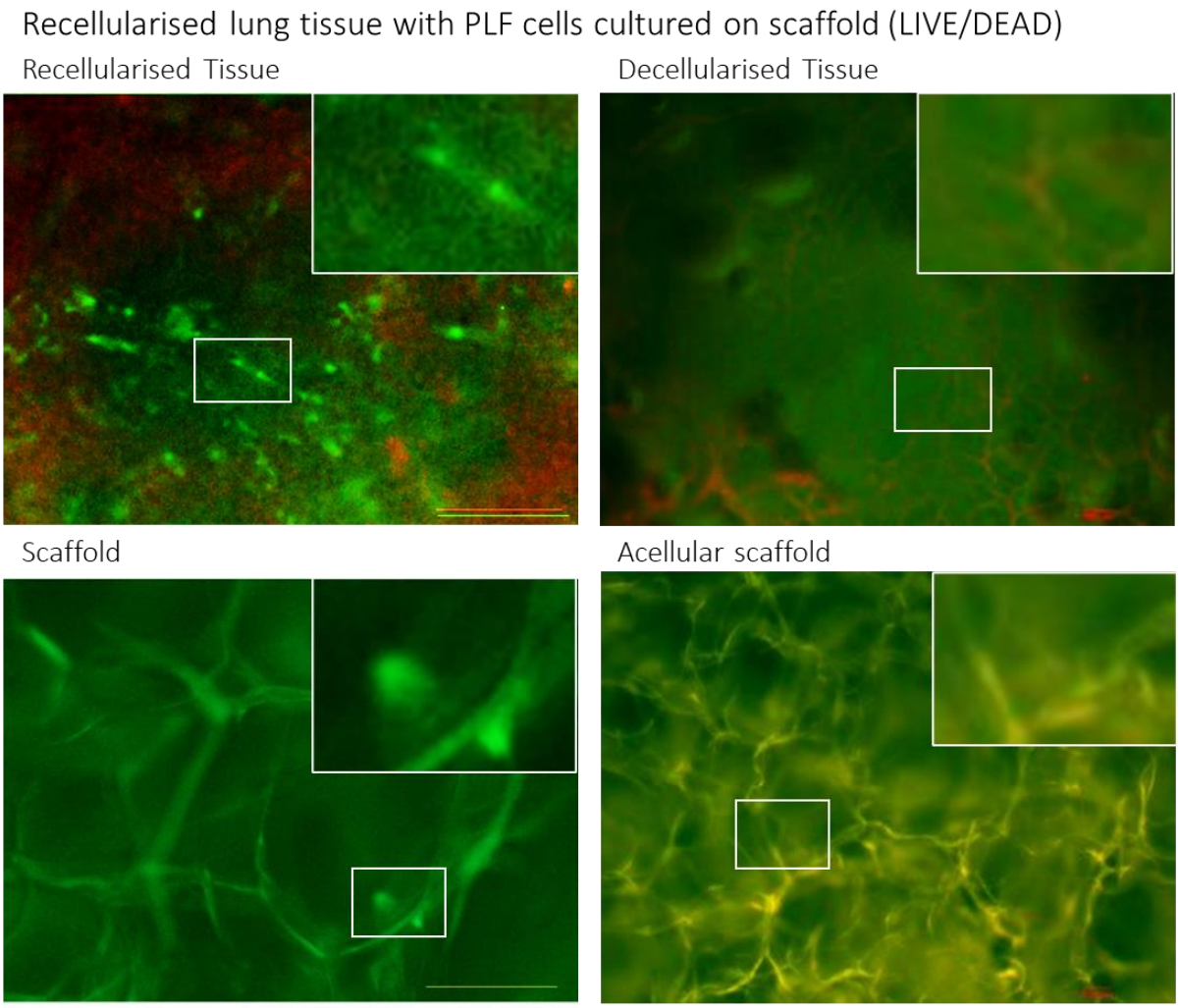

Figure 5.34: Assessing PLF migration from tissue to scaffold. LIVE/DEAD images show viable cells on recellularised tissues, but very few on scaffolds, suggesting low levels of migration. Decellularised tissue and acellular scaffolds were used as negative controls.

NanoDrop and PicoGreen results show that recellularised tissues had a significant increase in DNA quantity compared to control decellularised tissues ($p < 0.001$ for both), but scaffolds placed on tissues had no significant difference in DNA quantity compared to control empty scaffolds ($p > 0.05$ for both) (**Fig 5.35**). This indicates that PLFs did not migrate to Surgispon scaffolds in significant numbers, similarly to35FLH experiments.

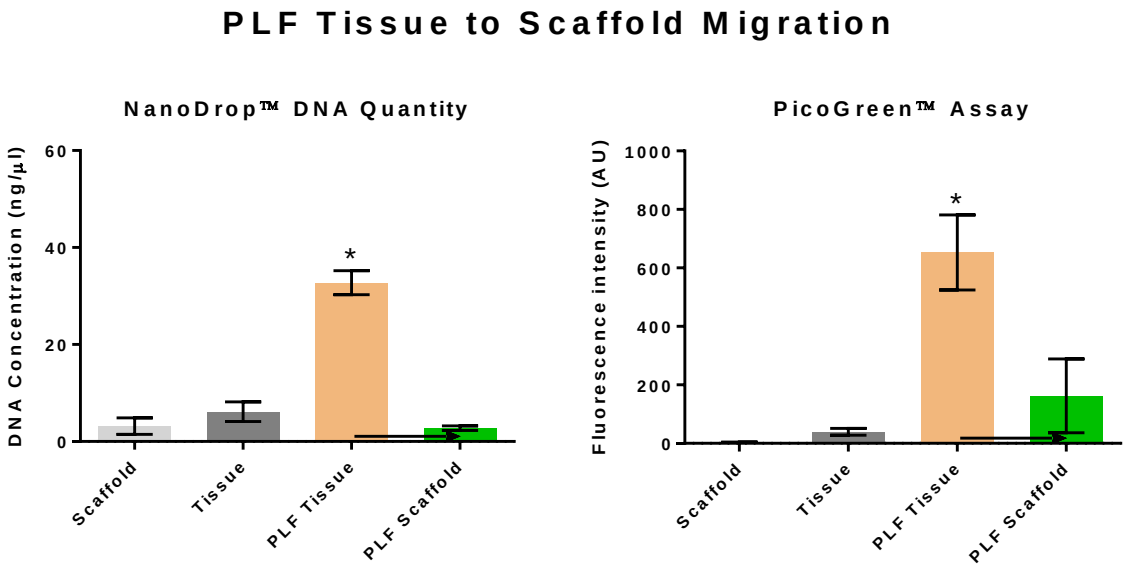

Figure 5.35: PLF migration from recellularised tissue to empty scaffolds. NanoDrop and PicoGreen assays ran on controls (empty scaffolds and decellularised tissue), on tissue recellularised with PLF cells (ORANGE), and on empty scaffolds placed on these tissues (GREEN). (*): $p<0.001$.

5.4.8.5 D-PLF/PLEC co-cultures

30,000 D-PLFs were seeded onto decellularised lung tissue followed by 30,000 PLECs, these cells were fluorescently labelled: PLECs with red fluorescence and D-PLFs with green fluorescence. A Surgispon scaffold was placed onto the seeding site, and after 7 days of culture the tissues and scaffolds were imaged in order to investigate cell migration from the recellularised lung tissue to the scaffold **(Fig 5.36).**

Fluorescent images showed that both PLECs and D-PLFs were attached to tissue and featured a healthy morphology. A higher number of PLECs were observed on the scaffolds when compared to D-PLFs, this is most likely due to D-PLFs no longer proliferating. Similarly to the reverse situation (scaffold to tissue), migration occurred but only for PLECs. The Surgispon

scaffold in contact with recellularised tissue showed attached and viable PLECs after 7 days.

However, there were no D-PLFs observed on scaffolds, indicating no D-PLF migration.

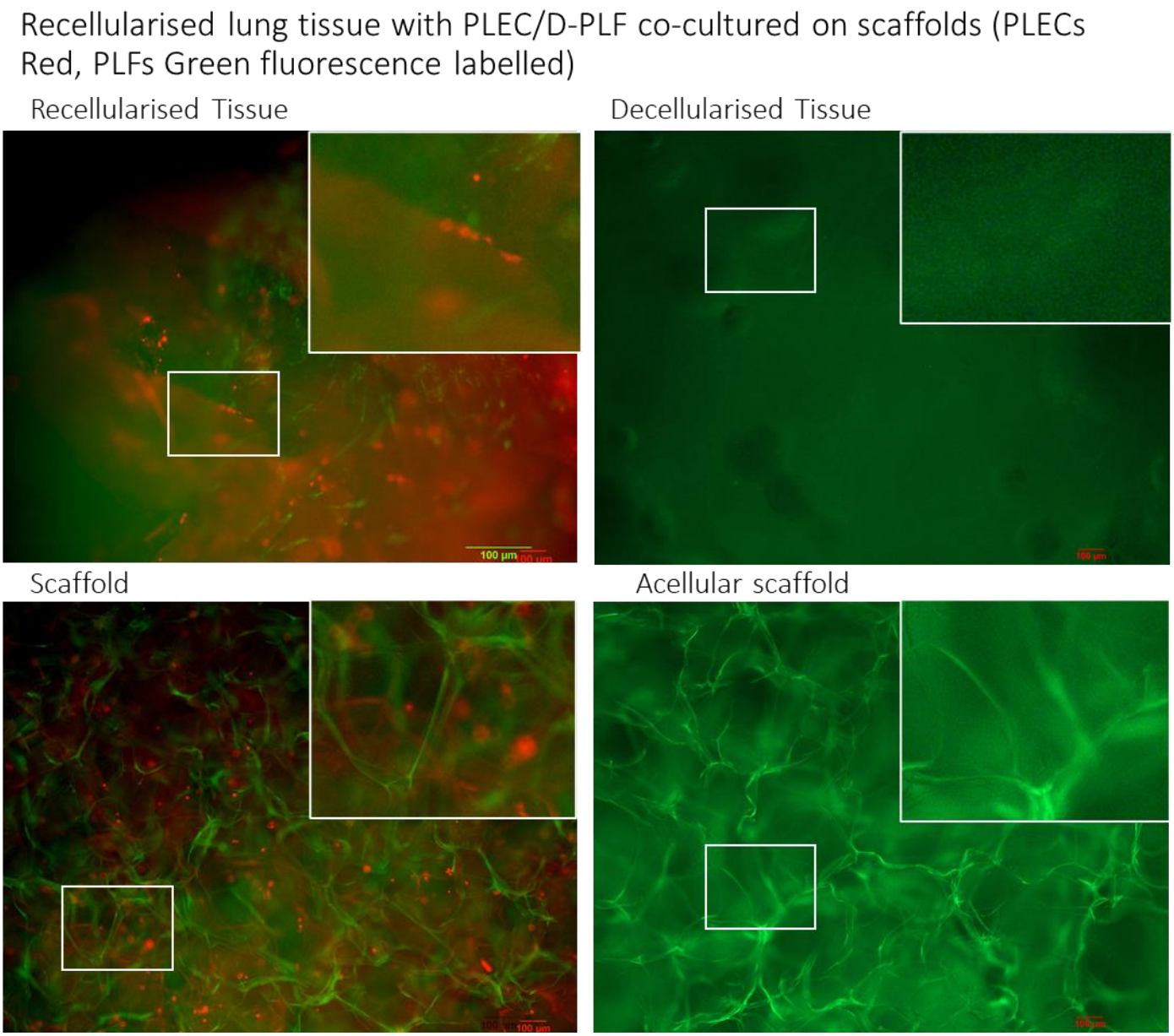

Figure 5.36: Assessing PLEC/D-PLF co-culture migration from tissue to scaffold. Cells are fluorescently labelled, PLECs in red, D-PLFs in green. Fluorescent images show PLEC and D-PLF successfully cultured on scaffolds, with PLECs migrating to tissue, no migration seen for D-PLFs.

The NanoDrop and PicoGreen assays could only quantify the amount of DNA on tissues and scaffolds, showing migration (**Fig 5.37**). They could not characterize the cell type that had migrated, but from observing the images in **Figure.5.36**, it is clear that any migration seen can be attributed to PLECs. A significant increase in DNA quantity was seen from the empty scaffold control when compared to D-PLF/PLEC co-culture scaffolds ($p<0.0001$ for both), and a significant increase was also seen from decellularised tissue control when compared to tissue next to seeded Surgispon scaffold ($p<0.0001$ for both), indicating that migration had occurred.

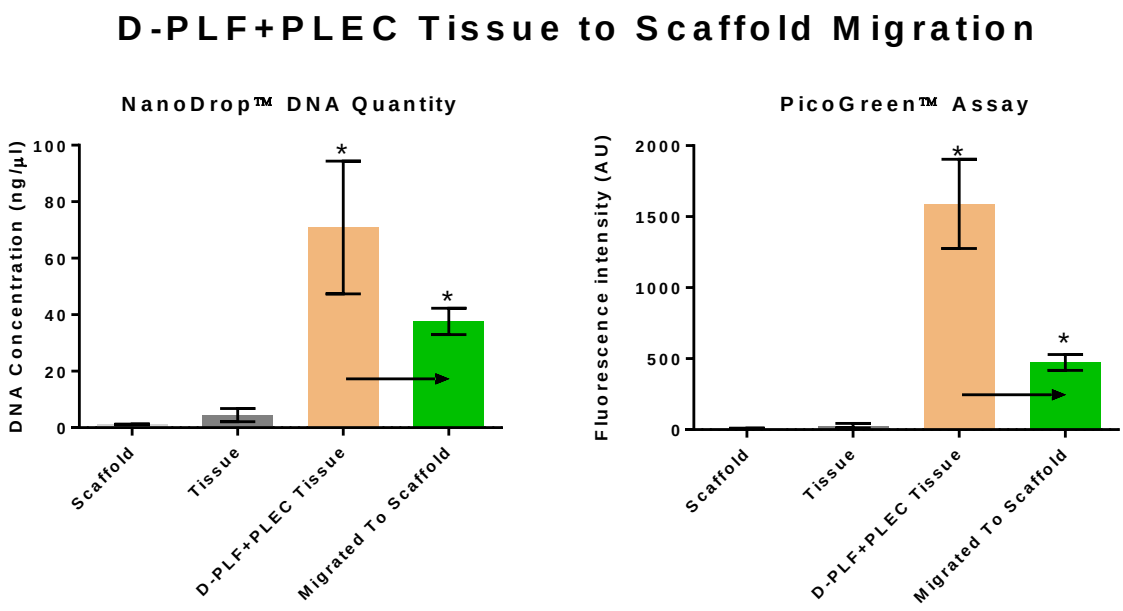

Figure 5.37: D-PLF+PLEC co-culture migration from recellularised tissue to scaffold. NanoDrop and PicoGreen assays ran for controls (empty scaffolds and decellularised tissue), on D-PLF+PLEC recellularised tissue (ORANGE/GREEN), and on empty scaffolds placed on these tissues (GREEN). Migration was observed only for PLECs, (*): $p>0.001$.

5.4.6 Cell Migration Comparison

As well as showing PicoGreen and NanoDrop assay results for DNA quantity for each experiment, the results are aggregated in **Figure 5.38** in order to compare migration between cell types. For scaffold to tissue migration, epithelial cell types (A549 and PLEC) migrated significantly more than fibroblast cell types (35FLH and PLF), ($p<0.001$ for NanoDrop, ns for PicoGreen), but demonstrated the greatest extent of migration when in a D-PLF/PLEC co-culture, significantly greater than migration seen with just PLEC cells ($p<0.001$ for both). Less migration was seen in the inverse situation, namely cell migration from tissue to scaffold. However, the trends are similar, with epithelial cells migrating more than fibroblasts, and the co-cultured PLECs migrating significantly more than other situations ($p<0.01$ for NanoDrop, ns for PicoGreen).

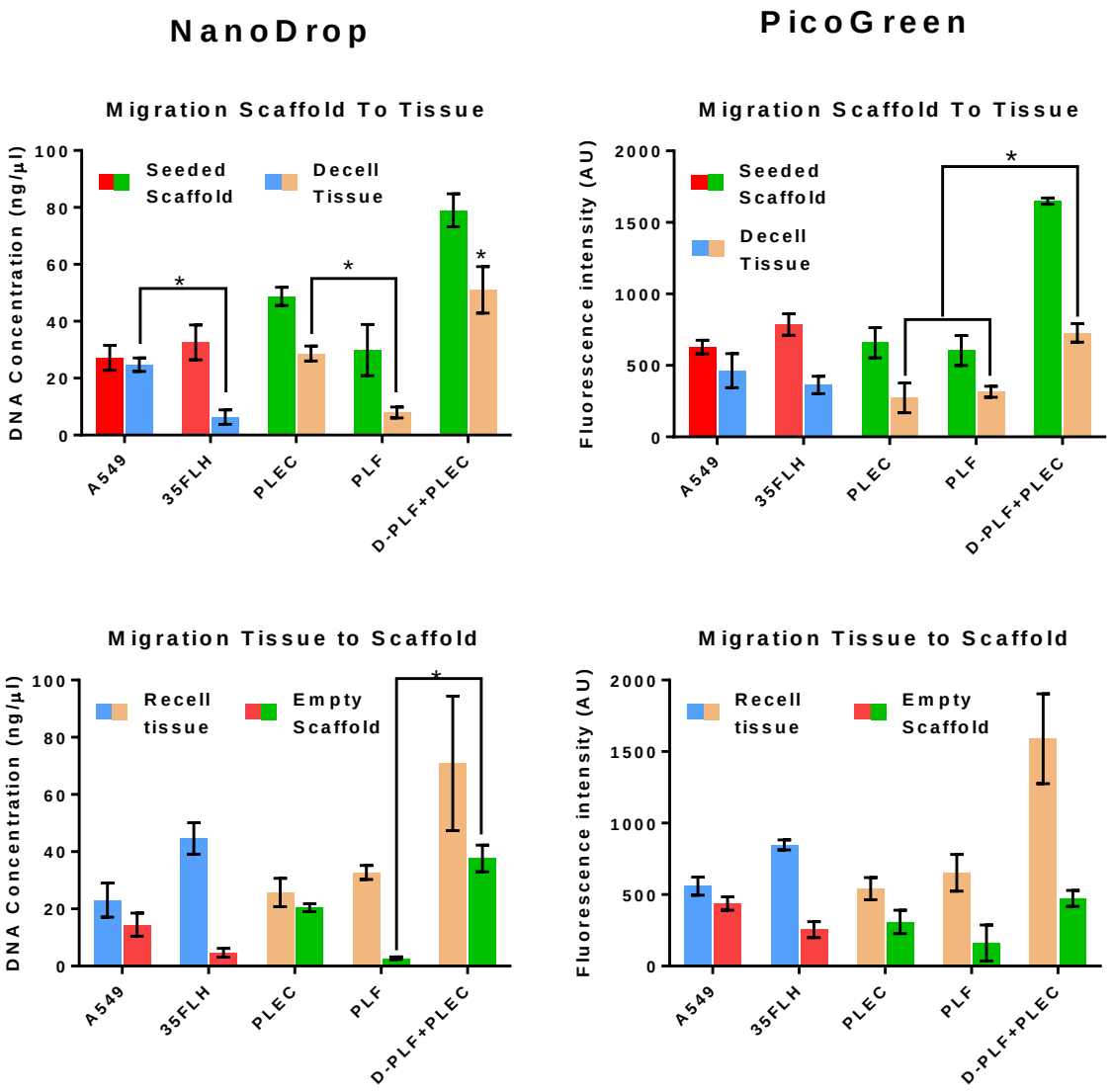

Figure 5.38: Summary of DNA quantification of cell migration, both from scaffold to tissue and from tissue to scaffold. For the scaffold to tissue migration, seeded scaffolds were placed onto decellularised tissue, for the tissue to scaffold migration, empty scaffolds were placed onto recellularised tissue. For cell lines, tissue is blue and scaffold is red. For primary cells, tissue is orange and scaffold is green.

5.5 Discussion

5.5.1 Primary Porcine Cell Culture on Surgispon

Cell attachment studies are important for understanding cell signalling pathways, biomaterial studies, development of tissue-on-a-chip/organ-on-a-chip models, effects of biochemical treatments/environmental stimuli on cell adhesion, and the potential of drug treatments. Cell adhesion has a critical role in cell communication and regulation as well as development and maintenance of tissue (Khalili and Ahmad, 2015). 3D cell culture gives us a better understanding of *in vivo* cellular behaviour and is important in order to produce *in vivo*-like data (Justice et al., 2009).

Both pan-cytokeratin (epithelial marker) and vimentin (fibroblast marker) markers indicated that epithelial and fibroblast cells were respectively isolated from dissection of porcine lungs, and the designation of PLEC and PLF were accurate. Data from alamarBlue and LIVE/DEAD viability assays as well as PicoGreen DNA quantification assay all indicated that PLECs were successfully cultured on Surgispon scaffolds over 21 days and were viable, proliferating and attached to Surgispon scaffolds (**Fig 5.4**). Surgispon scaffolds have a similar structure to lung tissue and they show potential as a lung model, with the ability to successfully culture primary lung cells using these scaffolds. PLFs were also cultured on Surgispon scaffolds, as alveolar fibroblasts contribute to alveoli structure and epithelial cell growth, and are part of the ECM protein production process (Chaubey et al., 2008). Results were similar to PLEC results, with increased cell density from days 7-14 and 14-21 (**Figs 5.5, 5.6)**, indicating that PLFs are viable and proliferating. The ability to culture both lung epithelial cells and lung fibroblasts adds to the potential of Surgispon as a lung model.

With Surgispon supporting culture of PLECs and PLFs individually, co-cultures of D-PLFs and PLECs together were tested, with the deactivated PLFs serving as a feeder layer, similar to *in vivo.* It is important to create these 3D co-culture systems to mimic *in vivo* cell growth environment. Research showed that 3D co-culture of lung fibroblasts and epithelial cells demonstrated the importance of underlying mechanisms of cell-cell communication, with Horie and colleagues co-culturing stromal cancer-associated fibroblasts with A549 cells on 3D collagen gels, showing that fibroblasts had increased invasion of A549 cells in cell-cell interactions and resulted in increased gel contraction (Horie et al., 2012). Successful co-culture of PLECs and D-PLFs on Surgispon indicate how this scaffold can potentially be used for 3D co-culture systems as a preclinical platform for study.

5.5.2 PLEC Differentiation on Surgispon

Lung epithelial cells are specialized for different functions. These are: basal cells, secretory cells, ciliated cells and alveolar type I/II (AT1/2). Lung airway basal cells can generate differentiated cells in adults during both steady and epithelial repair states (Rock et al., 2011). Lung epithelial cell repair requires rapid cell proliferation, evidence suggests that basal cells function as stem cells for this repair (Rawlins et al., 2007). Basal cells and AT2 cells have been grown in 3D culture systems and have created self-organising structures and organoids (Barkauskas et al., 2017). Epithelial-fibroblast co-cultures in air-liquid interface (ALI) culture systems improve the differentiation of respiratory epithelial cells and promotes organoid structural formation (Albers et al., 2016). These studies allow the study of epithelial cells and their differentiation pathways in 3D.

Surgispon has been shown to be a suitable 3D cell culture scaffold for primary porcine cells, namely PLECs and PLFs, with these cells attaching and proliferating on Surgispon for up to 21

days cell culture. Surgispon scaffolds also have the potential to support an air-liquid interface (ALI) and sphere culture as shown by PLEC differentiation, forming spheroids and organoids over time when cultured, while this was not observed with other scaffold experiments. Transwell inserts can be used to form an ALI (with cells grown on a porous membrane suspended partly in media) these are limited to 2D culture. A porous 3D sponge presents the potential for a 3D ALI and more biologically relevant differentiation and spheroid formation, in line with the sphere culture protocol that this differentiation protocol was based on (STEMCELL Technologies, 2019).

By only submerging half the Surgispon scaffold in media, these differentiation experiments allowed a 3D ALI to form, with the liquid media feeding the scaffold bottom half while the top half was exposed to air. Only these differentiation experiments were cultured in this manner, which does raise the question of whether the format of using half the usual media promotes differentiation, or if the use of Matrigel and sphere culture is the driver of differentiation, or if successful differentiation of PLECs into spheroids requires both. Further study is required to break down this process and determine what factors are necessary for differentiation, as only this experimental format resulted in the formation of spheroids from PLECs cultured on Surgispon.

Both PneumaCult-ALI commercial media and CFAD in-house media were shown to successfully result in spheroid formation with this differentiation protocol, meaning CFAD can be used for future experiments due to the ease of access and cost effectiveness. There was variation in spheroid size between each media type (both with and without supplements) and over time, but these differences were not significant and represent more of a trend. Mean spheroid diameter remained between 100-200 μm from days 2-14 for all media types, but the

range in diameters increased for all media types over time. Three main factors to investigate further would be the effect of spheroid diameter (is it better to have smaller or larger spheroids, would they still develop into functional bronchospheres?), how larger spheroids develop (do smaller spheres grow over time or is it a fusion between multiple smaller spheres?), and the effect of media supplements on spheroid formation and development (what are the differences between CFAD and CFAD+ in terms of bronchospheres, are the added growth factors having any measurable effect?) Overall, the variation between diameters for each media is not significant, may simply be biological variation, but should still be subject to further study.

Antibody staining and characterisation experiments revealed that a population of PLECs stained positive for p63 (stem/progenitor cells), and when under sphere culture conditions on Surgispon scaffolds, PLECs differentiated into cells that stained positive for mucin 5AC, potentially indicating the presence of ciliated cells or goblet cells (**Figs 5.12-5.14**). Broncospheres often feature ciliated/goblet cell types (Sprott et al., 2020), meaning that the spheroids formed from PLEC differentiation may be similar to bronchospheres. More should be done to identify these differentiated PLEC populations, while some cells stained positive for mucin 5AC, additional staining and gene expression work should be done, as well as higher resolution imaging to observe the presence of cilia, and how these cilia move.

Negative staining for SPC (surfactant protein C, AT2 cell marker) and podoplanin (AT1 cell marker) indicated there were no populations of AT1 or AT2 cells (**Fig.5.13**) but further characterisation work should be done in order to identify cell subpopulations within PLECs, both before and after differentiation protocol, performing further staining and gene expression analysis.

5.5.3 Porcine Lung Tissue Decellularisation

The porcine lung tissue decellularisation protocol was checked using DNA quantification assays NanoDrop and PicoGreen, as well as DAPI fluorescent staining (**Fig 5.15-5.16**). There is no universally accepted definition for tissue decellularisation but there are three main issues that need to be addressed: decellularised tissue should not contain more than 50 ng of DNA per mg dry weight, DNA fragments should not be longer than 200 bp, and there should not be any visible nuclear components in the ECM (Hillebrandt et al., 2019). If these factors can be observed through this decellularisation protocol, it can be determined to be successful and the tissue is decellularised and ready for experimentation. The average dry weight of decellularised tissue pieces was 228 mg with to DNA content of 485 ng (data from NanoDrop), resulting in ~2 ng of DNA per mg dry weight, well below the 50 ng stated above. Alongside this, DAPI imaging was used to determine that no nuclear components were visible (**Fig.5.15**). The only factor that isn't addressed is the DNA base pair length as there were no experiments done to determine DNA length on decellularised tissue, this should be addressed in future experiments to reinforce the decellularisation procedure. Despite this, the DNA per dry weight and DAPI imaging still both solidify the decellularisation procedure as effective on porcine lung tissue.

Compared to native control tissue, the decellularised samples showed a significant 98.47% reduction in DNA concentration (DNeasy assay, **Fig 5.16**), compared to 96.56% from PicoGreen. Additional DAPI imaging also only indicated that background autofluorescence was the only signal from decellularised lung tissue (**Fig 5.15**), with the vast majority of cells stripped from the tissue and only the ECM remaining. These results indicate the effective decellularisation of porcine lungs compared with native lung tissue, previous research

showed that decellularisation of tissues can provide up to 99% reduction in DNA concentration from decellularised tissue compared to native tissue (Simsa et al., 2018).

Decellularisation of lung tissue with detergent showed great potential to lyse/remove cells and to create 3D scaffolds for *ex vivo* lung tissue engineering. However, when detergent was used for the decellularisation process, it can be damaging to the ECM due to activation of metalloproteinases that can degrade ECM proteins. These ECM proteins are important for cell attachment and growth of cells on decellularised tissue (Wallis et al., 2011). The condition of decellularised porcine lung tissue ECM should be investigated in future work to ensure that major ECM proteins are retained after the decellularisation process.

The remaining tissue ECM after decellularisation was shown to support culture of A549, 35FLH, PLEC, PLF and D-PLF/PLEC co-cultures (**Fig. 5.17**), indicating that the ECM was potentially not damaged to the point where it cannot support cells, meaning that this protocol is robust for producing decellularised tissue for cell culture, providing an ideal biological scaffold for lung cell culture (O'Neill et al., 2013c), as recellularised tissue can show organ specific functions for short period of time and present a promise for future *in vivo* experiments (Tsuchiya et al., 2014). Recellularised tissues showed a similar cell structure compared to control porcine lung tissue when imaged with DAPI (**Fig 5.17**). These porcine lung tissues are used for the recellularisation process and function as a proof of concept study in combination with Surgispon, namely to test how cells would migrate to or from Surgispon *in vivo* if implanted to an injury site in the lung. However, it should be noted that the density, shape and composition of decellularised tissue cannot be easily controlled which limits use in tissue engineering (Zitnay et al., 2018).

5.5.4 Cell migration

A combination of Surgispon scaffolds and de/recellularised lung tissues were used to study migration, with an aim to investigate the use of Surgispon as a transplant vehicle for cells to access damaged sites, such as in emphysema. Epithelial cells A549 and PLEC were shown to migrate from Surgispon scaffolds to decellularised tissues, and from recellularised tissues to Surgispon scaffolds (**Figs 5.18, 5.19, 5.22, 5.23**), indicating they may be able to migrate to disease sites from cell-seeded Surgipon, or if Surgispon is placed onto a disease site it may attract cells, giving potential for Surgispon as an *in vivo* therapy for emphysema as well as an alveolar model. This cell migration from scaffold to tissue and proliferation of the migrated cells on tissue helps these cells to create their own ECM and eventually would become the bond between tissue and scaffolds (O'Brien, 2011). In addition, there was an increased number of migrated of PLECs observed in D-PLF/PLEC co-cultures, potentially either due to the D-PLF feeder layer resulting in more PLEC proliferation and therefore more migrated cells, or due to the D-PLF feeder layer increasing the rate or percentage of epithelial migration, the cause of which is not clear and requires further study. For transplant scaffolds, it would be more biologically relevant to include both fibroblasts and epithelial cells, meaning these co-cultures warrant further study, especially to determine if D-PLF migration is possible.

Far less migration was seen for fibroblasts 35FLH and PLF (**Figs 5.20, 5.21, 5.24. 5.25**). This may be due to the low stiffness of Surgispon, as fibroblast migration is linked to matrix stiffness and softer surfaces have been shown to inhibit lung fibroblast migration (Asano et al., 2017), to the collagen composition (particularly collagen VI) of Surgispon affecting fibroblast migration and adhesion (Theocharidis et al., 2016), or to the presence of populations of myofibroblasts, as these adhere to ECM with increased strength compared to

other fibroblast types (Knüppel et al., 2018). It may also be due to the fibroblasts depositing ECM on the scaffold and increasing their adherence, this is the original purpose of using PLFs and D-PLFs on Surgispon in combination with epithelial cells. Due to the importance of lung fibroblast migration in conditions such as fibrosis, it would be valuable for further work to examine fibroblast migration by studying Surgispon material properties, stiffness, and 35FLH/PLF identity.

Scaffolds must provide a suitable environment for cell-cell interaction, cell migration, cell proliferation and cell differentiation for a successful application in tissue engineering. Migration of cells along and/or across the tissue is an important part of tissue formation and tissue regeneration (Bružauskaitė et al., 2016). COPD causes irritated/injured areas in the airway, and the repair process for this injured tissue is initiated through epithelial cell migration, proliferation and progressive differentiation (Grainge and Davies, 2013), making migration a vital part of lung tissue engineering, and something that any successful lung tissue model should be capable of.

When cells migrate to scaffolds, scaffolds can provide directional migration and can promote and guide cell growth *in vivo* (Berns et al., 2014). Cell migration to scaffolds is crucial to achieve functional vascularisation following the implantation of scaffolds for *in vivo* studies (Ko et. al., 2013). Recent studies showed the importance of using acellular scaffolds (decellularised tissue) for proof of concept studies as it can be recellularised with epithelial cells and can be maintained *ex vivo* for several days (Gilpin and Wagner, 2018). To this end, migration should be investigated further, particularly the lack of fibroblast migration, and the activity/functionality of cells after migration over the long term. Time lapse imaging should be performed to get a clearer picture of how migration is occurring, in what locations, and at

what rates. LIVE/DEAD staining revealed that a small number of cells were dead on scaffolds, suggesting that either these cells had migrated and then died on scaffolds.

Co-culture systems can assist in cell differentiation, promote tissue homeostasis, metabolism, growth and repair (Paschos et al., 2015). Epithelial–fibroblast communication plays an important role for healthy lungs as dysfunctional communication is usually observed in COPD (Osei et al., 2016). Co-culture of D-PLFs and PLECs resulted in significant PLEC migration from scaffold to tissue, but no D-PLFs migration. As PLFs did not migrate, it was unlikely that deactivated PLFs would have the ability to migrate as deactivation only halts their position in the cell cycle.

There are many parameters that can affect cell migration. Key physical influences are adhesion, stiffness and topology of the extracellular environment (Charras and Sahai, 2014). ECM is a meshwork of both structural and functional proteins assembled in unique tissue-specific architectures that provides a cell-specific microenvironment. Numerous studies have confirmed the potential effects of ECM ultrastructure and mechanics upon cell behaviour, migration, and differentiation (Brown and Badylak, 2014). Even with the numerous similarities of Surgispon scaffolds to lung tissue, decellularised tissue provides the closest microenvironment to lung tissue, this is shown by migration to decellularised tissue being greater than migration to acellular scaffolds. This migration from scaffold to tissue highlights the ability of Surgispon scaffolds and a potential role in cell delivery to lung tissue.

Scaffolds with ECM-similar structures can promote cell attachment and proliferation, especially in the case of collagen-based scaffolds. Collagen is typically fabricated into porous spongy scaffolds (like Surgispon) or nanofibrous scaffolds, both of which have different effects on cell migration due to the pore diameter and interconnectivity, and even isotropy of pore

arrangement. These scaffold types are beneficial for tissue engineering across many different tissue types, including lung (Lee and Kim, 2018). The microstructure of Surgispon and the pore interconnectivity and alignment should be investigated further to see what effect it has on migration. Aligned collagen scaffolds can guide cell migration faster than a scaffold with a random structure, while also elongating the cells. While porous scaffolds are often characterised through the pore diameter measurement, it is also important to extract pore network structure and interconnectivity. This was attempted with uCT measurements but more should be done in terms of 3D measurements to track pores through the scaffold in slices and determine interconnectivity. Other scaffold factors to study include pore size, pore wall alignment and pore transport pathways, on both the migration of individual cells or bulk invasion. Pore sizes above 100 µm has been shown to be necessary to evenly distribute cells across a scaffold. This is dependent on high alignment of pores in the direction of travel, if Surgispon is to be used for cell delivery or recruitment then pore wall alignment should be carefully optimised. Cell elongation is also stated as a factor to measure due to the effect on migration, this should also be further tested in Surgispon to see if migrated cells have an elongated morphology (Ashworth et al., 2018). Particularly in fibre based collagen scaffolds, alignment and pore diameter can significantly change the pore network structure as well as direction of cell migration (Park et al., 2020). Cell proliferation and migration are affected by alignment of scaffold architecture and the addition of other factors such as fibrin (Pawelec et al., 2014).

The effects of these on lung epithelial cells and lung fibroblasts is unknown and should be tested in order to optimise migration, especially for lung fibroblasts (Seong et al., 2017). Surgispon scaffolds feature natural variation in pore diameter, arrangement and alignment, ideally different scaffolds can be tested to determine what effect each of these factors have

on cell alignment, in order to promote fibroblast migration. It is possible that experiments with epithelial cells used scaffolds with a favourable pore structure for migration, while experiments with fibroblasts used scaffolds with unfavourable pore structure, this is unlikely due to the numerous biological and technical repeats but scaffold structure should still be analysed for these experiments.

Scaffold chemical coating should also be investigated, namely the effect of collagen/fibronectin coating on migration. Coating was only tested in terms of attachment and viability in the previous experimental chapters, it should also be tested in terms of migration as the addition of collagen to scaffolds modulates migration to tissue, as shown by a study that compared alginate with alginate-collagen porous scaffolds. Alginate-only scaffolds featured cell agglomeration and limited migration, while alginate-collagen scaffolds had increased migration from scaffold to tissue, supporting fibroblast proliferation, ECM deposition, and local growth factor secretion. Surgispon is already composed of collagen, but a mixture of different collagen types may affect migration. In addition, it should be investigated whether or not cells cultured on Surgispon or tissue have local growth factor section, as this can amplify other local cellular events (Guillaume et al., 2015).

Another approach for modifying Surgispon scaffolds is through compression, with studies aiming to construct denser collagen scaffolds through plastic compression and creating a far denser structural network within the scaffold. However, the alignment of collagen fibres and pores is random in this approach and the result is not always an aligned structure; as well as the fact that a denser network within the scaffold may affect cell migration (Zitnay et al., 2018).

5.5.5 Future Work

Surgispon and decellularised lung tissue present a potential system for effective *in vitro* study of primary lung cell attachment, proliferation, metabolism, and migration. However, further work is needed in order to properly characterize each step of this process and reinforce subsequent experiments.

Due to the effects of autofluorescence, other imaging modalities should be explored, such as multiphoton (can image deep into Surgispon and uses infrared wavelengths which avoids overlap peak autofluorescence wavelengths), scanning electron microscopy (SEM, can investigate single cell morphology and attachment without the effect of autofluorescence) and additional μCT imaging, imaging an entire scaffold in 2D slices and following pores through the structure to determine pore interconnectivity, diameter and alignment, all of which are important factors for cell growth and migration.

Surgispon should also be subject to further mechanical testing, tensile testing at a constant strain along different axes (transverse, longitudinal), in order to determine stiffness and other important factors for cell culture. These factors should also be tested for different pore alignments, to see if different pore structures affect the overall mechanical properties, as well as whether Surgispon compression will result in a more favorable pore density without adverse effects on migration. If Surgispon is too stiff, coatings and other treatments (further investigation of crosslinking protocol) should be considered to ensure it is as close as possible to the stiffness of lung ECM.

The effect of chemical coatings on stiffness should also be investigated, along with the effects on cell migration, as chemical coatings were only tested with regards to cell attachment, proliferation and viability.

In addition, the structure of Surgispon and the decellularised lung tissue ECM should both be tested using protein analysis methods such as SDS-PAGE or Western blotting, both to determine the chemical composition of these structures, as well as to see if fibroblast culture produces additional ECM materials, and in general how cell culture affects the chemical composition of these structures over the long term. It is necessary to ensure that there are no negative biological effects such as inflammation or reduced ECM production, especially if these scaffolds are to be used *in vivo*.

Overall, while Surgispon scaffolds present a potentially promising platform for translational lung research, it is vital to perform more studies with primary cells to reveal more about Surgispon as a scaffold, as well as interactions with cells and tissues.

Chapter 6

Summative discussion, conclusion and future directions

6.1 Discussion

6.1.1 COPD

Chronic obstructive pulmonary disease (COPD) is characterized by limitation of airflow and reduced lung function (Britton, 2003). It is progressive, irreversible (Alshabanat et al., 2015) and a major public health issue, costing the NHS over £850 million and causing over 30,000 deaths every year (NICE report, 2018). Cigarette smoking is the main cause of COPD and the majority of smokers are at risk of developing significant airflow obstruction (Ryu et al., 2001; Rennard and Vestbo, 2006)

Exposure to noxious particles or gas causes alveolar abnormalities (emphysema) and air flow limitation (chronic bronchitis), which are the characteristics of COPD (Vogelmeier et al., 2017), but emphysema and chronic bronchitis usually occur together. Chronic bronchitis is the inflammation of the lining of the bronchial tubes, characterized by a daily cough and excess mucus production, while in emphysema the alveoli are damaged/destroyed (Poh et al., 2017).

There is currently no cure for COPD. Treatment usually depends on the symptoms and requires different treatments for individuals (Poh et al., 2017). In COPD, lung tissue cannot regenerate the damaged tissue which results in organ dysfunction. Recent studies into lung stem cell biology and tissue-engineered biomaterials led to advances in lung tissue engineering research (Hogan et al., 2014). Tissue-specific stem cells may increase the regeneration of lung tissue, however, COPD treatment with mesenchymal stem cells (MSCs) showed neither any adverse effects nor any differences in pulmonary function tests or quality of life indicators (Akram et al., 2016). If stem cells were injected directly into lung tissue, there would be no control over where cells would be directed. It is more likely that cells would be

led to existing alveolar walls instead of the areas where normal tissues have been lost due to COPD, which shows the importance of using scaffolds in lung tissue engineering. With a scaffold, a higher concentration of cells can be localized to the damaged area by using the 3D structure as a vehicle (Andrade et al., 2007).

6.1.2 Lung tissue engineering solutions

Lung tissue has a complex structure and 3D scaffolds are commonly used for *in vitro* modelling. Lung tissue scaffolds can be composed of a number of different materials, such as natural polymers (e.g. collagen, gelatine), donor extracellular matrix (ECM) (e.g. decellularised tissue), synthetic polymers (e.g. poly-Ɛ-caprolactone (PCL)) and composites of synthetic and natural materials (e.g. decorin-gelatin-PCL). These materials can be used to create alveolar-like structures with high porosity and elasticity (O'Leary et al., 2015). Of these scaffold materials some of the most commonly used are hydrogels, decellularised tissue and porous natural polymers.

Collagen-based hydrogels are widely used for *in vitro* respiratory tissue engineering applications, but the high water content makes them difficult to work with and they have a tendency to collapse *in vivo* due to their weak mechanical properties (Naito et al., 2011). Decellularised tissue provides a natural scaffold which maintains the tissue-specific architecture and signalling factors (Macchiarini et al., 2008; Crapo et al., 2011; Gonfiotti at el., 2014). However, decellularised scaffolds presents their own challenges, such as the requirement for donors and the limits on mass-production, as well as the decellularisation processes posing some risk to the existing ECM structure (Haykal et al., 2012).

Porous natural polymer scaffolds can address some issues encountered with both decellularised tissues and hydrogels. Porous scaffolds can be mass-produced and therefore

are suitable for high-throughput, are compatible with lung tissue due to their natural source material, and feature suitable mechanical properties, similar to those of lung tissue (Lyons et al., 2008).

In this study a porous natural polymer is used as a scaffold for lung tissue engineering. Surgispon® gelatine haemostatic sponge is commercially available, has the potential to mimic the alveolar structure and can be used for cell growth/differentiation in order to generate an alveolar-like structure, for both *in vitro* research and *in vivo* implantation.

6.1.3 Using a porous gelatine scaffold

Lungs have a complex 3D structure that is constantly mechanically stimulated by ventilation (expansion and compression), and features a complex combination of unique cell types. Simple 2D cell monolayers are not suitable for the replacement of lost lung tissue, as opposed to studies in other organs and tissues such as skin, cartilage, heart, and muscle, which used either biological or synthetic 3D scaffolds to increase the efficiency of complex tissue regeneration (Price et al., 2010; Petersenet al., 2010; Ott et al., 2010).

Collagen-based porous sponges are used as a 3D scaffold to enhance lung regeneration and/or repair lung defects (Itoi et al., 2001; Neuringer and Randell, 2004; Andrade et al., 2007). As collagen is the main protein type in the lung ECM, it is thought to be a suitable candidate as a natural polymer scaffold for lung tissue engineering studies (Nakamura et al., 2000). In addition, 3D porous scaffolds share many similar characteristics with *in vivo* pulmonary alveoli (Sun et al., 2012).

Using a 3D porous sponge scaffold composed of lung ECM proteins (collagen/gelatine) would mimic the 3D microenvironment of lung tissue, and the pores would resemble *in vivo* alveoli.

This kind of scaffold may give more insight on cellular behaviours in the *in vivo* lung microenvironment.

Lung alveoli have a porous structure with an average pore size diameter of 200-300 µm. However, there are smaller pores between alveoli called Pores of Kohn, which creates a bigger range of pore sizes in the *in vivo* lung. As well as this range of pore sizes, alveoli also have an elastic structure in order to expand and contract, and have a Young's modulus of approx. 1-6 kPa (Asano et al., 2017; Bou Jawde et al., 2020; Liu and Tschumperlin, 2011; Polio et al., 2018). Stiffness is an important factor to consider as lung disease often affects tissue stiffness, with fibrosis increasing stiffness (15-100 kPa) and emphysema decreasing it, as well as lung tissue also increasing in stiffness with age (Asano et al., 2017). It is vital to use a scaffold or material which has a similar stiffness to the *in vivo* lung, commonly used research materials such as glass (50-90 GPa) or tissue culture plastic (1.8-3.1 GPa) have a high stiffness and are limited in their accuracy of mimicking lung tissue *in vivo*. Porous scaffolds such as Surgispon generally have a lower stiffness (3-10 kPa) and can function as a better mimic of the *in vivo* alveoli compared to standard lab ware (Buckley et al., 2008). However, the Young's modulus and mechanical stiffness of Surgispon was not measured during this project, it would be useful to do further work to determine Surgispon Young's modulus with more accuracy and to see how it varies between batches, as well as whether or not it changes after crosslinking or time submerged in solution.

6.1.4 Surgispon suitability as material

Surgispon is cheap, easy to obtain, commercially mass-produced and easy to handle during experimentation. The presence of pores that are similar in size to alveoli, the complex 3D shape, and a similar stiffness, all point to Surgispon as a potential candidate for a 3D cell

scaffold for lung tissue engineering studies. Surgispon pore size ranged from 50-400 µm (as seen in **Figs 3.4, 3.8**, and **3.15**) mimicking both standard alveoli and the intra-alveolar pores of Kohn. These pores were interconnected (see **Fig.3.16-17**), allowing for potential gas exchange throughout the whole scaffold as well as potential cell-cell interactions through adjacent pores.

However, Surgispon is composed of water-soluble dehydrated collagen (gelatine) and would not survive long-term in a cell culture environment or *in vivo*, untreated scaffolds disintegrated after three days in liquid at cell culture conditions (see **Figs3.5-6**). Through crosslinking with gluteraldehyde (GTA) vapour the structural integrity of Surgispon was maintained while in solution, and the scaffolds were stable in cell culture media over the long term (>60 days, see **Fig.3.13**), regardless of serum content. Scaffolds also demonstrated their viscoelasticity by expanding when incubated in liquid, and contracting when dried (see **Fig.3.14**). This indicates that under mechanical stresses in the *in vivo* lung, Surgispon could potentially survive and expand/contract. Surgispon also changed weight depending on the presence of serum in the incubated liquid (see **Fig.3.12**), indicating that serum proteins may adsorb to Surgispon scaffolds, presenting a more favourable microenvironment for cell culture as it indicates that Surgispon may be able to take up native lung ECM proteins *in vivo*, increasing biocompatibility. In addition, despite the crosslinking with toxic GTA vapour, Surgispon did not exhibit any cytotoxicity due to an effective washing process, meaning that crosslinked Surgispon was suitable for cell culture. However, testing with liquid GTA did result in cytotoxic scaffolds (see **Fig.3.10**), so only vapour GTA was used throughout this project.

6.1.5 Lung cell line culture on Surgispon

Epithelial cells are the main cell type in the lung alveoli, and fibroblasts are the main cell type of lung connective tissue. In addition, epithelial cells showed greater proliferation in the presence of fibroblasts, as previously discussed in **Section 4.1**. Due to this, both epithelial and fibroblast cell lines were used with Surgispon in order to optimize cell seeding on the scaffold before moving onto more biologically-relevant primary cells. However, as both A549 epithelial and 35FLH fibroblasts are human in origin, they present ideal cell lines in order to test Surgispon as a mimic for the human alveoli microenvironment and potential testing of cell-based lung tissue engineering approaches towards COPD.

Both A549 and 35FLH cells were successfully cultured in 3D on Surgispon scaffolds, demonstrating attachment (**Fig.4.13**), metabolic activity (**Fig.4.15**) and proliferation on the 3D structure. In order to successfully assess cell proliferation and viability, the cell metabolic assay alamarBlue was used, after several optimisation steps. In combination with the dsDNA quantification assay PicoGreen, alamrBlue was used throughout the project in order to determine if cells were viable and proliferating on Surgispon scaffolds.

Chemical coatings were also tested in order to investigate their effect on cell attachment and proliferation. These coatings were made up of the lung connective tissue/ECM proteins collagen and/or fibronectin. However, as Surgispon itself is made up of gelatine, it was already a suitable platform for cell culture, meaning that a chemical coating was not required for effective cell culture, and experiments with coated and uncoated scaffolds resulted in no significant differences (**Figs 4.16** and **4.20**). These results all indicate that Surgispon is suitable for use as a cell scaffold due to successfully cell culture and ease of use, both for *in vitro* and *in vivo* work.

However, one drawback of Surgispon in scientific research is that collagen/gelatine are autofluorescent, producing signal across most wavelengths of visible light as fluorescence (**Fig.4.17**). This makes it challenging to image these scaffolds with fluorescence, such as when using fluorescent labels DAPI, LIVE/DEAD assays, or secondary antibodies. Fluorescent signals from these labels have to compete with background autofluorescence, meaning that the effectiveness of standard imaging is decreased. Decreasing the effect of autofluorescence would improve Surgispon as a scaffold as it would be easier to image the 3D structure, some methods include using an intense light source (such as a laser) to bleach the fluorescence or using an imaging wavelength outside of the autofluorescence range (such as infrared).

While A549 and 35FLH were both successfully cultured separately as single cell types on Surgispon scaffolds, it was more biologically relevant to co-culture these cells when attempting to create a microenvironment similar to that of the alveoli, where both cell types are found in close proximity and make up the alveolar structure. Surgispon was also suitable for co-culture of A549 and deactivated 35FLH (**Fig.4.26**), further increasing the accuracy of this scaffold as an *in vivo* mimic of a basic alveoli. 35FLH cells were deactivated for co-culture with A549 for a number of reasons: firstly, these fibroblasts could still produce ECM proteins when deactivated which coats Surgispon in preparation for A549 cells to grow on; secondly, fibroblasts make up a small portion of the alveoli, without deactivation these cells would proliferate and grow to unrealistic numbers on the scaffold; lastly, excessive fibroblast proliferation *in vivo* is a causative factor in fibrosis, and would create a pathological model rather than a physiological model (McAnulty 2007; Wang *et al*. 2018). For these reasons, 35FLH cells were deactivated for co-culture with A549 cells on Surgispon.

A549 cells grown on Surgispon had a tendency to grow around the perimeter of pores (**Figs.4.13, 4.18**, **4.21**), this mimics the alveolar structure *in vivo*, where a thin wall surrounds an air space, meaning that Surgispon has the potential to culture compact groups of cells located around pores, which would be a more effective transplant than suspended cells or cell monolayers. This shows the further potential of Surgispon as a transplant material or for use with *ex vivo* lung materials, as well as for pre-clinical study of cell-cell or cell-ECM interactions across multiple cell types in a 3D microenvironment.

6.1.6 Primary lung cell culture on Surgispon

Advancing in biological complexity from cell lines to primary lung cells was a natural next step. Rodent models would not have been suitable as a comparison to humans due to their different lobe division and far faster respiratory rate. Pigs presented a more accurate model due to their similar lung size, lung anatomy and incidence of lung disease to humans. Porcine lung epithelial cells (PLECs) and porcine lung fibroblasts (PLFs) were obtained and also used to test Surgispon as a candidate scaffold material for a more clinically-relevant cell type.

Both PLECs and PLFs attached (**Figs.5.4**, **5.6**) metabolised (**Figs.5.3, 5.5**) and proliferated on Surgispon scaffolds, similarly to previous cell line experiments. This shows that Surgispon can culture both immortalized cell lines and lung primary cells, with the latter being directly obtained from a lung structure. This further reinforces the idea that Surgispon can function as a scaffold *in vivo*, as they successfully cultured *ex vivo* primary cells.

In addition to passive proliferation, PLECs were differentiated on Surgispon scaffolds (**Fig.5.14-5.15**), indicating more cellular *in vivo* processes that can be performed on a porous 3D scaffold *in vitro*. PLECs were shown to have populations of p63-positive stem/progenitor cells, meaning they could potentially be characterised as distal airway stem cells. When

differentiated, populations of PLECs stained positive for mucin 5AC, indicating differentiation into ciliated cells, as this population was not present when cultured under normal conditons in 2D. However, these results were only determined with antibody staining, further characterisation is necessary to investigate PLEC differentiation on Surgispon, including protein/gene expression analysis (Western blot, flow cytometry) and functional assays (do the mucin 5AC-positive cells have cilia, are the other cells functional).

PLEC differentiation via spheroid culture resulted in the formation of spheroids/organoids. This is something that has been observed in previous studies, where basal cells and pneumocyte type II cells have self-organised into organoid structures (Barkauskas et. al., 2017). The fact that PLECs also self-organised into organoid structures on Surgispon suggests that they may contain a population of basal progenitor cells. These basal cells are important as they have been shown to function as stem cells for lung regeneration/repair (Rawlins et. al., 2007). With Surgispon supporting some degree of cell differentiation, it has a potential role as a vehicle for differentiated cells that have a role in lung regeneration, which is lacking in the lung tissue of COPD patients.

The differentiation protocol should be investigated, as both Matrigel and Pneumacult-ALI media were used with Surgispon to initiate differentiation, but it is unclear which one (or both) contributes to the differentiation process, and if it would occur with just one of these factors. The organoids were mainly observed with brightfield and fluorescence microscopy and would benefit from further analysis, especially if they can be extracted from the scaffold and sliced, in order to perform histology and cross-sectional staining to characterise the morphology and cell types. Determining any changes from PLECs to spheroids would be

beneficial, as well as culturing spheroids over the long term and checking for functional changes.

In order to test Surgispon as a vehicle for cells to rescue areas of damaged lung tissue, migration of cells to and from Surgispon was tested in combination with decellularised lung tissue. Areas affected by emphysema in COPD are destroyed and contain few to no cells, meaning that a decellularised lung environment is also a mimic of a pathological environment. A better mimic would be a sample with no ECM, featuring a hole in an alveoli with a surrounding 3D microenvironment containing cells. Holes in alveoli caused by emphysema could be potentially rescued by Surgispon in one of two ways. Surgispon could be cultured with biologically-relevant cells and then used as a vehicle to deliver these cells directly to the damaged site, with the cells migrating from the scaffold to the damaged and surrounding tissue, potentially initiating repair, plugging the hole or fusing the Surgispon to the tissue. The other option is that empty Surgispon scaffolds could be implanted onto the damaged site, encouraging surrounding cells to migrate to the scaffold and potentially fuse the Surgispon to the tissue or begin to plug the hole. However, there were limitations to the migration experiments, with little migration observed for fibroblast cells and from tissue to scaffold. Further work is still needed to increase fibroblast migration and obtain a greater degree of migration overall but there is still evidence for the possibility of using Surgispon as a platform for migration *in vivo*.

Regardless of method, if Surgispon can be localized to the damaged area and partially or fully fill in the hole or repair damaged sites, it would be beneficial to the lung tissue, as the hole results in trapped air in the alveoli, which damages the surrounding structure more due to the disruption to normal ventilation. Surrounding cells are also inflamed, meaning the

damage is widespread. A limitation is the lack of a clinically-accurate disease model, in the absence of alveolar-like structures containing holes and adjacent inflamed tissue, the alternative was decellularised lung tissue, which contains the microstructures and ECM organization of the lung while containing no functional cells. A permit to obtain COPD-affected lung tissue was applied for during this project, but ethical and Health Research Authority approval was not obtained within the timeframe of this project.

As mentioned earlier there were two experimental methodologies that were investigated: either Surgispon scaffolds containing cultured cells (cell lines or primary cells) were implanted on decellularised porcine lung tissue; or empty Surgispon scaffolds were implanted on recellularised (cell lines or primary cells) porcine lung tissue. The aim of the former was to investigate cell migration from scaffold to tissue (**Figs 5.19-5.28**), and the aim of the latter was to investigate cell migration from tissue to scaffold (**Figs 5.29-5.38**). There was significantly more migration seen from epithelial A549 and PLECs in both directions when compared to fibroblast 35FL and PLFs (**Fig.5.39**). There may be a number of reasons for the decreased fibroblast migration, such as fibroblasts attaching with greater strength to substrates, and producing ECM proteins that further increase their attachment strength. These cells also have a larger surface area for attachment when compared to epithelial cells (Nothdurft et al., 2015). Any number of these reasons may have decreased their ability to detach and migrate to the adjacent substrate.

These migration experiments were limited and could be improved, as migration is an important aspect that requires further study. Firstly, scaffolds and tissue were only analysed after 7 days, and this only gives one time point of data, it would be more relevant to track cell migration over time using time lapse imaging, and to observe cell activity over a longer period

of time, such as 21 days, in order to see how the cells attach and proliferate, and if there are changes in morphology or functionality. In addition, the scaffold and tissue should be separated after a certain time (7, 14 or 21 days) to see how the migrated cells react and if they can remain viable over the long term. While human tissue was applied for during this project, I also recognise that one way to make this migration experiment more comprehensive would be to use human tissue, especially emphysematous COPD tissue with existing damage so the scaffolds can be applied directly to the damage site. Finally, simply tracking cells with microscopy isn't sufficient, and the gene/protein expression of cells should also be determined, both before and after migration and culture.

Migration from Surgispon to decellularised tissue demonstrates the potential of Surgispon as a vehicle for cells to localise to a damaged site within the lung, and as an experimental methodology for cell-based lung repair/regeneration therapies. However, different cell seeding densities should be explored, as the current methodology using 30,000 cells may not be sufficient to elicit change in the tissue after migration, ideally this should be repeated with 100,000 and 500,000 cells as these preliminary experiments indicate the need for future work.

Migration from recellularised tissue into empty Surgispon scaffolds indicates that may be able to attract cells from adjacent tissues and be used as a focusing point for cells onto areas of damaged tissue for potential self-repair, this is an avenue of research worth exploring due to COPD-affected lungs having limited self-repair due to damaged and missing ECM (Castaldi et al. 2014), meaning that any contribution Surgispon may be able to make to the repair process would be valuable. But as described in previous paragraphs, these migration experiments

require further and more comprehensive study, as understanding cell migration and repair mechanisms can help accelerate research into lung disease.

6.2 Limitations

6.2.1 Surgispon Properties

There were a number of limiting factors concerning Surgispon as a material. Firstly, the use of glutaraldehyde (GTA) as a crosslinking agent for Surgispon was a necessary choice, but GTA is toxic both to cells and researchers and alternative crosslinking methods may reduce risk in experimentation. GTA use was still tolerated due to the effectiveness of GTA vapour as a crosslinking agent on the mechanical properties of Surgispon. Other options for crosslinking include UV and gamma radiation, while we had access to UV there was no access to gamma rays. Surgispon is already UV-crosslinked and UV-sterilised by the manufacturer Aegis Lifesciences, and in the native state is not suitable as it dissolves in solution. Further options included genipin (GP, a planet-derived substance that crosslinks in a similar manner to GTA but stains scaffolds a dark blue pigment), 1-ethyl-3-(3-dimethyl aminopropyl) carbodiimide (EDC, free carboxylic and amine groups react to form amide bonds), and microbial transglutaminase (mTG, an enzyme that catalyses acyl transfer reactions and links glutamine and lysine residues) (Yang et al., 2018), but overall GTA was chosen due to its previous use in our lab, widespread use in the literature, cost effectiveness, and effective crosslinking that allows scaffolds to maintain their integrity in solution over the long term.

Of Surgispon itself, further mechanical testing is required, to determine stiffness and Young's modulus (in order to compare this to native lung and decellularised tissues), shear strength and ability for repeated compression/expansion cycles, if this is to be used with alveoli it

should match these tissues as closely as possible, or at least be suitable for culturing cells from these tissues, as stiffness alone is an important metric for cell growth (Liu et al., 2010; Melo et al., 2014). Changes in mechanical properties could also be tracked throughout major stages of this project, including crosslinking, incubation in solution, cell culture, and when fused with decellularised tissues.

Concerning Surgispon porosity, pore interconnectivity needs further study, particularly to determine gas permeability through a layer of Surgispon (Kasai et al. 2016) and to see if there is variation in permeability, as this is linked to pore size (Han et al., 2020). Pore size should be investigated further with advanced imaging applications, especially scanning electron microscopy (SEM), measuring pore size, area, morphology and distribution, both across a 2D plane and throughout a 3D volume. Again, it would be beneficial to track these results with different stages of Surgispon treatment, namely crosslinking and incubation in solution, as well as determining if there is a preference for certain pore sizes when culturing cell lines/primary cells. Slicing of Surgispon was attempted in order to obtain this 3D image data, but scaffolds broke down before a slice could be obtained, whether using a microtome or wax embedding, and noting that pressure would likely depress the pores and decrease their size.

One of the main negative characteristics of Surgispon as a scaffold for lung tissue engineering studies was the autofluorescence (D et al., 2001). This autofluorescence was observed in blue, green and red channels with fluorescent microscopy, increasing image background and resulting in a lower signal-to-noise ratio when imaging fluorescently labelled cells. Techniques to reduce autofluorescence could be used as previously mentioned, including use of an intense light source (such as a laser) to bleach the fluorescence or using an imaging wavelength outside of the autofluorescence range (such as infrared). However these

techniques must not affect the ability of Surgispon to act as a scaffold for cell growth after treatment, so fixatives and irreversible procedures would not be useful. Other imaging modalities that avoided fluorescence could also be explored, including SEM and phase-contrast microscopy.

6.2.2 Cell culture with Surgispon and decellularised tissues

When using primary cells, porcine tissue was chosen due to the lack of healthy or diseased human tissue. Ideally, human primary lung cells, including human distal airway stem cells and populations of cells from human alveoli would be used for culture experiments, as these would create the most accurate *in vitro* model when the objective is to create an alveolar-like structure. Attempts were made to secure human lung tissue but the timeframe for approval was beyond the scope of this project.

Decellularised porcine lung tissue was also used for experimentation, this was done with thick 2D lung tissue slices. Chunks of porcine lung tissue with a more 3D structure would be more biologically relevant as the *in vivo* lung structure is a complex 3D space. However, decellularising a 3D chunk of tissue would be more time-consuming and challenging, as the detergent would have to reach the centre, potentially resulting in longer incubation times which risks damage to all ECM in the lung sample (van Steenberghe et al., 2018). In addition, observing migration through a 3D chunk of tissue would also be more challenging.

The effects of chemical coatings on stiffness and other mechanical properties of Surgispon and decellularised tissue should also be investigated, along with the effects on cell migration, as chemical coatings were only tested with regards to cell attachment, proliferation and viability.

In addition, the structure of Surgispon and the decellularised lung tissue ECM should both be tested using protein analysis methods such as SDS-PAGE or Western blotting, both to determine the chemical composition of these structures, as well as to see if fibroblast culture produces additional ECM materials, and in general how cell culture affects the chemical composition of these structures over the long term. It is necessary to ensure that there are no negative biological effects such as inflammation or reduced ECM production, especially if these scaffolds are to be used *in vivo*.

While Pneumacult-ALI media was used during the differentiation of PLECs, the protocol followed used Matrigel to establish sphere culture conditions. It is unclear whether or not the Pneuamcult-ALI media or the Matrigel were the chief factors in differentiation, this should be investigated in order to optimise PLEC differentiation. In addition, it is important to establish if Surgispon can support an air-liquid interface (ALI) for the development of a functional model. Airflow is very important for alveoli and the lung, airflow through Surgispon should be tested. During PLEC differentiation, Surgispon was half submerged in media to mimic an ALI, but it is unclear whether or not the cells were at the interface, as the bottom half were in media as usual but the top half were exposed to air with no media. The ALI protocol should be optimised so that cells are exposed to both air and liquid, in order to see if this affects PLEC differentiation and results in functional cells. Further functional airflow or gas exchange testing would also be useful, for example using a lung-similar bioreactor to generate an ALI and airflow.

A major limitation was the lack of analytical techniques used, as through the course of this project the main techniques were fluorescence imaging and antibody staining. Other

techniques should be used, such as gene/protein expression analysis (such as PCR, flow cytometry or Western blot), mechanical testing, time-lapse imaging,

6.3 Future Work

Potential future work for this project would essentially involve either humanising aspects of the model or increasing the complexity of the model, both in order to increase the clinical relevance and increase the accuracy of the Surgispon scaffold as an alveolar-like structure.

In terms of humanisation, human primary lung cells would be used, both from healthy and COPD-affected donors. Other aspects of cell culture such as media and Matrigel would need to be replaced with human protein substitutes in order to best humanise the model, but this would increase the cost and make the model less easy to access. Human lung tissue could also be used for decellularisation experiments.

In terms of complexity, aspects from the lung microenvironment could be incorporated into the Surgispon model, such as vascularisation (including endothelial cells in models, testing their attachment and ability to grow capillary-like structures and co-culture with lung-relevant cell types), gas exchange (including differentiated and functional pneumocyte type I in models), mechanical ventilation (using a bioreactor to put biologically-relevant stresses/pressures onto Surgispon scaffolds in order to imitate inspiration and expiration through compression and expansion) and the use of different functional alveolar cell types (further differentiating primary cells into functional populations of AT1s, mucus-producing goblet cells, surfactant-producing AT2s, and macrophages).

Other additional experiments to run include investigating the Surgispon structure alongside the decellularised tissue ECM, using both protein and gene analysis before and after cell

culture. The ECM is a vital component in this lung tissue engineering approach and it is important to analyse it using methods other than imaging. Mechanical studies should also be performed, looking at the mechanical properties of native Surgispon, as well as the mechanical effect of expansion and contraction as these are the conditions encountered *in vivo*.

In addition, long-term experiments could be performed to see the maximum limits of Surgispon *in vivo* or cell culture conditions, in order to see if vapour crosslinked Surgispon has a limit after which it will begin to dissolve into solution. This would be relevant for *in vivo* implantation of Surgispon in order to see if/when it disintegrates and what remains. *In vivo* animal work implanting Surgispon would allow for clinically-relevant data to be obtained, firstly implanting either empty or cell-seeded Surgispon under the skin to check for an immune response, then moving to the lungs of health and diseased models and tracking the effects over the long term. Migration *in vivo* should also be assessed, investigating Surgispon *in vivo* as a vehicle for cells/growth factors or as a physical aid for punctured alveoli in emphysema. Does Surgispon dissolve or is it accepted by the tissue, and what are the effects on this part of the tissue? Cells that migrate to or from the Surgispon should also be investigated.

6.4 Potential Clinical Applications

Surgispon shows promise for a role in research of lung physiology and pathology, acting as a possible model for alveoli, accelerating pre-clinical work towards cell therapies and treatments for various lung diseases, including asthma and COPD. However, Surgispon also has potential clinical applications, namely when applied directly to diseased COPD lung tissue *in vivo.*

One role for Surgispon is as a vehicle for cell therapies, relevant lung cells can be cultured on a Surgispon scaffold as a tissue engineering approach towards COPD, and the whole scaffold can be implanted onto a disease site, such as emphysematous tissue or inflamed areas. These cells may then migrate to the implant site and reduce the local symptoms, potentially repairing damage to the tissue. The alternate role is for Surgispon to attract cells to itself *in vivo*: by implanting just Surgispon (with no cells) to a disease site, it may promote cell growth and migration at the damaged site. Surgispon presents a structured matrix for cell growth, is composed of a suitable material (gelatine) and contains alveolar-scale pores for cell attachment and growth. The presence of Surgispon scaffolds at damaged sites in the lung may promote healing via encouraging cell growth and attracting biochemical factors.

However, there are many steps to go and this project presents early work in presenting Surgispon at a pre-clinical and clinical level.

6.5 Final Conclusion/Summary

Lung disease is the third highest cause of death worldwide, and the second highest cause of readmission to hospitals in the UK. This causes major social and financial burdens on healthcare and the NHS, meaning that research into lung diseases such as COPD is a necessity. We demonstrated here that the porous gelatine sponge Surgispon is cheap and easy to obtain, yet has the potential to be a powerful experimental platform into studying lung microstructure and potential cell-based therapies towards COPD and other lung diseases. While Surgispon is mainly used as a haemostatic sponge for clinical use, we demonstrate that it has applications in research and lung tissue engineering. Surgispon has been made available as a 3D scaffold for culture of many types of lung cell, whether immortalized or primary, and has showed potential for differentiation, migration and interactions with lung tissue. Further

research into Surgispon as a scaffold for cell-based therapies into lung disease is recommended. By accelerating research into these diseases, cell-based therapies are a prospective therapy or cure for the millions of people affected by lung diseases worldwide.

References

Aaron, S.D., 2014. Management and prevention of exacerbations of COPD. BMJ 349. https://doi.org/10.1136/bmj.g5237

Abel, G.A., Penson, R.T., Joffe, S., Schapira, L., Chabner, B.A., Lynch, T.J., 2006. Direct-to-consumer advertising in oncology. The Oncologist 11, 217–226. https://doi.org/10.1634/theoncologist.11-2-217

Ahmed, E.M., 2015. Hydrogel: Preparation, characterization, and applications: A review. J. Adv. Res. 6, 105–121. https://doi.org/10.1016/j.jare.2013.07.006

Albers, S., Thiebes, A.L., Gessenich, K.L., Jockenhoevel, S., Cornelissen, C.G., 2016. Differentiation of respiratory epithelium in a 3-dimensional co-culture with fibroblasts embedded in fibrin gel. Multidiscip. Respir. Med. 11, 6. https://doi.org/10.1186/s40248-016-0046-3

Albert, R.K., Connett, J., Bailey, W.C., Casaburi, R., Cooper, J.A.D., Criner, G.J., Curtis, J.L., Dransfield, M.T., Han, M.K., Lazarus, S.C., Make, B., Marchetti, N., Martinez, F.J., Madinger, N.E., McEvoy, C., Niewoehner, D.E., Porsasz, J., Price, C.S., Reilly, J., Scanlon, P.D., Sciurba, F.C., Scharf, S.M., Washko, G.R., Woodruff, P.G., Anthonisen, N.R., 2011. Azithromycin for Prevention of Exacerbations of COPD. N. Engl. J. Med. 365, 689–698. https://doi.org/10.1056/NEJMoa1104623

Allard, B., Panariti, A., Martin, J.G., 2018. Alveolar Macrophages in the Resolution of Inflammation, Tissue Repair, and Tolerance to Infection. Front. Immunol. 9. https://doi.org/10.3389/fimmu.2018.01777

Almadhoun, K., Sharma, S., 2020. Bronchodilators, in: StatPearls. StatPearls Publishing, Treasure Island (FL).

Al-Nasiry, S., Geusens, N., Hanssens, M., Luyten, C., Pijnenborg, R., 2007. The use of Alamar Blue assay for quantitative analysis of viability, migration and invasion of choriocarcinoma cells. Hum. Reprod. 22, 1304–1309. https://doi.org/10.1093/humrep/dem011

Andersson, C.K., Bergqvist, A., Mori, M., Mauad, T., Bjermer, L., Erjefält, J.S., 2011. Mast cell–associated alveolar inflammation in patients with atopic uncontrolled asthma. J. Allergy Clin. Immunol. 127, 905-912.e7. https://doi.org/10.1016/j.jaci.2011.01.022

Andersson, C.K., Mori, M., Bjermer, L., Löfdahl, C.-G., Erjefält, J.S., 2009. Novel site-specific mast cell subpopulations in the human lung. Thorax 64, 297–305. https://doi.org/10.1136/thx.2008.101683

Andrade, C.F., Wong, A.P., Waddell, T.K., Keshavjee, S., Liu, M., 2007a. Cell-based tissue engineering for lung regeneration. Am. J. Physiol. Lung Cell. Mol. Physiol. 292, L510-518. https://doi.org/10.1152/ajplung.00175.2006

Andrade, C.F., Wong, A.P., Waddell, T.K., Keshavjee, S., Liu, M., 2007b. Cell-based tissue engineering for lung regeneration. Am. J. Physiol.-Lung Cell. Mol. Physiol. 292, L510–L518. https://doi.org/10.1152/ajplung.00175.2006

Anser Medical - SURGISPON gelatin sponge [WWW Document], n.d. URL https://www.ansermedical.com/products/surgispon-gelatin-sponge/ (accessed 2.16.21).

Asano, S., Ito, S., Takahashi, K., Furuya, K., Kondo, M., Sokabe, M., Hasegawa, Y., 2017. Matrix stiffness regulates migration of human lung fibroblasts. Physiol. Rep. 5. https://doi.org/10.14814/phy2.13281

Bakhshandeh, B., Zarrintaj, P., Oftadeh, M.O., Keramati, F., Fouladiha, H., Sohrabi-jahromi, S., Ziraksaz, Z., 2017. Tissue engineering; strategies, tissues, and biomaterials. Biotechnol. Genet. Eng. Rev. 33, 144–172. https://doi.org/10.1080/02648725.2018.1430464

Balestrini, J.L., Niklason, L.E., 2015. Extracellular matrix as a driver for lung regeneration. Ann. Biomed. Eng. 43, 568–576. https://doi.org/10.1007/s10439-014-1167-5

Ballarin, A., Bazzan, E., Zenteno, R.H., Turato, G., Baraldo, S., Zanovello, D., Mutti, E., Hogg, J.C., Saetta, M., Cosio, M.G., 2012. Mast cell infiltration discriminates between histopathological phenotypes of chronic obstructive pulmonary disease. Am. J. Respir. Crit. Care Med. 186, 233–239. https://doi.org/10.1164/rccm.201112-2142OC

Barkauskas, C.E., Chung, M.-I., Fioret, B., Gao, X., Katsura, H., Hogan, B.L.M., 2017. Lung organoids: current uses and future promise. Development 144, 986–997. https://doi.org/10.1242/dev.140103

Barnes, P.J., 2019. Inflammatory endotypes in COPD. Allergy 74, 1249–1256. https://doi.org/10.1111/all.13760
Barnes, P.J., 2017. Cellular and molecular mechanisms of asthma and COPD. Clin. Sci. Lond. Engl. 1979 131, 1541–1558. https://doi.org/10.1042/CS20160487
Barnes, P.J., 2016. Inflammatory mechanisms in patients with chronic obstructive pulmonary disease. J. Allergy Clin. Immunol. 138, 16–27. https://doi.org/10.1016/j.jaci.2016.05.011
Barnes, P.J., 2008. Immunology of asthma and chronic obstructive pulmonary disease. Nat. Rev. Immunol. 8, 183–192. https://doi.org/10.1038/nri2254
Beers, M.F., Moodley, Y., 2017. When Is an Alveolar Type 2 Cell an Alveolar Type 2 Cell? A Conundrum for Lung Stem Cell Biology and Regenerative Medicine. Am. J. Respir. Cell Mol. Biol. 57, 18–27. https://doi.org/10.1165/rcmb.2016-0426PS
Belgrave, D.C.M., Simpson, A., Buchan, I.E., Custovic, A., 2015. Atopic Dermatitis and Respiratory Allergy: What is the Link. Curr. Dermatol. Rep. 4, 221–227. https://doi.org/10.1007/s13671-015-0121-6
Berne & Levy Physiology - 7th Edition [WWW Document], n.d. URL https://www.elsevier.com/books/berne-and-levy-physiology/koeppen/978-0-323-39394-2 (accessed 2.20.21).
Berns, E.J., Sur, S., Pan, L., Goldberger, J.E., Suresh, S., Zhang, S., Kessler, J.A., Stupp, S.I., 2014. Aligned neurite outgrowth and directed cell migration in self-assembled monodomain gels. Biomaterials 35, 185–195. https://doi.org/10.1016/j.biomaterials.2013.09.077
Bhatia, V.K., 2010. Interdiscursivity in professional communication: Discourse Commun. https://doi.org/10.1177/1750481309351208
Bizzintino, J., Lee, W.-M., Laing, I., Vang, F., Pappas, T., Zhang, G., Martin, A., Geelhoed, G., McMinn, P., Goldblatt, J., Gern, J., Le Souëf, P., 2011. Association between human rhinovirus C and severity of acute asthma in children. Eur. Respir. J. Off. J. Eur. Soc. Clin. Respir. Physiol. 37, 1037–1042. https://doi.org/10.1183/09031936.00092410
Bonnans, C., Chou, J., Werb, Z., 2014. Remodelling the extracellular matrix in development and disease. Nat. Rev. Mol. Cell Biol. 15, 786–801. https://doi.org/10.1038/nrm3904
Borra, R.C., Lotufo, M.A., Gagioti, S.M., Barros, F. de M., Andrade, P.M., 2009. A simple method to measure cell viability in proliferation and cytotoxicity assays. Braz. Oral Res. 23, 255–262. https://doi.org/10.1590/S1806-83242009000300006
Bou Jawde, S., Takahashi, A., Bates, J.H.T., Suki, B., 2020. An Analytical Model for Estimating Alveolar Wall Elastic Moduli From Lung Tissue Uniaxial Stress-Strain Curves. Front. Physiol. 11. https://doi.org/10.3389/fphys.2020.00121
Brand-Saberi, B.E.M., Schäfer, T., 2014. Trachea: Anatomy and Physiology. Thorac. Surg. Clin., Tracheal Surgery 24, 1–5. https://doi.org/10.1016/j.thorsurg.2013.09.004
Breeze, R.G., Wheeldon, E.B., 1977. The Cells of the Pulmonary Airways. Am. Rev. Respir. Dis. 116, 705–777. https://doi.org/10.1164/arrd.1977.116.4.705
Brill, S.E., Wedzicha, J.A., 2014. Oxygen therapy in acute exacerbations of chronic obstructive pulmonary disease. Int. J. Chron. Obstruct. Pulmon. Dis. 9, 1241–1252. https://doi.org/10.2147/COPD.S41476
Bronchial Anatomy: Overview, Gross Anatomy, Microscopic Anatomy [WWW Document], n.d. URL http://reference.medscape.com/article/1898852-overview#aw2aab6b3. (accessed 7.1.17).
Brown, B.N., Badylak, S.F., 2014. Extracellular matrix as an inductive scaffold for functional tissue reconstruction. Transl. Res. J. Lab. Clin. Med. 163, 268–285. https://doi.org/10.1016/j.trsl.2013.11.003
Brusselle, G.G., Joos, G.F., Bracke, K.R., 2011. New insights into the immunology of chronic obstructive pulmonary disease. Lancet Lond. Engl. 378, 1015–1026. https://doi.org/10.1016/S0140-6736(11)60988-4

Bružauskaitė, I., Bironaitė, D., Bagdonas, E., Bernotienė, E., 2016. Scaffolds and cells for tissue regeneration: different scaffold pore sizes—different cell effects. Cytotechnology 68, 355–369. https://doi.org/10.1007/s10616-015-9895-4

Burgel, P.-R., Nadel, J.A., 2004. Roles of epidermal growth factor receptor activation in epithelial cell repair and mucin production in airway epithelium. Thorax 59, 992–996. https://doi.org/10.1136/thx.2003.018879

Burgstaller, G., Oehrle, B., Gerckens, M., White, E.S., Schiller, H.B., Eickelberg, O., 2017. The instructive extracellular matrix of the lung: basic composition and alterations in chronic lung disease. Eur. Respir. J. 50. https://doi.org/10.1183/13993003.01805-2016

Burkhardt, R., Pankow, W., 2014. The Diagnosis of Chronic Obstructive Pulmonary Disease. Dtsch. Ärztebl. Int. 111, 834–846. https://doi.org/10.3238/arztebl.2014.0834

Burki, T.K., 2017. The economic cost of respiratory disease in the UK. Lancet Respir. Med. 5, 381. https://doi.org/10.1016/S2213-2600(17)30108-X

Burney, P.G.J., Patel, J., Newson, R., Minelli, C., Naghavi, M., 2015. Global and regional trends in COPD mortality, 1990–2010. Eur. Respir. J. 45, 1239–1247. https://doi.org/10.1183/09031936.00142414

Bustamante-Marin, X.M., Ostrowski, L.E., 2017. Cilia and Mucociliary Clearance. Cold Spring Harb. Perspect. Biol. 9. https://doi.org/10.1101/cshperspect.a028241

Byrne, A.J., Mathie, S.A., Gregory, L.G., Lloyd, C.M., 2015. Pulmonary macrophages: key players in the innate defence of the airways. Thorax 70, 1189–1196. https://doi.org/10.1136/thoraxjnl-2015-207020

Calle, E.A., Ghaedi, M., Sundaram, S., Sivarapatna, A., Tseng, M.K., Niklason, L.E., 2014. Strategies for Whole Lung Tissue Engineering. IEEE Trans. Biomed. Eng. 61, 1482–1496. https://doi.org/10.1109/TBME.2014.2314261

Calverley, P.M.A., Lee, A., Towse, L., van Noord, J., Witek, T.J., Kelsen, S., 2003. Effect of tiotropium bromide on circadian variation in airflow limitation in chronic obstructive pulmonary disease. Thorax 58, 855–860. https://doi.org/10.1136/thorax.58.10.855

Cao, X., Coyle, J.P., Xiong, R., Wang, Y., Heflich, R.H., Ren, B., Gwinn, W.M., Hayden, P., Rojanasakul, L., 2020. Invited review: human air-liquid-interface organotypic airway tissue models derived from primary tracheobronchial epithelial cells—overview and perspectives. In Vitro Cell. Dev. Biol. Anim. 1–29. https://doi.org/10.1007/s11626-020-00517-7

Carletti, E., Motta, A., Migliaresi, C., 2011. Scaffolds for tissue engineering and 3D cell culture. Methods Mol. Biol. Clifton NJ 695, 17–39. https://doi.org/10.1007/978-1-60761-984-0_2

Carreto-Binaghi, L.E., Aliouat, E.M., Taylor, M.L., 2016. Surfactant proteins, SP-A and SP-D, in respiratory fungal infections: their role in the inflammatory response. Respir. Res. 17, 66. https://doi.org/10.1186/s12931-016-0385-9

Castaldi, P.J., Dy, J., Ross, J., Chang, Y., Washko, G.R., Curran-Everett, D., Williams, A., Lynch, D.A., Make, B.J., Crapo, J.D., Bowler, R.P., Regan, E.A., Hokanson, J.E., Kinney, G.L., Han, M.K., Soler, X., Ramsdell, J.W., Barr, R.G., Foreman, M., Beek, E. van, Casaburi, R., Criner, G.J., Lutz, S.M., Rennard, S.I., Santorico, S., Sciurba, F.C., DeMeo, D.L., Hersh, C.P., Silverman, E.K., Cho, M.H., 2014. Cluster analysis in the COPDGene study identifies subtypes of smokers with distinct patterns of airway disease and emphysema. Thorax 69, 416–423. https://doi.org/10.1136/thoraxjnl-2013-203601

Cazzola, M., Donner, C.F., Hanania, N.A., 2007. One hundred years of chronic obstructive pulmonary disease (COPD). Respir. Med. 101, 1049–1065. https://doi.org/10.1016/j.rmed.2007.01.015

Central, P., 2012. Chronic obstructive pulmonary disease 2014 update (COPD Review). PulmCCM. URL http://pulmccm.org/main/2012/review-articles/chronic-obstructive-pulmonary-disease-2012-update-copd-review-lancet/ (accessed 7.12.17).

Chambers, D.C., Cherikh, W.S., Goldfarb, S.B., Hayes, D., Kucheryavaya, A.Y., Toll, A.E., Khush, K.K., Levvey, B.J., Meiser, B., Rossano, J.W., Stehlik, J., International Society for Heart and Lung Transplantation, 2018. The International Thoracic Organ Transplant Registry of the International Society for Heart and Lung Transplantation: Thirty-fifth adult lung and heart-lung transplant report-

2018; Focus theme: Multiorgan Transplantation. J. Heart Lung Transplant. Off. Publ. Int. Soc. Heart Transplant. 37, 1169–1183. https://doi.org/10.1016/j.healun.2018.07.020
Charalampidis, C., Youroukou, A., Lazaridis, G., Baka, S., Mpoukovinas, I., Karavasilis, V., Kioumis, I., Pitsiou, G., Papaiwannou, A., Karavergou, A., Tsakiridis, K., Katsikogiannis, N., Sarika, E., Kapanidis, K., Sakkas, L., Korantzis, I., Lampaki, S., Zarogoulidis, K., Zarogoulidis, P., 2015. Pleura space anatomy. J. Thorac. Dis. 7, S27-32. https://doi.org/10.3978/j.issn.2072-1439.2015.01.48
Charras, G., Sahai, E., 2014. Physical influences of the extracellular environment on cell migration. Nat. Rev. Mol. Cell Biol. 15, 813–824. https://doi.org/10.1038/nrm3897
Chaubey, A., Ross, K.J., Leadbetter, R.M., Burg, K.J.L., 2008. Surface patterning: Tool to modulate stem cell differentiation in an adipose system. J. Biomed. Mater. Res. B Appl. Biomater. 84B, 70–78. https://doi.org/10.1002/jbm.b.30846
Chen, P., Marsilio, E., Goldstein, R.H., Yannas, I.V., Spector, M., 2005a. Formation of lung alveolar-like structures in collagen-glycosaminoglycan scaffolds in vitro. Tissue Eng. 11, 1436–1448. https://doi.org/10.1089/ten.2005.11.1436
Chen, P., Marsilio, E., Goldstein, R.H., Yannas, I.V., Spector, M., 2005b. Formation of lung alveolar-like structures in collagen-glycosaminoglycan scaffolds in vitro. Tissue Eng. 11, 1436–1448. https://doi.org/10.1089/ten.2005.11.1436
Chen, Q., Liu, Y., 2020. Heterogeneous groups of alveolar type II cells in lung homeostasis and repair. Am. J. Physiol.-Cell Physiol. 319, C991–C996. https://doi.org/10.1152/ajpcell.00341.2020
Chen, Z.-H., Lam, H.C., Jin, Y., Kim, H.-P., Cao, J., Lee, S.-J., Ifedigbo, E., Parameswaran, H., Ryter, S.W., Choi, A.M.K., 2010. Autophagy protein microtubule-associated protein 1 light chain-3B (LC3B) activates extrinsic apoptosis during cigarette smoke-induced emphysema. Proc. Natl. Acad. Sci. U. S. A. 107, 18880–18885. https://doi.org/10.1073/pnas.1005574107
Cho, M.H., McDonald, M.-L.N., Zhou, X., Mattheisen, M., Castaldi, P.J., Hersh, C.P., Demeo, D.L., Sylvia, J.S., Ziniti, J., Laird, N.M., Lange, C., Litonjua, A.A., Sparrow, D., Casaburi, R., Barr, R.G., Regan, E.A., Make, B.J., Hokanson, J.E., Lutz, S., Dudenkov, T.M., Farzadegan, H., Hetmanski, J.B., Tal-Singer, R., Lomas, D.A., Bakke, P., Gulsvik, A., Crapo, J.D., Silverman, E.K., Beaty, T.H., NETT Genetics, ICGN, ECLIPSE and COPDGene Investigators, 2014. Risk loci for chronic obstructive pulmonary disease: a genome-wide association study and meta-analysis. Lancet Respir. Med. 2, 214–225. https://doi.org/10.1016/S2213-2600(14)70002-5
Clark, S.J., Zoumot, Z., Bamsey, O., Polkey, M.I., Dusmet, M., Lim, E., Jordan, S., Hopkinson, N.S., 2014. Surgical approaches for lung volume reduction in emphysema. Clin. Med. Lond. Engl. 14, 122–127. https://doi.org/10.7861/clinmedicine.14-2-122
Costa, C., Traves, S.L., Tudhope, S.J., Fenwick, P.S., Belchamber, K.B.R., Russell, R.E.K., Barnes, P.J., Donnelly, L.E., 2016. Enhanced monocyte migration to CXCR3 and CCR5 chemokines in COPD. Eur. Respir. J. 47, 1093–1102. https://doi.org/10.1183/13993003.01642-2015
Cranston, J.M., Crockett, A.J., Moss, J.R., Alpers, J.H., 2005. Domiciliary oxygen for chronic obstructive pulmonary disease. Cochrane Database Syst. Rev. CD001744. https://doi.org/10.1002/14651858.CD001744.pub2
Crupi, A., Costa, A., Tarnok, A., Melzer, S., Teodori, L., 2015. Inflammation in tissue engineering: The Janus between engraftment and rejection. Eur. J. Immunol. 45, 3222–3236. https://doi.org/10.1002/eji.201545818
D, Y., V, H., T, T., 2001. Photochemical effects and hypericin photosensitized processes in collagen. J. Biomed. Opt. 6, 52–57. https://doi.org/10.1117/1.1331559
Dale, T.P., Borg D'anastasi, E., Haris, M., Forsyth, N.R., 2019a. Rock Inhibitor Y-27632 Enables Feeder-Free, Unlimited Expansion of Sus scrofa domesticus Swine Airway Stem Cells to Facilitate Respiratory Research. Stem Cells Int. 2019, 3010656. https://doi.org/10.1155/2019/3010656
Dale, T.P., Borg D'anastasi, E., Haris, M., Forsyth, N.R., 2019b. Rock Inhibitor Y-27632 Enables Feeder-Free, Unlimited Expansion of Sus scrofa domesticus Swine Airway Stem Cells to Facilitate Respiratory Research. Stem Cells Int. 2019, 3010656. https://doi.org/10.1155/2019/3010656

Damous, L.L., Nakamuta, J.S., Saturi de Carvalho, A.E.T., Carvalho, K.C., Soares, J.M., Simões, M. de J., Krieger, J.E., Baracat, E.C., 2015. Scaffold-based delivery of adipose tissue-derived stem cells in rat frozen-thawed ovarian autografts: preliminary studies in a rat model. J. Assist. Reprod. Genet. 32, 1285–1294. https://doi.org/10.1007/s10815-015-0527-x

Dang-Tan, T., Zhang, S., Tavares, R.V., Stutz, M., Ismaila, A.S., Vaillancourt, J., Corriveau, D., Stanford, R.H., Lin, X., Nadeau, G.A., Simidchiev, A., Parsons, D., Sampalis, J.S., 2017. The Burden of Illness Related to Chronic Obstructive Pulmonary Disease Exacerbations in Québec, Canada. Can. Respir. J. 2017, 8184915. https://doi.org/10.1155/2017/8184915

De Grove, K.C., Provoost, S., Verhamme, F.M., Bracke, K.R., Joos, G.F., Maes, T., Brusselle, G.G., 2016. Characterization and Quantification of Innate Lymphoid Cell Subsets in Human Lung. PloS One 11, e0145961. https://doi.org/10.1371/journal.pone.0145961

Decramer, M., Janssens, W., Miravitlles, M., 2012. Chronic obstructive pulmonary disease. Lancet Lond. Engl. 379, 1341–1351. https://doi.org/10.1016/S0140-6736(11)60968-9

Delaere, P., Vranckx, J., Verleden, G., De Leyn, P., Van Raemdonck, D., Leuven Tracheal Transplant Group, 2010. Tracheal allotransplantation after withdrawal of immunosuppressive therapy. N. Engl. J. Med. 362, 138–145. https://doi.org/10.1056/NEJMoa0810653

DeQuach, J.A., Yuan, S.H., Goldstein, L.S.B., Christman, K.L., 2011. Decellularized porcine brain matrix for cell culture and tissue engineering scaffolds. Tissue Eng. Part A 17, 2583–2592. https://doi.org/10.1089/ten.TEA.2010.0724

Desai, T.J., Brownfield, D.G., Krasnow, M.A., 2014. Alveolar progenitor and stem cells in lung development, renewal and cancer. Nature 507, 190–194. https://doi.org/10.1038/nature12930

Dicpinigaitis, P.V., 2017. Effect of tobacco and electronic cigarette use on cough reflex sensitivity. Pulm. Pharmacol. Ther. 47, 45–48. https://doi.org/10.1016/j.pupt.2017.01.013

Elliott, M.J., De Coppi, P., Speggiorin, S., Roebuck, D., Butler, C.R., Samuel, E., Crowley, C., McLaren, C., Fierens, A., Vondrys, D., Cochrane, L., Jephson, C., Janes, S., Beaumont, N.J., Cogan, T., Bader, A., Seifalian, A.M., Hsuan, J.J., Lowdell, M.W., Birchall, M.A., 2012. Stem-cell-based, tissue engineered tracheal replacement in a child: a 2-year follow-up study. Lancet Lond. Engl. 380, 994–1000. https://doi.org/10.1016/S0140-6736(12)60737-5

Erjefält, J.S., 2014. Mast cells in human airways: the culprit? Eur. Respir. Rev. Off. J. Eur. Respir. Soc. 23, 299–307. https://doi.org/10.1183/09059180.00005014

Evans, K.V., Lee, J.-H., 2020. Alveolar wars: The rise of in vitro models to understand human lung alveolar maintenance, regeneration, and disease. Stem Cells Transl. Med. https://doi.org/10.1002/sctm.19-0433

Fahy, J.V., Dickey, B.F., 2010. Airway Mucus Function and Dysfunction. N. Engl. J. Med. 363, 2233–2247. https://doi.org/10.1056/NEJMra0910061

Falk, J.A., Minai, O.A., Mosenifar, Z., 2008. Inhaled and Systemic Corticosteroids in Chronic Obstructive Pulmonary Disease. Proc. Am. Thorac. Soc. 5, 506–512. https://doi.org/10.1513/pats.200707-096ET

Forey, B.A., Thornton, A.J., Lee, P.N., 2011. Systematic review with meta-analysis of the epidemiological evidence relating smoking to COPD, chronic bronchitis and emphysema. BMC Pulm. Med. 11, 36. https://doi.org/10.1186/1471-2466-11-36

Forsyth, N.R., Evans, A.P., Shay, J.W., Wright, W.E., 2003. Developmental differences in the immortalization of lung fibroblasts by telomerase. Aging Cell 2, 235–243. https://doi.org/10.1046/j.1474-9728.2003.00057.x

Forum of International Respiratory Societies, European Respiratory Society, 2017. The global impact of respiratory disease.

Freyman, T.M., Yannas, I.V., Gibson, L.J., 2001. Cellular materials as porous scaffolds for tissue engineering. Prog. Mater. Sci. 46, 273–282. https://doi.org/10.1016/S0079-6425(00)00018-9

Fuchs, S., Hollins, A.J., Laue, M., Schaefer, U.F., Roemer, K., Gumbleton, M., Lehr, C.-M., 2003. Differentiation of human alveolar epithelial cells in primary culture: morphological characterization and synthesis of caveolin-1 and surfactant protein-C. Cell Tissue Res. 311, 31–45. https://doi.org/10.1007/s00441-002-0653-5

Gagnon, P., Guenette, J.A., Langer, D., Laviolette, L., Mainguy, V., Maltais, F., Ribeiro, F., Saey, D., 2014. Pathogenesis of hyperinflation in chronic obstructive pulmonary disease. Int. J. Chron. Obstruct. Pulmon. Dis. 9, 187–201. https://doi.org/10.2147/COPD.S38934

GBD 2015 Mortality and Causes of Death Collaborators, 2016. Global, regional, and national life expectancy, all-cause mortality, and cause-specific mortality for 249 causes of death, 1980-2015: a systematic analysis for the Global Burden of Disease Study 2015. Lancet Lond. Engl. 388, 1459–1544. https://doi.org/10.1016/S0140-6736(16)31012-1

Gharib, S.A., Manicone, A.M., Parks, W.C., 2018. Matrix metalloproteinases in emphysema. Matrix Biol. J. Int. Soc. Matrix Biol. 73, 34–51. https://doi.org/10.1016/j.matbio.2018.01.018

Gilpin, S.E., Wagner, D.E., 2018. Acellular human lung scaffolds to model lung disease and tissue regeneration. Eur. Respir. Rev. Off. J. Eur. Respir. Soc. 27. https://doi.org/10.1183/16000617.0021-2018

Givi, M.E., Redegeld, F.A., Folkerts, G., Mortaz, E., 2012. Dendritic cells in pathogenesis of COPD. Curr. Pharm. Des. 18, 2329–2335. https://doi.org/10.2174/138161212800166068

Global Initiative for Asthma [WWW Document], n.d. . Glob. Initiat. Asthma - GINA. URL https://ginasthma.org/ (accessed 1.26.21).

Global Initiative for Chronic Obstructive Lung Disease [WWW Document], n.d. . Glob. Initiat. Chronic Obstr. Lung Dis. - GOLD. URL https://goldcopd.org/ (accessed 1.30.21).

Goldklang, M., Stockley, R., n.d. Pathophysiology of Emphysema and Implications. Chronic Obstr. Pulm. Dis. 3, 454–458. https://doi.org/10.15326/jcopdf.3.1.2015.0175

Gotts, J.E., Matthay, M.A., 2013. Cell Therapy for Lung Disease. Chest 143, 1525–1527. https://doi.org/10.1378/chest.12-2993

Grainge, C.L., Davies, D.E., 2013. Epithelial Injury and Repair in Airways Diseases. Chest 144, 1906–1912. https://doi.org/10.1378/chest.12-1944

Guilliams, M., De Kleer, I., Henri, S., Post, S., Vanhoutte, L., De Prijck, S., Deswarte, K., Malissen, B., Hammad, H., Lambrecht, B.N., 2013. Alveolar macrophages develop from fetal monocytes that differentiate into long-lived cells in the first week of life via GM-CSF. J. Exp. Med. 210, 1977–1992. https://doi.org/10.1084/jem.20131199

Hamid, R., Rotshteyn, Y., Rabadi, L., Parikh, R., Bullock, P., 2004. Comparison of alamar blue and MTT assays for high through-put screening. Toxicol. In Vitro 18, 703–710. https://doi.org/10.1016/j.tiv.2004.03.012

Hancock, D.B., Eijgelsheim, M., Wilk, J.B., Gharib, S.A., Loehr, L.R., Marciante, K.D., Franceschini, N., van Durme, Y.M.T.A., Chen, T.-H., Barr, R.G., Schabath, M.B., Couper, D.J., Brusselle, G.G., Psaty, B.M., van Duijn, C.M., Rotter, J.I., Uitterlinden, A.G., Hofman, A., Punjabi, N.M., Rivadeneira, F., Morrison, A.C., Enright, P.L., North, K.E., Heckbert, S.R., Lumley, T., Stricker, B.H.C., O'Connor, G.T., London, S.J., 2010. Meta-analyses of genome-wide association studies identify multiple loci associated with pulmonary function. Nat. Genet. 42, 45–52. https://doi.org/10.1038/ng.500

Harkema, J.R., Carey, S.A., Wagner, J.G., 2016. The Nose Revisited: A Brief Review of the Comparative Structure, Function, and Toxicologic Pathology of the Nasal Epithelium: Toxicol. Pathol. https://doi.org/10.1080/01926230600713475

Herbert, R.A., Janardhan, K.S., Pandiri, A.R., Cesta, M.F., Miller, R.A., 2018. Chapter 22 - Nose, Larynx, and Trachea, in: Suttie, A.W. (Ed.), Boorman's Pathology of the Rat (Second Edition). Academic Press, Boston, pp. 391–435. https://doi.org/10.1016/B978-0-12-391448-4.00022-8

Herbst, R.S., Heymach, J.V., Lippman, S.M., 2008. Lung Cancer. N. Engl. J. Med. 359, 1367–1380. https://doi.org/10.1056/NEJMra0802714

Herth, F.J.F., Slebos, D.-J., Criner, G.J., Shah, P.L., 2017. Endoscopic Lung Volume Reduction: An Expert Panel Recommendation - Update 2017. Respiration 94, 380–388. https://doi.org/10.1159/000479379

Herzog, W., Leonard, T.R., Joumaa, V., Mehta, A., 2008. Mysteries of muscle contraction. J. Appl. Biomech. 24, 1–13. https://doi.org/10.1123/jab.24.1.1

Hild, M., Jaffe, A.B., 2016. Production of 3-D Airway Organoids From Primary Human Airway Basal Cells and Their Use in High-Throughput Screening. Curr. Protoc. Stem Cell Biol. 37, IE.9.1-IE.9.15. https://doi.org/10.1002/cpsc.1

Hillebrandt, K.H., Everwien, H., Haep, N., Keshi, E., Pratschke, J., Sauer, I.M., 2019. Strategies based on organ decellularization and recellularization. Transpl. Int. 32, 571–585. https://doi.org/10.1111/tri.13462

Hinz, B., Phan, S.H., Thannickal, V.J., Galli, A., Bochaton-Piallat, M.-L., Gabbiani, G., 2007. The Myofibroblast: One Function, Multiple Origins. Am. J. Pathol. 170, 1807–1816. https://doi.org/10.2353/ajpath.2007.070112

Hirsch, F.R., Scagliotti, G.V., Mulshine, J.L., Kwon, R., Curran, W.J., Wu, Y.-L., Paz-Ares, L., 2017. Lung cancer: current therapies and new targeted treatments. The Lancet 389, 299–311. https://doi.org/10.1016/S0140-6736(16)30958-8

Hodge, S., Hodge, G., Scicchitano, R., Reynolds, P.N., Holmes, M., 2003. Alveolar macrophages from subjects with chronic obstructive pulmonary disease are deficient in their ability to phagocytose apoptotic airway epithelial cells. Immunol. Cell Biol. 81, 289–296. https://doi.org/10.1046/j.1440-1711.2003.t01-1-01170.x

Holgate, S.T., 2013. Mechanisms of Asthma and Implications for Its Prevention and Treatment: A Personal Journey. Allergy Asthma Immunol. Res. 5, 343–347. https://doi.org/10.4168/aair.2013.5.6.343

Hollenhorst, M.I., Richter, K., Fronius, M., 2011. Ion Transport by Pulmonary Epithelia [WWW Document]. J. Biomed. Biotechnol. https://doi.org/10.1155/2011/174306

Hoogendoorn, M., Feenstra, T.L., Hoogenveen, R.T., Al, M., Mölken, M.R., 2010. Association between lung function and exacerbation frequency in patients with COPD. Int. J. Chron. Obstruct. Pulmon. Dis. 5, 435–444. https://doi.org/10.2147/COPD.S13826

Horie, M., Saito, A., Mikami, Y., Ohshima, M., Morishita, Y., Nakajima, J., Kohyama, T., Nagase, T., 2012. Characterization of human lung cancer-associated fibroblasts in three-dimensional in vitro co-culture model. Biochem. Biophys. Res. Commun. 423, 158–163. https://doi.org/10.1016/j.bbrc.2012.05.104

Hsia, C.C.W., Hyde, D.M., Weibel, E.R., 2016. Lung Structure and the Intrinsic Challenges of Gas Exchange. Compr. Physiol. 6, 827–895. https://doi.org/10.1002/cphy.c150028

Hsu, K., Williamson, J.P., Peters, M.J., Ing, A.J., 2018. Endoscopic Lung Volume Reduction in COPD: Improvements in Gas Transfer Capacity Are Associated With Improvements in Ventilation and Perfusion Matching. J. Bronchol. Interv. Pulmonol. 25, 48–53. https://doi.org/10.1097/LBR.0000000000000445

Hu, G., Zhou, Y., Tian, J., Yao, W., Li, J., Li, B., Ran, P., 2010. Risk of COPD from exposure to biomass smoke: a metaanalysis. Chest 138, 20–31. https://doi.org/10.1378/chest.08-2114

Hussell, T., Bell, T.J., 2014. Alveolar macrophages: plasticity in a tissue-specific context. Nat. Rev. Immunol. 14, 81–93. https://doi.org/10.1038/nri3600

Hyde, D.M., Tyler, N.K., Putney, L.F., Singh, P., Gundersen, H.J.G., 2004. Total number and mean size of alveoli in mammalian lung estimated using fractionator sampling and unbiased estimates of the Euler characteristic of alveolar openings. Anat. Rec. A. Discov. Mol. Cell. Evol. Biol. 277A, 216–226. https://doi.org/10.1002/ar.a.20012

Ikeda, Y., Iwakiri, S., Yoshimori, T., 2009. Development and characterization of a novel host cell DNA assay using ultra-sensitive fluorescent nucleic acid stain “PicoGreen.” J. Pharm. Biomed. Anal. 49, 997–1002. https://doi.org/10.1016/j.jpba.2009.01.022

Ingenito, E.P., Sen, E., Tsai, L.W., Murthy, S., Hoffman, A., 2010. Design and testing of biological scaffolds for delivering reparative cells to target sites in the lung. J. Tissue Eng. Regen. Med. 4, 259–272. https://doi.org/10.1002/term.237

Innes, A.L., Carrington, S.D., Thornton, D.J., Kirkham, S., Rousseau, K., Dougherty, R.H., Raymond, W.W., Caughey, G.H., Muller, S.J., Fahy, J.V., 2009. Ex vivo sputum analysis reveals impairment of

protease-dependent mucus degradation by plasma proteins in acute asthma. Am. J. Respir. Crit. Care Med. 180, 203–210. https://doi.org/10.1164/rccm.200807-1056OC

Janahi, I., Rehman, A., Baloch, H.N.U.A., 2018. Corticosteroids and Their Use in Respiratory Disorders. pp. 47–96. https://doi.org/10.5772/intechopen.72147

Jasper, A.E., McIver, W.J., Sapey, E., Walton, G.M., 2019. Understanding the role of neutrophils in chronic inflammatory airway disease. F1000Research 8. https://doi.org/10.12688/f1000research.18411.1

Jiménez-Ruiz, C.A., Andreas, S., Lewis, K.E., Tonnesen, P., van Schayck, C.P., Hajek, P., Tonstad, S., Dautzenberg, B., Fletcher, M., Masefield, S., Powell, P., Hering, T., Nardini, S., Tonia, T., Gratziou, C., 2015. Statement on smoking cessation in COPD and other pulmonary diseases and in smokers with comorbidities who find it difficult to quit. Eur. Respir. J. 46, 61–79. https://doi.org/10.1183/09031936.00092614

Jungebluth, P., Alici, E., Baiguera, S., Blomberg, P., Bozóky, B., Crowley, C., Einarsson, O., Gudbjartsson, T., Le Guyader, S., Henriksson, G., Hermanson, O., Juto, J.E., Leidner, B., Lilja, T., Liska, J., Luedde, T., Lundin, V., Moll, G., Roderburg, C., Strömblad, S., Sutlu, T., Watz, E., Seifalian, A., Macchiarini, P., 2011. Tracheobronchial transplantation with a stem-cell-seeded bioartificial nanocomposite: a proof-of-concept study. Lancet Lond. Engl. 378, 1997–2004. https://doi.org/10.1016/S0140-6736(11)61715-7

Justice, B.A., Badr, N.A., Felder, R.A., 2009. 3D cell culture opens new dimensions in cell-based assays. Drug Discov. Today 14, 102–107. https://doi.org/10.1016/j.drudis.2008.11.006

Khalili, A.A., Ahmad, M.R., 2015. A Review of Cell Adhesion Studies for Biomedical and Biological Applications. Int. J. Mol. Sci. 16, 18149–18184. https://doi.org/10.3390/ijms160818149

Khoor, A., Gray, M.E., Singh, G., Stahlman, M.T., 1996. Ontogeny of Clara cell-specific protein and its mRNA: their association with neuroepithelial bodies in human fetal lung and in bronchopulmonary dysplasia. J. Histochem. Cytochem. Off. J. Histochem. Soc. 44, 1429–1438. https://doi.org/10.1177/44.12.8985135

Kim, V., Criner, G.J., 2013a. Chronic Bronchitis and Chronic Obstructive Pulmonary Disease. Am. J. Respir. Crit. Care Med. 187, 228–237. https://doi.org/10.1164/rccm.201210-1843CI

Kim, V., Criner, G.J., 2013b. Chronic Bronchitis and Chronic Obstructive Pulmonary Disease. Am. J. Respir. Crit. Care Med. 187, 228–237. https://doi.org/10.1164/rccm.201210-1843CI

Kim, V., Oros, M., Durra, H., Kelsen, S., Aksoy, M., Cornwell, W.D., Rogers, T.J., Criner, G.J., 2015. Chronic bronchitis and current smoking are associated with more goblet cells in moderate to severe COPD and smokers without airflow obstruction. PloS One 10, e0116108. https://doi.org/10.1371/journal.pone.0116108

Klein, S.G., Hennen, J., Serchi, T., Blömeke, B., Gutleb, A.C., 2011. Potential of coculture in vitro models to study inflammatory and sensitizing effects of particles on the lung. Toxicol. Vitro Int. J. Publ. Assoc. BIBRA 25, 1516–1534. https://doi.org/10.1016/j.tiv.2011.09.006

Kleinman, H.K., Luckenbill-Edds, L., Cannon, F.W., Sephel, G.C., 1987. Use of extracellular matrix components for cell culture. Anal. Biochem. 166, 1–13. https://doi.org/10.1016/0003-2697(87)90538-0

Knudsen, L., Ochs, M., 2018a. The micromechanics of lung alveoli: structure and function of surfactant and tissue components. Histochem. Cell Biol. 150, 661–676. https://doi.org/10.1007/s00418-018-1747-9

Knudsen, L., Ochs, M., 2018b. The micromechanics of lung alveoli: structure and function of surfactant and tissue components. Histochem. Cell Biol. 150, 661–676. https://doi.org/10.1007/s00418-018-1747-9

Knüppel, L., Heinzelmann, K., Lindner, M., Hatz, R., Behr, J., Eickelberg, O., Staab-Weijnitz, C.A., 2018. FK506-binding protein 10 (FKBP10) regulates lung fibroblast migration via collagen VI synthesis. Respir. Res. 19. https://doi.org/10.1186/s12931-018-0768-1

Ko, F.W.S., Hui, D.S.C., 2012. Air pollution and chronic obstructive pulmonary disease. Respirol. Carlton Vic 17, 395–401. https://doi.org/10.1111/j.1440-1843.2011.02112.x

Koblinski, J.E., Wu, M., Demeler, B., Jacob, K., Kleinman, H.K., 2005. Matrix cell adhesion activation by non-adhesion proteins. J. Cell Sci. 118, 2965–2974. https://doi.org/10.1242/jcs.02411

Kohansal, R., Martinez-Camblor, P., Agustí, A., Buist, A.S., Mannino, D.M., Soriano, J.B., 2009. The natural history of chronic airflow obstruction revisited: an analysis of the Framingham offspring cohort. Am. J. Respir. Crit. Care Med. 180, 3–10. https://doi.org/10.1164/rccm.200901-0047OC

Kotaru, C., Schoonover, K.J., Trudeau, J.B., Huynh, M.-L., Zhou, X., Hu, H., Wenzel, S.E., 2006. Regional fibroblast heterogeneity in the lung: implications for remodeling. Am. J. Respir. Crit. Care Med. 173, 1208–1215. https://doi.org/10.1164/rccm.200508-1218OC

Kotton, D.N., Morrisey, E.E., 2014. Lung regeneration: mechanisms, applications and emerging stem cell populations. Nat. Med. 20, 822–832. https://doi.org/10.1038/nm.3642

Kristin M. Hutchins, n.d. Effect of Chemical Crosslinking on Properties of Polymer Microbeads: A Review [WWW Document]. ResearchGate. http://dx.doi.org/10.13179/canchemtrans.2015.03.04.0245

Kruk, D.M.L.W., Heijink, I.H., Slebos, D.-J., Timens, W., ten Hacken, N.H., 2018. Mesenchymal Stromal Cells to Regenerate Emphysema: On the Horizon? Respiration 96, 148–158. https://doi.org/10.1159/000488149

Kubo, H., 2012. Tissue engineering for pulmonary diseases: Insights from the laboratory. Respirology 17, 445–454. https://doi.org/10.1111/j.1440-1843.2012.02145.x

Kumar, A., Anjum, F., 2020. Lung Transplantation, in: StatPearls. StatPearls Publishing, Treasure Island (FL).

Kummer, W., Lips, K.S., Pfeil, U., 2008. The epithelial cholinergic system of the airways. Histochem. Cell Biol. 130, 219–234. https://doi.org/10.1007/s00418-008-0455-2

Kurz, F.T., Kampf, T., Buschle, L.R., Schlemmer, H.-P., Heiland, S., Bendszus, M., Ziener, C.H., 2015. Microstructural Analysis of Peripheral Lung Tissue through CPMG Inter-Echo Time R2 Dispersion. PLoS ONE 10, e0141894. https://doi.org/10.1371/journal.pone.0141894

Lambrecht, B.N., Hammad, H., 2013. Asthma: the importance of dysregulated barrier immunity. Eur. J. Immunol. 43, 3125–3137. https://doi.org/10.1002/eji.201343730

Lang, M.R., Fiaux, G.W., Gillooly, M., Stewart, J.A., Hulmes, D.J., Lamb, D., 1994. Collagen content of alveolar wall tissue in emphysematous and non-emphysematous lungs. Thorax 49, 319–326. https://doi.org/10.1136/thx.49.4.319

Lee, D.F., Salguero, F.J., Grainger, D., Francis, R.J., MacLellan-Gibson, K., Chambers, M.A., 2018. Isolation and characterisation of alveolar type II pneumocytes from adult bovine lung. Sci. Rep. 8, 11927. https://doi.org/10.1038/s41598-018-30234-x

Li, C.-W., Wang, G.-J., 2012. 8 - MEMS manufacturing techniques for tissue scaffolding devices, in: Bhansali, S., Vasudev, A. (Eds.), MEMS for Biomedical Applications, Woodhead Publishing Series in Biomaterials. Woodhead Publishing, pp. 192–217. https://doi.org/10.1533/9780857096272.3.192

Ling, T.-Y., Liu, Y.-L., Huang, Y.-K., Gu, S.-Y., Chen, H.-K., Ho, C.-C., Tsao, P.-N., Tung, Y.-C., Chen, H.-W., Cheng, C.-H., Lin, K.-H., Lin, F.-H., 2014. Differentiation of lung stem/progenitor cells into alveolar pneumocytes and induction of angiogenesis within a 3D gelatin – Microbubble scaffold. Biomaterials 35, 5660–5669. https://doi.org/10.1016/j.biomaterials.2014.03.074

Liu, F., Mih, J.D., Shea, B.S., Kho, A.T., Sharif, A.S., Tager, A.M., Tschumperlin, D.J., 2010. Feedback amplification of fibrosis through matrix stiffening and COX-2 suppression. J. Cell Biol. 190, 693–706. https://doi.org/10.1083/jcb.201004082

Liu, F., Tschumperlin, D.J., 2011. Micro-mechanical characterization of lung tissue using atomic force microscopy. J. Vis. Exp. JoVE. https://doi.org/10.3791/2911

Liu, M., Skinner, S.J., Xu, J., Han, R.N., Tanswell, A.K., Post, M., 1992. Stimulation of fetal rat lung cell proliferation in vitro by mechanical stretch. Am. J. Physiol. 263, L376-383. https://doi.org/10.1152/ajplung.1992.263.3.L376

Liu, Y., Kumar, V.S., Zhang, W., Rehman, J., Malik, A.B., 2015. Activation of type II cells into regenerative stem cell antigen-1(+) cells during alveolar repair. Am. J. Respir. Cell Mol. Biol. 53, 113–124. https://doi.org/10.1165/rcmb.2013-0497OC

Llames, S., García-Pérez, E., Meana, Á., Larcher, F., del Río, M., 2015. Feeder Layer Cell Actions and Applications. Tissue Eng. Part B Rev. 21, 345–353. https://doi.org/10.1089/ten.teb.2014.0547

López-Campos, J.L., Tan, W., Soriano, J.B., 2016. Global burden of COPD. Respirol. Carlton Vic 21, 14–23. https://doi.org/10.1111/resp.12660

Lowery, E.M., Brubaker, A.L., Kuhlmann, E., Kovacs, E.J., 2013. The aging lung. Clin. Interv. Aging 8, 1489–1496. https://doi.org/10.2147/CIA.S51152

Lozano, R., Naghavi, M., Foreman, K., Lim, S., Shibuya, K., Aboyans, V., Abraham, J., Adair, T., Aggarwal, R., Ahn, S.Y., AlMazroa, M.A., Alvarado, M., Anderson, H.R., Anderson, L.M., Andrews, K.G., Atkinson, C., Baddour, L.M., Barker-Collo, S., Bartels, D.H., Bell, M.L., Benjamin, E.J., Bennett, D., Bhalla, K., Bikbov, B., Abdulhak, A.B., Birbeck, G., Blyth, F., Bolliger, I., Boufous, S., Bucello, C., Burch, M., Burney, P., Carapetis, J., Chen, H., Chou, D., Chugh, S.S., Coffeng, L.E., Colan, S.D., Colquhoun, S., Colson, K.E., Condon, J., Connor, M.D., Cooper, L.T., Corriere, M., Cortinovis, M., de Vaccaro, K.C., Couser, W., Cowie, B.C., Criqui, M.H., Cross, M., Dabhadkar, K.C., Dahodwala, N., De Leo, D., Degenhardt, L., Delossantos, A., Denenberg, J., Des Jarlais, D.C., Dharmaratne, S.D., Dorsey, E.R., Driscoll, T., Duber, H., Ebel, B., Erwin, P.J., Espindola, P., Ezzati, M., Feigin, V., Flaxman, A.D., Forouzanfar, M.H., Fowkes, F.G.R., Franklin, R., Fransen, M., Freeman, M.K., Gabriel, S.E., Gakidou, E., Gaspari, F., Gillum, R.F., Gonzalez-Medina, D., Halasa, Y.A., Haring, D., Harrison, J.E., Havmoeller, R., Hay, R.J., Hoen, B., Hotez, P.J., Hoy, D., Jacobsen, K.H., James, S.L., Jasrasaria, R., Jayaraman, S., Johns, N., Karthikeyan, G., Kassebaum, N., Keren, A., Khoo, J.-P., Knowlton, L.M., Kobusingye, O., Koranteng, A., Krishnamurthi, R., Lipnick, M., Lipshultz, S.E., Ohno, S.L., Mabweijano, J., MacIntyre, M.F., Mallinger, L., March, L., Marks, G.B., Marks, R., Matsumori, A., Matzopoulos, R., Mayosi, B.M., McAnulty, J.H., McDermott, M.M., McGrath, J., Memish, Z.A., Mensah, G.A., Merriman, T.R., Michaud, C., Miller, M., Miller, T.R., Mock, C., Mocumbi, A.O., Mokdad, A.A., Moran, A., Mulholland, K., Nair, M.N., Naldi, L., Narayan, K.M.V., Nasseri, K., Norman, P., O'Donnell, M., Omer, S.B., Ortblad, K., Osborne, R., Ozgediz, D., Pahari, B., Pandian, J.D., Rivero, A.P., Padilla, R.P., Perez-Ruiz, F., Perico, N., Phillips, D., Pierce, K., Pope, C.A., Porrini, E., Pourmalek, F., Raju, M., Ranganathan, D., Rehm, J.T., Rein, D.B., Remuzzi, G., Rivara, F.P., Roberts, T., De León, F.R., Rosenfeld, L.C., Rushton, L., Sacco, R.L., Salomon, J.A., Sampson, U., Sanman, E., Schwebel, D.C., Segui-Gomez, M., Shepard, D.S., Singh, D., Singleton, J., Sliwa, K., Smith, E., Steer, A., Taylor, J.A., Thomas, B., Tleyjeh, I.M., Towbin, J.A., Truelsen, T., Undurraga, E.A., Venketasubramanian, N., Vijayakumar, L., Vos, T., Wagner, G.R., Wang, M., Wang, W., Watt, K., Weinstock, M.A., Weintraub, R., Wilkinson, J.D., Woolf, A.D., Wulf, S., Yeh, P.-H., Yip, P., Zabetian, A., Zheng, Z.-J., Lopez, A.D., Murray, C.J., 2012. Global and regional mortality from 235 causes of death for 20 age groups in 1990 and 2010: a systematic analysis for the Global Burden of Disease Study 2010. The Lancet 380, 2095–2128. https://doi.org/10.1016/S0140-6736(12)61728-0

Ma, J., Rubin, B.K., Voynow, J.A., 2018. Mucins, Mucus, and Goblet Cells. Chest 154, 169–176. https://doi.org/10.1016/j.chest.2017.11.008

Ma, L., Gao, C., Mao, Z., Zhou, J., Shen, J., Hu, X., Han, C., 2003. Collagen/chitosan porous scaffolds with improved biostability for skin tissue engineering. Biomaterials 24, 4833–4841. https://doi.org/10.1016/S0142-9612(03)00374-0

Macchiarini, P., Jungebluth, P., Go, T., Asnaghi, M.A., Rees, L.E., Cogan, T.A., Dodson, A., Martorell, J., Bellini, S., Parnigotto, P.P., Dickinson, S.C., Hollander, A.P., Mantero, S., Conconi, M.T., Birchall, M.A., 2008. Clinical transplantation of a tissue-engineered airway. Lancet Lond. Engl. 372, 2023–2030. https://doi.org/10.1016/S0140-6736(08)61598-6

Mackay, D., Haw, S., Ayres, J.G., Fischbacher, C., Pell, J.P., 2010. Smoke-free legislation and hospitalizations for childhood asthma. N. Engl. J. Med. 363, 1139–1145. https://doi.org/10.1056/NEJMoa1002861

Mannino, D.M., Buist, A.S., 2007. Global burden of COPD: risk factors, prevalence, and future trends. Lancet Lond. Engl. 370, 765–773. https://doi.org/10.1016/S0140-6736(07)61380-4

Mansouri, N., SamiraBagheri, null, 2016. The influence of topography on tissue engineering perspective. Mater. Sci. Eng. C Mater. Biol. Appl. 61, 906–921. https://doi.org/10.1016/j.msec.2015.12.094
Mason, R.J., 2006. Biology of alveolar type II cells. Respirology 11, S12–S15. https://doi.org/10.1111/j.1440-1843.2006.00800.x
Matrigel Matrix | Extracellular Matrix | Corning [WWW Document], n.d. URL https://www.corning.com/emea/en/products/life-sciences/products/surfaces/matrigel-matrix.html (accessed 4.28.21).
Mehta, A.C., Thaniyavarn, T., Ghobrial, M., Khemasuwan, D., 2015. COmmon congenital anomalies of the central airways in adults. Chest 148, 274–287. https://doi.org/10.1378/chest.14-1788
Melo, E., Garreta, E., Luque, T., Cortiella, J., Nichols, J., Navajas, D., Farré, R., 2014. Effects of the decellularization method on the local stiffness of acellular lungs. Tissue Eng. Part C Methods 20, 412–422. https://doi.org/10.1089/ten.TEC.2013.0325
Metz, M., Grimbaldeston, M.A., Nakae, S., Piliponsky, A.M., Tsai, M., Galli, S.J., 2007. Mast cells in the promotion and limitation of chronic inflammation. Immunol. Rev. 217, 304–328. https://doi.org/10.1111/j.1600-065X.2007.00520.x
Mikus, J., Steverding, D., 2000. A simple colorimetric method to screen drug cytotoxicity against Leishmania using the dye Alamar Blue®. Parasitol. Int. 48, 265–269. https://doi.org/10.1016/S1383-5769(99)00020-3
Miller, F.D., Kaplan, D.R., 2012. Mobilizing endogenous stem cells for repair and regeneration: are we there yet? Cell Stem Cell 10, 650–652. https://doi.org/10.1016/j.stem.2012.05.004
Minervini, F., Kestenholz, P.B., Paolini, V., Pesci, A., Libretti, L., Bertolaccini, L., Scarci, M., 2018. Surgical and endoscopic treatment for COPD: patients selection, techniques and results. J. Thorac. Dis. 10, S3344–S3351. https://doi.org/10.21037/jtd.2018.06.156
Morales-Nebreda, L., Misharin, A.V., Perlman, H., Budinger, G.R.S., 2015. The heterogeneity of lung macrophages in the susceptibility to disease. Eur. Respir. Rev. 24, 505–509. https://doi.org/10.1183/16000617.0031-2015
Mullen, P.D., Hersey, J.C., Iverson, D.C., 1987. Health behavior models compared. Soc. Sci. Med. 24, 973–981. https://doi.org/10.1016/0277-9536(87)90291-7
Nkadi, P.O., Merritt, T.A., Pillers, D.-A.M., 2009. An Overview of Pulmonary Surfactant in the Neonate: Genetics, Metabolism, and the Role of Surfactant in Health and Disease. Mol. Genet. Metab. 97, 95–101. https://doi.org/10.1016/j.ymgme.2009.01.015
Nothdurft, F.P., Fontana, D., Ruppenthal, S., May, A., Aktas, C., Mehraein, Y., Lipp, P., Kaestner, L., 2015. Differential Behavior of Fibroblasts and Epithelial Cells on Structured Implant Abutment Materials: A Comparison of Materials and Surface Topographies. Clin. Implant Dent. Relat. Res. 17, 1237–1249. https://doi.org/10.1111/cid.12253
O'Brien, F.J., 2011. Biomaterials & scaffolds for tissue engineering. Mater. Today 14, 88–95. https://doi.org/10.1016/S1369-7021(11)70058-X
O'Brien, J., Wilson, I., Orton, T., Pognan, F., 2000. Investigation of the Alamar Blue (resazurin) fluorescent dye for the assessment of mammalian cell cytotoxicity. Eur. J. Biochem. 267, 5421–5426. https://doi.org/10.1046/j.1432-1327.2000.01606.x
Ochs, M., Nyengaard, J.R., Jung, A., Knudsen, L., Voigt, M., Wahlers, T., Richter, J., Gundersen, H.J.G., 2004. The number of alveoli in the human lung. Am. J. Respir. Crit. Care Med. 169, 120–124. https://doi.org/10.1164/rccm.200308-1107OC
O'Driscoll, B.R., Howard, L.S., Davison, A.G., British Thoracic Society, 2008. BTS guideline for emergency oxygen use in adult patients. Thorax 63 Suppl 6, vi1-68. https://doi.org/10.1136/thx.2008.102947
Oldham, M.J., Moss, O.R., 2019. Pores of Kohn: forgotten alveolar structures and potential source of aerosols in exhaled breath. J. Breath Res. 13, 021003. https://doi.org/10.1088/1752-7163/ab0524
O'Neill, J.D., Anfang, R., Anandappa, A., Costa, J., Javidfar, J., Wobma, H.M., Singh, G., Freytes, D.O., Bacchetta, M.D., Sonett, J.R., Vunjak-Novakovic, G., 2013a. Decellularization of human and porcine

lung tissues for pulmonary tissue engineering. Ann. Thorac. Surg. 96, 1046–1055; discussion 1055-1056. https://doi.org/10.1016/j.athoracsur.2013.04.022
O'Neill, J.D., Anfang, R., Anandappa, A., Costa, J., Javidfar, J., Wobma, H.M., Singh, G., Freytes, D.O., Bacchetta, M.D., Sonett, J.R., Vunjak-Novakovic, G., 2013b. Decellularization of Human and Porcine Lung Tissues for Pulmonary Tissue Engineering. Ann. Thorac. Surg. 96, 1046–1056. https://doi.org/10.1016/j.athoracsur.2013.04.022
O'Neill, J.D., Anfang, R., Anandappa, A., Costa, J., Javidfar, J., Wobma, H.M., Singh, G., Freytes, D.O., Bacchetta, M.D., Sonett, J.R., Vunjak-Novakovic, G., 2013c. Decellularization of Human and Porcine Lung Tissues for Pulmonary Tissue Engineering. Ann. Thorac. Surg. 96, 1046–1056. https://doi.org/10.1016/j.athoracsur.2013.04.022
Osei, E.T., Noordhoek, J.A., Hackett, T.L., Spanjer, A.I.R., Postma, D.S., Timens, W., Brandsma, C.-A., Heijink, I.H., 2016. Interleukin-1α drives the dysfunctional cross-talk of the airway epithelium and lung fibroblasts in COPD. Eur. Respir. J. 48, 359–369. https://doi.org/10.1183/13993003.01911-2015
Overview | Chronic obstructive pulmonary disease in over 16s: diagnosis and management | Guidance | NICE [WWW Document], n.d. URL https://www.nice.org.uk/guidance/ng115 (accessed 1.26.21).
Pahal, P., Avula, A., Sharma, S., 2020. Emphysema, in: StatPearls. StatPearls Publishing, Treasure Island (FL).
Papi, A., Bellettato, C.M., Braccioni, F., Romagnoli, M., Casolari, P., Caramori, G., Fabbri, L.M., Johnston, S.L., 2006. Infections and airway inflammation in chronic obstructive pulmonary disease severe exacerbations. Am. J. Respir. Crit. Care Med. 173, 1114–1121. https://doi.org/10.1164/rccm.200506-859OC
Parameswaran, H., Majumdar, A., Suki, B., 2011. Linking microscopic spatial patterns of tissue destruction in emphysema to macroscopic decline in stiffness using a 3D computational model. PLoS Comput. Biol. 7, e1001125. https://doi.org/10.1371/journal.pcbi.1001125
Paschos, N.K., Brown, W.E., Eswaramoorthy, R., Hu, J.C., Athanasiou, K.A., 2015. Advances in tissue engineering through stem cell-based co-culture. J. Tissue Eng. Regen. Med. 9, 488–503. https://doi.org/10.1002/term.1870
Patel, S.J., Teach, S.J., 2019. Asthma. Pediatr. Rev. 40, 549–567. https://doi.org/10.1542/pir.2018-0282
Peng, Y.Y., Glattauer, V., Ramshaw, J.A.M., 2017. Stabilisation of Collagen Sponges by Glutaraldehyde Vapour Crosslinking [WWW Document]. Int. J. Biomater. https://doi.org/10.1155/2017/8947823
Petersen, T.H., Calle, E.A., Zhao, L., Lee, E.J., Gui, L., Raredon, M.B., Gavrilov, K., Yi, T., Zhuang, Z.W., Breuer, C., Herzog, E., Niklason, L.E., 2010a. Tissue-Engineered Lungs for in Vivo Implantation. Science 329, 538–541. https://doi.org/10.1126/science.1189345
Petersen, T.H., Calle, E.A., Zhao, L., Lee, E.J., Gui, L., Raredon, M.B., Gavrilov, K., Yi, T., Zhuang, Z.W., Breuer, C., Herzog, E., Niklason, L.E., 2010b. Tissue-engineered lungs for in vivo implantation. Science 329, 538–541. https://doi.org/10.1126/science.1189345
Phan, S.H., 2012. Genesis of the Myofibroblast in Lung Injury and Fibrosis. Proc. Am. Thorac. Soc. 9, 148–152. https://doi.org/10.1513/pats.201201-011AW
Pillai, S.G., Ge, D., Zhu, G., Kong, X., Shianna, K.V., Need, A.C., Feng, S., Hersh, C.P., Bakke, P., Gulsvik, A., Ruppert, A., Lødrup Carlsen, K.C., Roses, A., Anderson, W., Rennard, S.I., Lomas, D.A., Silverman, E.K., Goldstein, D.B., ICGN Investigators, 2009. A genome-wide association study in chronic obstructive pulmonary disease (COPD): identification of two major susceptibility loci. PLoS Genet. 5, e1000421. https://doi.org/10.1371/journal.pgen.1000421
Plopper, C.G., Smiley-Jewell, S.M., Miller, L.A., Fanucchi, M.V., Evans, M.J., Buckpitt, A.R., Avdalovic, M., Gershwin, L.J., Joad, J.P., Kajekar, R., Larson, S., Pinkerton, K.E., Van Winkle, L.S., Schelegle, E.S., Pieczarka, E.M., Wu, R., Hyde, D.M., 2007. Asthma/allergic airways disease: does postnatal exposure to environmental toxicants promote airway pathobiology? Toxicol. Pathol. 35, 97–110. https://doi.org/10.1080/01926230601132030
PneumaCult™-ALI Medium for Airway Epithelial Cell Culture | STEMCELL Technologies [WWW Document], n.d. URL https://www.stemcell.com/pneumacult-ali-medium.html (accessed 4.28.21).

Polio, S.R., Kundu, A.N., Dougan, C.E., Birch, N.P., Aurian-Blajeni, D.E., Schiffman, J.D., Crosby, A.J., Peyton, S.R., 2018. Cross-platform mechanical characterization of lung tissue. PloS One 13, e0204765. https://doi.org/10.1371/journal.pone.0204765

Possa, S.S., Leick, E.A., Prado, C.M., Martins, M.A., Tibério, I.F.L.C., 2013. Eosinophilic Inflammation in Allergic Asthma. Front. Pharmacol. 4. https://doi.org/10.3389/fphar.2013.00046

Pottier, N., Maurin, T., Chevalier, B., Puisségur, M.-P., Lebrigand, K., Robbe-Sermesant, K., Bertero, T., Cardenas, C.L.L., Courcot, E., Rios, G., Fourre, S., Lo-Guidice, J.-M., Marcet, B., Cardinaud, B., Barbry, P., Mari, B., 2009. Identification of Keratinocyte Growth Factor as a Target of microRNA-155 in Lung Fibroblasts: Implication in Epithelial-Mesenchymal Interactions. PLOS ONE 4, e6718. https://doi.org/10.1371/journal.pone.0006718

Putcha, N., Drummond, M.B., Connett, J.E., Scanlon, P.D., Tashkin, D.P., Hansel, N.N., Wise, R.A., 2014. Chronic Productive Cough is Associated with Death in Smokers with Early COPD. COPD 11, 451–458. https://doi.org/10.3109/15412555.2013.837870

Qian, Z., Travanty, E.A., Oko, L., Edeen, K., Berglund, A., Wang, J., Ito, Y., Holmes, K.V., Mason, R.J., 2013. Innate Immune Response of Human Alveolar Type II Cells Infected with Severe Acute Respiratory Syndrome–Coronavirus. Am. J. Respir. Cell Mol. Biol. 48, 742–748. https://doi.org/10.1165/rcmb.2012-0339OC

Quent, V.M.C., Loessner, D., Friis, T., Reichert, J.C., Hutmacher, D.W., 2010. Discrepancies between metabolic activity and DNA content as tool to assess cell proliferation in cancer research. J. Cell. Mol. Med. 14, 1003–1013. https://doi.org/10.1111/j.1582-4934.2010.01013.x

Quezada, W., Make, B., 2016. Interventional Options for COPD- LVRS, Bronchoscopic Therapies and the Future. Chronic Obstr. Pulm. Dis. Miami Fla 3, 446–453. https://doi.org/10.15326/jcopdf.3.1.2015.0171

Qureshi, H., Sharafkhaneh, A., Hanania, N.A., 2014. Chronic obstructive pulmonary disease exacerbations: latest evidence and clinical implications. Ther. Adv. Chronic Dis. 5, 212–227. https://doi.org/10.1177/2040622314532862

Rabe, K.F., Hurd, S., Anzueto, A., Barnes, P.J., Buist, S.A., Calverley, P., Fukuchi, Y., Jenkins, C., Rodriguez-Roisin, R., van Weel, C., Zielinski, J., Global Initiative for Chronic Obstructive Lung Disease, 2007. Global strategy for the diagnosis, management, and prevention of chronic obstructive pulmonary disease: GOLD executive summary. Am. J. Respir. Crit. Care Med. 176, 532–555. https://doi.org/10.1164/rccm.200703-456SO

Ramamoorthy, S., Cidlowski, J.A., 2016. Corticosteroids-Mechanisms of Action in Health and Disease. Rheum. Dis. Clin. North Am. 42, 15–31. https://doi.org/10.1016/j.rdc.2015.08.002

Rampersad, S.N., 2012. Multiple Applications of Alamar Blue as an Indicator of Metabolic Function and Cellular Health in Cell Viability Bioassays. Sensors 12, 12347–12360. https://doi.org/10.3390/s120912347

Raredon, M.S.B., Rocco, K.A., Gheorghe, C.P., Sivarapatna, A., Ghaedi, M., Balestrini, J.L., Raredon, T.L., Calle, E.A., Niklason, L.E., 2016. Biomimetic Culture Reactor for Whole-Lung Engineering. BioResearch Open Access 5, 72–83. https://doi.org/10.1089/biores.2016.0006

Ravi, M., Paramesh, V., Kaviya, S.R., Anuradha, E., Solomon, F.D.P., 2015. 3D Cell Culture Systems: Advantages and Applications. J. Cell. Physiol. 230, 16–26. https://doi.org/10.1002/jcp.24683

Rawlins, E.L., Ostrowski, L.E., Randell, S.H., Hogan, B.L.M., 2007. Lung development and repair: Contribution of the ciliated lineage. Proc. Natl. Acad. Sci. 104, 410–417. https://doi.org/10.1073/pnas.0610770104

Reece, T.B., Mitchell, J.D., Zamora, M.R., Fullerton, D.A., Cleveland, J.C., Pomerantz, M., Lyu, D.M., Grover, F.L., Weyant, M.J., 2008. Native lung volume reduction surgery relieves functional graft compression after single-lung transplantation for chronic obstructive pulmonary disease. J. Thorac. Cardiovasc. Surg. 135, 931–937. https://doi.org/10.1016/j.jtcvs.2007.10.069

Rehan, V.K., Torday, J.S., 2014. The Lung Alveolar Lipofibroblast: An Evolutionary Strategy Against Neonatal Hyperoxic Lung Injury. Antioxid. Redox Signal. 21, 1893–1904. https://doi.org/10.1089/ars.2013.5793

Rehman, A., Amin, F., Sadeeqa, S., 2018. Prevalence of asthma and its management: A review. JPMA J. Pak. Med. Assoc. 68, 1823–1827.
Reis, R.L., Neves, N., Mano, J.F., Gomes, M., Marques, A., Azevedo, H., 2008a. Natural-Based Polymers for Biomedical Applications. Nat.-Based Polym. Biomed. Appl. XXIII–XXV.
Reis, R.L., Neves, N.M., Mano, J.F., Gomes, M.E., Marques, A.P., Azevedo, H.S., 2008b. Natural-Based Polymers for Biomedical Applications. Elsevier.
Rennard, S.I., Vestbo, J., 2006. COPD: the dangerous underestimate of 15%. The Lancet 367, 1216–1219. https://doi.org/10.1016/S0140-6736(06)68516-4
Rizzo, D.C., 2015. Fundamentals of Anatomy and Physiology. Cengage Learning.
Robinson, H.C., 2016. Respiratory Conditions Update: Restrictive Lung Disease. FP Essent. 448, 29–34.
Rock, J.R., Gao, X., Xue, Y., Randell, S.H., Kong, Y.-Y., Hogan, B.L.M., 2011. Notch-Dependent Differentiation of Adult Airway Basal Stem Cells. Cell Stem Cell 8, 639–648. https://doi.org/10.1016/j.stem.2011.04.003
Rokicki, W., Rokicki, M., Wojtacha, J., Dżeljijli, A., 2016. The role and importance of club cells (Clara cells) in the pathogenesis of some respiratory diseases. Kardiochirurgia Torakochirurgia Pol. Pol. J. Cardio-Thorac. Surg. 13, 26–30. https://doi.org/10.5114/kitp.2016.58961
Rosenberg, Sharon R., Kalhan, R., 2017. Recent advances in the management of chronic obstructive pulmonary disease. F1000Research 6, 863. https://doi.org/10.12688/f1000research.9819.1
Rosenberg, Sharon R, Kalhan, R., 2017. Recent advances in the management of chronic obstructive pulmonary disease. F1000Research 6. https://doi.org/10.12688/f1000research.9819.1
Sachs, N., Papaspyropoulos, A., Zomer-van Ommen, D.D., Heo, I., Böttinger, L., Klay, D., Weeber, F., Huelsz-Prince, G., Iakobachvili, N., Amatngalim, G.D., de Ligt, J., van Hoeck, A., Proost, N., Viveen, M.C., Lyubimova, A., Teeven, L., Derakhshan, S., Korving, J., Begthel, H., Dekkers, J.F., Kumawat, K., Ramos, E., van Oosterhout, M.F., Offerhaus, G.J., Wiener, D.J., Olimpio, E.P., Dijkstra, K.K., Smit, E.F., van der Linden, M., Jaksani, S., van de Ven, M., Jonkers, J., Rios, A.C., Voest, E.E., van Moorsel, C.H., van der Ent, C.K., Cuppen, E., van Oudenaarden, A., Coenjaerts, F.E., Meyaard, L., Bont, L.J., Peters, P.J., Tans, S.J., van Zon, J.S., Boj, S.F., Vries, R.G., Beekman, J.M., Clevers, H., 2019. Long-term expanding human airway organoids for disease modeling. EMBO J. 38, e100300. https://doi.org/10.15252/embj.2018100300
Salathe, M., 2002. Effects of β-agonists on airway epithelial cells. J. Allergy Clin. Immunol. 110, S275–S281. https://doi.org/10.1067/mai.2002.129412
Salciccioli, J.D., Marshall, D.C., Shalhoub, J., Maruthappu, M., Carlo, G.D., Chung, K.F., 2018. Respiratory disease mortality in the United Kingdom compared with EU15+ countries in 1985-2015: observational study. BMJ 363, k4680. https://doi.org/10.1136/bmj.k4680
Salvi, S.S., Barnes, P.J., 2009. Chronic obstructive pulmonary disease in non-smokers. The Lancet 374, 733–743. https://doi.org/10.1016/S0140-6736(09)61303-9
Santis, M.M.D., Bölükbas, D.A., Lindstedt, S., Wagner, D.E., 2018. How to build a lung: latest advances and emerging themes in lung bioengineering. Eur. Respir. J. 52. https://doi.org/10.1183/13993003.01355-2016
Schreiber, W.G., Morbach, A.E., Stavngaard, T., Gast, K.K., Herweling, A., Søgaard, L.V., Windirsch, M., Schmiedeskamp, J., Heussel, C.P., Kauczor, H.-U., 2005a. Assessment of lung microstructure with magnetic resonance imaging of hyperpolarized Helium-3. Respir. Physiol. Neurobiol., Structure and Function in the Periphery of the Lung 148, 23–42. https://doi.org/10.1016/j.resp.2005.05.002
Schreiber, W.G., Morbach, A.E., Stavngaard, T., Gast, K.K., Herweling, A., Søgaard, L.V., Windirsch, M., Schmiedeskamp, J., Heussel, C.P., Kauczor, H.-U., 2005b. Assessment of lung microstructure with magnetic resonance imaging of hyperpolarized Helium-3. Respir. Physiol. Neurobiol. 148, 23–42. https://doi.org/10.1016/j.resp.2005.05.002
Schyns, J., Bureau, F., Marichal, T., 2018. Lung Interstitial Macrophages: Past, Present, and Future. J. Immunol. Res. 2018. https://doi.org/10.1155/2018/5160794
Seemungal, T.A.R., Wilkinson, T.M.A., Hurst, J.R., Perera, W.R., Sapsford, R.J., Wedzicha, J.A., 2008. Long-term erythromycin therapy is associated with decreased chronic obstructive pulmonary

disease exacerbations. Am. J. Respir. Crit. Care Med. 178, 1139–1147. https://doi.org/10.1164/rccm.200801-145OC
Sethi, S., 2010. Infection as a comorbidity of COPD. Eur. Respir. J. 35, 1209–1215. https://doi.org/10.1183/09031936.00081409
Seyer, J.M., Hutcheson, E.T., Kang, A.H., 1976. Collagen polymorphism in idiopathic chronic pulmonary fibrosis. J. Clin. Invest. 57, 1498–1507. https://doi.org/10.1172/JCI108420
Seys, L.J.M., Verhamme, F.M., Schinwald, A., Hammad, H., Cunoosamy, D.M., Bantsimba-Malanda, C., Sabirsh, A., McCall, E., Flavell, L., Herbst, R., Provoost, S., Lambrecht, B.N., Joos, G.F., Brusselle, G.G., Bracke, K.R., 2015. Role of B Cell–Activating Factor in Chronic Obstructive Pulmonary Disease. Am. J. Respir. Crit. Care Med. 192, 706–718. https://doi.org/10.1164/rccm.201501-0103OC
Sharafkhaneh, A., Hanania, N.A., Kim, V., 2008. Pathogenesis of Emphysema. Proc. Am. Thorac. Soc. 5, 475–477. https://doi.org/10.1513/pats.200708-126ET
Shigemura, M., Lecuona, E., Sznajder, J.I., 2017. Effects of hypercapnia on the lung. J. Physiol. 595, 2431–2437. https://doi.org/10.1113/JP273781
Siddiqi, A., Sethi, S., 2008. Optimizing antibiotic selection in treating COPD exacerbations. Int. J. Chron. Obstruct. Pulmon. Dis. 3, 31–44.
Siddiqui, F.M., Diamond, J.M., 2018. Lung transplantation for chronic obstructive pulmonary disease: past, present, and future directions. Curr. Opin. Pulm. Med. 24, 199–204. https://doi.org/10.1097/MCP.0000000000000452
Siddiqui, N.A., Mansour, M.K., Nookala, V., 2020. Bullous Emphysema, in: StatPearls. StatPearls Publishing, Treasure Island (FL).
Silverman, E.K., 2020. Genetics of COPD. Annu. Rev. Physiol. 82, 413–431. https://doi.org/10.1146/annurev-physiol-021317-121224
Simsa, R., Padma, A.M., Heher, P., Hellström, M., Teuschl, A., Jenndahl, L., Bergh, N., Fogelstrand, P., 2018. Systematic in vitro comparison of decellularization protocols for blood vessels. PLoS ONE 13. https://doi.org/10.1371/journal.pone.0209269
Singh, R., Mackay, A.J., Patel, A.R., Garcha, D.S., Kowlessar, B.S., Brill, S.E., Donnelly, L.E., Barnes, P.J., Donaldson, G.C., Wedzicha, J.A., 2014. Inflammatory thresholds and the species-specific effects of colonising bacteria in stable chronic obstructive pulmonary disease. Respir. Res. 15, 114. https://doi.org/10.1186/s12931-014-0114-1
Sinyor, B., Concepcion Perez, L., 2020. Pathophysiology Of Asthma, in: StatPearls. StatPearls Publishing, Treasure Island (FL).
Sprott, R.F., Ritzmann, F., Langer, F., Yao, Y., Herr, C., Kohl, Y., Tschernig, T., Bals, R., Beisswenger, C., 2020. Flagellin shifts 3D bronchospheres towards mucus hyperproduction. Respir. Res. 21, 222. https://doi.org/10.1186/s12931-020-01486-x
Stegemann-Koniszewski, S., Jeron, A., Gereke, M., Geffers, R., Kröger, A., Gunzer, M., Bruder, D., 2016. Alveolar Type II Epithelial Cells Contribute to the Anti-Influenza A Virus Response in the Lung by Integrating Pathogen- and Microenvironment-Derived Signals. mBio 7. https://doi.org/10.1128/mBio.00276-16
Stenton, C., 2008. The MRC breathlessness scale. Occup. Med. 58, 226–227. https://doi.org/10.1093/occmed/kqm162
Suissa, S., Patenaude, V., Lapi, F., Ernst, P., 2013. Inhaled corticosteroids in COPD and the risk of serious pneumonia. Thorax 68, 1029–1036. https://doi.org/10.1136/thoraxjnl-2012-202872
SURGISPON [WWW Document], n.d. URL https://www.aegis-lifesciences.com/web-page/surgispon.html (accessed 2.16.21).
Swann, W.B., Wenzlaff, R.M., Tafarodi, R.W., 1992. Depression and the search for negative evaluations: More evidence of the role of self-verification strivings. J. Abnorm. Psychol. 101, 314–317. https://doi.org/10.1037/0021-843X.101.2.314
Takahashi, K., Yamanaka, S., 2006. Induction of Pluripotent Stem Cells from Mouse Embryonic and Adult Fibroblast Cultures by Defined Factors. Cell 126, 663–676. https://doi.org/10.1016/j.cell.2006.07.024

Taylor, A.E., Finney-Hayward, T.K., Quint, J.K., Thomas, C.M.R., Tudhope, S.J., Wedzicha, J.A., Barnes, P.J., Donnelly, L.E., 2010. Defective macrophage phagocytosis of bacteria in COPD. Eur. Respir. J. 35, 1039–1047. https://doi.org/10.1183/09031936.00036709

Technologies, S., 2019. How to Culture Human Bronchial Epithelial Cells as Airway Organoids. https://doi.org/10.17504/protocols.io.4u5gwy6

Terry, P.B., Traystman, R.J., 2016. The Clinical Significance of Collateral Ventilation. Ann. Am. Thorac. Soc. 13, 2251–2257. https://doi.org/10.1513/AnnalsATS.201606-448FR

The Global Asthma Report 2014 [WWW Document], n.d. URL http://www.globalasthmareport.org/2014/ (accessed 1.26.21).

Theocharidis, G., Drymoussi, Z., Kao, A.P., Barber, A.H., Lee, D.A., Braun, K.M., Connelly, J.T., 2016. Type VI Collagen Regulates Dermal Matrix Assembly and Fibroblast Motility. J. Invest. Dermatol. 136, 74–83. https://doi.org/10.1038/JID.2015.352

Thulborn, S.J., Mistry, V., Brightling, C.E., Moffitt, K.L., Ribeiro, D., Bafadhel, M., 2019. Neutrophil elastase as a biomarker for bacterial infection in COPD. Respir. Res. 20, 170. https://doi.org/10.1186/s12931-019-1145-4

Todd, J.L., Palmer, S.M., 2010. Lung transplantation in advanced COPD: is it worth it? Semin. Respir. Crit. Care Med. 31, 365–372. https://doi.org/10.1055/s-0030-1254076

Toskala, E., Kennedy, D.W., 2015. Asthma risk factors. Int. Forum Allergy Rhinol. 5, S11–S16. https://doi.org/10.1002/alr.21557

Tsolaki, V., Pastaka, C., Kostikas, K., Karetsi, E., Dimoulis, A., Zikiri, A., Koutsokera, A., Gourgoulianis, K.I., 2011. Noninvasive Ventilation in Chronic Respiratory Failure: Effects on Quality of Life. Respiration 81, 402–410. https://doi.org/10.1159/000317138

Tsuchiya, T., Sivarapatna, A., Rocco, K., Nanashima, A., Nagayasu, T., Niklason, L.E., 2014. Future prospects for tissue engineered lung transplantation. Organogenesis 10, 196–207. https://doi.org/10.4161/org.27846

Valipour, A., Slebos, D.-J., Herth, F., Darwiche, K., Wagner, M., Ficker, J.H., Petermann, C., Hubner, R.-H., Stanzel, F., Eberhardt, R., IMPACT Study Team, 2016. Endobronchial Valve Therapy in Patients with Homogeneous Emphysema. Results from the IMPACT Study. Am. J. Respir. Crit. Care Med. 194, 1073–1082. https://doi.org/10.1164/rccm.201607-1383OC

van Helvoort, H.A.C., Heijdra, Y.F., Heunks, L.M.A., Meijer, P.L.M., Ruitenbeek, W., Thijs, H.M.H., Dekhuijzen, P.N.R., 2006. Supplemental oxygen prevents exercise-induced oxidative stress in muscle-wasted patients with chronic obstructive pulmonary disease. Am. J. Respir. Crit. Care Med. 173, 1122–1129. https://doi.org/10.1164/rccm.200512-1957OC

van Noord, J.A., Aumann, J.L., Janssens, E., Verhaert, J., Smeets, J.J., Mueller, A., Cornelissen, P.J.G., 2006. Effects of tiotropium with and without formoterol on airflow obstruction and resting hyperinflation in patients with COPD. Chest 129, 509–517. https://doi.org/10.1378/chest.129.3.509

van Steenberghe, M., Schubert, T., Gerelli, S., Bouzin, C., Guiot, Y., Xhema, D., Bollen, X., Abdelhamid, K., Gianello, P., 2018. Porcine pulmonary valve decellularization with NaOH-based vs detergent process: preliminary in vitro and in vivo assessments. J. Cardiothorac. Surg. 13, 34. https://doi.org/10.1186/s13019-018-0720-y

Vijayan, V.K., 2013. Chronic obstructive pulmonary disease. Indian J. Med. Res. 137, 251–269.

Vogelsinger, H., Halank, M., Braun, S., Wilkens, H., Geiser, T., Ott, S., Stucki, A., Kaehler, C.M., 2017. Efficacy and safety of nasal high-flow oxygen in COPD patients. BMC Pulm. Med. 17, 143. https://doi.org/10.1186/s12890-017-0486-3

von Dincklage, J.J., Ball, D., Silvestri, G.A., 2013. A review of clinical practice guidelines for lung cancer. J. Thorac. Dis. 5, S607–S622. https://doi.org/10.3978/j.issn.2072-1439.2013.07.37

Wagers, A.J., 2012. The stem cell niche in regenerative medicine. Cell Stem Cell 10, 362–369. https://doi.org/10.1016/j.stem.2012.02.018

Wagner, D.E., Bonvillain, R.W., Jensen, T.J., Girard, E.D., Bunnell, B.A., Finck, C.M., Hoffman, A.M., Weiss, D.J., 2013. Can Stem Cells be Used to Generate New Lungs? Ex Vivo Lung Bioengineering with Decellularized Whole Lung Scaffolds. Respirol. Carlton Vic 18. https://doi.org/10.1111/resp.12102

Wallis, J.M., Borg, Z.D., Daly, A.B., Deng, B., Ballif, B.A., Allen, G.B., Jaworski, D.M., Weiss, D.J., 2011. Comparative Assessment of Detergent-Based Protocols for Mouse Lung De-Cellularization and Re-Cellularization. Tissue Eng. Part C Methods 18, 420–432. https://doi.org/10.1089/ten.tec.2011.0567

Wang, C., de Mochel, N.S.R., Christenson, S.A., Cassandras, M., Moon, R., Brumwell, A.N., Byrnes, L.E., Li, A., Yokosaki, Y., Shan, P., Sneddon, J.B., Jablons, D., Lee, P.J., Matthay, M.A., Chapman, H.A., Peng, T., 2018. Expansion of hedgehog disrupts mesenchymal identity and induces emphysema phenotype. J. Clin. Invest. 128, 4343–4358. https://doi.org/10.1172/JCI99435

Wang, L., Zhao, Yannan, Yang, F., Feng, M., Zhao, Yazhen, Chen, X., Mi, J., Yao, Y., Guan, D., Xiao, Z., Chen, B., Dai, J., 2020. Biomimetic collagen biomaterial induces in situ lung regeneration by forming functional alveolar. Biomaterials 236, 119825. https://doi.org/10.1016/j.biomaterials.2020.119825

Wang, Y., Lu, Y., Wu, Y., Sun, Y., Zhou, Y., Ma, Q., Zheng, Y., Yu, Q., Cao, Y., Chen, G., Zhang, T., Dai, X., Ren, T., Ma, Y., Zuo, W., 2019. Alveolar Differentiation Potency of Human Distal Airway Stem Cells Is Associated with Pulmonary Pathological Conditions. Stem Cells Int. 2019, e7123078. https://doi.org/10.1155/2019/7123078

Wang, Y., Xu, J., Meng, Y., Adcock, I.M., Yao, X., 2018. Role of inflammatory cells in airway remodeling in COPD. Int. J. Chron. Obstruct. Pulmon. Dis. 13, 3341–3348. https://doi.org/10.2147/COPD.S176122

Watson, A., Phipps, M.J.S., Clark, H.W., Skylaris, C.-K., Madsen, J., 2019. Surfactant Proteins A and D: Trimerized Innate Immunity Proteins with an Affinity for Viral Fusion Proteins. J. Innate Immun. 11, 13–28. https://doi.org/10.1159/000492974

Weibel, E.R., 1999. Understanding the limitation of O2 supply through comparative physiology. Respir. Physiol. 118, 85–93. https://doi.org/10.1016/S0034-5687(99)00084-5

Weill, D., Benden, C., Corris, P.A., Dark, J.H., Davis, R.D., Keshavjee, S., Lederer, D.J., Mulligan, M.J., Patterson, G.A., Singer, L.G., Snell, G.I., Verleden, G.M., Zamora, M.R., Glanville, A.R., 2015. A consensus document for the selection of lung transplant candidates: 2014--an update from the Pulmonary Transplantation Council of the International Society for Heart and Lung Transplantation. J. Heart Lung Transplant. Off. Publ. Int. Soc. Heart Transplant. 34, 1–15. https://doi.org/10.1016/j.healun.2014.06.014

Weiss, D.J., Bertoncello, I., Borok, Z., Kim, C., Panoskaltsis-Mortari, A., Reynolds, S., Rojas, M., Stripp, B., Warburton, D., Prockop, D.J., 2011. Stem Cells and Cell Therapies in Lung Biology and Lung Diseases. Proc. Am. Thorac. Soc. 8, 223–272. https://doi.org/10.1513/pats.201012-071DW

White, E.S., 2015. Lung Extracellular Matrix and Fibroblast Function. Ann. Am. Thorac. Soc. 12, S30–S33. https://doi.org/10.1513/AnnalsATS.201406-240MG

Widysanto, A., Mathew, G., 2020. Chronic Bronchitis, in: StatPearls. StatPearls Publishing, Treasure Island (FL).

Wilk, J.B., Chen, T.-H., Gottlieb, D.J., Walter, R.E., Nagle, M.W., Brandler, B.J., Myers, R.H., Borecki, I.B., Silverman, E.K., Weiss, S.T., O'Connor, G.T., 2009. A genome-wide association study of pulmonary function measures in the Framingham Heart Study. PLoS Genet. 5, e1000429. https://doi.org/10.1371/journal.pgen.1000429

Yamamoto, Y., Gotoh, S., Korogi, Y., Seki, M., Konishi, S., Ikeo, S., Sone, N., Nagasaki, T., Matsumoto, H., Muro, S., Ito, I., Hirai, T., Kohno, T., Suzuki, Y., Mishima, M., 2017. Long-term expansion of alveolar stem cells derived from human iPS cells in organoids. Nat. Methods 14, 1097–1106. https://doi.org/10.1038/nmeth.4448

Yusen, R.D., Edwards, L.B., Dipchand, A.I., Goldfarb, S.B., Kucheryavaya, A.Y., Levvey, B.J., Lund, L.H., Meiser, B., Rossano, J.W., Stehlik, J., International Society for Heart and Lung Transplantation, 2016. The Registry of the International Society for Heart and Lung Transplantation: Thirty-third Adult Lung and Heart-Lung Transplant Report-2016; Focus Theme: Primary Diagnostic Indications for Transplant. J. Heart Lung Transplant. Off. Publ. Int. Soc. Heart Transplant. 35, 1170–1184. https://doi.org/10.1016/j.healun.2016.09.001

Zacharias, W.J., Frank, D.B., Zepp, J.A., Morley, M.P., Alkhaleel, F., Kong, J., Zhou, S., Cantu, E., Morrisey, E.E., 2018. Regeneration of the lung alveolus by an evolutionarily conserved epithelial progenitor. Nature 555, 251–255. https://doi.org/10.1038/nature25786

Zhang, W.-J., Lin, Q.-X., Zhang, Y., Liu, C.-T., Qiu, L.-Y., Wang, H.-B., Wang, Y.-M., Duan, C.-M., Liu, Z.-Q., Zhou, J., Wang, C.-Y., 2011a. The reconstruction of lung alveolus-like structure in collagen-matrigel/microcapsules scaffolds in vitro. J. Cell. Mol. Med. 15, 1878–1886. https://doi.org/10.1111/j.1582-4934.2010.01189.x

Zhang, W.-J., Lin, Q.-X., Zhang, Y., Liu, C.-T., Qiu, L.-Y., Wang, H.-B., Wang, Y.-M., Duan, C.-M., Liu, Z.-Q., Zhou, J., Wang, C.-Y., 2011b. The reconstruction of lung alveolus-like structure in collagen-matrigel/microcapsules scaffolds in vitro. J. Cell. Mol. Med. 15, 1878–1886. https://doi.org/10.1111/j.1582-4934.2010.01189.x